Politecnico di Milano

IV Facoltà di Ingegneria

Master Degree in Mechanical Engineering

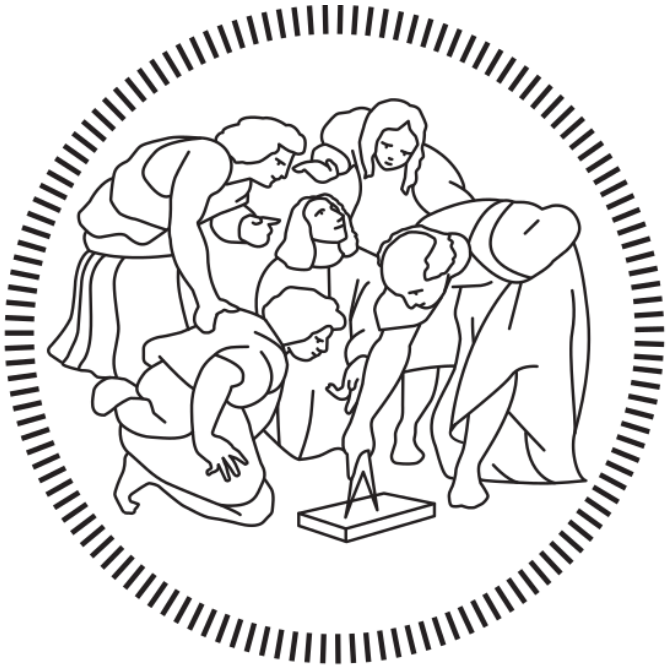

GRADUATION THESIS

Lateral Dynamics of a Sidecar Vehicle

Definition of a simplified model and parameters optimization

Supervisor

Prof. Stefano Melzi

Co-Supervisor

Ing. Giuseppe Guerra

Author

Simone Dovico

Academic Year 2017-2018

Summary

Summary of Figures

Summary of Tables

1 Introduction

Our study will be focused on the lateral dynamics of a sidecar vehicle. In particular, we will focus on the formulation of a simple mathematical model able to predict the lateral behaviour of the vehicle, and to identify the issues of this particular kind of vehicle. The final goal is the optimization of some critical parameter, to find the most stable sidecar configuration.

This project will proceed with the following steps:

- Formulation of a simplified two-dimensional model coherent with the vehicle-dynamics theory that can predict the lateral dynamics of the sidecar vehicle;
- Building-up of a prototype, to be coupled with the motorcycle presented in the next chapter;
- Execution of a series of tests, performing different manoeuvres, with the vehicle equipped with the necessary sensors and data acquisition systems;
- Validation of the mathematical model on the basis of the output coming from the campaign test;
- Set-up of maths able to calculate the sensitivity analysis, and an optimization algorithm to define a set of design variables and then define an optimal set of vehicle parameters.

There is a challenge in this particular type of vehicle: because of its geometry, with no symmetry and with the major amount of masses on a side of the vehicle, and the side wheel placed forward to the rear one and not aligned with it, the modelling is not a trivial business; while other types of three wheeled vehicle has the engine and the driver placed in the middle plane of the vehicle, making the mathematical simulation pretty similar to well known models.

A sidecar is surely more stable than a motorcycle: with the presence of the side wheel, and some drive skill, no (reasonable) ground surface will stop you. You will never drop an outfit down on ice, snow, gravel or mud, although you may slide a little or a lot. Hitting a greasy manhole cover, a pot hole or a curb, will be no longer a “tankslapping” experience. Any of the three tires can blow without instant loss of control.
You have much higher defense.
When a car hits the solo motorcycle head-on, the impact causes the rear of the cycle to lift. This catapults the hapless rider and passenger into the windscreen of the car. He may fly over the car
into oncoming traffic behind the car. With the sidecar, most of the added weight is behind the centre of mass of the cycle. When a car hits our three-wheel vechicle, also head-on, the added weight of the sidecar keeps the rear down. The front wheel, fork and the nose of the sidecar collapse and absorb the impact. You and your passenger will walk away on your legs...
You and your passenger can enjoy the comfort of a car well, almost. Some sidecars come with a hood or hardtop, radio, telecom, mirror, upholstery, fan, and heater.
But on the other hand we have some disadvantages like reduction of the performance expected of your solo. It will have an increased gasoline, tires, chains, sprockets, and spokes consumption.
Accessibility to some cycle parts could be reduced, especially on the right side. The sidecar frame may interfere with removal of alternator covers or other engine components.
The ride is harsher because of the stiffer suspension needed. Hitting a bump with any of the three wheels will jar both rider and passenger. You may hit more bumps as it is easier to hit the bump than to wrench your way around them. On a solo motorcycle you simply glide by with little effort.
You must have patience to learn an entirely new set of riding habits. You must forget your previous motorcycle experience, except the basic motorcycle controls. It is easier for a non-motorcyclist to learn to pilot a sidecar rigm, than it is for the average long term soloist. The amateur has nothing to forget.

1.1 A Short History of Sidecars

From the earliest days of motorcycling to the present day, motorcyclists have pondered the problem of transporting their women. Some girl friends or wives endured the agonies of bumpy rides on the back of a motorcycle, sitting on the "flapper bracket" or rear seat. How they got there, is another matter for the bikes of those days had not have a clutch nor a gearbox nor even a kick starter.
Others could not be persuaded to ride on the rear of the motorcycle in such an ungainly manner, and for them the designers of the pioneer motorcycles tried several approaches to accommodate them.
As far back as 1895, a French newspaper offered a prize for the best idea to carry a passenger on a bike. The sidecar idea took the honours but no one did anything about it. A similar contest took place in the United States. Nothing came of these contests. But the first sidecars vehicle are invented even before the invention of motorcycles between the XIX and the XX centuries, as an extension of bicycles of the period with the same aims expressed above, of increasing the carriage capacity of these kind of vehicles; so a French Army officer, Jean Bertoux, added an extended structure equipped with a back on the rear wheel of his bicycle.

Figure 1-1 Jean Bertoux sidecar model

In the sidecar evolution from the first model of Jean Bertoux the trailer came first. The lady sat on a comfortably cushioned wicker work seat mounted between two bicycle wheels, which was towed behind the motorcycle. This was a very undesirable place to be. The noisy, smoky motorcycle was popping and banging up front. It threw up dust, mud, rocks, and whatever else man and nature paved roads with, in those days. There had to be a better way for a loving twosome to share the joys of motorcycling. Besides, it was not uncommon for the bent towbar to break off unexpectedly, which led to the motorcyclist turning his head to one side and asking “Are you still there, dear”? and added to the apprehension of the damsel.

Figure 1-2 De Dion tricycle with trailer

They next tried the fore-carriage, or fore-car. This was another comfortable wicker seat slung between two wheels attached to the front forks. It replaced the front wheel. At least the intrepid passenger could see where she was going even if the driver could not. The driver had to move his head to look around the passenger, thus compromising safety. It left a lot of room for improvement, including protection from the elements, nature, and the road ahead. Besides, the flimsy front end carriage section often broke.
There is a lot to write about the development of this a little weird vehicle: every conutry developed its own approach, British as well germans as well americans – and italians of course! - all them created their own 'three-wheeled motorcycle'. We have dedicated the appendix B to the history of Sidecar for each country: please refer to it for further details, while we report in the following just some information about today vehicles production.

1.2 Modern Sidecars

While motorcycles have advanced very rapidly the last few decades, motorcycle sidecar design technology has fallen behind. It is not uncommon to see sidecars of the 1960's (or earlier) coupled to sophisticated 2000's models motorcycles.
An example of modern technology applied to sidecar design is the electrically adjustable motorcycle lean control by Vern Goodwin. This enables correct lean adjustment for sidecar loading, or for combatting cross winds. When used while in motion it makes steering easier. The finest example of sidecar technology is the turbo-diesel, three-wheel drive, two-wheel steering Corda from Sweden.

Figure 1-3 Corda sidecar

Look for a price tag of 300,000 Swedish Crowns or over $ 40,000. Only a fortunate few will ever drive one. The fully enclosed sidecar seats two people in comfort. The rig handles like a well mannered sports car. It can turn to the right as quickly and as easily as it can turn to the left. This is very unusual for any sidecar rig. The unitized frame provides support for the motorcycle. It features a 71 hp VW engine and automatic transmission, motorcycle wheels, sidecar wheel, and a sidecar body. Its massive fuel tank provides a 1200 km touring range. Top speed is greater than 105 mph.
Sidecar performance requires certain physical changes to the motorcycle. The sidecar is not an appendage like a set of saddlebags. The motorcycle, its size and power, is taken into account when considering a sidecar. They exist, as interdependent units, one to the other. No showroom motorcycle is suitable for sidecar use without certain changes.
It is not just the sidecar, but features of the sidecar on the motorcycle. A sidecar manufacturer's job is not over when he finishes a sidecar. The way an outfit handles depends on how the sidecar is mounted and the motorcycle preparations made to accept the sidecar.
There are three categories to examine in any sidecar. First, the sidecar. A manufacturer must consider the final use his customer will have, in addition to particular features of the sidecar itself.

Figure 1-4 Goldwing and Ural modern sidecars

The design must compliment the motorcycle, not detract from it. The sidecar is useless by itself.
Next, the sidecar must mount to the motorcycle to create a dual track vehicle from a single track vehicle. The structure is only as good as the foundation. A strong mounting system is essential. The mounts must attach to the main frame and spread the loads uniformly. They must not slide, rotate, or shift. They must not bend or crush the frame.

1.3 Sidecar competitions

As for the traditional motorcycles, sidecars are used for race until the dawn of motorcycling, while the asymmetry of the vehicle imposes a particular and scenic driving technique to the driver and also the passenger to push the vehicle to the limit. As said before, the geometrical asymmetry but also the

asymmetry in the weight distribution heavily influences the dynamics of the vehicle: in the sidecar is present a yaw motion caused by the traction of the engine in the acceleration phase, and the action of the brakes that cause a rotation in the opposite verse.

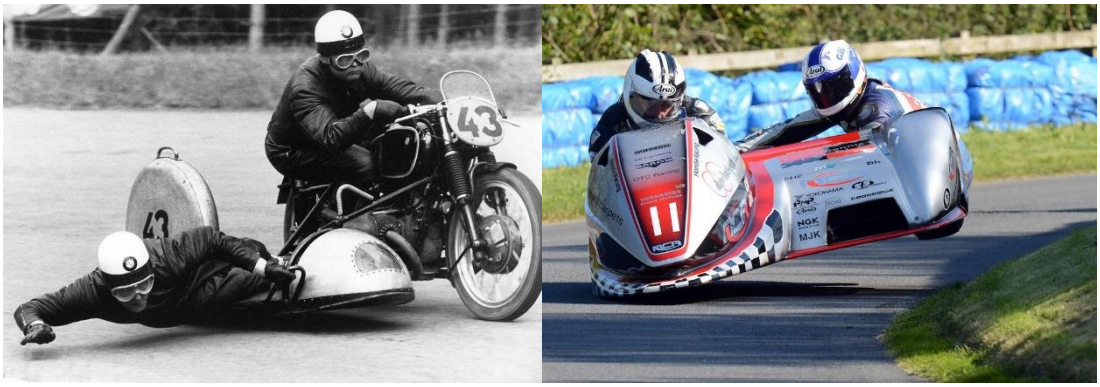

Figure 1-5 first and modern race sidecars

Sidecar racing events exist in Motocross (see Sidecarcross), Enduro, Grasstrack, Trial, road racing and Speedway with sidecar classes. The sport has followers in Europe, the United States, Japan, Australia and New Zealand. The sidecars are often classed by age or engine size, with historic sidecar racing often being more popular than its modern counterpart.

Older classes in road racing generally resemble solo motorcycles with a platform attached, where modern racing sidecars are low and long and borrow much technology from open wheel race cars. In all types of sidecar racing there is a rider and a passenger who work in unison to make the machine perform, as they would be almost unrideable without the passenger in the correct position.

Road racing sidecars began to change away from normal motorcycle development in the 1950s with them becoming lower and using smaller diameter wheels and they kept the enclosed "dustbin fairing" banned in solo competition in 1957. By the 1970s, they were using wide slick tyres with a square car like profile, the rider kneeled behind the engine instead of sitting on a seat and the motor of choice was generally a 500 cc two stroke. In the late 1970s sidecars began to appear with hub centre steering and later the engines moved to the rear of the rider, to lower the centre of gravity further still, making the sidecar very long. Sidecars raced in the world championship known as Superside are all hub centre long monocoque framed machines, the most common being LCR, ART or Windle, with 1000 cc four-cylinder four-stroke engines, the most popular being the Suzuki GSX-R1000.

These at club and national level are known as Formula One sidecars, as opposed to Formula Two. Formula Two sidecars are short front engined bikes, which must have a frame made of steel tube and have leading link forks as monocoques and hub centre steering is banned. Engines are 350 cc two strokes or 600 cc four strokes. F2 sidecars are raced in their own championship but are often on track at the same time as the F1s, but competing for their own points. Since 1990 at the Isle of Man TT, the Sidecar TT has been solely contested by Formula Two sidecars as Formula Ones were deemed too fast, then lapping at 108 mph (174 km/h) average. By 2006 however, F2s were faster than this lapping at 116 mph (187 km/h).

2018 record was set on a 18 mins 59 sec 018/1000 by the Birchalls, at a 119,250 mph average speed. The solo machine driven by Peter Hickman lapped at 134,403 mph: it’s easy to figure out how close is the sidecar performance ...

2 Sidecar Modelling

2.1 Hypothesis of the simplified model

Before we can start with the modelling of the system is necessary to impose some hypothesis in order to reduce the number of equations and the complexity of the equations of motion of the vehicle, aiming to obtain a set of linear equations that are the easiest to manage and at the same time can explain the behaviour of ta real sidecar vehicle.

Since we are analysing a vehicle with a singular geometry and we want to avoid the use of a three-dimensional approach to the problem we can formulate the following hypothesis considering the vehicle half a way between a two-wheeled vehicle, like a motorcycle, and a four wheeled one like a car:

_ the vertical motion of the vehicle is neglected

_ we don't consider pitch and roll motions

_ we neglect the aerodynamic forces

_ we neglect the rolling resistance motion at the wheels

_ we neglect the gyroscopic effect at the wheels

_ the elasto-kinematic effect of the suspensions is not considered

_ we neglect the self-aligning torque at the pneumatic tyre

_ we consider the system as made only by rigid bodies

_ we neglect the longitudinal slippage at pneumatic tyres

_ each manoeuvre is made imposing the steering angle at the front wheel

_ we consider the combined friction in the pneumatic tyres

_ Load transfer is considered

_ Driver and passengers are modelled as material points

We want now to describe in a more detailed way the reasons that leaded us to formulate the below listed hypothesis. Since we want to analyse the lateral dynamics of the vehicle in a simplified formulation the vertical motion gives us an additional degree of freedom and thus we are not interested, in this phase, in the comfort analysis; the vertical motion involves even the pitch and roll motions that will add other two degrees of freedom and equations to the set of equations of motion that can be neglected due to the small values assumed by pitch and roll during the lateral motion of the vehicle. For what concern the resistant forces, we can consider that the manoeuvres are performed at low speed so in general their quantity is quite low, but we have a better explanation in the dedicate paragraph; the gyroscopic effect becomes low because it is function of the rotational speed of the wheel, and so the rolling resistance at the pneumatic tyre adding the small value of the force arm. The other reasons are our aim to simplify as much as possible the system of equations; for the aerodynamic forces we can neglect them following the reasons explained for the other resistant forces even if their implementation inside the model gives a lower complexity due to the relative simple formulation. The elasto-kinematic of the suspensions is given by the elements connecting the suspension elements to each other or the frame like bushing; in motorcycles those elements are quite absent and in our vehicle we have only one suspension system, in addition the ealsto-

kinematics doesn't change too much the results but in the other hand increases the number of degree of freedom and equations. Since the self-aligning torque is the given by the shifting of the lateral force towards the direction of motion, the relative arm falls inside the contact pact and is about few milimeters it can be neglected considering that all the other forces acting on the vehicle has higher values. The elements of the system are considered rigid in order to limit the number of degree of freedom and equations of the system leading a more simple one as our aim is because considering the bodies and the joints connecting them deformable leads to exponential increase of the degree of freedom as we have to consider the strains of the bodies and the relative displacements between them, given by the joints, during the vehicle motion. The longitudinal slippages can be neglected as we are not interested in the longitudinal dynamics of the vehicle and considering a simpler modelling of the longitudinal forces inside the combined friction, as we will see in the relative paragraph with the aim of simplifying as much as possible the set of equation. The load transfer is implemented considering the suspension system as rigid, a consideration not far from the real case since the vehicle has only the front suspension; due to the presence of the third wheel the load transfer takes into account both lateral and longitudinal accelerations considering the variation of vertical load inside the cornering force modelling. Driver and passengers as said are considered material points located on the seats, we will see the reasons in the dedicated paragraph. The steering angle is given as input parameter since we are not using a driver model because it needs to define a quickness and visual length of the driver to follow a trajectory leading to complexity of the model.

Le sopra elencate ipotesi sono state formulate alla luce del problema da analizzare, quindi la dinamica laterale del sidecar, ma anche in funzione del veicolo su cui andrà effettuata la validazione di tale modello; volendo garantire una maggiore generalità del modello alcune ipotesi, come l'assenza di sistemi di sospensione, potranno portare a modifiche delle ipotesi e ad aggiunte in termini di equazioni o gradi di libertà nelle equazioni di moto del sistema, in ogni caso le ipotesi di maggior peso per il modello quali l'utilizzo di un modello bidimensionale e l'assenza di forze aerodinamiche, resistenza al rotolamento ed effetti giroscopici rimarranno valide.

2.1.1 Aerodynamic Forces

A body that moves in a fluid is subjected to resistant force given by the interaction between its surface and the fluid, in the case of a vehicle between the vehicle and the air around it. Those interactions called aerodynamic forces are made of three components with the following formulations

$$\begin{aligned} F_d &= \frac{1}{2}\rho_a V^2 S C_d \\ F_l &= \frac{1}{2}\rho_a V^2 S C_l \\ M_{aer} &= \frac{1}{2}\rho_a V^2 S b C_m \end{aligned} \qquad [2.1]$$

Where we can see the dependence from the air density, the cross section of the vehicle and the relative speed between vehicle and air, since we don't consider the wind effect the speed is the vehicle one, and another dimensionless coefficient. The three coefficients are given from experimental test on the vehicle in a wind tunnel and are function of the dimensions and shape of the vehicle.

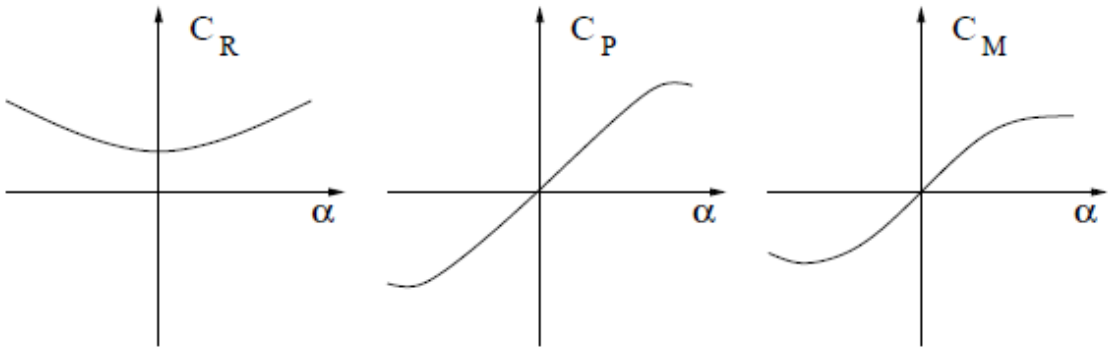

Figure 2-1 drag, lift and aerodynamic moment coefficients

We report above a typical trend of the three coefficients for a wing profile.

In case of a vehicle, and in particular for the longitudinal dynamics, we are interested in the drag force that represents one of the resistant forces to the system motion. If we want to introduce this resistance inside the model we need to split the drag force in two components as the vehicle speed during the manoeuvre has a longitudinal and lateral component

$$F_{dx} = \frac{1}{2}\rho_a V_x^2 S_x C_{dx}$$
$$F_{dy} = \frac{1}{2}\rho_a V_y^2 S_y C_{dy} \qquad [2.2]$$

As we can see from the above formulations we need to know the drag coefficients in longitudinal and lateral direction and also the relative cross section area of the vehicle. Since we perform the simulations and the test with low speed resulting in a small value of this component with respect to other forces like cornering or inertial once, and due to the complexity of calculating the coefficients to perform the aerodynamic forces, we can think in this first stage of the project to neglect this resistant component.

2.1.2 Rolling Resistance

One of the resistance components acting on vehicle is the rolling resistance, usually considered in the study of the longitudinal dynamics is made of two terms. The loss of energy in tire deformation also results in a non-symmetric distribution of the normal tire load over the contact patch. When the tire is static, then the distribution of normal load in the contact patch is symmetric with respect to the centre of the contact patch. However, when the tires are rotating the normal load distribution is non-symmetric producing a shifting of the resultant force towards the motion direction

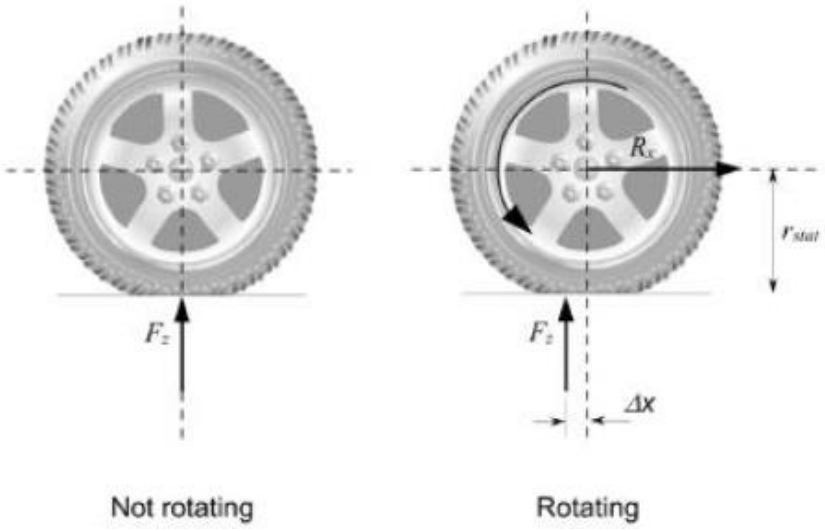

Figure 2-2 shift of the vertical load for a wheel

The contact patch is generated by the action of the normal load on the wheel and the difference of stiffness between tire and road, since the tire is less stiff than the road is subjected to higher deformations responsible also to the reduction of the rolling radius that can be calculated as

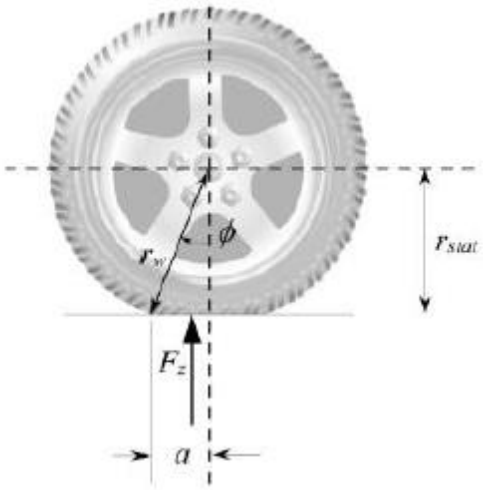

$$r_{stat} = r_w - \frac{F_z}{k_{wr}}$$

$$r_{stat} < r_{eff} < r_w$$

Figure 2-3 effictive wheel radius

As we can see from the figure above the generated arm is so small that remains inside the contact patch and so the resulting moment can be neglected with respect to the other forces acting on the vehicle, even if it is not too complex to introduce in the model since its coefficient vary between 0.01 and 0.04. we start the modelling of the vehicle without the rolling resistance then in a second time we added it in the simplest formulation proposed by Paceijcka (BOH) proposed as the product between a coefficient f_v, the vertical load acting on the single tyre F_z and the effective radius of the wheel

$$R_{rol} = f_v F_z r_{stat} \qquad [2.3]$$

Since we noticed that the real vehicle disseats more energy than the modelled one without rolling resistance.

2.1.3 Pilot and passengers modelling

Starting from the considerations done in the previous paragraphs we see the pilot and passengers on board the vehicle as concentrated masses placed in the three seats of the sidecar, but now we want to motivate more in detail our choice.

Starting from the model of a car we can see that the occupants of the vehicle they are seen as punctual masses because of the large dimensions of the vehicle and because the location of the occupants doesn't affect too much the position of the centre of gravity of the vehicle and this is due to the larger mass and dimension of the vehicle with respect to the passenger body. On the other hand we have smaller vehicles like motorcycles where the mass of pilot and passenger is a big part of the mass of the entire vehicle and so the location of the occupants and even their position on board can change the position of the centre of gravity of the motorcycle.

The vehicle we are analysing, as we said before, can be seen half a way between a car and a motorcycle, but for what concern the mass distribution is more similar to a motorcycle because of the compact dimensions of the vehicle; this leads to the fact that changing the location of the vehicle's occupants and even their number we change the position of the centre of gravity of the vehicle and the vertical load on each wheel.

The human body has its own distribution of masses most of it concentrated in the head and the torso, but in our modelling we can see it as a concentrated mass because the sitting position is with torso and head placed over the vehicle seats, in this case the major amount of the weight of the occupants falls on the seat due to the position assumed on the vehicle with the only except of the legs, and considering that the pilot and the passengers follows the move of the sidecar during the motion; this is true if we analyse road vehicle, because for race applications the positions on board of the pilot and passenger changes and even the assumption that they doesn't move during the motion of the vehicle is not valid as the driver is leaned forward the front of the vehicle and the passenger changes his position depending on the turn direction.

2.2 System mass geometry

With the above hypothesis and before we start write the equations of motion of the vehicle we have to take a look at the geometry of the system we are studying in order to simplify it any more if possible. At first we notice that once the motorcycle is connected to the sidecar we have no symmetry along both longitudinal and lateral directions; this is caused by the forward shifting of the side wheel with respect to the rear one and the alignment of the front and rear wheel on a side of the vehicle. In this case we can't collapse the rear and side wheel in a unique wheel as we usually do for the Single Track Model of four wheeled vehicles.

In addition the steering system is placed only on a side of the vehicle, since it is the one of the motorcycle, that doesn't have any kinematics and reduction ratios. Otherwise than a car here the angle given to the handlebar is the same to the one saw at the front wheel. With those considerations the final model is made of two aligned wheel rigidly connected, where the front one is able to rotate, and a side wheel shifted forward the rear one.

Looking at the mass geometry of the system we can see that the centre of masses of the unladen vehicle is not at a half of the gauge but shifted towards the motorcycle because the engine is located on the motorcycle on a side of the vehicle and, as said in the previous paragraph, it is also influenced by the location and number of occupants

Considering the particular influences on the position of the centre of gravity we have to define some configuration of masses before the start the model in order to set the centre of gravity of the vehicle:

. Only the Driver

. Partial Load

. Full Load

Since the unladen vehicle is meaningless the first configuration has only the vehicle and the Driver located on the corresponding seat located on the motorcycle, this leads to a shifting of the centre of gravity towards the motorcycle and so to handling issues, as we will see in the next paragraphs, depending on the manoeuvres performed.

The Partial Load configuration prescribe the presence of the driver and a passenger, where the driver is located as in the previous configuration while the passenger is located inside the sidecar, on the longitudinal middle plane of the sidecar frame and forward the side wheel. In this case we can see a better mass distribution with the centre of gravity nearer the longitudinal middle plane of the vehicle.

The Full Load prescribe the presence of the driver and two passengers, while the first one is located as in the previous configuration the second one is seat in correspondence to the passenger seat of the motorcycle leading to a shifting of the centre of gravity towards the motorcycle and the rear of the vehicle

Nella prima l'unica massa concentrata presente sarà il pilota posizionato in corrispondenza della sella in corrispondenza della moto; nella seconda configurazione avremo la presenza del pilota situato sempre sulla sella anteriore della moto e di un passeggero posto sul sedile del carrozzino, si è optato per tale disposizione degli occupanti poiché ritenuta la più probabile con un veicolo del genere; in ultimo si è scelta una configurazione con l'aggiunta di un ulteriore passeggero posizionato sulla sella posteriore della motocicletta. Sulla base della configurazione scelta dall'utente è stata creata un'opportuna sotto funzione che definisce la posizione del baricentro, la massa totale del veicolo, il suo momento d'inerzia lungo l'asse z e la distribuzione delle forze verticali sulle tre ruote, prendendo come punto di riferimento delle distanze il perno ruota posteriore della motocicletta.

In each configuration we set the centre of gravity of each body of the vehicle and its position with respect to the rear wheel of the motorcycle; all data are given by a 3D cad software with which the vehicle is designed and then we define the mass and position of the driver and passengers. The mass of the vehicle is obtained summing up the mass of each body

While the position of the centre of gravity is calculated using the Mass Geometry Theory

$$M = \sum_{i=1}^{N} m_i \qquad [2.4a]$$

$$x_G = \frac{1}{M}\sum_{i=1}^{N} x_i m_i \qquad [2.4b]$$

$$y_G = \frac{1}{M}\sum_{i=1}^{N} y_i m_i \qquad [2.4c]$$

And with them the Inertia moment along the z axis using the Theory of Huygens-Steiner

$$J_{zG} = J_{zb} + J_{zs} - \sum_{i=1}^{n} m_i d_i^2 \qquad [2.5]$$

Where the inertia moment of the motorcycle and the sidecar are referred to the rear wheel centre like the distances d.

Now that we know all the geometrical and inertial properties of the vehicle we can calculate the vertical forces acting on each wheel in static position by a vertical equilibrium of forces

$$F_{zf} + F_{zr} + F_{zs} - Mg = 0 \qquad [2.6]$$

An equilibrium to the rotation on the longitudinal plane with respect to the rear wheel contact point

$$F_{zf}p + F_{zs}b_s - Mgb = 0 \qquad [2.7]$$

An equilibrium to the rotation on the lateral plane with respect to the rear wheel contact point

$$F_{zs}s - Mgw = 0 \qquad [2.8]$$

At the end of the routine we have the following output defining the geometry of the vehicle that we can see in Appendix A figures 1 2 3 noticing the shifting of the centre of gravity, going to the first to the last configuration, towards the rear side of the vehicle leading to an oversteering behaviour of the vehicle and to issues of side wheel detaching, in the first one, performing clockwise turns.

2.3 Traction and Braking Systems

Since we are considering a combined friction model, in other words we have the simultaneous presence of a lateral and longitudinal force in the contact patch between tyre and ground is interesting to know more about the traction and braking systems equipped on sidecars and how can be modelled in an easy way.

2.3.1 Hypothesis and model of the engine

For what concern the traction system, the vehicle is moved by an internal combustion engine of low-medium size for vehicle traction, in particular a motorcycle, made by Hartford, a Taiwanese builder.

Figure 2-4 Zongshen 230 cc engine

We dealing with a single cylinder 230 cc displacement internal combustion engine, it has two valves in the cylinder head moved by a cam shaft; the engine is cooled by air cooling system and fed by a carburetor injection system and an air filter able to purify the air from impurities and at the same time reduce the gas dynamic noise of the aspiration system. In the outlet of the engine we have a three ways catalytic converter able to reduce the pollutant emissions as prescribed by the EURO 3 regulation. From this engine we take the torque curves at maximum and minimum admission, corresponding to maximum and minimum opening of the throttle valve

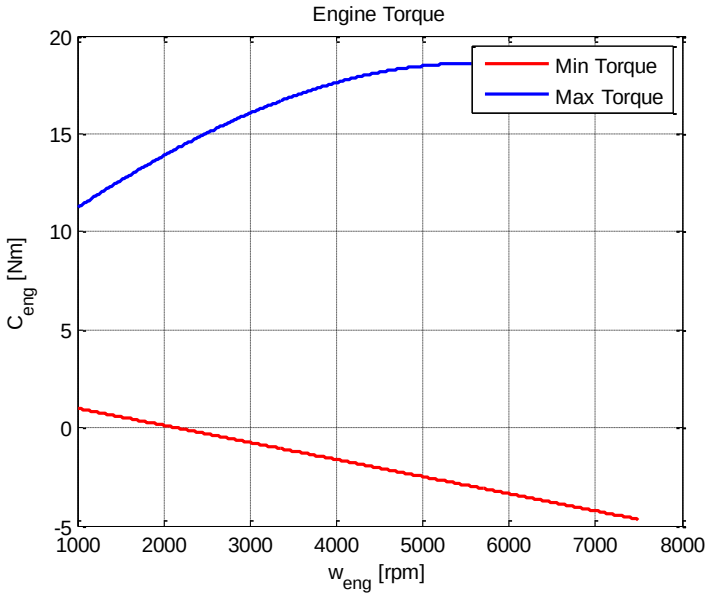

Figure 2-5 Miximum and minimum admission curves

Both curves are necessary to determine the engine torque at any admission level by a linear interpolating formula

$$C_m = \gamma_e C_{max} + (1 - \gamma_e) C_{min} \quad [2.8]$$

As the engine is used for vehicle traction in series to the engine we have a five gears gearbox with a final chain transmission. The engine is coupled to the gearbox by a wet multidisc clutch that helps the driver to engage each gear and start the vehicle motion.

$$\omega_w = \frac{\omega_m}{\tau_{gb}\tau_f}$$

$$C_w = \eta_{gb}\eta_f \frac{C_m}{\tau_{gb}\tau_f}$$

All data about the gearbox and the final transmission in terms of gear ratios are listed in the vehicle data sheet in Attachment B.

For the calculation of the torque given to the driving wheel we follow two similar ways that uses the same interpolation formula to compute the engine torque but changing the input parameters to the model. The first one takes as input the engine curves the admission level the speed rotation of the driving wheel and the gear used for the manoeuvre; the wheel rotation is used to get the rotation speed of the crankshaft passing through the transmission and the admission is used to calculate the engine operative curve. With the input data and a linear interpolation we reach the operative point of the engine in terms of torque, then getting again through the transmission we finally have the torque at the driving wheel.

The other approach follows the same procedure for the calculation of the driving wheel torque, but taking as input instead the admission rate the vehicle speed; we use it in a proportional-integral close loop cycle where the difference between the two speeds are multiplied by the two gains properly set up defining in that way the new engine admission rate

$$\gamma_e = k_i errI + k_p err \quad [2.10a]$$

$$err = V - V_0 \quad [2.10b]$$

$$errI = errI + err \quad [2.10c]$$

At the end of the calculation process we check that the operative point is inside of the operative range of the engine otherwise we provide an increase or decrease of the gear doing again the calculation of the torque.

Since we are using a motorcycles vehicle the torque is given only to the rear wheel of the vehicle even if in modern types of sidecar the engine torque is driven to both rear and side wheel. On the other hand, as we will see later the braking torque is provided to all wheels by braking system.

2.3.2 Hypothesis and model of the braking system

As we said we are looking both at the acceleration and the braking phases, where the last is important if we want to stop the vehicle in quick and safety way. A brake is a mechanical pneumatic hydraulic or electric system actioned by driver and able to provide to the wheels a torque in and opposite direction to its rotation and most cases the energy dissipated by the brakes is transformed in heat that must be taken out of the braking zone.

The most diffuse braking system is the hydraulic one that is made of a pump one or more calipers pads and braking disks.

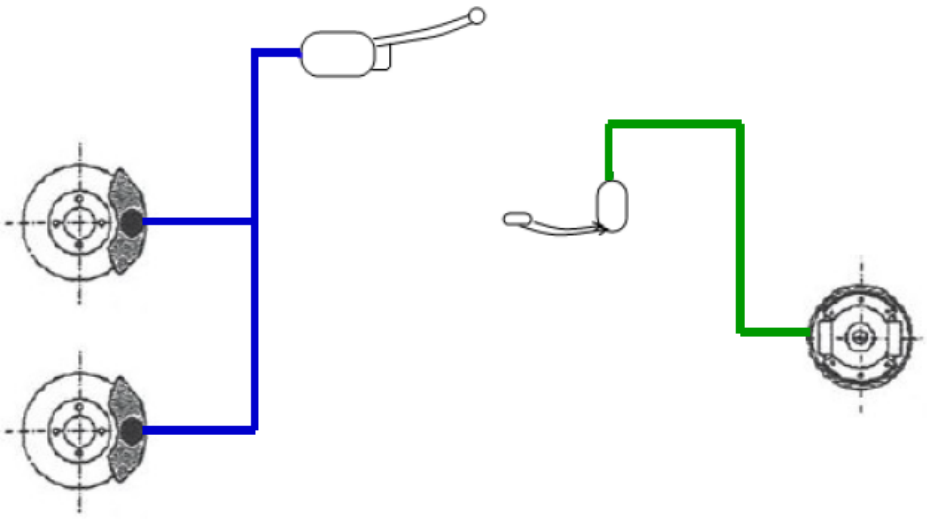

Figure 2-6 Braking system diagram

The driver, pushing a lever or a pedal, moves the piston of a pump that increases the pressure inside the ducts and then the increase of pressure moves the pads inside the caliper towards the braking disk; the disk is rigidly connected to the wheel and the increase of friction between the pads and the disk slows down the rotational speed of the wheel, generating heat that is blow off to from the pads and calipier by the air flow that surrounds the wheel and the disk itself by convection. This particular system is powerful and can guarantee high braking torques with little motion of the lever because of the reaching of high pressures due to the incompressibility of the oil and the section and the number of the pistons moving the pads.

Figure 2-7 Braking system components

The other kind of braking system is an ancient type actioned by a mechanical system that uses instead of a caliper a drum while the other components are wires, or rods, that connect the drum to the lever or pedal and the pads that even in this case are the friction elements that are responsible to the energy dissipation.

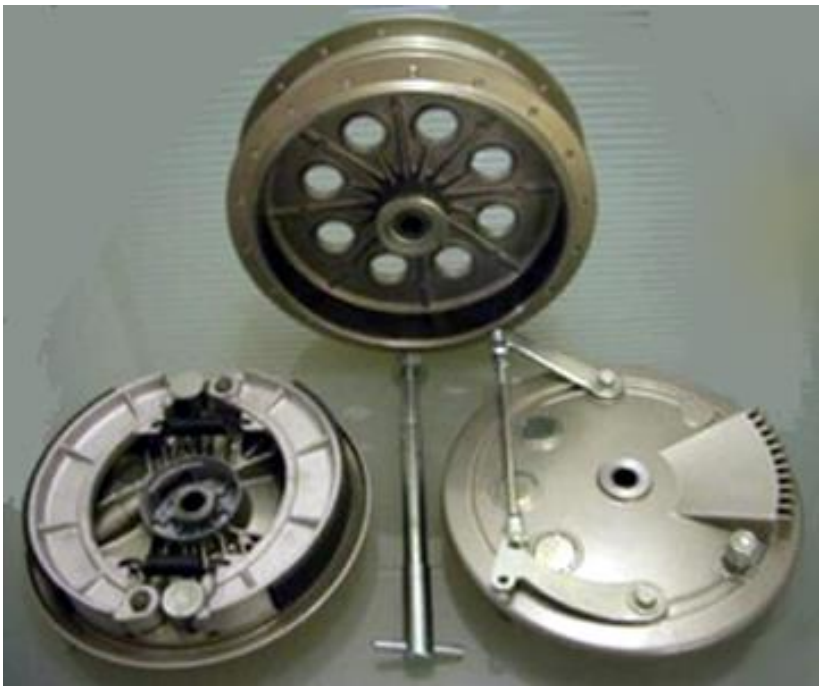

Figure 2-8 Drum brakes

The drum can be seen as circular plate where are fixed the springs and the mechanism that moves the pads against the hub of the wheel, in fact most of this kind of braking systems are placed in the hub of the wheel that makes difficult to dissipate the heat generated during that braking phase. To brake the wheel the driver pushes the lever actioning the wires or rod and so the mechanisms inside the drum that generates a rotation of the pads, fixed at an end to a hinge, that gets in contact with the inner part of the wheel hub.

Now that we have an idea on how a braking system works we focus on the modelling of the braking system used on a sidecar, and on our vehicle; the main issue looking at the geometry of the sidecar is that we have a system half a way between a motorcycle and a car since the presence of three wheels but with the rear and the side one not aligned on the same axle like in a car and with two different lines like a motorcycle so the first problem is to guarantee the simultaneous braking at all wheels and the yaw rotation during braking caused by presence of the side wheel.

The vehicle that we are studying is equipped with a drum type braking system where the front drum is actuated by a lever placed on the handlebar and the rear and side drums are actuated simultaneously by a pedal placed on the right footplate of the motorbike.

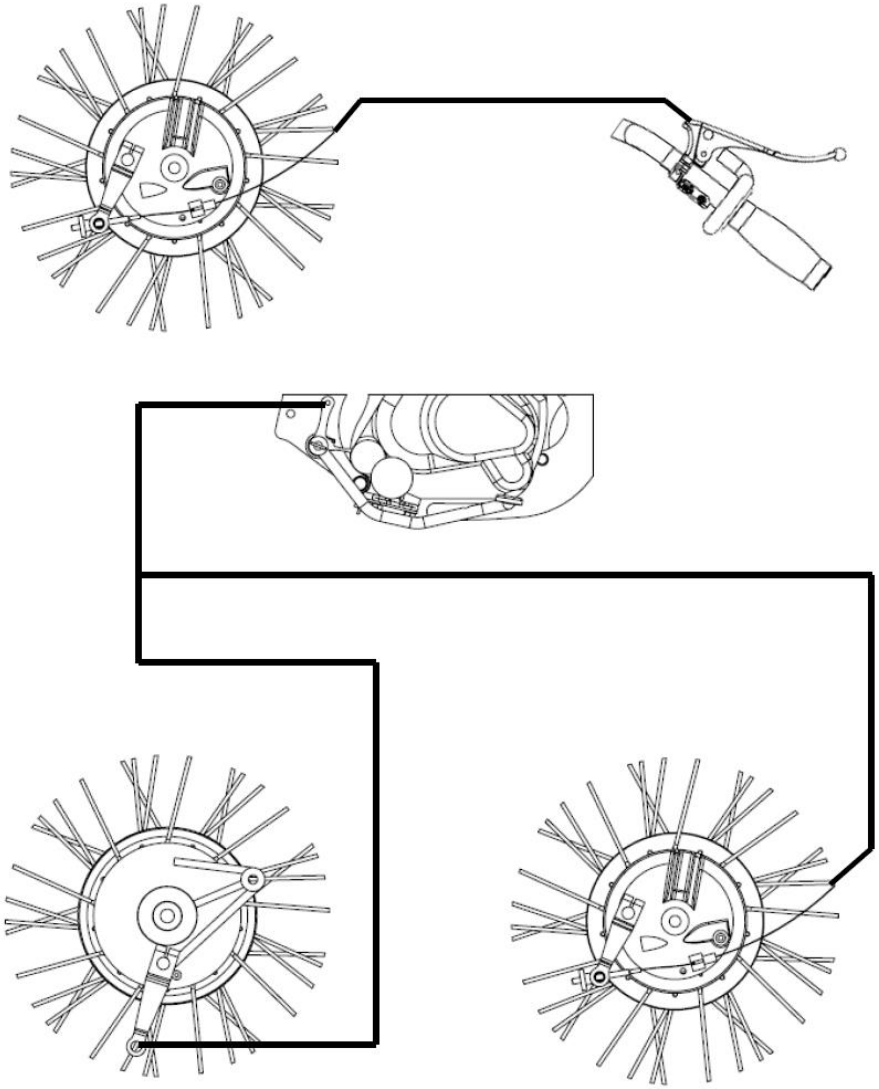

Figure 2-9 Sidecar Sterling MK V braking scheme

Where we can see that to actuate the front and side brakes there's a wire connecting the lever or pedal to the drum while for the rear one the connection is made by a rod, this is because the rear brake is in line with the pedal otherwise the other needs several rods connected by hinges that makes the system more expensive and complex than a wire. In the above figure we can see the coupling system used to actuate at the same time the rear and side drum made with a plate welded on the hinge of the pedal; this simple solution guarantee reliability to the braking system and an easy disassemble when we want to remove the sidecar from the motorbike.

The modelling of this kind of system is quite simple once we know the geometry and the friction coefficient between pad and hub, we need to make some equilibrium at the rotation on some components of the system taking as input the force loading the lever/pedal; let's start analysing the front braking line

$$F_l * l_5 = T_f * l_6 \qquad [2.11]$$

Then we study the force flow at the rear and side drum that follow the same procedure

$$F_p * l_3 = T_r * l_2 \quad [2.12]$$

$$F_p * l_3 = T_s * l_7 \quad [2.13]$$

Since we have the forces getting to the drum we take a look at how the force is transformed into the braking torque at the wheel

$$F_i 2a = T_i l_4 \quad [2.14a]$$

$$N_{ci}(s_t - \mu_t r_t) = F_i h_t \quad [2.14b]$$

$$N_{ti}(s_t + \mu_t r_t) = F_i h_t \quad [2.14c]$$

And then the braking torque can be calculated as

$$M_{brk} = \mu_t (N_{ti} + N_{ci}) \frac{D_t}{2} \quad [2.15]$$

3 Dynamic model of a sidecar vehicle

The hypothesis assumed in the previous chapter are at the basis to the lateral dynamics of the vehicle, that is given by writing a set of equations able to study its behaviour on a curved path. We are going to use simple model of the vehicle placed on a plane consisting of three solid wheels connected by lines that represents the frame of the vehicle; only the front wheel is able to rotate around the z axis to model the steering angle of the motorcycle and placed on the left side of the sidecar. All bodies have no mass that is concentrated in the centre of gravity of the vehicle setted up by the procedure explained in the previous chapter.

Since the set of equations of motion describing the bi-dimensional multi-body system are second order partial derivative and we can't handle them by hand on a paper sheet, so we need to use a software for numerical calculation were the equations are implemented inside a function; this function is then taken numerically integrated with the Runge-Kutta 45 algorithm, ode45c in Matlab.

In this phase of the study all the equations, kinematics and dynamic, and the equations of motion themselves are given in their non-linear formulation because the displacements and the variation of the degrees of freedom is large so we don't have an equilibrium condition to which define a linearization while the model needs a validation process to be sure that represents the behaviour of a real vehicle.

3.1 Selection of the reference system

When we want to study a mechanical system we must select the set of degrees of freedom and a system of coordinates to which define the kinematics and the set of equations of motion. Recalling that our aim is to obtain a simple dynamic model we use two bi-dimensional reference systems one fixed and one moving with respect to vehicle centre of gravity; then the selection of the degrees of freedom leads us to choose between three approaches.

In the first approach the motion of the vehicle is described by a series of rotations about the centre of instantaneous rotation (CIR) which changes its position instant by instant

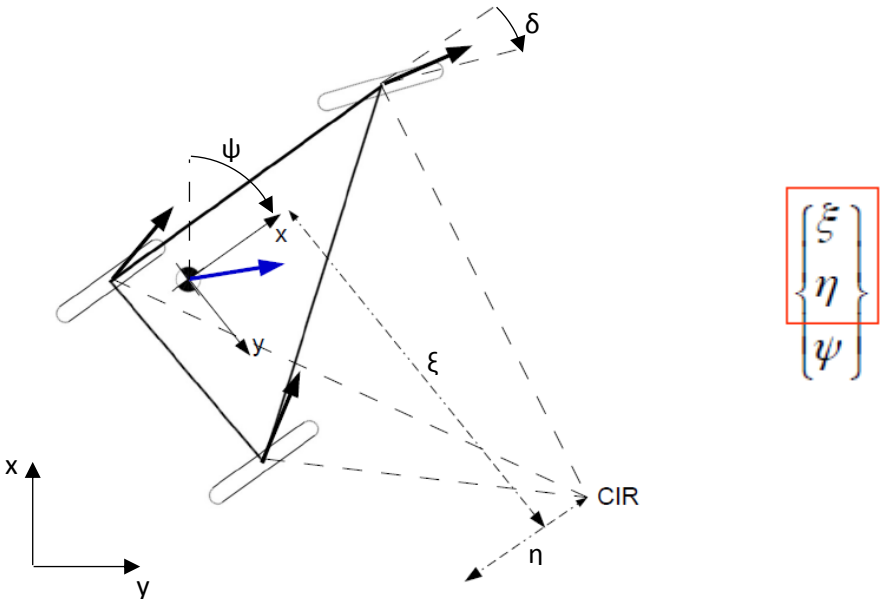

Figure 3-1 Reference system I approach

The second approach uses quantities closely linked to the motion of the vehicle in the local reference system, like the yaw rate and the projection of the vehicle speed along the local reference system

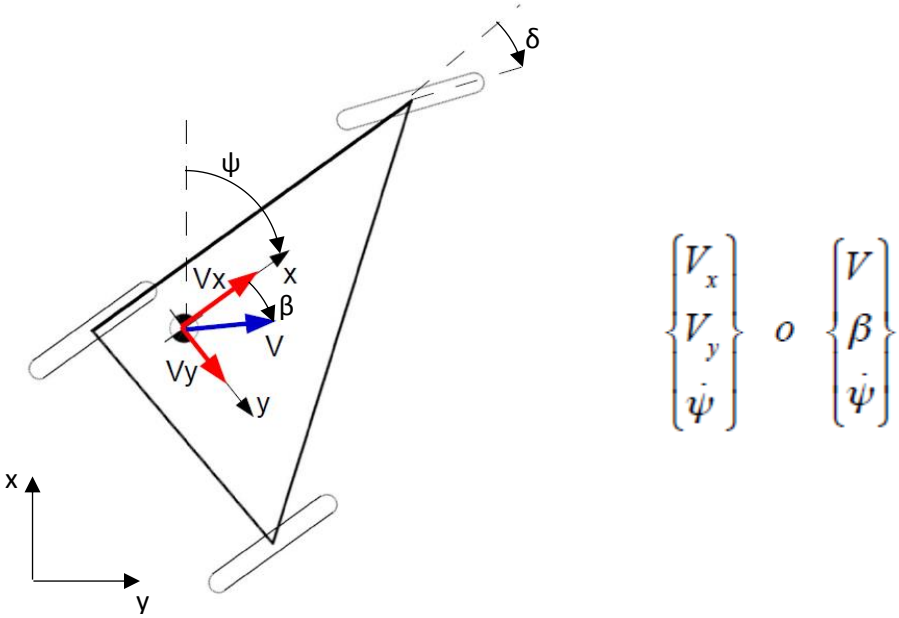

$$\begin{Bmatrix} V_x \\ V_y \\ \dot{\psi} \end{Bmatrix} \quad o \quad \begin{Bmatrix} V \\ \beta \\ \dot{\psi} \end{Bmatrix}$$

Figure 3-2 Reference system II approach

With this approach we can even use instead of the projections of the vehicle speed the side slip angle of the vehicle and its speed

The third and last approach uses as degrees of freedom the coordinates of the centre of gravity, of the vehicle, in the global reference system and the yaw angle.

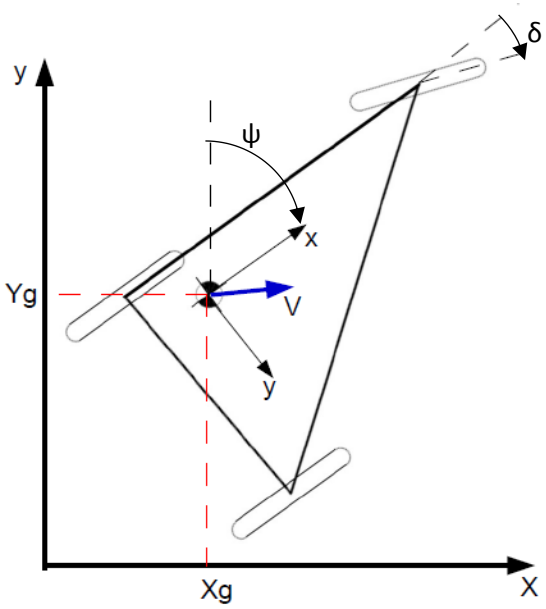

$$\begin{Bmatrix} X_G \\ Y_G \\ \psi \end{Bmatrix}$$

Figure 3-3 Reference system III approach

After this short description we chose the second approach to study the dynamics of our vehicle as it is that is more intuitive and gives in an easy way all outputs we are looking for to study the behaviour of the vehicle.

3.2 Kinematic analysis of a sidecar vehicle

Chosen the reference system and the number of degree of freedom we analyse the kinematics of the vehicle in order to define the links between velocities and acceleration of the bodies defining the vehicle and the degrees of freedom.

3.2.1 Front wheel kinematics

We start form the front wheel that is the more complex due to the presence of the steering angle; to calculate the velocities of the centre of the wheel we write its position with respect to the centre of gravity of the vehicle.

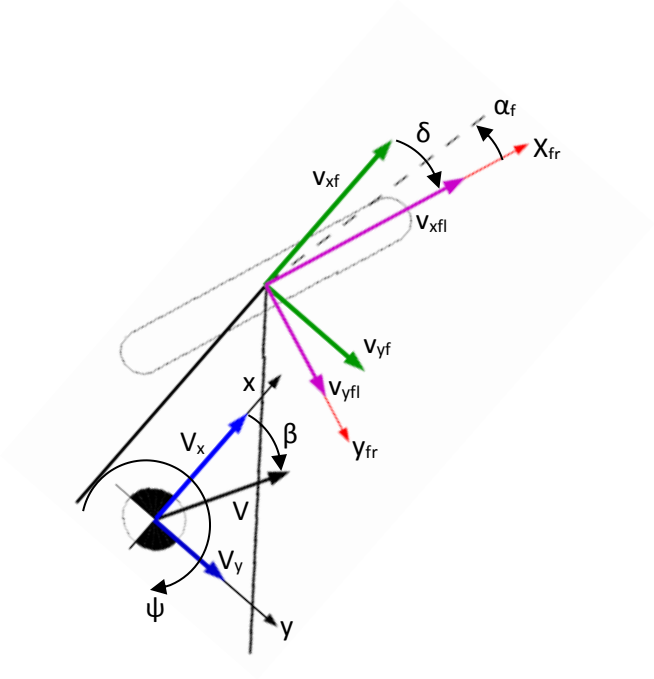

Figure 3-4 Front wheel kinematics

We define a local reference system fixed with the longitudinal axis of the wheel where we project the speed vector, tangent to the trajectory in the front wheel centre; its position is made of two components along the longitudinal and lateral directions, we derive, with respect to time, the projected formulation getting the expressions of local longitudinal and lateral speed with respect to the degrees of freedom

$$V_f = \frac{d(F-G)}{dt} = \overrightarrow{V_G} + \vec{\omega} \wedge (F-G) = V_x\vec{\imath} + V_y\vec{\jmath} + \dot{\psi} \wedge (F-G) \qquad [3.1a]$$

$$(F-G) = a\vec{\imath} - w\vec{\jmath} \qquad [3.1b]$$

$$v_f = V_x\vec{\imath} + V_y\vec{\jmath} + \dot{\psi}\vec{k} \wedge a\vec{\imath} - \dot{\psi}\vec{k} \wedge w\vec{\jmath} \qquad [3.1c]$$

$$\begin{cases} v_{xf}^r = V_x - \dot{\psi}w = (V\cos\beta - \dot{\psi}w)\cos\delta + (V\sin\beta + \dot{\psi}a)\sin\delta \\ v_{yf}^r = V_y + \dot{\psi}a = (V\sin\beta + \dot{\psi}a)\cos\delta - (V\cos\beta - \dot{\psi}w)\sin\delta \end{cases} \qquad [3.1d]$$

The above system of equation is used to define the formulation of the side slip angle for the front wheel with respect to the degrees of freedom

$$\alpha_f = \tan^{-1}\left(\frac{v_{yf}^r}{v_{xf}^r}\right) = \tan^{-1}\left(\frac{\left(V\cos\beta - \dot{\psi}w\right)\cos\delta + \left(V\sin\beta + \dot{\psi}a\right)\sin\delta}{\left(V\cos\beta - \dot{\psi}w\right)\cos\delta + \left(V\sin\beta + \dot{\psi}a\right)\sin\delta}\right) \qquad [3.2]$$

We can easily notice the dependence of the steering angle inside the side slip angle and the degrees of freedom we choose for the modelling, but also the presence of some terms due to the extension of the model in lateral direction, that are not present in the Single Track Model.

3.2.2 Rear wheel kinematics

In a similar way we calculate the speed components at the rear wheel that seems simpler due to the absence of the steering angle. We go on writing the formulation of the position of the wheel centre and with a derivation in time domain we get the two speed components projected on the local reference system fixed to the wheel.

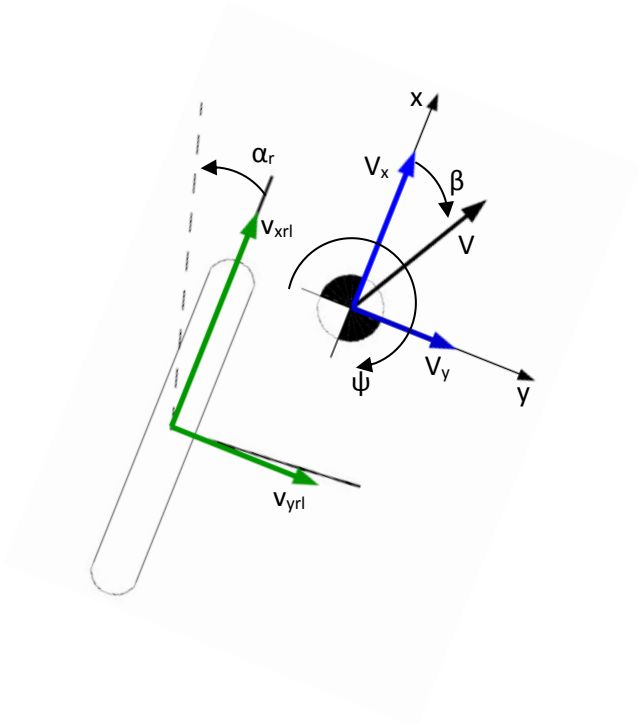

Figure 3-5 Rear wheel kinematics

$$V_r = \frac{d(R-G)}{dt} = \overrightarrow{V_G} + \vec{\omega} \wedge (R-G) = V_x\vec{\imath} + V_y\vec{\jmath} + \dot{\psi} \wedge (R-G) \qquad [3.3a]$$

$$(R-G) = -b\vec{\imath} + w\vec{\jmath} \qquad [3.3b]$$

$$v_r = V_x\vec{\imath} + V_y\vec{\jmath} - \dot{\psi}\vec{k} \wedge b\vec{\imath} + \dot{\psi}\vec{k} \wedge w\vec{\jmath} \quad [3.3c]$$

$$\begin{cases} v_{xr}^r = V_x + \dot{\psi}w = V\cos\beta + \dot{\psi}w \\ v_{yr}^r = V_y - \dot{\psi}b = V\sin\beta - \dot{\psi}b \end{cases} \quad [3.3d]$$

We can then define the side slip angle at the rear wheel as follows

$$\alpha_r = \tan^{-1}\left(\frac{v_{yr}^r}{v_{xr}^r}\right) = \tan^{-1}\left(\frac{V\cos\beta + \dot{\psi}w}{V\sin\beta - \dot{\psi}b}\right) \quad [3.4]$$

In this case we can notice that the local reference system is aligned with the vehicle one cause the wheel can rotate only along its y axis and even in this latter case we have some components caused by the lateral expansion of the vehicle.

3.2.3 Side wheel kinematics

For what concern the side wheel the equation set of the wheel centre speed is similar to the rear wheel even if we can have the presence of a toe angle at this will that remains constant during the motion of the vehicle contrarily to the steer angle at the front wheel

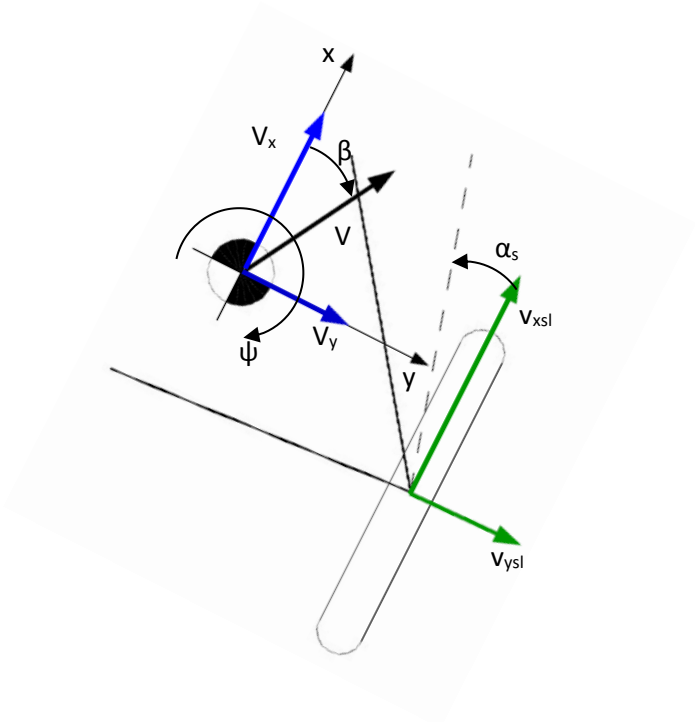

Figure 3-6 Side wheel kinematics

$$V_s = \frac{d(S-G)}{dt} = \overrightarrow{V_G} + \vec{\omega} \wedge (S-G) = V_x\vec{\imath} + V_y\vec{\jmath} + \dot{\psi} \wedge (S-G) \quad [3.5a]$$

$$(S-G) = -(b-b_s)\vec{\imath} + (s-w)\vec{\jmath} \quad [3.5b]$$

$$v_s = V_x\vec{\imath} + V_y\vec{\jmath} - \dot{\psi}\vec{k} \wedge (b-b_s)\vec{\imath} + \dot{\psi}\vec{k} \wedge (s-w)\vec{\jmath} \quad [3.5c]$$

$$\begin{cases} v_{xs}^r = V_x + \dot{\psi}(s-w) = \left[V\cos\beta - \dot{\psi}(s-w)\right]\cos\lambda + \left[V\sin\beta + \dot{\psi}(b-b_s)\right]\sin\lambda \\ v_{ys}^r = V_y - \dot{\psi}(b-b_s) = \left[V\sin\beta + \dot{\psi}(b-b_s)\right]\cos\lambda - \left[V\cos\beta - \dot{\psi}(s-w)\right]\sin\lambda \end{cases} \quad [3.5d]$$

As in the other cases we define the side slip angle at the side wheel

$$\alpha_s = \tan^{-1}\left(\frac{v_{ys}^r}{v_{xs}^r}\right) = \tan^{-1}\left\{\frac{\left[V\sin\beta + \dot{\psi}(b-b_s)\right]\cos\lambda - \left[V\cos\beta - \dot{\psi}(s-w)\right]\sin\lambda}{\left[V\cos\beta - \dot{\psi}(s-w)\right]\cos\lambda + \left[V\sin\beta + \dot{\psi}(b-b_s)\right]\sin\lambda}\right\} \quad [3.6]$$

In the modelling process we introduced this angle: the toe angle, that remains constant during the motion of the system only to get a more realistic model thus this parameter is simple to introduce in the equations and, as said is always constant.

3.3 Pneumatic tyres and contact forces

We want to give a description of the different types of pneumatic tyres equipped on sidecar vehicles along years and their different characteristics and interactions with the road.

3.3.1 Pneumatic tyres

The first Sidecars, as the vehicle we are studying, were equipped with motorcycle tyres of big diameter because they were motorcycles with a cart added on a side, so this kind of pneumatic tyre has a toroidal cross section area that defines an elliptical contact patch and a higher lateral stiffness than tyres used on cars.

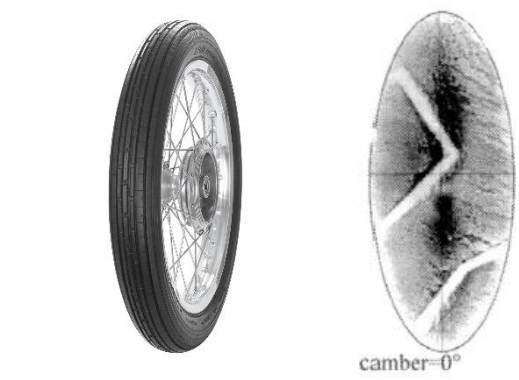

Figure 3-7 Motorcycle pneunmatic tyre

In modern Sidecars vehicles we can see the use of pneumatic tyres typically equipped on cars with a dimeter around 14” inches, that contrarily to motorcycles one has a rectangular cross section area and a rectangular contact patch and a lower lateral stiffness; this choice is due to the fact that sidecars doesn’t need high roll angles to approach curved path but high steering angles.

Figure 3-8 Car pneumatic tyre

The use of car pneumatic tyres need a change in the front and rear suspension and braking systems of the motorcycle because the rim used for the tyre.

3.3.2 Tyre and wheel contact model

During the study of the dynamic of a vehicle it is important to define a model of the interaction between tyre and road able to represent the real behaviour of that interaction describing all forces and torques generated in the contact patch with respect to input given to the tyres like speed, slippages and side slip angle, roll angle if we are considering a motorcycle tyre and the vertical load.

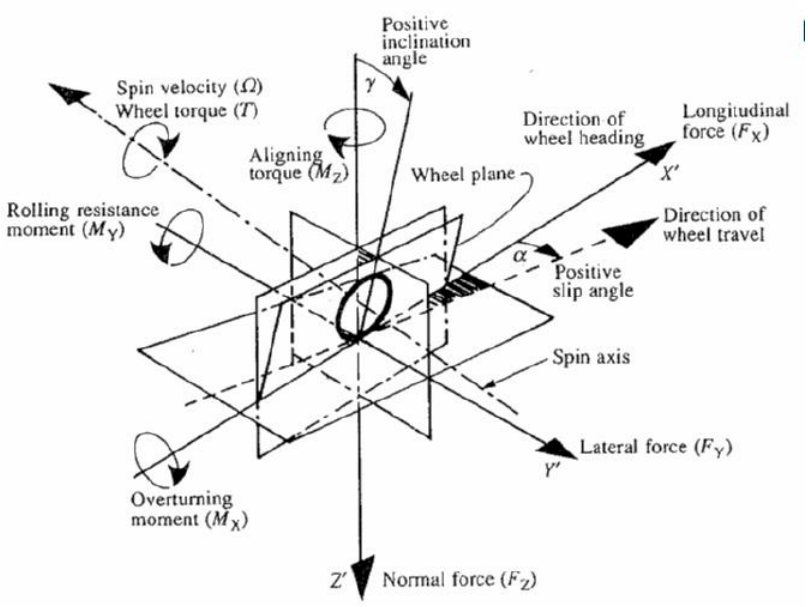

Figure 3-9 force and moments acting on a wheel

Unlike the Culombian friction model, where we have a single contact point between road and tyre, in reality we have a contact area given by the deformation of the tyre in radial direction caused by the vertical load. Inside this contact patch are generated three forces and three torques:

- Vertical load
- Longitudinal force
- Lateral force
- Self-aligning torque
- Roll torque
- Rolling resistance torque

In the following of the vehicle modelling we consider only the three forces acting inside the contact patch because each the arm of each moment falls inside the contact patch and is enough small to get the torque negligible with respect to the.

3.3.2.1 The Magic Formula of Pacejka

To model the behaviour of a tyre we have several kinds of models with different complexity, but for our analysis we choose to use the Magic Formula of Pacejka. It is a semi-empirical model that is able to calculate the steady-state tyre force and moment characteristics to use in vehicle dynamics. The interpolating formula takes as input the vertical force, the side slip angle or longitudinal slip, depending of the kind of force we are looking for, the camber and roll angle generating as output the lateral or longitudinal force acting inside the contact patch.

$$y(x) = D\sin\{Ctan^{-1}[Bx - E(Bx - tan^{-1}Bx)]\} \quad [3.7]$$

The curve produced by the model passes through the origin reaches a maximum then subsequently tends to a horizontal asymptote; to match the curve to the experimental one a vertical and horizontal shifting are added explaining some phenomena like ply-steer in the tyre.

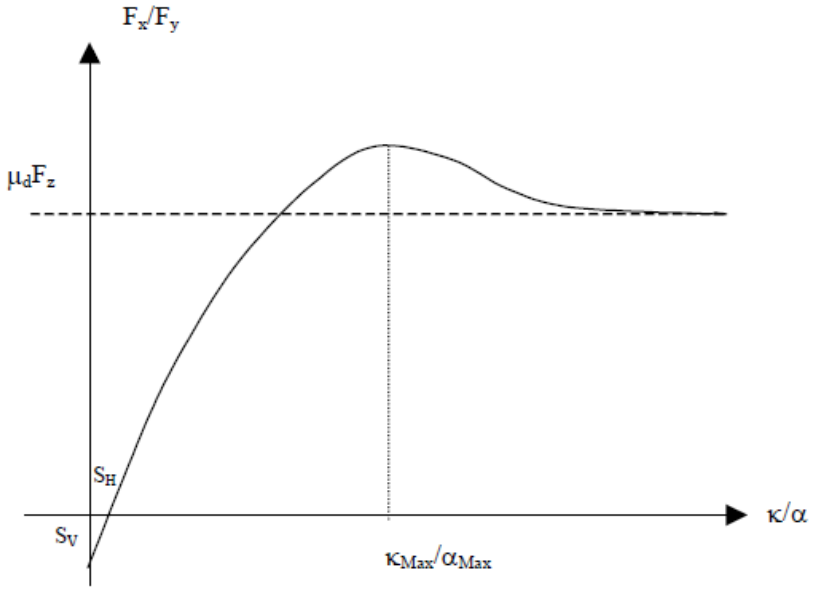

Figure 3-10 Magic Formula output

In our vehicle model we want to calculate only the lateral forces with this Magic Formula as we are most interested in the lateral dynamics of the Sidecar; in particular we approached the problem with two different formulation for the tyre model where the first one uses the macro coefficients inside the interpolating formula while the other one prescribe the use of the micro coefficient to calculate the lateral forces.

With the micro coefficient we have:

$$F_{yi} = D\sin\{C\tan^{-1}[B(\alpha_i + S_h)]\} + S_v \quad [3.8]$$

With the macro coefficients we have:

$$F_{yi} = D_\alpha F_z \begin{bmatrix} \sin\{C_\alpha \tan^{-1}[B_\alpha \alpha - E_\alpha(B_\alpha \alpha - \tan^{-1} B_\alpha \alpha)]\} + \\ \sin\{C_\varphi \tan^{-1}[B_\varphi \varphi - E_\varphi(B_\alpha \varphi - \tan^{-1} B_\alpha \varphi)]\} \end{bmatrix} \quad [3.9]$$

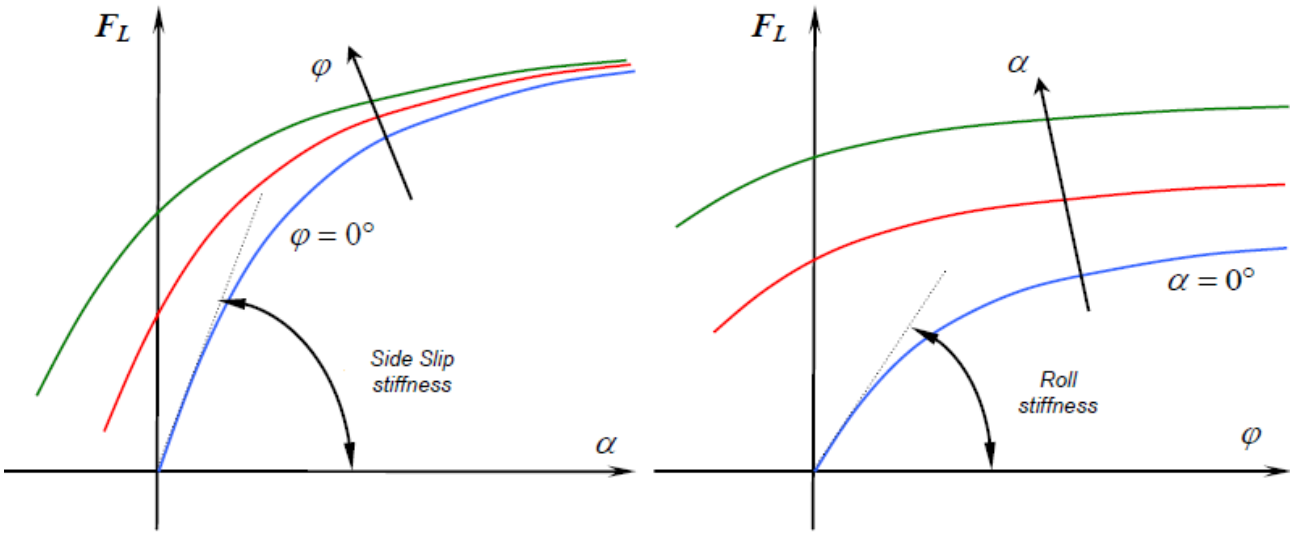

Figure 3-6 relationship between slip angle and roll angle

In the first case the micro coefficients and the links between the inputs we described above is inside the coefficients B C D as shown in the Attachment X, while in the second formulation, proposed by Prof. Cossalter, the links between the input is clear especially; we can notice two similar formulation, the first one depending on the side slip angle and the other depending on the roll motion of the vehicle.

Since the approach is semi-empirical it needs some experimental test to gain the coefficients which are determined on a test pneumatic tyre and a test machine where we can vary all the input data for the Magic Formula and collecting each force record. With all the recorded data from the tests we perform an optimization with the minimum least squares that gives the coefficients we are looking for. The process to obtain the macro coefficients is so long and needs lot of test on a particular test machine while the amount of tests to obtain the micro coefficients is even higher.

3.3.3 Combined friction model

The model shown in the previous paragraph to generate a single contact force considers the only presence of longitudinal or lateral force in the contact patch except the vertical one; but in reality inside the contact patch we have the simultaneously presence of both lateral and longitudinal forces. Since the maximum obtainable force in the contact patch is the vertical one multiplied by the friction coefficient we want to know the dependence between lateral and longitudinal forces; from experimental tests we can define a surface able to define the lateral force as function of longitudinal one and side slip angle

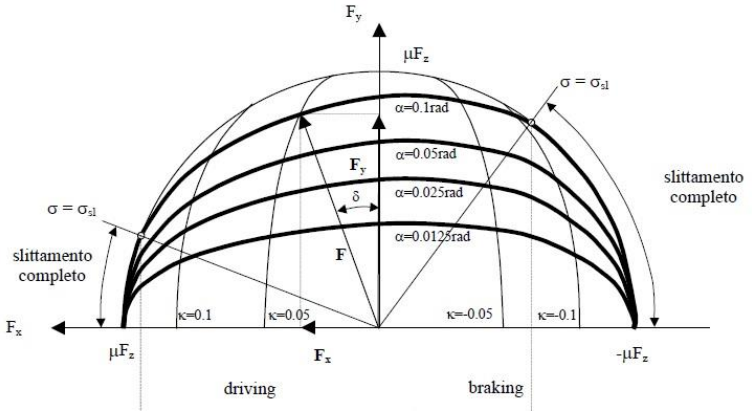

Figure 3-7 Combined friction

As we can notice the elliptical surface is divided in two zones, one corresponding to the traction longitudinal force and the other to the braking force, while we can clearly see that increasing the longitudinal component the lateral one tends to decrease till zero in correspondence to the maximum allowable longitudinal force.

It is now necessary to introduce this link inside the Magic Formula between the lateral and longitudinal forces; if are using the micro-coefficients this link is already present inside the coefficient D

$$D_0 = \frac{d_4 F_z}{(1 + d_7 \gamma^2)} \qquad [3.10a]$$

$$D = \sqrt{D_0^2 - F_x^2} \qquad [3.10b]$$

Otherwise if we want to use the macro-coefficient we can follow the approach used by prof. Cossalter that introduce a corrective coefficient at the beginning of the Magic Formula that is able to reduce the lateral force increasing the longitudinal:

$$F_{yi} = \sqrt{\left(1 - \frac{F_x}{F_{x0}}\right)} D_\alpha F_z \begin{bmatrix} \sin\{C_\alpha \tan^{-1}[B_\alpha \alpha - E_\alpha (B_\alpha \alpha - \tan^{-1} B_\alpha \alpha)]\} \\ + \sin\{C_\varphi \tan^{-1}[B_\varphi \varphi - E_\varphi (B_\alpha \varphi - \tan^{-1} B_\alpha \varphi)]\} \end{bmatrix} \qquad [3.11]$$

Where the term F_{x0} is the maximum allowable longitudinal force inside the contact patch:

$$F_{x0} = \mu_x F_z \qquad [3.12]$$

3.4 Lateral Sidecar Dynamics

Knowing the kinematics of the system we can know proceed to write the non-linear equation of motion for the sidecar; we use non-linear equations since we are studying the motion in large of the system with high variations of the degrees of freedom so, for example the steering angle can't be linearized.

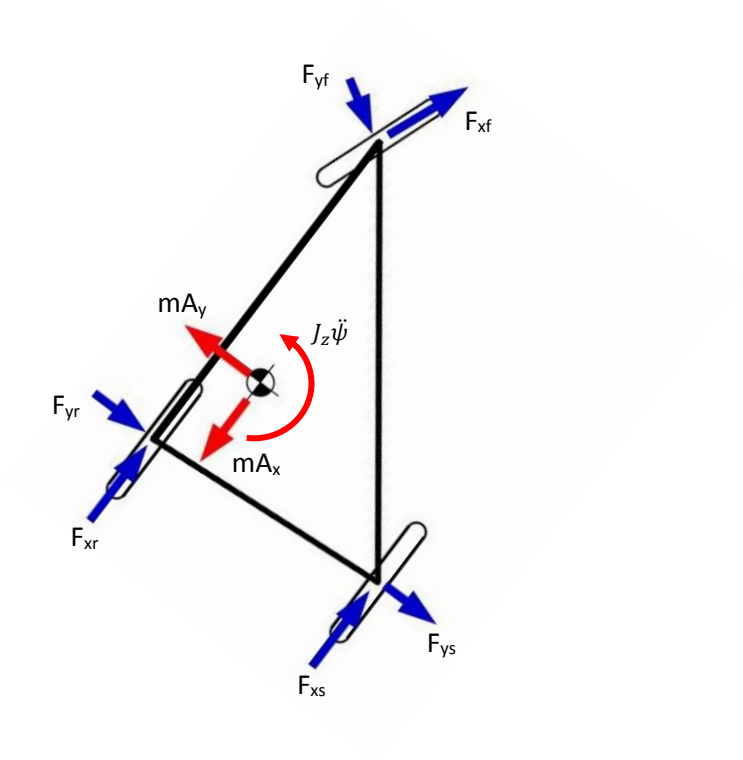

Figure 3-8 Forces acting on the sidecar

With this aim we go on writing three dynamic equilibriums along the three directions of motion: the longitudinal, the lateral and the rotation around the centre of gravity; we consider as reference system a right-handed trail of vectors with positive verse in agreement with the running direction of the vehicle.

$$\begin{cases} -ma_x + F_{xf}\cos\delta - F_{yf}\sin\delta + F_{xs} + F_{xr} = 0 \\ -ma_y + F_{xf}\sin\delta + F_{yf}\cos\delta + F_{ys} + F_{yr} = 0 \\ -J_z\ddot{\psi} + F_{xf}w\cos\delta - F_{yf}w\sin\delta + F_{xf}a\sin\delta + F_{xf}a\cos\delta \\ -F_{xs}(s-w) - F_{ys}(b-b_s) - F_{yr}b + F_{xr}w = 0 \end{cases} \quad [3.13]$$

We know proceed adding the kinematics links inside the equations of motion in order to reveal the chosen degrees of freedom inside the equations.

$$\begin{cases} \dot{v}_x = {}^1/_m\left(F_{xf}\cos\delta - F_{yf}\sin\delta + F_{xs} + F_{xr}\right) + \dot{\psi}v_y \\ \dot{v}_y = {}^1/_m\left(F_{xf}\sin\delta + F_{yf}\cos\delta + F_{ys} + F_{yr}\right) - \dot{\psi}v_x \\ \ddot{\psi} = {}^1/_{J_z}\begin{pmatrix} F_{xf}w\cos\delta - F_{yf}w\sin\delta + F_{xf}a\sin\delta + F_{xf}a\cos\delta \\ -F_{xs}(s-w) - F_{ys}(b-b_s) - F_{yr}b + F_{xr}w \end{pmatrix} \end{cases} \quad [3.14]$$

We can now define two different operating conditions, to simplify at most the motion equations set: one for the acceleration, and one for braking.

In acceleration, the only action is the driving torque applied to the rear wheel of the motorcycle. All the other longitudinal forces are negligible, seen that we have assumed a longitudinal contact simplified according to the Magic Formula.

In braking, the motion equation set is as above presented, with three brakes on the three wheels. Another condition to be considered is the presence of a roll angle between the motorcycle and the sidecar, laying in the longitudinal-lateral plane; this result in a convergency angle to the side wheel, modifying the equation set as follows:

$$\begin{cases} \dot{v}_x = {}^1\!/_m \left(F_{xf}\cos\delta - F_{yf}\sin\delta + F_{xs}\cos\lambda + F_{xr} + F_{ys}\sin\lambda\right) + \dot{\psi}v_y \\ \dot{v}_y = {}^1\!/_m \left(F_{xf}\sin\delta + F_{yf}\cos\delta + F_{ys}\cos\lambda + F_{yr} - F_{xs}\sin\lambda\right) - \dot{\psi}v_x \\ \ddot{\psi} = {}^1\!/_{J_z} \begin{pmatrix} F_{xf}w\cos\delta - F_{yf}w\sin\delta + F_{xf}a\sin\delta + F_{xf}a\cos\delta - \\ +F_{xs}(s-w) - F_{ys}(b-b_s) - F_{yr}b + F_{xr}w \end{pmatrix} \end{cases} \quad [3.15]$$

To perform the simulation of the lateral dynamics of the vehicle we load the data sheet of the sidecar and then, as said in the previous chapters, we select the mass configuration, the type of engine and tyres we want to equip and finally we define the initial guess in terms of maximum steering angle, initial speed and simulation duration

$$\begin{cases} \delta_{max} \\ V_0 \\ t_f \end{cases}$$

We can also define different kind of manoeuvres defining the time history of the steering angle and the turn direction considering as positive steering angle a left turn and negative a right one.

Then the model solves the above system of equation in matrix form using the Runge-Kutta numerical integration method

$$\dot{z} = [A]z \quad [3.16a]$$

$$\dot{z} = \begin{Bmatrix} \dot{v}_x \\ \dot{v}_y \\ \ddot{\psi} \\ v_x \\ v_y \\ \dot{\psi} \end{Bmatrix} \quad z = \begin{Bmatrix} v_x \\ v_y \\ \dot{\psi} \\ x \\ y \\ \psi \end{Bmatrix} \quad [3.16b]$$

In theory if the system is linear the matrix [A] contains the coefficients necessary to solve the linear system but as we are using non-linear equation of motion the matrix is an integrating function that solves the following equations to define the vector z

$$\begin{cases} \alpha_f = \tan^{-1}\left(\frac{v_{yf}^r}{v_{xf}^r}\right) \\ \alpha_r = \tan^{-1}\left(\frac{v_{yr}^r}{v_{xr}^r}\right) \\ \alpha_s = \tan^{-1}\left(\frac{v_{ys}^r}{v_{xs}^r}\right) \end{cases} \quad [3.17a]$$

$$\begin{cases} C_m = C_m(\gamma_m, \omega_m, \tau_g) \\ F_{xr} = \eta_{gb}\eta_{tf}\frac{C_m}{r_w\tau_{tot}} \end{cases} \quad [3.17b]$$

$$\begin{cases} F_{yf} = F_y(\alpha_f) \\ F_{yr} = F_y(\alpha_r) \\ F_{ys} = F_y(\alpha_s) \end{cases} \quad [3.17c]$$

$$\begin{cases} -ma_x + F_{xf}\cos\delta - F_{yf}\sin\delta + F_{xs} + F_{xr} = 0 \\ -ma_y + F_{xf}\sin\delta + F_{yf}\cos\delta + F_{ys} + F_{yr} = 0 \\ -J_z\ddot{\psi} + F_{xf}w\cos\delta - F_{yf}w\sin\delta + F_{xf}a\sin\delta + F_{xf}a\cos\delta \\ -F_{xs}(s-w) - F_{ys}(b-b_s) - F_{yr}b + F_{xr}w = 0 \end{cases} \quad [3.17d]$$

Since the model of the lateral forces depends on the vertical load acting on the wheel we implement inside the integrating function the load transfer routing that calculate for every ten steps the instantaneous vertical load on each wheel.

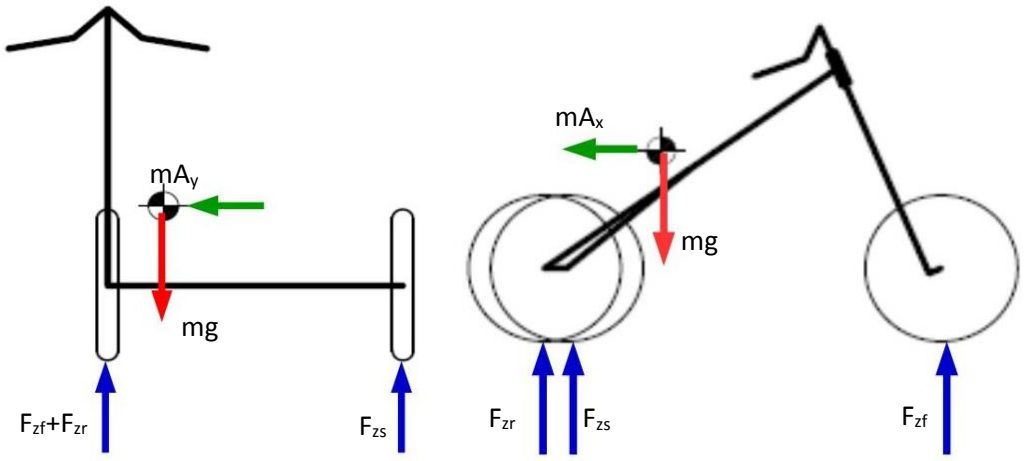

Figure 3-9 Lateral and longitudinal load transfer

In a similar way seen in the previous chapter for the calculation of the static vertical load we perform an equilibrium in vertical direction and two equilibriums at the rotation with respect to the rear wheel contact point, one in the longitudinal plane and the other on the longitudinal one, but in this case we consider the two inertial forces acting on the centre of gravity

$$F_{zf} + F_{zr} + F_{zs} - Mg = 0 \qquad [3.18a]$$

$$F_{zf}p + F_{zs}(b - b_s) - Mgb - MA_x h_G = 0 \qquad [3.18b]$$

$$F_{zs}s - Mgw - MA_y h_G = 0 \qquad [3.18c]$$

The integration of this set of equations gives, as seen, all the quantities we need to compute the trajectory and the speed of the vehicle performing a defined manoeuvre, but to have a complete view of the dynamic behaviour of the vehicle we need more data; to do that we run again the integrating function that takes as input the time vector and the z matrix, that are the output of the integration procedure, obtaining as output a matrix of twenty-one columns and a number of rows equal to the time vector

$$\{\dot{v}_x(t)\ \dot{v}_y(t)\ \ddot{\psi}(t)\ v_x(t)\ v_y(t)\ \dot{\psi}(t)\ F_{ys}(t)\ F_{yr}(t)\ F_{ys}(t)\ \beta(t)\ \delta(t)\ \alpha_f(t)\ \alpha_r(t)\ \alpha_s(t)\ F_{zf}(t)\ F_{zr}(t)\ F_{zs}(t)\ a_y(t)\ C_w(t)\ C_m(t)\ \omega_m(t)\}$$

With this matrix and the output coming from integration we can create the graph in Appendix B showing the behaviour of the vehicle with this model; the shape of the curves changes as function of the manoeuvre and the configuration we select for the vehicle. At this stage the model is theoretically correct, so the forces, velocities and accelerations goes in the right direction as function of the input data but to be sure that the model represents the behaviour of a real vehicle we need to validate it as shown later.

3.4.1 Steering Torque calculation

One of main issues in driving a vehicle is tiredness of the driver that is related to the comfort and to the force that he needs to drive the vehicle; in this section we focus on the force needed to drive the Sidecar because in other vehicle like cars or trucks the solution is adding in the steering line a system, hydraulic or electric, able to reduce the resistant torque at the steering wheel but in motorcycles is not possible to add a similar system in addition our vehicle is half way between a motorcycle and a car.

After this little introduction we start the analysis of the steering torque with the approach used by professor Cossalter in his book “Motorcycles Dynamic” where he calculates the resistant torque at the steer as the summary of the moments at the steering axle, isolating this part of the motorcycle considering the forces and weights loading the front axle of the vehicle in a steady state curve. Since our purpose is to compute the steering torque along not a steady state curve but a general manoeuvre we start from the considerations made by professor Cossalter writing an equilibrium of moments at the steering axle considering the whole vehicle and not only the front section.

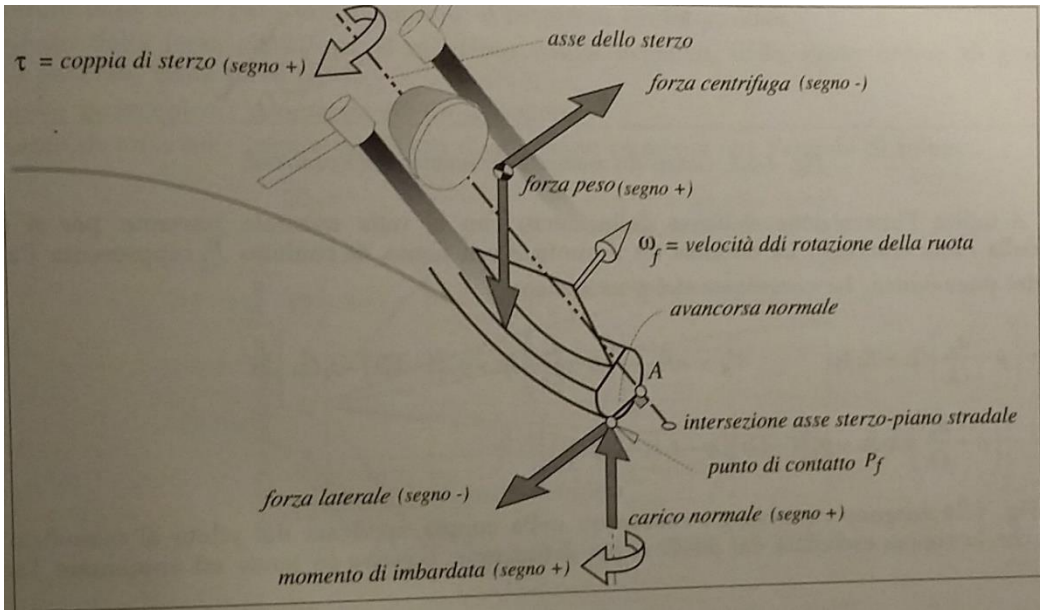

Figure 3-10 Steering Torque calculation proposed by V. Cossalter

As the steering axle is not perpendicular with the ground we must project all forces acting on the vehicle on a plane perpendicular to the steering axle to calculate their arms; the calculation is quite easy since we know all the vehicle geometry and the steering axle doesn't change it's angle during the motion of the vehicle, the only quantities that changes during the motion are the trailer arms of the cornering forces.

As said in the previous chapter the trailer arm is the shifting of the lateral force toward the direction of motion that generates the self-aligning torque of the tyre; taking a look at the numbers we can see that the trailer arms are small with respect to the arms of the forces, so in a first approximation we consider the forces applied in the wheel centre projection on the ground obtaining the following expressions for the forces arms

$$\begin{cases} a_v = r_w \tan\varepsilon \cos\delta - \dfrac{\sqrt{1-(\sin\delta \sin\varepsilon)^2}}{\cos\varepsilon} d \\ b_n = (p - a_v)\cos\varepsilon \\ c_n = [(p - b_s) + a_v]\cos\varepsilon \\ x_{Gn} = (a + a_v)\cos\varepsilon \end{cases} \quad [3.19]$$

And the final formulation of the steering torque

$$M_{steer} = ma_y x_{Gn} + ma_x w - J_z\ddot{\psi} - F_{yr}b_n - F_{ys}c_n - F_{yf}a_v\cos\delta - F_{xs}s - F_{xf}a_v\sin\delta \quad [3.20]$$

4 Experimental tests and model validation

At this stage we have a mathematical model of the vehicle whose output quantities are coherent with the theory, but it needs to be validate by the output of a real vehicle; the validation process tells us if all the modelling assumptions and the models themselves are coherent with a real vehicle and if the model and the vehicle are not coherent we have to re-introduce some neglected hypothesis or change the modelling approach getting from the bi-dimensional to the tri-dimensional one.

This phase of our study needs the built up of a vehicle prototype that must be equipped with sensors, and after a series of tests we can confront the outputs coming from the mathematical model with the once got from the prototype and finally do the necessary corrections on the model.

4.1 Prototype built up

To perform the experimental tests we need a prototype vehicle and since we already have the motorcycle in this paragraph we will see the design of the only frame of the sidecar; we start the design from an already existing prototype presented in the master degree thesis "*Realizzazione del prototipo di un sidecar con l'utilizzo di tecniche di prototipazione virtuale*" of Ing. DavideBassi. This first design of the frame is made with the 3D modelling software SolidWorks 2012 and composed by a rectangular closed path with a central stiffening element, to reduce the lateral deformation, made of hollowed circular cross section that realize the skeleton of the sidecar, then we add some stiffening elements inside the rectangular frame to increase the torsional stiffness and the mass of the sidecar.

Figure 4-11 Sidecar prototype frame

The section of each element of the frame is selected in order to obtain a stiff structure able to endure to the loads coming from the motorcycle and the contact patch, to optimize the mass of the vehicle because a too heavy vehicle will affect the performances of the vehicle while a too light one will get overturning issues in clockwise turn direction affecting the safety of the vehicle. For this reason, and to have a coherent design with the motorcycle, we use 25 mm diameter and 3 mm thick for the perimetric part of the frame and 18 mm diameter 2 mm thick for the stiffening rods; the number of internal rod is limited to reduce the weight of the vehicle taking to account that on the frame we have to add the coach, where the passenger seats.

A particular case is the rear rod, originally thought as torsional stiffening element, is then used to place the lower hinge of the suspension system for the coach.

The wheel is connected to the frame by wheel pin that take the wheel fixed during the motion of the vehicle; our wheel pin is fixed by two supports to the frame because we use as side wheel the same wheel equipped at the front fork of the motorcycle. To endure the forces coming from the side wheel contact patch we fix one end of the pin directly to the frame by plate while the other end is supported by another plate connected to the frame by a two bended tubes of 25 mm diameter and 3 mm thick to limit the vertical and bending displacements of the wheel pin end.

All the plates and the junctions elements of the frame are cut with a laser machine and bended, where necessary, with an automatic bending machine while the tubes of the frame are cut by a hand cutter for metals and then bended with a hand pneumatic machine. We used a 3 mm thick tubes not only for the reasons above but even because a low thickness tube showed some deformation along the cross section during the bending phase; all the elements of the frame are then welded together with a MIG hand welding machine.

Figure 4-12 Prototype frame realization

Now let's take a look on how the sidecar frame is connected to the motorcycle; since the vehicle can run with or without the sidecar we thought about a connection made of five removable points, three in the lower part of the motorcycle and other two in the upper part; all the connection elements are made of rods tubes about 25 mm diameter and 2.5 mm thick and spherical hinges at the end of the tubes.

On the front part of the vehicle we have two connection points, one in the lower part of the motorcycle and precisely on the left engine plate made by an extension of the frame with a spherical hinge for the sidecar part and only a plate with a housing for the hinge on the motorcycle side. The upper joint is made of a two sections curved tube of 25 mm diameter and 2.5 mm thick that goes from 2/3 of the gauge of the sidecar to the housing under the tank of the motorcycle; this housing is realized by two machined aluminium element embracing the motorcycle frame

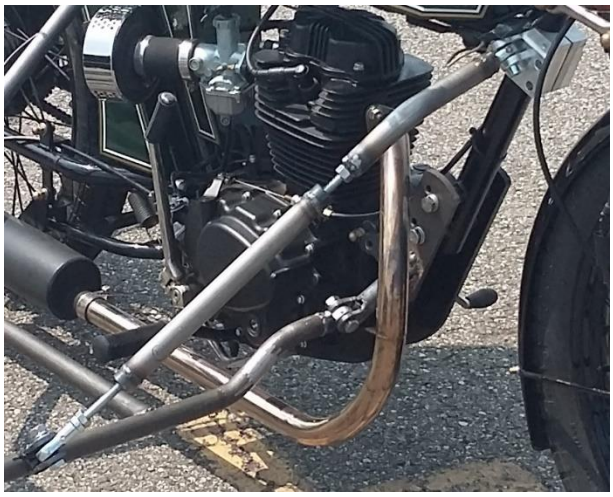

Figure 4-13 Front upper and lower joints

The third connection point between sidecar and motorcycle is placed in the central part of the vehicle going form the under the pilot seat of the motorcycle to the sidecar frame, even in this case we have a rod with the same characteristics of the previous one with a tow machined aluminium elements that embrace the motorcycle frame.

Figure 4-14 Central joint

In the rear part of the vehicle we have two lower joints, like the lower front one realized from an extension of the sidecar frame with a spherical hinge while the other one is made of a sloped rod with the characteristics of the front one going from the middle of the sidecar frame to the rear wheel centre support.

Figure 4-15 Rear lateral and longitudinal joints

The front and rear lower joints have to keep the sidecar fixed to the motorcycle in lateral and longitudinal direction while the slopped rear rod must resist the longitudinal forces acting on the vehicle; instead all the upper joints has to prevent the relative rotation between the sidecar and the motorcycle during the vehicle motion and realize a rigid vehicle. All connecting rods are made of right threaded end and a left threaded one as we can modify the camber and toe angles of the vehicle varying the rods length while the side wheel shifting is modified thanks to buttonholes on the supports of the pin wheel.

Otherwise the other elements, the connections of the sidecar to the motorcycle on the motorbike side are realized by machining processes in Alluminium, except the rear one that is made of a Steel plate. They are thought and realized in such a way that they can be easily removed from the motorcycle frame without modifying it for the sidecar connection.

Figure 4-16 Elements of connection between motorcycle and sidecar

The last particular element in the prototype is the side brake connection system; as said we use as side wheel a front one equipped with the prescribed drum brake, to ac this brake we connect the wire to the rear brake pedal through a modify to the pedal itself.

Figure 4-17 Coupling between rear and side brake system

As we can see from the picture we add a lever to the brake pedal where we directly connect the wire of the side brake, the cover of the wire is stopped by a plate fixed to the rear engine plate. The lever is made of steel, so we can weld it to the pedal, and its length is calculated in order to obtain the same force acting the rear brake rod.

4.2 Acquisition data system

To make the comparison of the results coming from the mathematical model and the once from the experimental tests is necessary to equip the vehicle we choose to perform the test on the track with an acquisition data system able to measure, from the physical model, the quantities we need under a graphic shape; with this aim we use an existing system, already present on the market, who's target is to measure several parameters on two or four wheeled vehicles. That kind of systems are made of a Data Logger, a central unit able to read and record the measured data coming from the internal and external sensors and finally send them through an usb socket to a pc, and then a series of sensors of different kind able to measure the quantities that the designer wants to take under control.

The data logger is produced by aim sportline and has two accelerometers inside that are usually used to acquire the speed and the accelerations along longitudinal and lateral directions of the vehicle; to acquire the signals from the other sensors we have some circular connectors socket that connects the sensors wiring line from each sensor to the data logger.

Figure 4-18 Data Logger

As we can see, on this model, we have three circular sockets on the front side of the box and each of this connector has a different function:

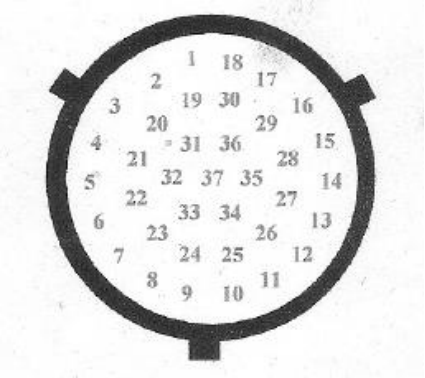

Figure 4-19 Data Logger 37 pin socket

In the first one, the 37 lines, are placed all the 13 analogic channels that the system can acquire without expansions box; for the channels are requested so much lines because a single sensor needs a power, signal and ground line to be acquired from the data logger

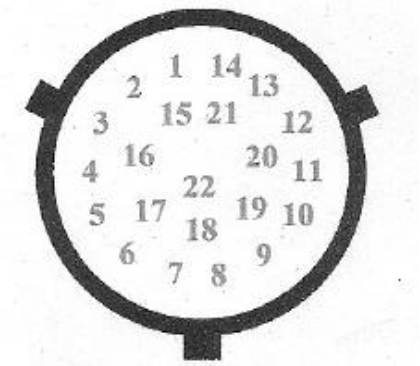

Figure 4-20 Data Logger 22 pin socket

The second one, a 22 channels line socket, is used to provide power to the entire system from the battery of the vehicle, to acquire a certain number of digital channel like rpm, front and rear wheel speed from the sensors already installed on the vehicle and the output connector for the data download.

Figure 4-21 Data logger CAN BUS socket

The last one on the right side of the data logger is used to connect the data acquisition system to the can bus line of the vehicle in order to record other quantities that the control units and the sensors of the vehicle exchanges on this line; as on our vehicle we don't have a can line this wiring line is connected but not used.

4.2.1 Sensor types used on the vehicle

On the market we have several types of sensor able to give the measurement of the quantities needed to the designer to analyse the behaviour of a vehicle; for our purpose on the vehicle selected for the tests we used accelerometers, potentiometers.

An accelerometer is an instrument able to measure the vibrations acting on a system, the function principle of this sensor is a one degree of freedom system made of a sprung mass suspended on a spring and damper in parallel

The frequency response function of this simple system is used to get the measurement of the acceleration we are looking for where when the M mass in the accelerometer is accelerated to the value xpp there be a force responsible for the acceleration of the mass; but if M doesn't move with respect to the case the force will come only from the spring, so thus the force is linearly dependent to the displacement of the spring this value of x0 is a measurement of the acceleration xpp.
Taking a look at the market we have several types of accelerometers, used for automotive purposes, due to the method used to get the measurement of the acceleration:

_ piezoelectric
_ MEMS

The piezoelectric get a response to the deformation of a material sensible to electric impulses, proportional to the acceleration of the system; this type of sensor are most used in case of crashes or vibration thus they are not suitable for constant acceleration measurements because of the principles at the basis of the piezoelectric displacement measurement. Otherwise they present high output tension signals, compact dimensions and very high natural frequencies, characteristics necessary to study impulsive phenomena.

The principle used for MEMS sensors is the same as the other ones but they are made of a micromachined material where when the system is subjected to an acceleration it's deformation gets a measure of the acceleration. The low cost technological process and the compact dimensions and the principles at the basis of the measurement makes them suitable for automotive purposes;

Figure 4-22 Accelerometer G101

in particular we use G101 sensors built up by RMG Tech s.r.l. that can be mono axial or biaxial accelerometers, the difference between the two sensors is that the first one is able to collect the measure in one direction as the second one measure the acceleration along two axis at the same time, so with a single sensor we can collect two measure channels. For what concern the output we have three wires getting from the sensor:

the red one is the power tension at 5V that represent the target tension, the black is the ground wire of the electric circuit and the white one is the signal tension and representing the measure of the sensor in terms of electric tension; in case of biaxial accelerometer we can see a couple of white wires that collect separately the measurements in the two different directions while, as the sensor is only one the power is get by two wires. In our tests the accelerometers are not used only to compare the accelerations of the vehicle but to get the speed of the centre of each wheel along the longitudinal and lateral directions, with those information we can't get the slip angles even integrating the signals because they need the use of

optical sensors like laser torches but as said before we can obtain the accelerations of each wheel centre so we can compare them with the local accelerations of the wheels coming from the mathematical model.

The other type of sensor used for our project are potentiometers, sensors able to get the measurement of length or distance in different ways;

the function principle of those sensors is that the distance that we want to measure is proportional to the voltage given by an electrical circuit inside the sensor, but how is the electrical circuit made of? Is quite simple to answer using the Ohm law: as we can see from the figure the sensor is made of a resistance powered by the principal line, an electric cursor runs over the resistance so adding a voltmeter between the cursor and an end of the resistance we have the measure of the distance covered by the potentiometer

Figure 4-23 Linear Potentiometer

on our vehicle we use two types of potentiometers, the first one is the linear one functioning exactly like the theory prescribes, but for our purpose is used to get the value of the steering angle of the vehicle so is fixed by a plate at the handlebar to the mobile end of the sensor while it's body is connected to the frame of the bike by a rotational joint.

The potentiometer is not fixed to the frame by its end but on the body of the sensor because in this case we can use the same sensor to calculate a clockwise and anticlockwise rotation at the same time without replacing the sensor and it leads to measure all types of manoeuvre we want.
The other distance sensor used is a wire linear potentiometer that uses the function principle of an angular potentiometer, connected to a wire, the rotation of the sensor is proportional to the length of the wire and as the diameter of the reel is constant the relationship between angular and linear motion is linear.

For our purpose this sensor is used to measure the rotation of the throttle handle that gives us the admission rate to the engine; using the same principle of the wire sensor to transform the linear in an angular one we fixed the sensor to the handlebar by a plate and the end of the wire is enveloped around the handle, the wire is kept tangential to the throttle handle by adding some returns to the system.

4.2.2 Acquisition data system wiring

Now that we have an idea of how the sensors works and the acquisition data is made of we have to place the sensors and the wiring on the vehicle and connect the sensors to the data logger we used a pre-existing wiring used on race motorbike that has more available sockets that we need for our tests.

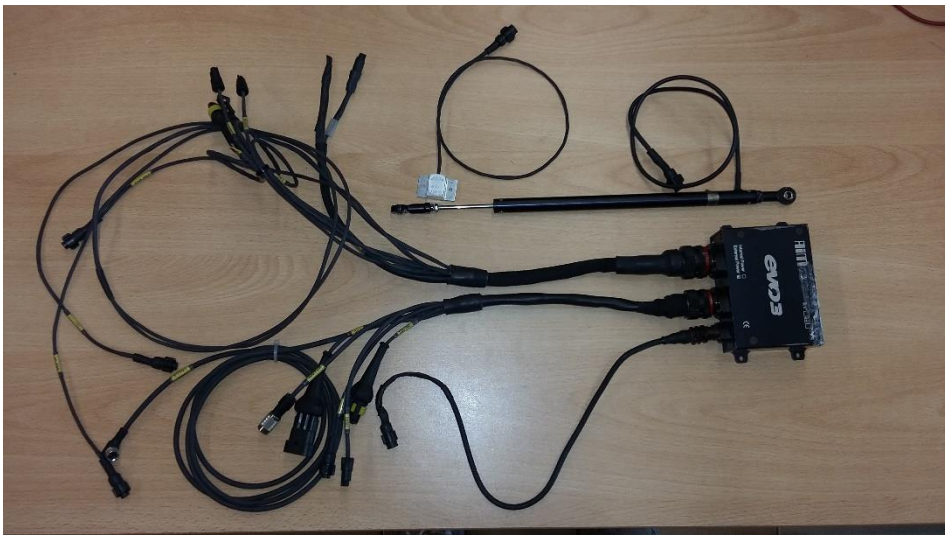

Figure 4-24 Acquisition Data system

The first thing to do is place the sensors and the data logger on the vehicle, placing the last one on the baggage rack of the bike over the rear wheel axle in order to use the accelerometers inside the logger to calculate the accelerations of the wheel;

Figure 4-25 Data Logger positioning on the vehicle

then the biaxial accelerometers as close as possible to the wheel axles, for the front wheel we use a moulded iron plate fixed to the fork right foot of the vehicle centred with the front wheel axle

Figure 4-26 Front biaxial accelerometer positioning

the same is done for the lateral wheel accelerometer fixed with another moulded iron plate, in this case the plate is placed on the right side of the wheel but on the inner side of the of the axle support, between the support and the wheel hub where we have a long spacer so the accelerometer is protected in case of crash during the tests.

Figure 4-27 Side biaxial accelerometer positioning

The linear potentiometer, with the system presented in the previous paragraph, is placed in the front part of the frame close to the steering axle and the handlebar in order to obtain the shortest lever as possible

Figure 4-28 Steering angle potentiometer

While the linear potentiometer used for measurement of the engine admission is fixed by a plate to the right rear mirror of the bike in order to be as close as possible to the throttle command.

Figure 4-29 Throttle position sensor potentiometer

The last sensors we add to the system are two linear potentiometers used to measure the force acting on the braking system;

Looking at the figures we notice that one end of each sensor is fixed to the frame, or handlebar, of the bike to keep it fixed during the braking phase while the other end is connected to the lever/pedal and its rotation produces a displacement that the sensor is able to measure; with this aim the moving end of the potentiometer is placed as far as possible from the centre of rotation of the pedal/lever to highlight even the smallest displacements. Thus we are not using a load cell able to give the force in Newton we calculate the force acting on each brake as the product of a mass and the gravity acceleration and we can calibrate the sensor only changing the weight connected to the lever/pedal.
As said using an existing wiring we at first connect the data logger to the electric power of the battery, placed in the rear part of the fuel tank, making all the wiring pass close to the frame and under the fuel tank we bring two channel on the front of the vehicle that are used for the steering angle potentiometer and the throttle positions sensor one then we have three channels connectors under the fuel tank used for the front wheel accelerometer by using a special wiring line made ad hoc between the accelerometer and the channel sockets and the third one is used to acquire the RPM signal with its own wire connection to the ignition coil; the last accelerometer, placed on the lateral wheel is connected by two sockets placed on the rear part of the vehicle with another wiring line made ad hoc for the sensor the last line we used is the usb one placed under the pilot seat that is the socket where we connect the pc to the data logger to download the data.
Reminding the first paragraph we can see a loss of channels in this system, in fact to acquire the vehicle speed and its trajectory during the manoeuvre we use a GPS chronometer placed closed to the centre of masses of the vehicle as we can have a precise measure to confront with the data given by the mathematical model, but as the vehicle is compact we placed the chronometer on the handlebar of the motorbike so the pilot can easily read the vehicle speed on the chronometer screen;

Figure 4-30 Chronometer positioning

the biggest problem in this system is that we have two different subsystems that acquire different data separately and with different starting instant because the GPS chronometer start its acquisition when the vehicle moves as the other one starts the acquisition in a time chosen by the user, but we will see that in detail in the following section.
The last thing to do on the acquisition data system before performing the tests is the calibration of the sensors inside the analysis software, this is necessary in order to obtain the right measure from each channel and rapidly identify any single channel inside the list, so we connect the pc to the data logger switched on and run the analysis software. Going in the calibration section of the software we select the channel corresponding to the sensor we want to set up, for example we start from the steering angle channel, at first we go to the “online” window where we can see the real time measure of the sensors in voltage and writing down the values corresponding to zero and maximum degrees in both directions.

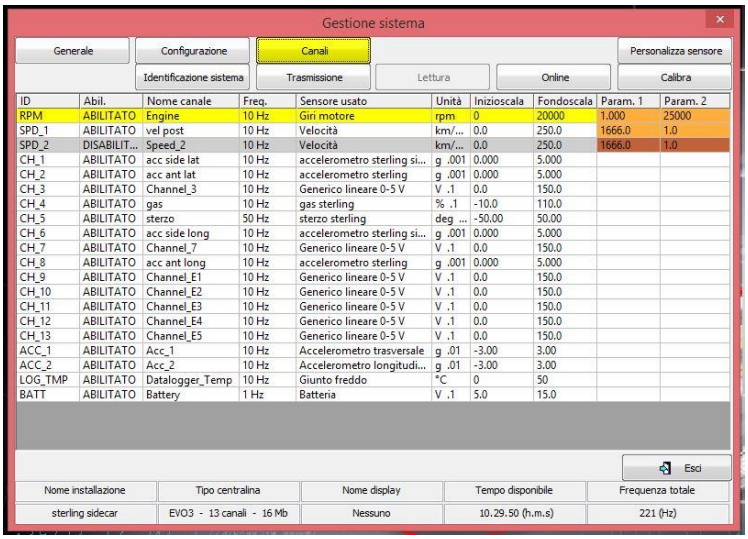

ID	Abil.	Nome canale	Freq.	Sensore usato	Unità	Inizioscala	Fondoscala	Param. 1	Param. 2
RPM	ABILITATO	Engine	10 Hz	Giri motore	rpm	0	20000	1.000	25000
SPD_1	ABILITATO	vel post	10 Hz	Velocità	km/...	0.0	250.0	1666.0	1.0
SPD_2	DISABILIT...	Speed_2	10 Hz	Velocità	km/...	0.0	250.0	1666.0	1.0
CH_1	ABILITATO	acc side lat	10 Hz	accelerometro sterling si...	g .001	0.000	5.000		
CH_2	ABILITATO	acc ant lat	10 Hz	accelerometro sterling	g .001	0.000	5.000		
CH_3	ABILITATO	Channel_3	10 Hz	Generico lineare 0-5 V	V .1	0.0	150.0		
CH_4	ABILITATO	gas	10 Hz	gas sterling	% .1	-10.0	110.0		
CH_5	ABILITATO	sterzo	50 Hz	sterzo sterling	deg ...	-50.00	50.00		
CH_6	ABILITATO	acc side long	10 Hz	accelerometro sterling si...	g .001	0.000	5.000		
CH_7	ABILITATO	Channel_7	10 Hz	Generico lineare 0-5 V	V .1	0.0	150.0		
CH_8	ABILITATO	acc ant long	10 Hz	accelerometro sterling	g .001	0.000	5.000		
CH_9	ABILITATO	Channel_E1	10 Hz	Generico lineare 0-5 V	V .1	0.0	150.0		
CH_10	ABILITATO	Channel_E2	10 Hz	Generico lineare 0-5 V	V .1	0.0	150.0		
CH_11	ABILITATO	Channel_E3	10 Hz	Generico lineare 0-5 V	V .1	0.0	150.0		
CH_12	ABILITATO	Channel_E4	10 Hz	Generico lineare 0-5 V	V .1	0.0	150.0		
CH_13	ABILITATO	Channel_E5	10 Hz	Generico lineare 0-5 V	V .1	0.0	150.0		
ACC_1	ABILITATO	Acc_1	10 Hz	Accelerometro trasversale	g .01	-3.00	3.00		
ACC_2	ABILITATO	Acc_2	10 Hz	Accelerometro longitudi...	g .01	-3.00	3.00		
LOG_TMP	ABILITATO	Datalogger_Temp	10 Hz	Giunto freddo	°C	0	50		
BATT	ABILITATO	Battery	1 Hz	Batteria	V .1	5.0	15.0		

Figure 4-31 Channel list

With those data we go to the calibration window selecting the type of measure we want to obtain “Angle” and inserting them in the cells on the left side while a curve with three points blue points and a red line appears in the middle of the window clicking on “calculate curve” button, finally we give a name to the sensor and save it then return to the channel window and select the calibrated sensor for the channel corresponding to the steering angle

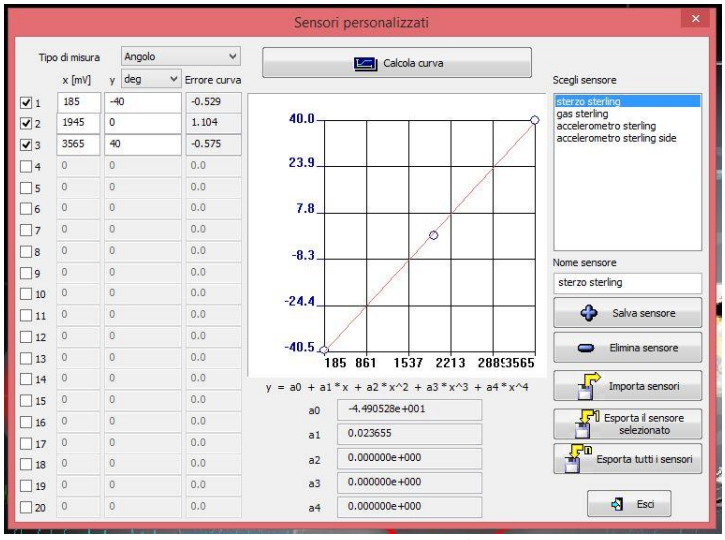

Figure 4-32 Steer sensor conditioning

We do the same procedure to calibrate the throttle position sensor taking the values at closed throttle valve and at fully opened, as the valve goes only from zero to full open two points are enough to get the regression line

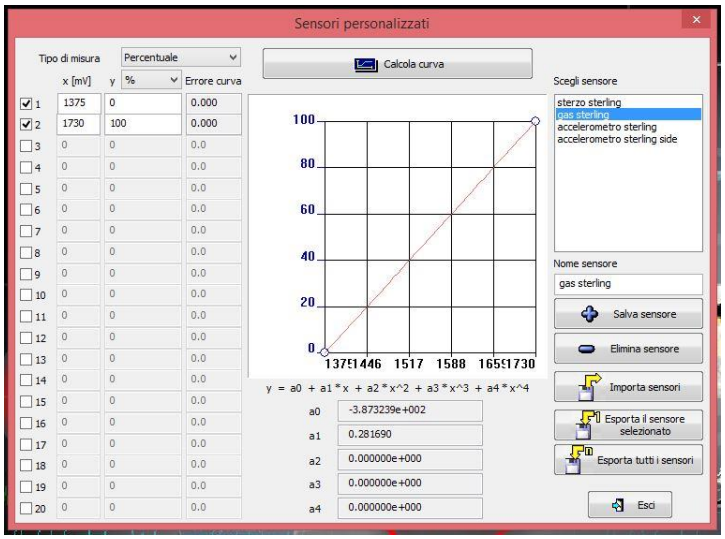

Figure 4-33 TPS sensor conditioning

Now that we know how to calibrate the sensors we end calibrating the two biaxial accelerometers, in this case as the sensor is the same for two channels, one longitudinal and one lateral, the procedure can be done only in one direction: we select the measure type, in this case acceleration in g scale, give a rotation to the accelerometer in direction of negative acceleration noting the corresponding voltage value and then rotating the sensor in the positive acceleration direction noting again the corresponding voltage value. We pot those values in the cells corresponding to the ordinate axis of the calibration curve as in the ordinate one we put the value -5 g and 5 g, corresponding to the maximum acceleration that the sensor can measure and obtaining the regression curve

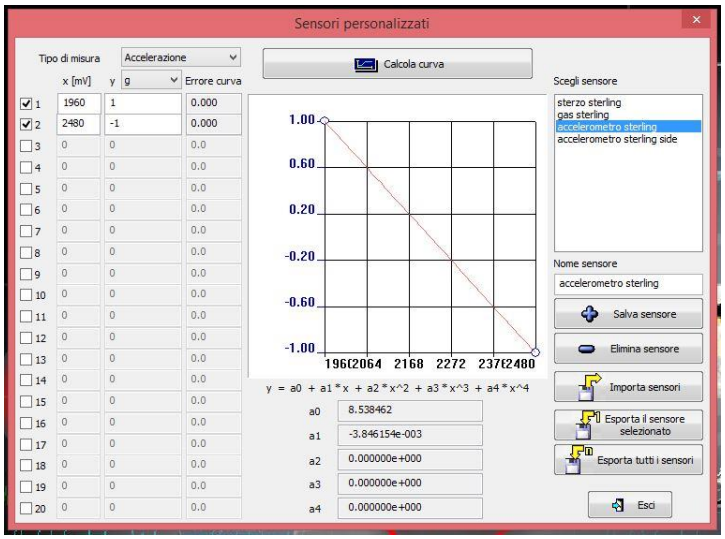

Figure 4-34 Front Accelerometer conditioning

As the sensor on the side wheel is different from the one on the front wheel we do the procedure again for this biaxial accelerometer and as we can see from the obtained curves, the maximum and minimum values and the coefficients of the curves are different

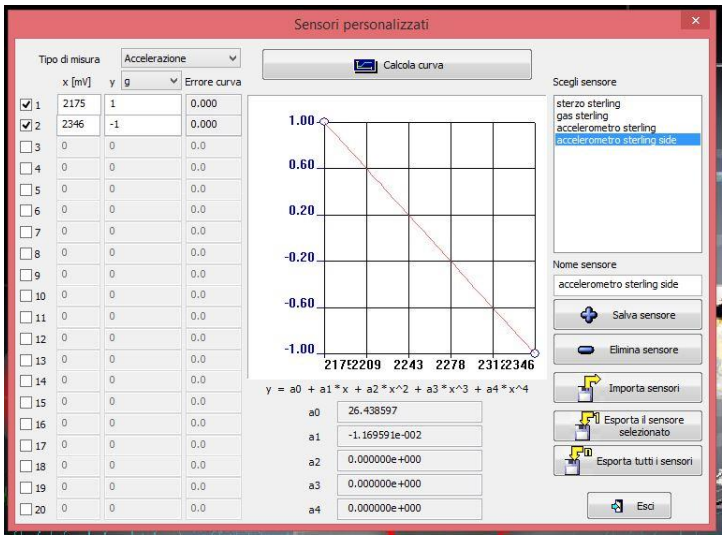

Figure 4-35 Side accelerometer conditioning

At the end we select the saved accelerometers in the channel list for the ones corresponding to the front longitudinal and lateral accelerations and for the side longitudinal and lateral accelerations.

The last sensors we have to calibrate are the potentiometers used to measure the force acting on the two braking systems. Since the potentiometers has different length and the leverages acting the brakes changes from front to rear brake system we have two different calibrations, one for each system.
As shown before, we are interested in the force acting on the lever/pedal in terms of mass multiplied by the gravity acceleration so to calibrate the sensor we consider the voltage value at zero, 3 Kg and 5 Kg. as we can see from the figure the calibration of this kind of sensor is not perfectly linear but enough to consider it as linear.

4.3 Experimental Tests

Now the vehicle is ready and equipped with an acquisition data system we have to define a series of tests that can help us in the validation of the mathematical model described in the previous chapter and a place where perform them in a safety way. Let's start from the place, is obvious that perform our experimental test along the streets is not safe for us and for other people so we decide to go to a track where if we have an issue during a run the pilot will stop the vehicle in a safe way without hurting the staff or other people, the track we choose is the CREA test track for agriculture machines that is commonly used to make test on heavy machines used in the fields but is even used for phonometric tests on road vehicle

Figure 4-36 CREA test track

The circuit, as we can see is made of two straight lines connected by two long turns and a large pane space in the middle of the circuit; the speed admitted on the track is quite low from 30 Km/h to a maximum of 60 Km/h, a range suitable for our tests, but now let's get in detail on each run we choose to perform.

Straight line _ for this test we start from the square in the middle of the track taking the vehicle in the middle of the straight road, then we accelerate the vehicle till 40 Km/h opening the throttle valve and when we reach that speed the pilot maintains the speed for some seconds and then decelerates without using brakes till the vehicle stops

As we start each run at the square in the middle of the circuit we made the test two times, the first one between the start line and the turn and the second between the turn and the finish line.
This test is needed to know if the model of the engine we made is correct or not but even to validate the model of contact between pneumatic tyre and road explained in the previous chapter.

Steering pad _ this manoeuvre consist in a short straight line before the vehicle enters a turn in which the steering angle is linearly increased trying to maintain the speed as constant as possible. We performed those runs inside the square in the middle of the circuit as we need a larger space then the gauge of the track.

The test was made four times two times for steering direction at the speed of 20 Km/h and 25 Km/h, we need to validate separately the right and the left steering direction because of the presence of the side wheel and the not symmetrical geometry of the vehicle while the difference of speed at which we perform the manoeuvre is only to have more data to validate the model.

Wave manoeuvre _ this test was made on the straight lines of the track and it consists in varying the steering angle from left to right with the aim to realize a sinusoidal wave with constant amplitude while increasing its frequency.

Even in this case we performed several runs to obtain a more precise manoeuvre and data set at different speed going from 15 Km/h and 20 Km/h; as we can notice the speed of the runs are quite low this is due to the fact that this manoeuvre is quite dangerous for the pilot and increasing the speed and the frequency of the steering the vehicle becomes unstable as the side wheel detaches from the ground

Step Steer _ even those last manoeuvres were performed on the straight lines of the track as it consists only in an acceleration till the test speed and at a certain point on the track the pilot gives a sudden steer angle in a direction and then release the steer with the aim of the pilot to avoid a sudden obstacle on the road.

Before starting with the test campaign we perform some checks on the vehicle as to be sure of some characteristic parameters of the vehicle like the forward shifting of the side wheel, the camber angle of side wheel and the motorcycle and the toe angle.
The first one is simply measured by linear meter considering the distance, on the longitudinal axis, between the rear wheel centre of the motorcycle and the side wheel centre; the camber angle is measured with an inclinometer, a device similar to a level, that is able to measure the slope of a plane; using the inclinometer as it was the string of a circumference we measure the camber of the side wheel.

Since the static camber angle of the front wheel is the same as the rear one we measure the camber on this last wheel placing the inclinometer between two points of the motorcycle frame.

Figure 4-37 Camber angle check on the test track

For what concern the toe angle we place two metal bars one aligned with the side wheel and the other with the front and rear wheels of the motorcycle, the bars have a length of 2,5 m while measuring the distance between the two bars at each end we can easily calculate the toe angle.

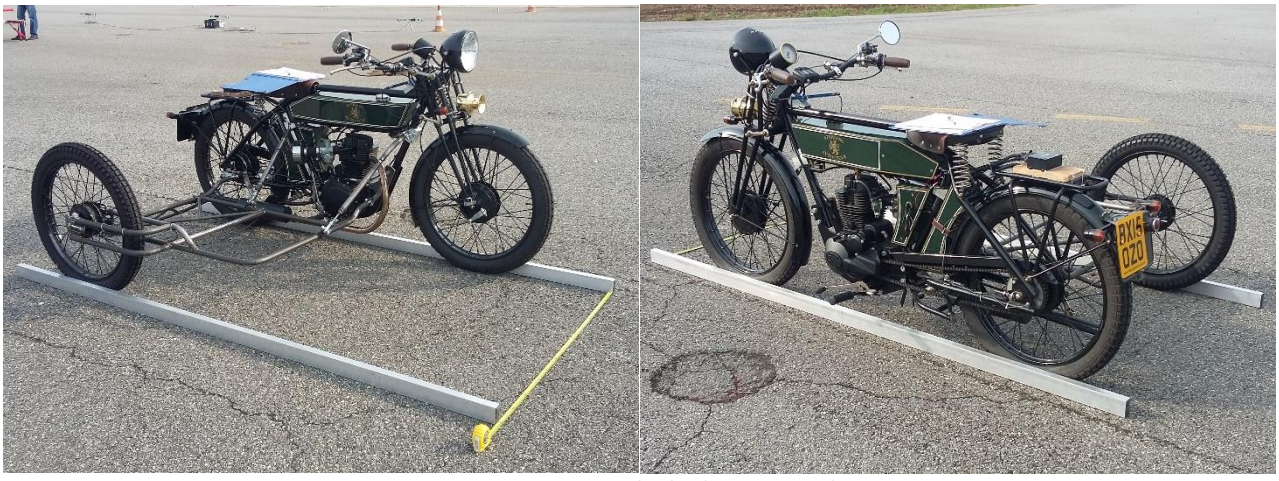

Figure 4-38 Toe angle check on test track

This check is necessary in order to be sure that there's no camber and toe on the vehicle wheels defining a standard configuration and if they have a different value we can act on the linkage of the sidecar and the buttonhole of the side wheel to set them to zero.

As usual we perform the test four times at different speed in order to have the behaviour of the vehicle while steering on the left and right side because of the reasons explained for the steering pad manoeuvre; the speed is kept quite low even in this is case because of the dangerous of the manoeuvre as when giving a sudden and high steering angle in clockwise verse the side wheel tends to detach from the road getting the vehicle in instability.
We have other data with which we can make a detailed validation of the vehicle because using the geometry of the track we collected the data coming from the turns joining the two straight lines between the square where the start and stop lines are placed.
In addition we performed a braking test accelerating the vehicle from zero to 40 Km/h and then braking with the pedal and the lever along a straight line; this is done to validate the mathematical model of the brakes and see if the vehicle, due to the not symmetric geometry of the wheels and so the brakes, gives a yaw rotation during the braking phase

Figure 4-39 Experimental test on CREA track

4.4 Validation process

As said in the in the previous paragraphs the validation consists in make a comparison between the outputs coming from the mathematical model and the once coming out from the prototype tests, but a first problem is to be sure that the dimensions of the two vehicles, the mathematical and real one, are the same and the second problem is what kind of output we can confront.
To answer the first question we put the vehicle on his wheels and with a length measurement instrument, in our case a meter, we take:

- The base length of the vehicle, the distance from the rear wheel centre and the front wheel one
- The gauge of the vehicle, the distance between the middle plane of the rear wheel and the middle plane of the side wheel
- The side wheel forward length, the distance between the wheel centre of the rear and side wheel

After we wrote down those quantities we must put them into the mathematical model in order to have the same vehicle but we make this check because the prototype is a handcrafted one so bends cuts and welded joints may not respect at all the once given by the CAD model because in the realization of the frame we didn't used automated bending machines and a welding mask in order to reduce as possible the costs of the prototype. We have also to check if the masses, and so the static loads, of the vehicle are equivalent to the same quantities given by the CAD model; to do this verification we use three weight scales in this way. We put the three weight scales under each wheel of the vehicle reading the measure and then we sum up the values getting the total mass of the unladen vehicle and making a comparison with the value given by the CAD model and adjusting it in the mathematical program inputs if necessary.

We do the same procedure on the laden vehicle with only the driver and the driver plus a passenger but before calculating the mass of the entire vehicle we have to measure the mass of the driver and the passenger in order to make a proper comparison with the CAD model obtaining the following results:

As we can see, considering that the CAD model is completely rigid and has rigid joints, we can say that the CAD model and the prototype are not too different so the prototype is well realized even if in the validation process we will use the data coming from the real model, this check will help us to find some data, like the vehicle moments of inertia, in an easier way making less tests on the prototype.

4.4.1 Rearrangement of the experimental data

From the description of the data analysis system we get that we are using two system to calculate some parameters of the vehicle that doesn't directly communicate one with the other so at the beginning we have to realign all the data and collect them in a single data file that is easier to use during the confrontation, to do that we export all the recorded data from the software "Race Studio 2" to a standard format that can be loaded on Matlab;

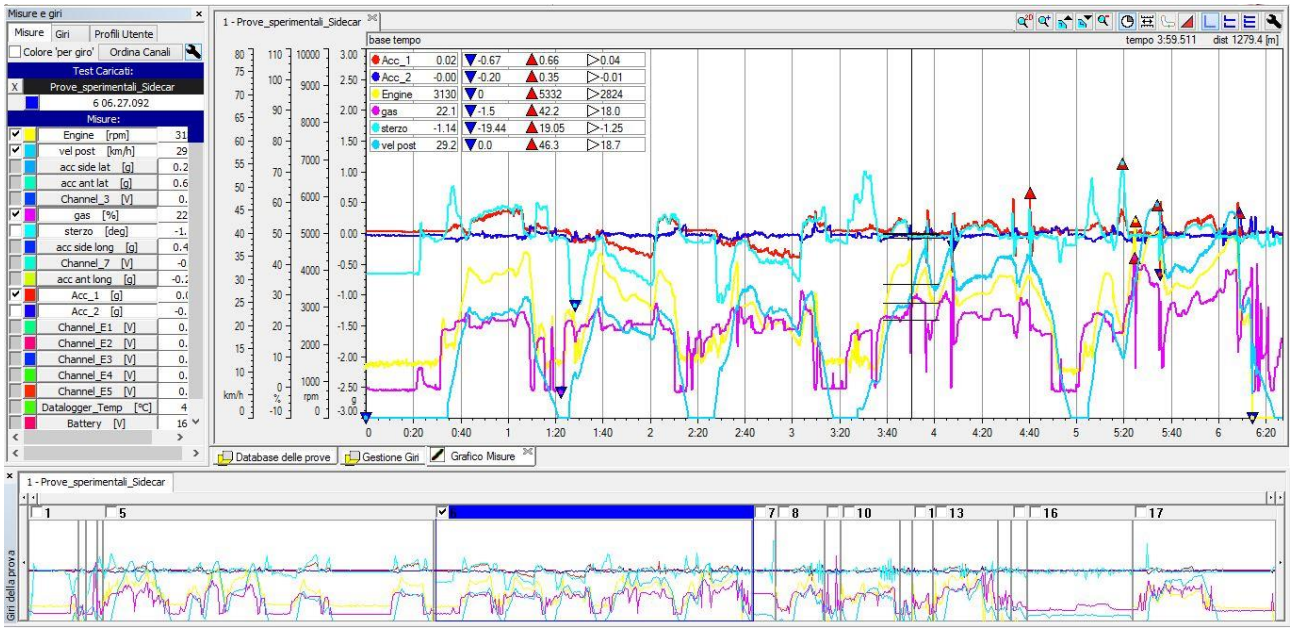

Figure 4-40 Data view in Race Studio 2 software

for the exported file we select the data of the entire campaign test choosing the folder and the extraction format then finally the program asks which channels we want to export in both time and space base. The export procedure is the same for data coming from the data logger and the chronometer noting that the

challenge of this work phase is that the data are collected with different sampling frequencies and different acquisition start time as explained in the previous sections; so knowing the issues we confront the speed of the vehicle coming from the gps with the speed, measured by the data logger, of the rear wheel centre on the same chart to have overall view of the situation

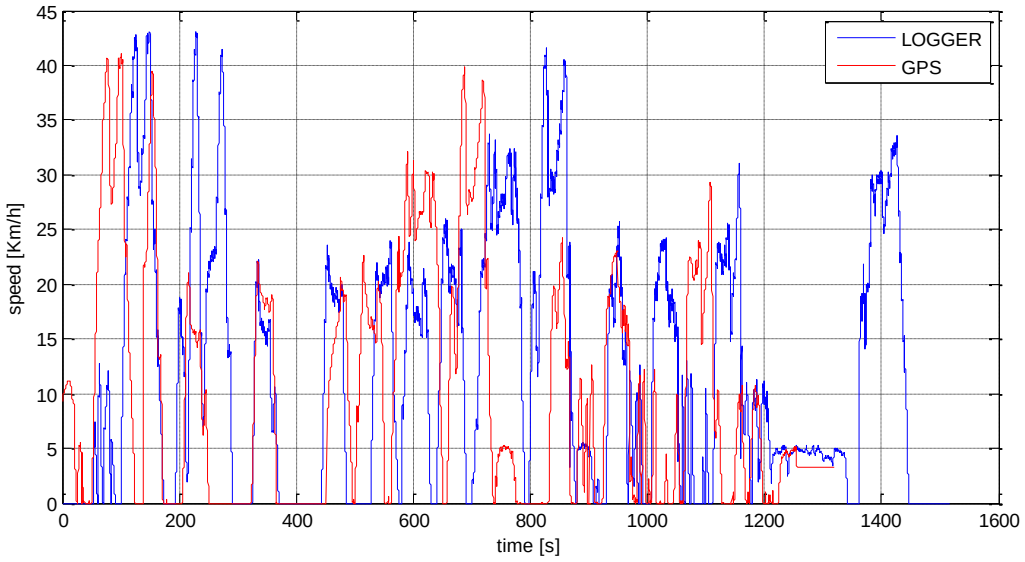

Figure 4-41 Data imported from data logger and chronometer

as we can see there are some zones of the plots where the two speed are zero identifying the instants where the vehicle is not running so we make a first cut of the dataset in subsets where the speed is greater than zero, obtaining 27 records for the data logger and 54 for the chronometer; the records are too much because with this first cut we have even records corresponding to the tests we are looking for and other where we realign the vehicle to start a new run.
The next step is to take a look not only to the speed but even to the other channel, in particular the trajectory of the vehicle, coming from the chronometer, and the steering angle, coming from the data logger. With the help of the simultaneous plot of the speeds as done for the first cut we collect the sections containing only the experimental tests presented in the previous paragraph building up a single data set for each test containing:

$$[t_{gps} \quad V_{gps} \quad lat \quad long \quad A_x \quad A_y \quad t \quad V_{rear} \quad a_{xf} \quad a_{yf} \quad a_{xr} \quad a_{yr} \quad a_{xs} \quad a_{ys} \quad \delta \quad rpm \quad tps]$$

But the problem of different sampling frequency is still present that is represented in a not perfect alignment of the two speed signals since the first six components belong to the chronometer and the other from the data logger; to solve this issue we use a linear interpolation function with the aim to extract the data coming from the gps chronometer with the same sampling frequency of the datalogger getting a set of records with the same number of points and finally realign the data using the cross-correlation function.

$$R_{xy}(\tau) = \frac{1}{T-\tau}\int_0^{T-\tau} x(t)y(t+\tau)dt \qquad [4.1]$$

This function used in signal analysis is used to identify the delay between two different signals multiplying the first signal for the second shifted by a quantity τ that is a time length in our case; getting more in detail we can't use the formulation presented above because our signals are not continuous but sampled obtaining a fixed number points per signal, so the cross-correlation can be rewritten in that way

$$R_{xr}(r) = \frac{1}{N-r}\sum_{i=1}^{N-r} x(i)\, y(i+r) \qquad [4.2]$$

For our purpose we can use a more intuitively and easy view of the correlation data using the normalized formulation, in this way the correlation varies only between 0 and 1 where the unity corresponds to the maximum correlation between the signals

$$\rho_{xy}(\tau) = \frac{R_{xy}(\tau)}{R_{xx}(0)R_{yy}(0)} \qquad [4.3]$$

Where Rxx and Ryy are the auto-correlation functions for x and y signals. We perform this procedure for each time records of the tests taking as x and y signals the rear wheel speed and the gps speed.

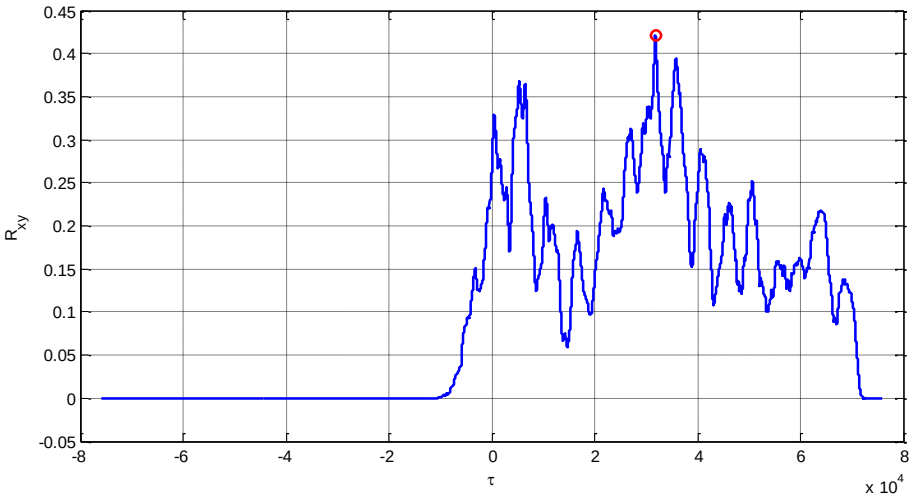

Figure 4-42 Crosscorrelation function for vehicle speed

With the time delay of each data set we can shift only the latitude and longitude time history coming from the chronometer and realign them with the data coming from the data logger and finally saving them in a single time history.
The setup of the data set for the validation procedure is not done yet since it the records needs another cut for two reasons; the first one is that in some cases the data are so long and this length take lot of time inside the validation software to be processed, as we can see later; the second one is more related to the modelling we have done for the Sidecar, in fact taking a better look to the dataset we see that it starts with vehicle in stationary position and then we accelerate it to the manoeuvre speed since in this section we have the release of the clutch in order to meet the matching point between the engine and the resistance power to start the motion of the vehicle but the release of the clutch is not implemented in the engine model. With this aim we cut the data sets close to the manoeuvre obtaining the following data set.

$$[t \quad V_{gps} \quad V_{rear} \quad lat \quad long \quad A_x \quad A_y \quad a_{xf} \quad a_{yf} \quad a_{xr} \quad a_{yr} \quad a_{xs} \quad a_{ys} \quad \delta \quad rpm \quad tps]$$

The last rearrangement of the data got from experimental test is made on the trajectory plots because, as we said before, this graph is given in terms of latitude and longitude but we have to compare it in X and Y displacement in meter. The changing of coordinates from geographic to cartesian can be easily done through a set of simple equations

$$\begin{cases} a = 6378137 \\ e^2 = 0.00669437999 \end{cases}$$

$$N = \frac{a}{\sqrt{[1 - e^2 \sin(lat)^2]}} \quad [4.4a]$$

$$\begin{cases} X = N \cos(lat) \cos(long) \\ Y = N \cos(lat) \sin(long) \end{cases} \quad [4.4b]$$

In the set of equations we will use only the first two since our problem is a planar and not tri-dimensional one; from the obtained cartesian coordinates we subtract its minimum value in order to start from the origin, but in some trajectory we can see an issue making a check, the total distance covered by the transformed curve is not the same as the distance channel for each test. To solve the problem we use the data given by the transformation set of equation to calculate the instant angle of the trajectory.
And then we reconstruct the correct trajectory from the distance channel using the trigonometric functions.

4.4.2 Mathematical model validation

The last step of the validation procedure is to modify the mathematical model presented in the previous chapter as it can take as input some data coming from the experimental test; in particular the model has to take in input the steering angle that defines the manoeuvre, the initial speed that are already given as input in the previous model; in the validation one we add as input the admission rate of the engine in form of percentage of throttle valve opening and the gear along the manoeuvre.

In output to the model we have, like in the previous case, the degrees of freedom of the system calculated from the integration procedure and we add the local accelerations of each wheel centre; the experimental once are got directly from the accelerometers while the mathematical are got deriving the speed of the centre of each wheel with respect to time

The speed of the vehicle and its trajectory, to make first comparison we plot those output results with the ones coming from the experimental tests over the same chart and looking if the obtained curves has the same shape.
The other output we need for this phase are the local accelerations of the wheel centre, to do that we add inside the integration function the formulas of the quantities we need previously derived from the expression of the wheel centre's speed

$$\vec{A}_f = \frac{d}{dt}\vec{V}_f = \vec{\imath}\left(\dot{V}_x + \ddot{\psi}w - V_y\dot{\psi} - a\dot{\psi}^2\right) + \vec{\jmath}\left(\dot{V}_y + a\ddot{\psi} + V_x\dot{\psi} + w\dot{\psi}^2\right) \quad [3.5a]$$

$$\begin{cases} a^l_{xf} = \left(\dot{V}_x + \ddot{\psi}w - V_y\dot{\psi} - a\dot{\psi}^2\right)\cos\delta + \left(\dot{V}_y + a\ddot{\psi} + V_x\dot{\psi} + w\dot{\psi}^2\right)\sin\delta \\ a^l_{yf} = -\left(\dot{V}_x + \ddot{\psi}w - V_y\dot{\psi} - a\dot{\psi}^2\right)\sin\delta + \left(\dot{V}_y + a\ddot{\psi} + V_x\dot{\psi} + w\dot{\psi}^2\right)\cos\delta \end{cases} \quad [3.5b]$$

$$\vec{A}_r = \frac{d}{dt}\vec{V}_r = \vec{\imath}\left(\dot{V}_x + \ddot{\psi}w - V_y\dot{\psi} + b\dot{\psi}^2\right) + \vec{\jmath}\left(\dot{V}_y - b\ddot{\psi} + V_x\dot{\psi} + w\dot{\psi}^2\right) \quad [3.6a]$$

$$\begin{cases} a^l_{xr} = \left(\dot{V}_x + \ddot{\psi}w - V_y\dot{\psi} + b\dot{\psi}^2\right) \\ a^l_{yr} = \left(\dot{V}_y - b\ddot{\psi} + V_x\dot{\psi} + w\dot{\psi}^2\right) \end{cases} \quad [3.6b]$$

$$\vec{A}_s = \frac{d}{dt}\vec{V}_s = \vec{\imath}\left(\dot{V}_x - \ddot{\psi}(w-s) - V_y\dot{\psi} + (b-b_s)\dot{\psi}^2\right) + \vec{\jmath}\left(\dot{V}_y - (b-b_s)\ddot{\psi} + V_x\dot{\psi} - (w-s)\dot{\psi}^2\right) \quad [3.7a]$$

$$\begin{cases} a_{xs}^l = \left(\dot{V}_x - \ddot{\psi}(w-s) - V_y\dot{\psi} + (b-b_s)\dot{\psi}^2\right) \\ a_{ys}^l = \left(\dot{V}_y - (b-b_s)\ddot{\psi} + V_x\dot{\psi} - (w-s)\dot{\psi}^2\right) \end{cases} \quad [3.7b]$$

We start the validation process form the straight line and in particular the constant speed phase where we can notice the right curvature of the trajectory and the difference between the mathematical one; this difference could be caused by the presence of ply-steer effects on the tyre that can gives a lateral force with zero steering angle, fact that explains why we have a right steering angle to keep the trajectory straight. In order to realign the trajectory we act on the Magic Formula shifts s_v and s_h; setting up those terms we can see the shifting of lateral accelerations of the wheels toward the real vehicle ones and even a decreasing of the vehicle speed profile obtaining the results listed in Attachment E

The next step is to work on the acceleration phase in straight line with which we validate the engine model; as in the previous case we look at the alignment of the real vehicle graph and the mathematical ones. At first we notice that the lateral accelerations are quite correct considering the presence of some noise in the experimental graphs but its mean value is coherent with the mathematical graph, while we see a big difference in the speed plot. In this case we add a loss in the engine model proportional to engine speed of rotation and another concentrated loss proportional to the complementary part of the engine admission,

In this way we have the curves of torque closer at low admission rate and then tends separate at high admission rate and we add another concentrated loss proportional to the complementary part of the engine admission. This loss in the engine model produces a reduction of the speed of the vehicle and its longitudinal accelerations, we increase the losses in terms of mass and its misalignment till the graph are overlapped as close as possible reaching the results in Attachment E.

With those parameters we obtain a good fitting of the curves for the straight line and right steering pad manoeuvres otherwise we can see an error in the central part of the left steering pad where the model speed is higher than the vehicle one and then tends to realign the results. In the wave path we can see that the model doesn't follow in a precise way the vehicle even if as in the case of straight line constant speed the oscillations are around one or two Km/h so we can think the speed constant along the manoeuvre.
The next phase is to look at the output coming from the two steering pad in order to decide if it is necessary to introduce in the model a first order approximation for the cornering forces like the relaxation length; taking a look at the results the trajectory is sufficiently overlapped and all the accelerations coming from the mathematical model are close to the real accelerations of the wheels, so at the end we can say that is not necessary to introduce the relaxation length inside the model. Since we don't know the exact coefficients of the tyres used for the Magic Formula of Pacejka we use the two steering pad results to set the coefficients.
For the Step steer manoeuvre acts like an impulse given to the mechanical system, so for the output is like to see the free response of the system; taking a look at the results for this manoeuvre we can say that the model response to the impulse is perfectly overlapped if we analyse the lateral accelerations while we have a little discrepancy in case of longitudinal accelerations probably caused by the not perfect modelling of the engine.
From the results listed in Attachment E we can clearly see that the accelerations coming from the vehicle have so much oscillation that is difficult to identify a trend in the signal; for a better understanding if the signal coming from the vehicle and the mathematical model are similar we calculate the mean and standard deviation of the error between the real vehicle curves and the mathematical model ones

$$err_i = (x_{iV} - x_{iM}) \quad [3.8a]$$

$$\mu_i^{err} = \frac{1}{N}\sum err_i \quad [3.8b]$$

$$\sigma_i^{err} = \frac{1}{N}\sum (err_i - \mu_i^{err})^2 \quad [3.8c]$$

Obtaining the results listed in the table of the Attachment E, and as we can see the errors are enough small and the data low dispersed around the corresponding mean value, low standard deviation.

Analysing the obtained results, after a rearrangement of the model, we can say that the model with the hypothesis we made at the beginning reproduce with a sufficient precision the lateral behaviour of a real sidecar vehicle.

4.4.3 Coefficients Adjustment

During the validation of the model we saw that the trajectory in some runs was not coherent with the mathematical model one while other quantities like the accelerations were overlapped; analysing the issues that could cause such a problem we identify it in the coefficients used for the Magic Formula of Pacejka. This because we are not using the real coefficients of those tyres but estimated ones from similar pneumatic tyres.
For this reason during the validation process we decide to perform an optimization of the coefficients along some manoeuvres using a minimization algorithm; for this procedure we used the constant speed test, that presents at the beginning a trajectory shifting to the right, and the steering pad left and right for 10 seconds length in order to not incur in the curve saturation and remain in the linear zone of the contact curve.
We will describe in detail in the next chapter how an optimization algorithm works, know we focus on the objective functions that are represented by the mean squared error between the real vehicle curve and the mathematical model one. The curves we are interested in are the Trajectory and the Lateral Acceleration of the vehicle. In the Lateral Acceleration case it is enough to calculate the squared error at each point of the curve and then calculate its mean value along the manoeuvre; a little complex procedure must be done for the Trajectory that is made of two time depending vectors, one representing the longitudinal displacement and the other the lateral one; the composition of the coordinates generates each point of the trajectory with which we can define the error between the curves.
The optimization proceeds using the Constraint Method because we have a multi-objective optimization that implement the simplex method as minimization function that operates changing the coefficients B, C, E and μ_y of the Magic Formula reaching an optimal set of values.

Roll-coefficients	
B	7.5
C	1.9539
E	0.3029
μ_y	0.9

Table 4.1 - Macro-coefficient for the Magic Formula

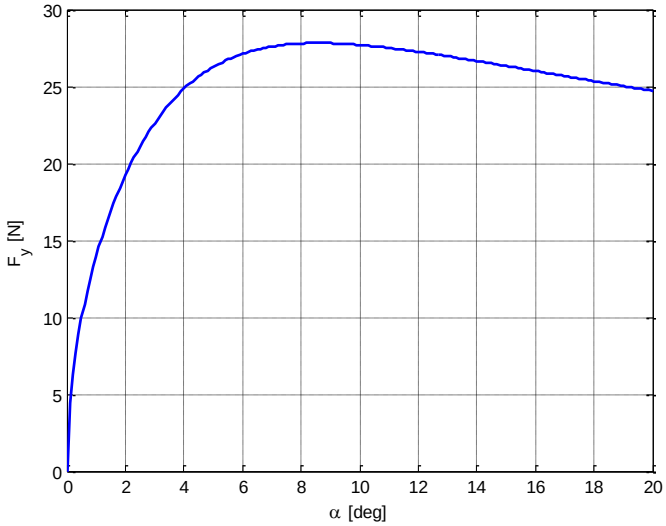

Figure 4-43 Lateral force vs slip angle curve

4.5 Additional Tests

During the campaign test we perform other additional runs with the variation of some vehicle parameters, lately used for the sensitivity analysis in the next chapter. The runs are the same as for the once used to validate the model but in this case we change one parameter at a time both on the real vehicle and in the mathematical model; this is done in order to see clearly the effect of the single parameter on the dynamics of the vehicle otherwise it is difficult to identify the effect of a single one.
The first change is on the forward shifting of the side wheel, in this case we put the wheel as forward as we can on its housing reaching a distance of 65 mm from the rear wheel of the motorcycle and paying attention to not apply a toe angle. Applying the same validation procedure used for the standard model, and changing the same parameter inside the mathematical model we get the results listed at the end of the Attachment E paragraph E.8, where we can clearly see that the two trajectories are quite overlap while the acceleration, especially the lateral ones have a drop from half of the manoeuvre till the end, that could be caused by a not perfect modelling of the engine, fact that causes even the drop in the vehicle speed. Considering the results of the whole test we can say that the model reproduces in a sufficient way the behaviour of the vehicle.
The second parameter we are going to change is the camber angle to the wheel, this is used not only as a check for the validation of the mathematical model but also to check and eventually set up the coefficients, related to the roll motion, inside the Magic Formula. As in the previous case we don't exactly know the tyre coefficients related to the roll motion, but following the same procedure seen in the previous paragraphs we can adjust in a simple way the coefficients considering the dynamics of the vehicle along some runs. With this approach we are sure that the model is sufficiently valid to perform the dynamics of a sidecar vehicle with different camber angles as shown in the Attachment E. Since in those additional tests we vary the camber angle, we used them not only as a check for the model validation but also to adjust the roll coefficient of the Magic Formula B_φ, C_φ, E_φ, performing the same procedure seen for the adjustment of the macro coefficients.

Roll-coefficients	
B_φ	9
C_φ	0.9394
E_φ	0.1398

Table 4.2 - Macro coefficients for roll for the Magic Formula

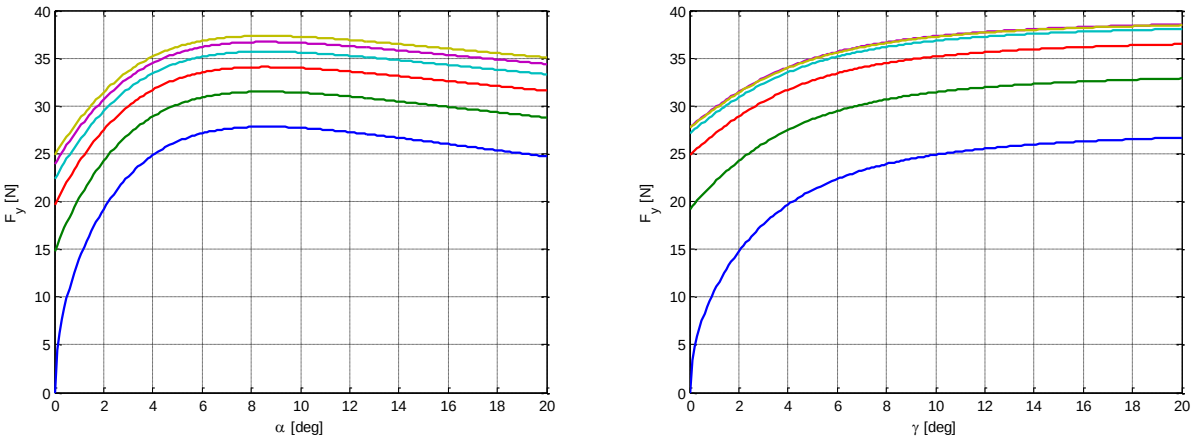

Figure 4-44 Lateral force function of slip and roll angles

5 Sensitivity Analysis

At this stage of our study we have a ready and valid model that can represent and predict the lateral dynamics of a Sidecar, now we want to identify the parameters that mostly affect the behaviour of the vehicle on a curved path inside the whole set of parameters. To identify the right parameters we perform a sensitivity analysis of the system that consist in the choice of some quantities we think affect the performance of the system and make them vary between two or three values inside a defined range. We vary a single parameter at a time in order to avoid the joint effect of two or more variables on the performances of the system.

The global Sensitivity Analysis helps us in this stage since it describes the behaviour of the system when we consider a high variation of the design variables, unlike the Local Sensitivity Analysis in which we see how little variations of design variables, around an equilibrium position, affects the whole system. On the other hand a Global Sensitivity analysis, considering high variable variations, requires higher computational costs of the algorithm while get a better understanding on the critical parameter of the mechanical system.

We will see in the optimization phase a more detailed sensitivity analysis based on linear correlation indexes.

5.1 Design Variables and Performances of the system

At the beginning we have to select a group of parameters as design variable that we think mostly affect the performances of the sidecar dynamics reaching the following set of variables

$$[b_b \ \gamma_r \ \lambda_s \ m_s \ v \ \delta]$$

The first choice falls on the forward shifting of the side wheel with respect to the rear one. This parameter affects the vertical load distribution on the three wheels and then the drivability and steering torque; its variation starts from zero where the side wheel is aligned with the rear wheel of the motorcycle and ends to a thoughtful value.

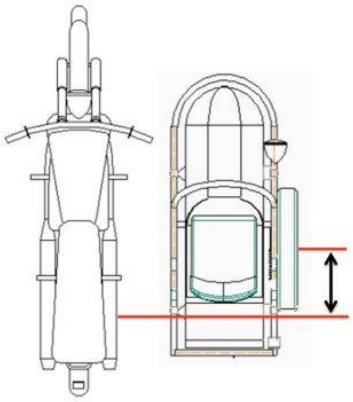

Figure 5-45 Froward shifting parameter variation

A second design variable is the lean out or “camber angle” or in the motorcycle field the roll angle given to the wheels, in our case is more similar to the camber angle of a car since it doesn’t change during the manoeuvre. This design variable affects the drivability of the vehicle acting on the cornering forces and it is obtained tilting the motorcycle and the sidecar one toward the other. The range of variation for this parameter is between -2.5 degrees getting to zero, corresponding to the wheels perpendicular with the

ground, and 5 degrees. A positive value means a rotation, of the side wheel, in the inner side of the vehicle, while a negative one the rotation in the opposite direction. The analysis is made over five levels and uses negative values to observe the dynamics changes over more than one level for each direction of wheel rotation

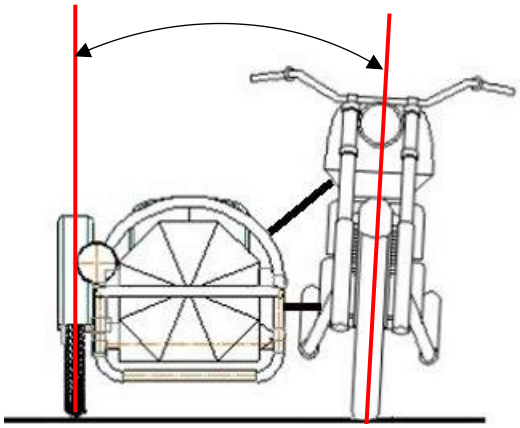

Figure 5-46 Camber angle parameter variation

A third design variable is the toe angle that represents a sort of convergence angle given to the side wheel on the plane parallel to the ground; the parameter influences the drivability of the vehicle changing the cornering force at the side wheel. Even in this case we make it vary between -5 degrees getting to zero, corresponding to the parallelism of all wheels and 5 degrees as shown in the following figure. A positive value corresponds to toe in rotation while a negative one to a toe out. Even in this case the variation is made over five levels to clearly observe the changes in both direction of rotation of the wheel.

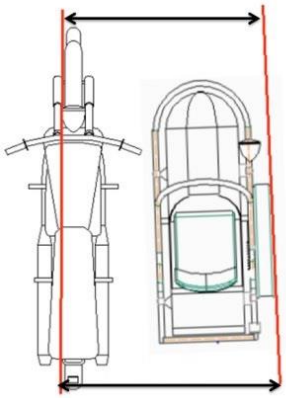

Figure 5-47 Toe angle parameter variation

The fourth design variable we select is the mass of the sidecar that, as for other vehicles, affect the performances of the system like acceleration and vertical load but in our case influences even the overturning tendency of the vehicle when performing right turns and so the safety of the sidecar. The variation of this variable is between the mass of the prototype and the same mass increased by the eighty percent.

The last two parameters selected for the sensitivity analysis are more related to the manoeuvre then the vehicle and are the initial speed of the at which we perform the run and the maximum steer angle of the

manoeuvre; the variation of those parameters are made over three levels as negative speed is meaningless and the steering angle start from zero with positive values corresponding to left curves and negative to right once.

The last two design variables we want to analyse for the sensitivity analysis are not characteristic parameters of the vehicle but characteristic of the manoeuvre we are going to perform and in particular are the Initial Speed of the vehicle and the maximum steering angle; both the parameter parameters affects the behaviour of the vehicle running a curved bath as the variation of the initial speed get an increase/decrease of the lateral acceleration request to maintain the given steering angle affecting the slip angle and then the cornering and vertical forces; in a similar way a variation of the steering angle get a similar variation of the lateral acceleration changing the slip angles and so the cornering forces and the load transfer.

For what concern the performances we want to analyse, as we are not performing an optimization, we consider all the output of the mathematical model and in particular the trajectory, lateral acceleration, vehicle speed, cornering forces and steering torque variations.

The architecture of the algorithm is the same presented in chapter 3 with the only difference that it runs several times to show the outputs for each level of a single design variable variation and plot the results on the same chart to easily identify the effect of the selected parameter.

The parameters are made vary along equi-spaced vectors of five levels in the following range different for each design variable; obtaining the results listed in Attachment F

$$\begin{cases} b_s = [0 \div 95\,mm] \\ \gamma_r = [0 \div 8°] \\ \lambda_s = [0 \div 4°] \\ m_s = [m_{s0} * 0{,}8 \div m_{s0} * 1{,}2] \\ v = [V_0\ V_0 + 5\ V_0 + 10] \\ \delta = [0.5\delta_0 \div 1.5\delta_0] \end{cases}$$

5.1.1 Sensitivity Analysis for a Steering Pad Left

The first manoeuvre we want to observe is a steering pad left, where the steering angle is linearly increased from zero to a maximum value:

$$\begin{cases} V_0 = 25\ {}^{Km}/_{h} \\ \delta_0 = 12° \\ t_f = 20\ s \end{cases}$$

The effect of the b_s parameter on the trajectory is an anticipation of the curve phase while keeping constant the lateral displacement covered during the manoeuvre. The lateral acceleration sees an increase in the first part, while ending in a decreasing of the maximum reached value. The slip angles have a particular behaviour during the steering pad: the front and side wheel's slip angles reduce in the final part of the manoeuvre, while the rear one gets an overall increase with the change of the parameter b_s. The β angle (related to the vehicle) during the manoeuvre is reduced while ending with the same value for all the runs. Taking a look at the contact forces they see quite the same behaviour as the corresponding slip angle,

while in the verticals we obtain an increase for the rear and side; for what concern the front wheel both lateral and vertical forces have no significant variations.

Analysing the effect of camber we can see an advance of the curve phase with an increase of the lateral displacement; that means that the lateral displacement increase for a positive variation, while the opposite leads to a decrease of lateral displacement. Looking at the lateral acceleration we see an increase of the maximum reached value, ranging from a negative to a positive variation of the camber angle. In the vehicle speed figure we notice a greater influence of the speed control loop for positive camber, while for negative one the speed tends to decrease, even if we try to maintain it. The only vehicle characteristic angle affected by this variation, is the beta one: it sees a progressive increase with the growth of the parameter change while, if we look at the wheel slip angles, we notice the opposite effect.

In effect, even if we are performing a left curve their values get progressively form positive to negative by increasing the camber angle; at the contrary the cornering and vertical forces see an increase of their values, going form negative to positive camber angles. We can either notice that the joint effect of the slip angles and vertical forces limits the variation in the lateral forces.

For the variation of toe parameter, as said, we give a positive and negative variation that gives a progressively closing of the trajectory for a positive increase; while we get an opening for its decreasing. We notice in figure F.1-3 the toe figure making the vehicle turn even, when the steering angle is zero. Looking at the lateral acceleration, not considering the first part of the diagram, we have an increase of the acceleration, driven by steering angle increase in the left direction, ending with higher values for toe out variation, figure F.1-7. In a similar way we notice a higher speed value during the manoeuvre for toe out variation, figure F.1-3. The slip angles see a global increase, in the side wheel, going from toe out to toe in; the same we see in the rear slip angle with the difference that all values tends to align to a positive value, corresponding to the direction of the turn; the same effect is observed in the front wheel with the difference that the final values increase for toe out variations, figure F.1-15. The cornering forces follows the same variations observed for the corresponding slip angle, figure F.1-15, while the verticals for the side and rear wheels get a first decrease and then an increase for a toe in variation and an opposite behaviour for a toe out one; in the front wheel we see the opposite behaviour seen for the other wheels, figure F.1-21.

For what concern the mass effect we see a global decrease of the curves with growth of the mass while in the beta angle and the cornering and vertical forces that sees an increase with the changing of the parameter, figures F.1-4, F.1-10, F.1-16, F.1-22.

The next phase is to look what happens when we change the initial speed at which we perform the manoeuvre: the trajectory shows a progressive opening of the curve with an increase of its radius as the speed grows; for what concern the speed profile it tend to drop down the quicker as higher initial speed is, even if we are trying to control and maintain the velocity along the manoeuvre. As a consequence of the higher radius of curvature the lateral acceleration decreases its maximum value with the initial speed vehicle, while the β angle shows a global increase as does the speed (the parameter under analysis); the yaw angle is not influenced too much by the initial speed. The slip angles at the wheels show an increase of the values in the first part of the manoeuvre followed by a drop of the maximum reached values, figure F.1-17. In the cornering forces we see a great influence of the slip angles in the trend of the curves, since have a first rapid increasing, by the vehicle speed change, and then a flattening of the curve, producing the reduction of the maximum value, figure F.1-17.

The maximum steer variation gets an early closure of the trajectory with a progressively decrease of the curve radius, figure F.1-6. The speed sees a gradual decreasing by the growth of the parameter, figure F.1-

6, while the lateral acceleration is increased, figure F.1-12. A particularity in this figure is that increasing the maximum steer in the final part of the manoeuvre the acceleration tends to decrease due to the reduction of radius. All the characteristic angles of the vehicle tend to increase with the parameter, figure F.1-12, while the slip angles and the cornering forces have a behaviour similar to the lateral acceleration, figures F.1-18; the front vertical force has a global increase; while the other two have a decrease in the first and central part of the manoeuvre and then tend to increase in the final section, figure F.1-24.

5.1.2 Sensitivity Analysis for a Steering Pad Right

Another manoeuvre we want to analyse is the right steering pad, with the same inputs as the steering pad left, except the direction of turning: it must be done paying attention if the design variables changes affects in a different way the behaviour of the vehicle because of the asymmetry given by the side wheel.

$$\begin{cases} V_0 = 22.5\ {}^{Km}/_{h} \\ \delta_0 = -12^{\circ} \\ t_f = 20\ s \end{cases}$$

The reduction of the initial speed is due to prevent the overturning effect in this manoeuvre.

The forward shifting of the side wheel increase produces an early closing of the trajectory, and the lateral acceleration of the vehicle increases as well; we either observe a progressive drop of the vehicle speed curve, even if we are trying to maintain the initial speed, figure F.2-1. The changes of the parameter produces a decrease of the front and side slip angles, while the rear one increases, figure F.2-13, with the consequent change of the cornering forces. We observe the increase of the rear vertical force and the decrease of the side one; while the front one doesn't see any variation, figure F.2-19. No changes are observed in the slip angle of the vehicle or the yaw rotation, but we see an increase of the steering torque with the increase of the wheel forward shifting.

The changes in the dynamics, due to the camber angle variation in this manoeuvre, are similar to the those analysed for the left steering pad, just in opposite way. Looking at the trajectory, the curves tend to anticipate the curve phase from a positive to a negative variation of the parameter, shown in figure F.2-2. The lateral acceleration, figure F.2-8, has the same behaviour reaching higher values for negative camber. The same conclusions can be held for the vehicle speed where we see a progressive decreasing of the curves, going from positive to negative values of the parameter, figure F.2-2. The vertical forces present a different behaviour: the front and rear show a decrease, with the increase of the camber angle; while the force on the side wheel is progressively decreased getting close to null values, figure F.2-20. All the characteristic angles of the vehicle present the opposite behaviour compared with the left steering pad, figures F.2-8 and F.2-14. The joint effect of vertical forces and slip angles brings an increase of the lateral forces, with the decrease of the considered parameter, figure F.2-14.

The toe angle otherwise gets a significant change in some of vehicle quantities, like the progressively advancing, and closing of the trajectory, the decrease of the vehicle speed going from toe in to toe out variation that we can observe in figures F.2-3. Taking a look at the vehicle characteristic angles we notice the decrease, in a different way, of both beta and yaw angles, as the toe angle gets higher, figure F.2-9. The opposite effect can be observed in the rear and side wheels slip angles; while the front wheel shows at first an increase, slowing down proceeding in the manoeuvre, and ending in a drop down of the maximum value, plotted in figure F.2-15. Going on with the analysis, we take a look at the vertical forces: the front and rear one follow the same variation with a first drop down and then a rise up with the run for toe in variation, and the opposite behaviour for a toe out; otherwise the front vertical force show the opposite trend than the other two with the overlapping point of the curves shifted forward along the time axis,

figure F.2-21. In figure F.2-15 we can see that the cornering forces, as said in the other cases, follow the behaviour of the slip angles as the vertical forces.

Considering the mass variation of the sidecar we notice a quite null effect except for the trajectory, tending to reduce the distance covered by the vehicle. We see a negative effect on the lateral acceleration, and the vehicle speed: due to the increase of the mass, both the quantities decrease; the mass increase reduces the yaw rate of the vehicle, as it requires more energy to rotate. Taking a look at the characteristic angles of the vehicle we can see a decrease of all slip angles, caused by the reduction of the speed, figures F.2-10 and figure F.2-16. The other effect of the mass increase is the growth of the vertical forces, effect enhanced by the load transfer for the rear and side once figure F.2-22. The joint effect of slip angles and vertical forces produces a quite null variation of the cornering forces, figure F.2-16.

Now we want to see the effect of the initial speed change in the behaviour of the sidecar performing the same manoeuvre. As for the previous manoeuvre, the trajectory covered by the vehicle shows an opening of the curvature with an increase of the radius for a growing initial speed, figure F.2-5. Even the trend of the vehicle speed shows a progressive drop of the final value with the increase of the initial speed; this happens despite the corrections of the seed control loop, figure F.2-5. The lateral acceleration shows a reduction of the maximum reached value due to the increase of the curvature radius with the parameter change, figure F.2-11. For what concern the characteristic angles we see the increase of the maximum β angle and a little decrease of the yaw one, figure F.2-11, while all the slip angles tend to decrease their values during the manoeuvre as shown in figure F.2-17. In figure F.2-23 we can see that the side vertical force has a progressive increase of its value, caused by the reduction of the lateral acceleration and so the load transfer while the other forces, after a first decrease, reached higher values in correspondence of higher initial speed. The joint effect of vertical forces and slip angles causes the drop of all the cornering forces drawn in figure F.2-17, where is stronger the effect of the slip angles as the theory prescribes.

Taking a look at the variation of the maximum steering angle for this manoeuvre, and analysing the figures F.2-6, F.2-12, F.2-18, F.2-24 we can notice that the dynamic, due to the parameters change, are the same as for the Steering pad left manoeuvre; the only thing that changes is the sign, for we are studying a right turn path.

5.2 Sidecar Dynamics Parameters Optimization

With the same parameters used for the first rough sensitivity analysis we want to perform an optimization of some performance indexes of the sidecar dynamics that from now are named as objective functions whose final aim is to define a set of optimal parameters that grant high drivability performances and safety of the vehicle while reducing the tardiness of the driver.

5.2.1 Selection of the objective function

As said before the design variable are the same as shown in the sensitivity analysis and the only thing to do is define a set of objective functions able to describe the optimization problem we want to solve.

Since we are looking to optimize the drivability performances of the system the best objective function that represents this problem is the maximum acceleration along a defined curved path while for what concern the safety of the vehicle we can define two objective function. The first one is given by the maximum yaw rotation of the vehicle in the braking phase along a straight line

A high yaw rotation produces a generation and consequently increase of cornering forces in the contact patch reducing at the same time the longitudinal braking one and so increasing the braking distance of the vehicle; on the other hand this yaw rotation can cause an overturning of the vehicle centred on the front wheel or an exposure of the side of the vehicle to possible impacts. The second objective function showing the safety of the vehicle is the minimum vertical load on the side wheel performing a right turn; in this case the reduction of vertical load in this situation increase the tends of the vehicle to overturning with the detachment of the wheel from the ground.

The yaw rotation function is obtained running a simulation of the vehicle along a straight line with the following input parameters

Input Data	
V_0 [Km/h]	50
δ_{max} [deg]	0
t_{end} [s]	4
F_p [N]	30
F_l [N]	15
Driver + Passenger	

Table 5.1 - First Simulation input data

While the overturning objective function comes from the simulation of the vehicle running a right turn steering pad with the following input parameters

Input Data	
V_0 [Km/h]	22.5
δ_{max} [deg]	-12
t_{end} [s]	15
Driver + Passenger	

Table 5.2 - Second Simulation input data

A fourth objective function that can be selected in order to increase the drivability of the vehicle is the maximum steering torque when performing a turn; we choose this function because the steering torque affects the tardiness of the driver while it must be greater than zero in order to give a better feeling of the curve to the driver.

This objective function is obtained simulating the run of a left steering pad with the following input parameters

Input Data	
V_0 [Km/h]	25
δ_{max} [deg]	12
t_{end} [s]	15
Driver + Passenger	

Table 5.3 - Third Simulation input data

Since any optimization algorithm uses a minimization architecture to reach the optimal set of design variable we have to rearrange the objective functions as they can be minimized. In particular we notice that we want to maximize only the lateral acceleration and the vertical load on the side wheel, so we consider the negative of those functions as they can be maximized when using a minimization algorithm.

5.2.2 Spearman Coefficient

Defined the objective functions we have to be sure that are all necessary for the optimization process, in other words we are looking what happens to the other function when we want to minimize one of them.

We can perform this procedure calculating the Spearman coefficient that calculate if exists any kind of monotonic correlation between two data, where they can be an output and input of a system or two design variables or two objective functions. This relationship can be obtained because the coefficient doesn't use the values of the data but the rank of the corresponding values inside the dataset

$$rank = \frac{1}{N}\sum_{i=1}^{N} rank_i \qquad [5.1]$$

And then the Spearman coefficient is obtained as

$$r_s = \frac{\sum_{i=1}^{N}\left[rank(y_{1,i}) - \overline{rank}(y_1)\right]\left[rank(y_{2,i}) - \overline{rank}(y_2)\right]}{\sqrt{\sum_{i=1}^{N}\left[rank(y_{1,i}) - \overline{rank}(y_1)\right]^2 \sum_{i=1}^{N}\left[rank(y_{2,i}) - \overline{rank}(y_2)\right]^2}} \qquad [5.2]$$

The Spearman can be calculate even for more than two data at the same time with the help of the Matlab command "`[rho,pv] = corr(fo,'type','Spearman')`" obtaining the following matrix

$$\begin{bmatrix} 1 & 0.7478 & -0.1447 & -0.7537 \\ 0.7478 & 1 & -0.2115 & -0.8938 \\ -0.1447 & -0.2115 & 1 & 0.3984 \\ -0.7537 & -0.8938 & 0.3984 & 1 \end{bmatrix}$$

The Spearman correlation matrix is a matrix whose number of rows and columns are equal to the number of objective functions and each element represent the level of linear correlation between each objective function, then we can have three different conditions:

- If ρ_{ij} tends to 1 we have a progressively strong direct correlation between the two objective functions
- If ρ_{ij} tends to -1 we have a progressively strong inverse correlation between the two objective functions
- If ρ_{ij} tends to 0 we have no direct correlation between the two objective functions

We can also notice that the terms on the diagonal are ones due to the fact that represents the autocorrelation of each objective function. The coefficients allow us to determine if we can delete some function to the optimization problem, in fact if the we have a strong direct linear correlation between functions minimizing the first one we minimize even the other, so we can optimize only one function obtaining a simple algorithm due to the fact that we are sure that we are minimizing even the other function.
Taking a look at the Spearman matrix we notice a high direct correlation only between the first and the second functions while we have a low direct correlation between the third and the fourth ones; for what concern the other functions we can see a high inverse correlation between the first and the forth functions and the second and the fourth otherwise the inverse correlation gets low between the first and the third functions and the second and the third. In conclusion we could think to delete the first or the second functions because of the high value of the correlation coefficient but they have a high inverse correlation with the other two functions, so we can finally say that none of the objective functions can be deleted from the optimization process due to the combination of the correlation coefficients. Even if we can think to simplify the algorithm deleting the first one from the process because of its meaning, in fact it represents the maximum acceleration of the vehicle and our vehicle is not focused on performances but on comfort while the other functions refer to safety and tardiness of the driver we prefer to optimize those ones.

5.2.3 Objective Functions Approximation

Taking a look at the problem we notice that the objective functions are calculated from a complex multi-body system performing different conditions so the algorithm will take more time to calculate the objective functions than for the optimization of the parameters, to solve this issue we can use an approximation architecture in order to obtain an interpolation function able to give the functions we are looking for from the given input with a lower computational cost; this approximation function is given by a Neural Network.

The neural network is an approximation algorithm based on the biological concept of a brain where we have neurons connected one to each other and the information is transmitted to each neuron that elaborates it, starting by this concept we built a network of elaborating units that take the values of a function, re-elaborates it and then transmit the new output to the next neurons and the process goes on up to the last layer of neurons that gives the final approximation, the neurons of the same layer works in parallel to speed up the approximation; every neuron takes as input the sum of the outputs of the neurons of the previous layer, or the starting sample, multiplied by a proper weight and shifted by a bias defined in the training phase. The output of each neuron is given passing by the activation function that is a not decreasing function like a linear, sigmoid or tangent one.

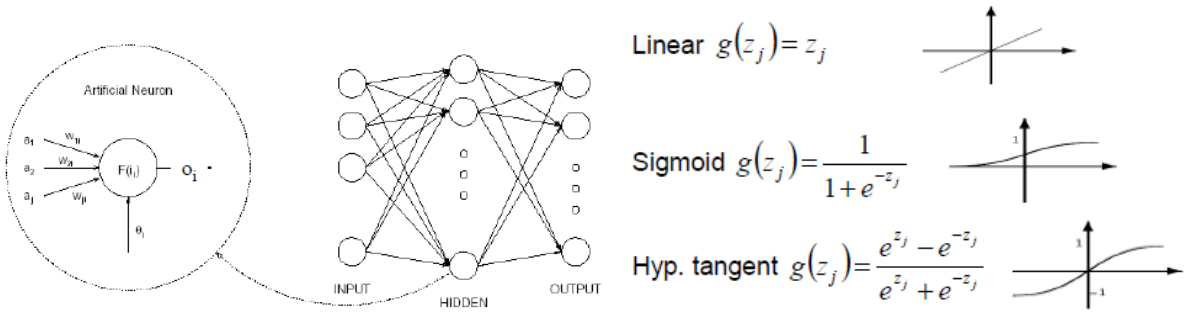

Figure 5-48 Neural Network architecture

The weights and the bias, for each neuron, are given during the training phase of the network by different rules, the one we use is the Back Propagation Learning Rule. This idea of this rule is to use the error between the output of the single neuron and the expected value of the neuron from the input data and then with the errors of all neurons minimize the squared sum of them setting the weights and bias.

$$E^2 = \frac{1}{2}\sum_{i=0}^{N_0} e_i^2 \qquad [5.3]$$

To do that the rule starts calculating the errors from the last layer where we have the final outputs and then propagates backwards the process to the previous layer knowing the expected values form the previous step. Weights and bias at first are guessed and then the rule optimize them minimizing the total squared error and the training phase stops while the generalized error function, after getting closer to the training one, starts increase

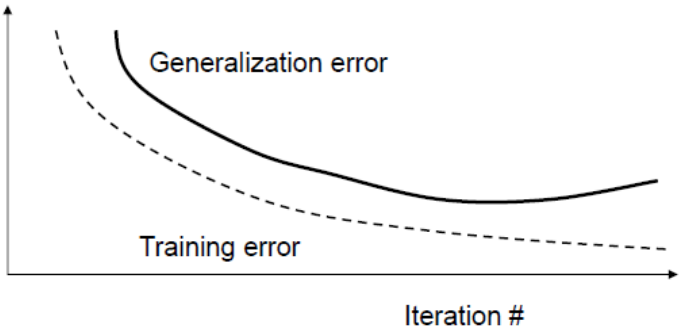

Figure 5-49 example of training graph

Because the increase of the error is the sign that are going to overtrain the Network and loose the general approximation instead of specializing on fitting the input data.
By the following steps we can define and train a neural network for every approximation from a generalized architecture:

- We start defining the design variables values that the algorithm has to take as input and the objective functions value that are its output, the populations are made of a small number of samples
- Then is useful to normalize the inputs and targets of the neural network in a range [-1 1] in order to obtain an easier and generalized training of the algorithm. After the training session we have to reconstruct the inputs and outputs of the algorithm

- In this phase we have to define the architecture of the Neural Network in terms of hidden layers, number of neurons for each layer and training function. For the last one we use the default option that follows the Levenberg-Marquardt training algorithm. As part of the architecture definition we set the percentage of samples and the maximum number of epochs for the training session of the network
- The next step is to train the neural network with the previous architecture in order to see if the algorithm approximates in the right way the starting problem and avoid the overtraining. At the end of the training phase we can add a string where we save the algorithm in order to avoid the training phase in the next runs

In this phase we change the numbers of layers of the Neural Network and the number of neurons for each layer till we obtain a sufficiently precise approximation of the objective function; using the following parameters inside the algorithm:

- Two hidden layers with 6 and 8 neurons
- 80% of the samples for the training
- 20% of the samples for the validation
- Maximum number of epochs 200

We obtain the following results for the approximation with a starting population of 10000 elements for each design variable

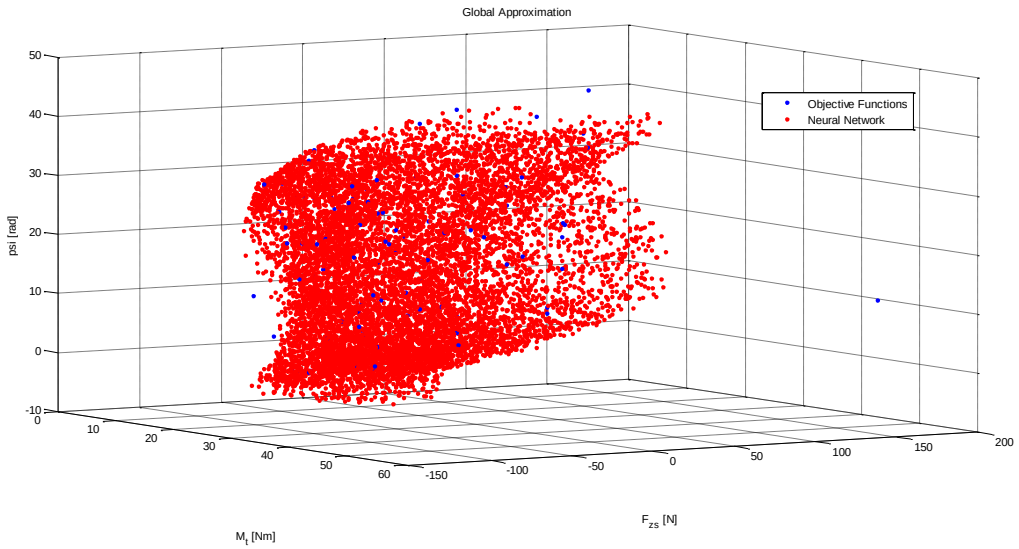

Figure 5-50 Objective functions approximation

As we can notice the simulated data well approximates the starting data without overtraining and going in details in the training of the algorithm we can see

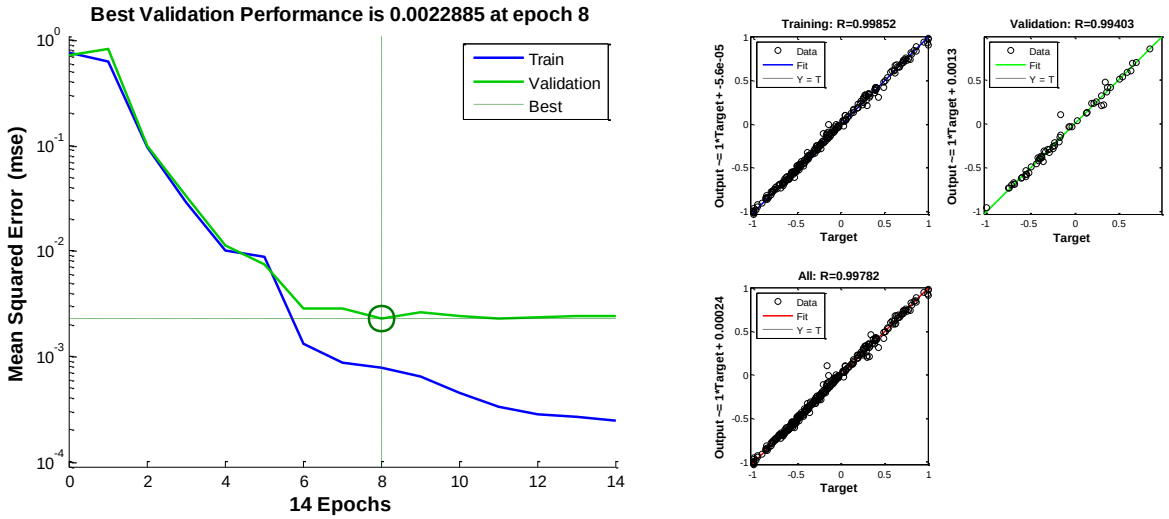

Figure 5-51 Training error and regression plots of objective functions

In the left diagram we can see that the mean squared error of the training and the validation phase are so small and close one to each other, then in the right diagram we can see that the starting data for each objective function falls on the regression line.

At the end of the process we can run the Neural Network with a larger number of samples then the starting once.

5.2.4 Optimization Algorithm

At this stage we have all the elements we need to perform an optimization algorithm for our problem, the last choice we have to do is the algorithm to perform the optimization. Looking at the set of architectures we studied for a multi-objective optimization we can discard the first and second order algorithms due to the fact that they need the first and second derivative of the objective functions that we don't have at disposal since they belong to a Neural Network; even the Pareto Optimal set is not the best choice for our problem because we want to perform a minimization with four design variables and the Pareto Optimal set needs an equi-spaced grid of element with a dimension equal to

$$n_{cdv} = n_v^{n_{dv}} \quad [5.4]$$

That contains all the possible combination of design variables element; it obvious that increasing the number of design variable and the number of elements the input matrix becomes bigger and the computational cost for the algorithm increases as well.

Our two options are to perform an equivalent objective function using the Weighted sum method or the Genetic Algorithm.

Since the Pareto Optimal set is too heavy to perform when dealing with more than two design variables we use the Constraint Method. The idea of this algorithm for multi-objective optimization problems is to perform the optimization considering only one objective function and use the other ones as constrain for the first one. What we do is impose the other objective functions lower than a certain level, different for each function, and then minimize the first one, varying the level ε of the constrain function inside a "for" loop; the final result is the definition of the Pareto optimal solutions in the objective functions space and in the corresponding design variables one. With this approach we use to different algorithm, the sqp and the

interior point to perform the constrained method where the first one is a method that solves, for every iteration a quadratic programming problem allowing us to mimic the Newton's method for a constrained problem. Then the second one constructs approximations inside the domain set building barriers against leaving it

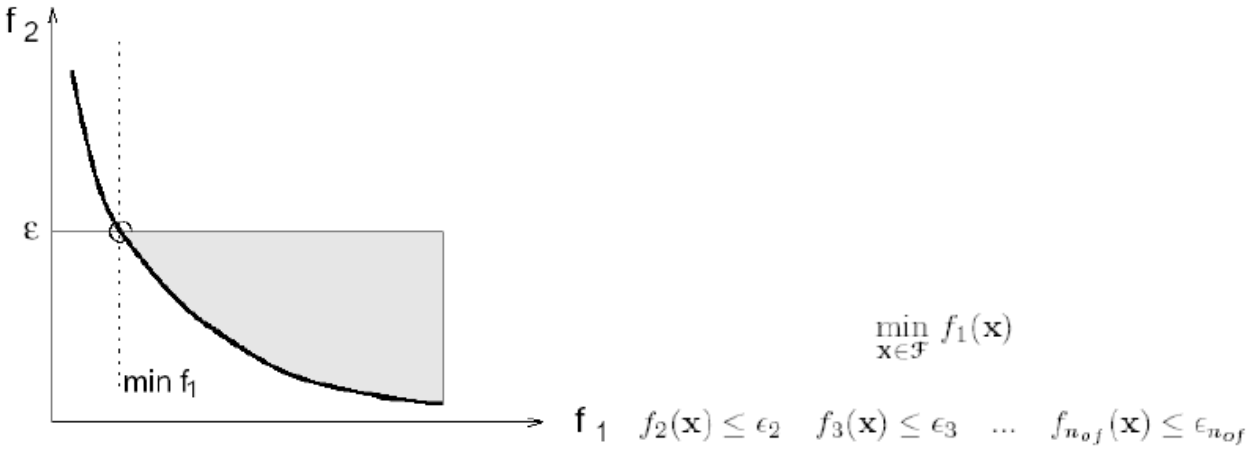

Figure 5-52 Constrain Method for two objective functions

This method is more powerful than the Weighted Sum because it can be used even when the Pareto Optimal set is not convex in the objective functions domain

Starting with the biological concept of the evolution of the species we try to implement it for a numerical problem of the maximization of a simple two variables function, shown in the previous paragraph, that represents a circumference, to do that we start selecting two random populations of samples in a certain range of values that represents the "parents" and calculating the fitness of the population. The design variables randomly vary in a defined range and are made about N of samples, where we set N equal to 200.

With the population of parents and its fitness values we go on with the coding phase, for this step we code the entire population in binary code generating a sequence of 1 and 0 of the length of n bits, that represents the elements of the population, the coding is necessary to generate the chromosomes for the next step of the algorithm.

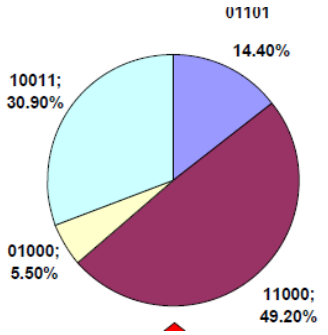

$$p_i = \frac{F_i}{\sum_N F_i}$$

Figure 5-53 wheel of fortune for genetic algorithm

Then we generate the offspring from the starting population with the crossover function. This function implements the wheel of fortune idea to select the elements of the population to breed and generate the

offspring, with this idea we set a probability of crossover and if some elements of the population falls into this crossover threshold some string of bits are mated otherwise they are propagated to next generation unchanged

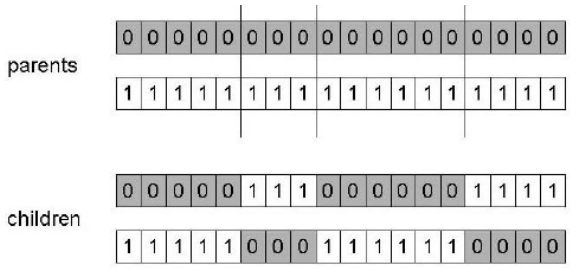

Figure 5-54 crossover process

After the crossover of the population and the generation of the offspring we can add a mutation phase, differently from the previous case we set a probability of mutation, a number between 0 and 1 is generated for each element of the offspring and if it falls within the mutation range one or more chromosomes of the element are mutated, typically changed from 0 to 1.
Then we have the decoding of the offspring from the binary code to the real one in order to generate the new population and calculate their fitness values.
The final step is to evaluate the best candidate that has to constitute the next generation selecting the elements with the higher fitness from the parents and the children populations by the discard function; this function selects as element for the next generation the once that has the highest fitness values from the parents and offsprings population.
All the previous steps have to be closed inside a loop in order to obtain a final population with highest fitness that corresponds to the solution for our optimization problem, in fact the stop condition for the algorithm is when the average fitness of the final population is the highest possible or if we reach the maximum number of generations.
For our case we set the algorithm with the following parameters:

- Number of bits 8
- Probability of mutation 0.5
- Maximum number of generations 200

The crucial part of this algorithm is how we generate the fitness of parents and children and since we have a multi-objective function the fitness can't be the output of the objective function. We create a routine where we use as fitness the inverse of the rank of the Pareto optimal solution of the population where the rank is the Pareto Optimal layer where the single solution belongs, following the next steps

- With the starting population of design variables we calculate the objective functions one to build up the matrix for the computation of Pareto Optimal set. This matrix is composed of j columns where the first once are the design variables, then we have the objective function, the "flag", the "rank" and the "fitness"
- The next step is to calculate the Pareto Optimal Solution with the sorting method as seen in the Passive Suspension Laboratory, where all the optimal solutions are flagged with a zero in the "flag" column and to these elements of the population we assign a rank equal to one.

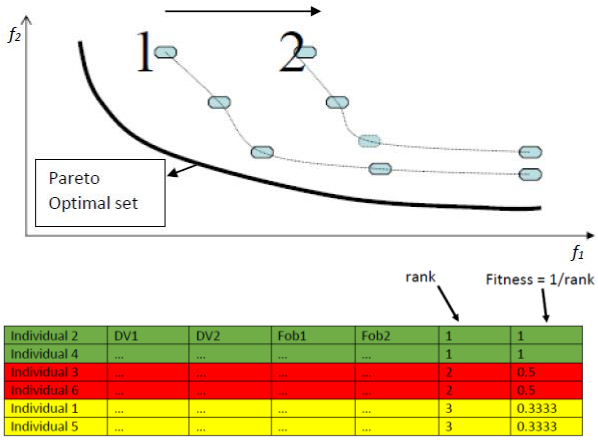

Figure 5-55 Pareto Optimal set layers

- Then we delete from the matrix the Pareto Solutions and then we perform again the sorting method, with the new matrix, obtaining a new set of Pareto Optimal solution at which we assign a rank increased by one with respect to the previous one
- We keep cycle that procedure storing the Pareto optimal solutions in the output matrix till the initial one is empty, progressively increase the ranks. The fitness is obtained by taking the inverse of the rank for each element of the population

From the explained algorithm we choose the last one to perform the optimization of the parameters of the vehicle as it is more robust to handle a large number of design variables. This algorithm uses as input a random population of 200 elements varying inside this range:

$$\begin{cases} b_s = [23.5 \div 95\ mm] \\ \gamma_r = [0 \div 8°] \\ \lambda_s = [0 \div 4°] \\ m_s = [m_{s0} * 0{,}8 \div m_{s0} * 1{,}2] \end{cases}$$

b_s [mm]	γ [deg]	λ [deg]	m_s [Kg]
52,84	3,88	1,19	25,68
32,77	0,83	0,84	25,66
…	…	…	…
43,77	0,71	4,51	28
58,86	1,34	4,71	26,14
…	…	…	…
95,46	2,42	4,55	35,26
74,94	1,92	0,99	24,25

Table 5.4 - Starting random population for the optimization algorithm

That bring the optimization algorithm to reach the following solution. In the following we report the results of the Genetic Algorithm

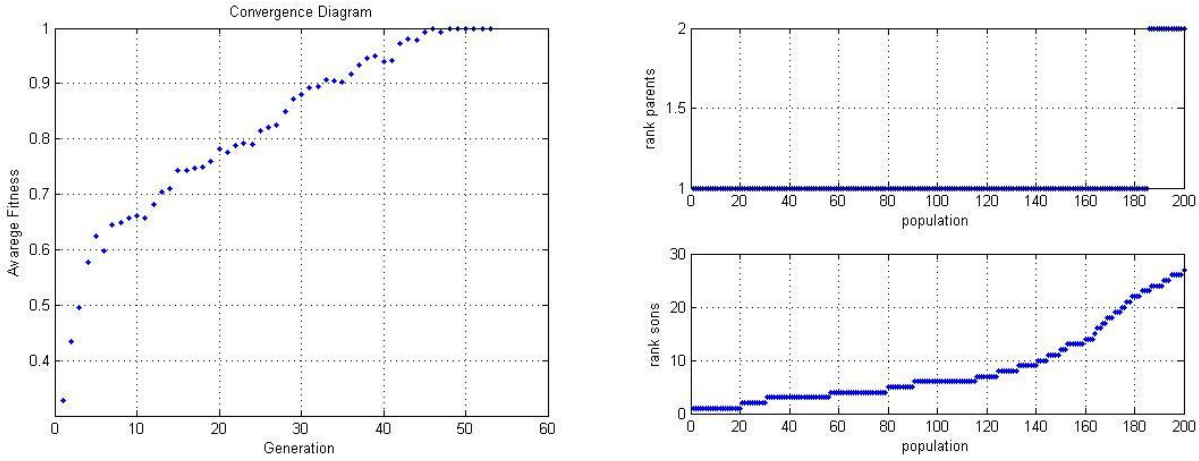

Figure 5-56 Mean Fittness and Ranks along the Generations

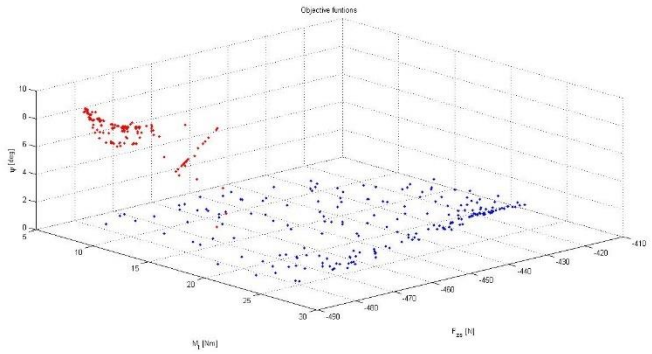

Figure 5-57 Initial and Optimal solutions in Objective functions space

On the lower figure we can see the evolution of the objective functions, from the first generation in blue dots from the last one representing the optimal set in red dots; in the left figure we can see the evolution of the mean fitness function of the analysed population along the generations and as we can notice the fitness is quite high starting just from the beginning and reaches value 1 in quite few generations, helped by the mutation and discard sub-routines. The last figure on the right shows in the upper part the rank of the parents along the generations while the lower the rank of the sons. In the following we report the optimal set used to verify the optimality of the solution but a larger dataset is listed in the Attachment F:

b_s [mm]	γ [deg]	λ [deg]	m_s [Kg]
42,28627	2,509804	0	27,64744

Table 5.5 - Optimal Set

At least we randomly extract a set of value from the obtained optimal population, and with those variables we run the model obtaining the results listed in Attachment G. At this stage we want to see if the optimization process increases the performances we are looking for, so we plot those results over the standard configuration curves of the vehicle for the manoeuvre of steering pad left, right and braking.

Looking at the results listed in the Attachment G we can see that, for what concern the selected objective functions the steering torque is quite the same as the standard vehicle for all the manoeuvre. The side wheel vertical force has a little increase in all the runs, sign that we are preventing the overturning issue; even the maximum rotation during the braking phase is a little reduced then for the standard vehicle. Taking a look at the lateral acceleration, even if we choose to not use that function in the routine, shows a little increase for the left curve while a decrease for the right one and in the central part of the braking. Globally we can say that the choose a set of parameters, that is not far from the standard configuration of the vehicle, optimizes the chosen performances of the sidecar even if the results shows a difficult of the optimization to reach an appreciable increase of the objective functions caused by the different behaviour of the vehicle performing left and right turns.

6 Conclusions

This project has the task to formulate a simple mathematical model able to describe the lateral dynamics of a sidecar vehicle. We started with simplyfying hypothesis, helping us in the reduction of the number of degrees of freedom and equations of motion; nonetheless, during the validation process we reintroduced some of them as the results were too far from the real vehicle. Then, writing the equations of motion for the vehicle followed, using a bi-dimensional multibody system with rigid bodies. This multibody set of equations required some sub-models to calculate the interactions between tyres and the road, and the torque to driving wheel.

Unfortunately, about tyres, the macro coefficients for the Magic Formula related to the real tyres were unavailable, and we were forced to use similar model ones. This implies that we have an additional uncertainty on the behaviour difference between the vehicle and the model. The same can be said for the engine model; as shown in the first chapters we used a simple interpolating formula to get the torque at the rear wheel; this formula does not take into account many non-linear behaviour of the engine. The clutch release, and the lag during acceleration and braking transitory are the heaviest. It is well known that a complete model of the engine requires many parameters to identify the correct behaviour, as well as the tyre's, and high calculation costs getting the entire model more difficult to define: in other word, some uncertainty about the modelling can be either due to modelling errors, in details too simplified equations, or to the tyre model.

To be sure that the model reproduces the behaviour of a real vehicle we built a third prototype of sidecar and used it to perform a set of chosen tests; comparing the model with the vehicle test runs we can define the accuracy of the model, to predict the behaviour of such a system: this is the validation of the model. In this phase we selected some tests not only to validate the lateral dynamics model, but also to set up and reduce the uncertainty of the contact and engine models, as described in the validation dedicated chapter. The challenging part of this phase was to set up the tyres and engine parameters, and then change the hypothesis or equations inside the model in an iterative way, in order to let the model to have the same behaviour as the vehicle.

As the model has beed successfully validated, we proceed changing a set of characteristic parameters for the vehicle and the manoeuvre: this is to see the changes in the Sidecar behaviour, in order to find the parameters that mostly affect the performances of the vehicle; this is mandatory to define the design variables for the next optimization phase. At the end of this phase we observe that the most influencing parameters are the camber and toe angles, while the increase of sidecar mass – and its distribution – reduces the tendency of overturning performing right curves.

With the design variables selected in the previous step, we perform an optimization of some relevant objective functions for our sidecar vehicle: since it is not a vehicle focused on performance, we preferred to optimize the safety of the sidecar. The results of the optimization showed that the standard configuration was close to the optimal solution found. The vehicle is enough safe even in the starting configuration; this is an expected result as this is the third prototype, where the previous two have already been modified during their testing phase.

During the modelling process, we faced some issues related to the peculiar kind of vehicle under study. The clearest one is the geometrical asymmetry: it was presented in the third chapter and is closely related to the construction: a motorcycle is joined to a cart with a single wheel, that brings the steering axle on a side of the vehicle and the wheel of the cart is shifted forward with respect to the rear one. With this configuration, we can see that the running on a straight line the vehicle tends to turn on the in the direction of the cart: so the driver has to give an angle to the steer to keep the vehicle running on a straight line.

The other one is related to the inertial characteristics, and in particular to the position of the centre of gravity, as shown in the first chapters. This mass distribution asymmetry causes a different behaviour while performing a left or a right turn: this is due to the load transfer during the manoeuvre. In effects, during a

left turn, the lateral acceleration increases the load on the side wheel, this makes the vehicle more stable. Otherwise, when performing a right turn with the same steering angle and approaching speed, we notice that the lateral acceleration and the load transfer tends to unload the side wheel. This can cause the detachment of side wheel from the road, leading to a non-stable and unsafe motion of the whole vehicle. As we can see from the sensitivity analysis, the only way to prevent this phenomenon is to increase the mass of the cart, or move it towards the wheel, even if this will be penalizing the performances of the vehicle.

Al the other parameter variations, do not affect the overturning effect of the sidecar.

In conclusion we can say that this kind of vehicle is not far, from a dynamic point of view, from a car; while, due to its compact dimensions, it is sensible to the actual drive configuration. In other words, the number of passengers and the weight of the vehicle affects not only the performances of the vehicle, but even its safety. Nonetheless it is more stable than a motorcycle, because of the presence of a side wheel, that prevents the vehicle to fall aside; at the same time, it not as safe as a car: the overturning especially with only the driver is a critical condition: so, at the end we can say that this work is focused to provide the designer a model helping to solve this important issue.

The optimal distribution of masses on the vehicle could be achieved using the presented model, inside an optimization algorithm, as we did for our objective functions.

As said before the critical issues of the model, except those related to the type of vehicle, are due to the engine and tyre model. The only way to solve them is to go on with a test campaign, following the already existing approaches, to calculate the exact coefficients of the tyres; while for the engine, the best thing to do, will be to formulate a simple model able to take into account the losses and lags of a small size internal combustion engine. For what concern the mathematical model, it will be better to expand the validation process with tests coming from other type sidecar, to be sure that the model is general.

We can eventually say that the model formulated in this document is fairly simple but general enough to analyse the lateral dynamics of a sidecar, establishing the starting tool that the designer can use to build or optimize a vehicle of this type.

6.1 Conclusions and Further Development

The work done in this thesis is just preparatory to a deeper study of the dynamics of sidecars to improve vehicle behaviour: the model, at the moment, tells us only how the vehicle moves and how it interacts with the ground.

From this point, the model can be used to analyse the loads coming from the road, to investigate how they are absorbed by the sidecar frame and transmitted to the motorcycle (and vice versa), and then to the driver and passengers. In this way a deeper handling and comfort analysis, is made much easier.

About the dynamics behaviour study, the model could be refined with additional field test on tyres and engine, to get a more detailed and realistic and actual model. For example, the release of the clutch should be modelled much better, even at the cost of an increasing complexity of the model itself.

Furthermore, the actual model could be completed adding some degrees of freedom: to start, taking into account the traction at the side wheel and up to a three-dimensional model that represents the complete dynamics of the system including the suspension’s kinematics and also, last but not least, to the introduction of the degrees of freedom due to movements of the driver and the passengers.

Another very important area of further development will be the study the stability of the system, to find critical velocities, eigenvalues and natural frequencies: this could be obtained by linearizing the motion equations, hence by developing the model in the opposite direction – simplifying it.

From the loads defined above, coming from the wheel, it will be possible to evaluate the frame loading, an analysis to be performed with a FEM approach. In this way, it will be possible to better define the size and the thickness of the tubes. Another analysis that can be done through the data of the optimization algorithm will be the definition of how the mass of the sidecar should be spread over the frame, in such a way to prevent as much as possible the overturning issue. For example, using the FEM data it can be possible to use different thickness of the tubes in some parts of the chassis to 'move' weight on one side or the other.

Based on the same data, it will be possible to study how to 'move' accessory components of the sidecar like battery, additional fuel tank, luggage and even the passenger seat, in such a way to place the centre of mass in the best position to improve the performance and the driveability of the vehicle.

This optimization can be done in a fast and easy way using the mathematical model presented in the previous chapters, avoiding the empirical method, used since today by all other sidecars manufacturer, to modify an existing prototype and see how the changes affects driveability and performances.

In conclusion, all the work done in this project is mainly an initial milestone to better understand and optimize a complex system like the sidecar.

The sidecar as an everyday-use vehicle is not appealing, but there is a large cluster of users that are interested to such a vehicle for leisure. For this reason, studying to obtain a safer and better performing vehicle is not only an academical research, as a series production of a safer and better driveable sidecars can be the key point to make sidecar fans much more satisfied of such a product.

Attachment A - Description of the company and the Vehicle

In this chapter we will present the company and the vehicle the sidecar will be coupled to, to realize the experimental test.

A.1 The RMG-Tech s.r.l. Company

RMG-Tech is a company born in 2005, involved in the mechanical coupled to electronics, I.e. the newly named mechatronic fields. The aim of the original partners was to create a company able to guarantee a high know-how and technological experience in the automotive related mechatronics field, specially in the motorcycles one. The company has a registered office in Cassina de' Pecchi (Mi) and the operative office in the industrial district of Melzo (Mi).

Figure A-58 two MK V vehicle produced in 2017

The primary operative field of the company is the automotive; but an enlarged area of interest comprehend general industry and buildings/construction. The purpose of RMG is to give outsourcing services, consultancy and realization of prototypes, as well as small productions for other companies operating in the above mentioned fields.

The business started in 2005 was focused on the realization of an electro-actuated gear shift for a small car with the construction of a prototype; in the meanwhile, from the company partner's experience the business goes on with some collaborations in the motorsport with the use of their products in races.

The RMG-Tech in motorsports cooperated with partners like Andreani Group, Team PSG-1 and Liberty in the World SuperBike Series, Team X-ONE in the Wolrd Endurance Championship, Scardino workshop for the repairs of structural issues on two-wheeled vehicles. Among the suppliers we have Kulite Semiconductors and DSPM for the electronic components and sensors while National Instruments and AIM-sportline for what concern the data acquisition system for vehicles.

In 2013 TBD Motor ltd of UK, owner of the motorcycle brand "The Black Douglas Motorcycles", commissioned to RMG-Tech the design and realization of a small series of motorcycles. With the year 2015 the production of those vehicles covered quite the whole production of the company, up to year 2017. In 2016, TBD motor decided to realize a sidecar vehicle, with the aim to evaluate the feasibility and refine the look for future

commercial developments. This was aimed to increase the range of The Black Douglas Motorcycles vehicles, with only a part of the huge cost of the development of a new vehicle.

Today, RMG-Tech range of devices and accessories for the design and production is dedicated to testing for vehicle components or end-production tests, for mechanical or other structural components, and, eventually, accessories for race vehicles.

All the primary activities are keep in the technical assistance to race teams for motorcycles races.

A.2 The Black Douglas Motorcycles - Sterling Autocycle Mk V

The Sterling MK V is the last model designed and realized on the basis of a Sterling motorcycle prototype, that holds “The Black Douglas Motorcycles” brand. The vehicle is unique, compared to the actual proposal of other builders, as the frame is of under barrel type, typical of 1920 motorcycles the company took inspiration from.

On the basis of the design realized by some artisans in a single prototype vehicle, the MK V version is the engineering result of RMG-Tech work on the commission of the manufacturer, TBD Motor ltd, with the aim to realize a small series of vehicles with that design. From 2015 the vehicle obtained the EURO 3 regulation approval, and is sold all over Europe and other countries like South Africa, Australia, New Zeland and Canada. The vehicle is available in two motorizations: 125 cc and 250cc.

Engines are supplied, already assembled and tested, by a Taiwanese supplier; it is based on 1970 Honda’s CG125: this family is equipped with air cooling system and carburettor fuel system. This engine has been choosen for its simplicity, and the coherent design with the motorcycle, permitting to realize the desired vintage look for the vehicle.

Figure A-59 Sterling mkV 230cc.

Several components of the motorcycle are designed and built ad hoc for this vehicle; just a few are bought off the shelf from suppliers like engine, braking system, lights and wheels. This choice is made due to the – obvious – absence of components with a design able to fit on a '20 motorcycle on the actual market.

The first step made by the company was to analyse and measure each component of the existing motorcycle, built by the artisan, and then design it using a 3D CAD software. In this way a digital archive is created where every part of the vehicle is present and can be easily declined in different versions.

Inside the 3D CAD software, the vehicle is digitally assembled; in this way the designer could check that all the modify to the prototype vehicle are compliant with the project constraints, all the parts couplings are correct and there were no interferences between moving parts and so on. A careful analysis and review of the geometrical dimensions of the motorcycle has been performed at the same time, and the best parameters have been found and chosen to obtain a vehicle with a good driveability and an easy feeling; this leads to a vehicle that can be used everyday, despite his uniqueness of a kind.

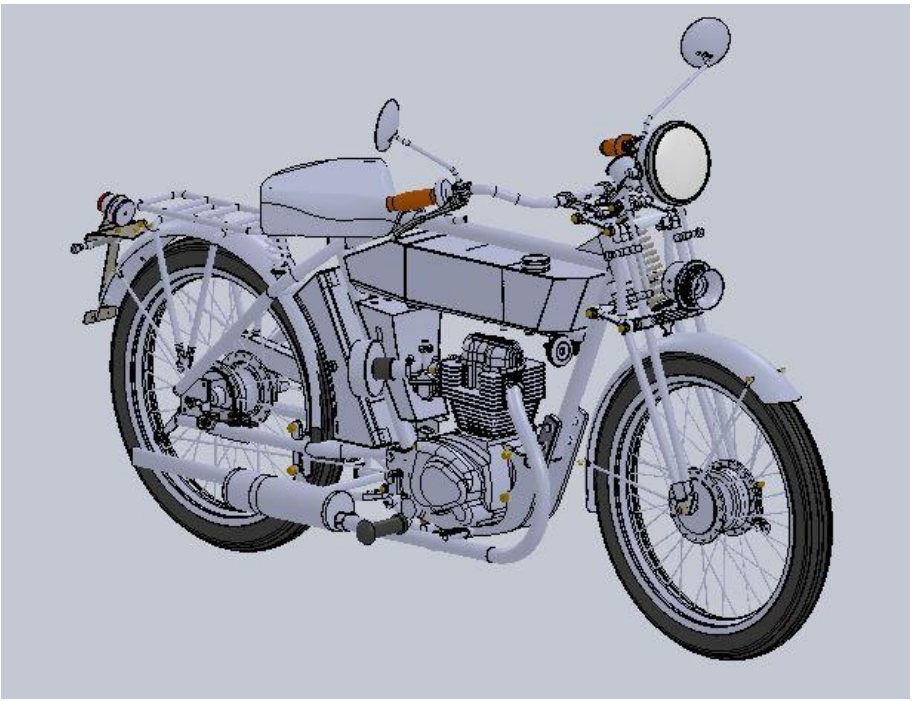

Figure A-3 Soldworks 3D model of the Sterling MK V

The following step was to commit the production of each designed component to external suppliers, in order to have the elements necessary to build the motorcycle, starting from the most important, the tubular frame.

Once obtained the first three prototypes, the esthetic design of the motorcycle was checked; this phase was conducted selecting the best matching version to the desired vintage style, or in other words, the components with the best look on the vehicle: in any case, keeping in mind at the same time the simplicity of production.

The first difference in the engineering of the vehicle, versus the prototype, was the use of lighter materials like high strength aluminium (Anticorodal and Ergal) on many parts, versus the the first prototype steel-based ones. This obviously was done in order to decrease the weight of the motorcycle. All the remaining structural parts, like the frame, are still made of hi-strenght steel, with the exception of the front fork that is a mix of

high strength steel and aluminium alloy. Eventually, all the bodywork is made of aluminium alloy named peraluman – while the fenders are made by stainless steel to lower the thickness to minimum.

Another major task of the project was realize a vehicle the easiest to assemble as possible, in such a way a skilled owner can provide to maintenance and customization of the motorcycle without too many and/or specific tools, or the need of a dedicated workshop.

For what concern the customization of the vehicle, the future owner can choose between 36 colours and 8 types of leathers for the seat, and between several accessories that can be added to the standard motorcycle, realizing a personal and unique vehicle.

Just a few examples: it is possible to add toolboxes and wicker basket to the rear luggage rack, that is at the same time designed to hold the passenger seat. The front headlight is available in two types, one of them has been realized ad-hoc for the vehicle. It is possible to mount a gear lever heel and toe or single, the choke control on the handlebar, several leather coverings for the boxes, the cables and so on, there is the possibility to choose a speedometer of different clock-type in two diameters and – eventually – to choose the finish of several parts in brass, or nickel-plated or copper instead of the standard black paint.

A.3 The Black Douglas Motorcycles - Military version and Sidecar coupling

The company started in november 2015 a program to develop a sidecar to couple to the Sterling MK V vechicle, already in production. Launch customer and key development was a canadian company named 4CMR, a non-profit created to remember the canadians died in the battle of Vimy, april 2017. Their aim was to obtain a working copy of the vehicles used by canadians (in effect triumphs) to run a commemorative tour in Canada for the 100th year of the battle.

Figure A-60 Example of Canadian Sidecar

The specification was simple: to copy an existing vehicle coupled to a Douglas bult in 1916, found in the collection of a private owner in Canada. During 2016 a prototype was built – time schedule was very tight – with geometrical parameters of first trial, copied mostly from the original 1916 vehicle.

Of course a number of issues were found in the prototype, and one entire year was needed to fix them. Unfortunately the complete vehicle 3D-model was ready and available to help during the design phase just after the first prototype was built. In any case, part of the work was done in another dissertation thesis named: "*Realizzazione del prototipo di un sidecar con l'utilizzo di tecniche di prototipazione virtuale*".

Figure A-61 First Sidecar Prototype

With this model a number of structural issues were corrected, as well as a number of improvement were possible. A second prototype was built during 2017, with all the improvement needed, suggested by the experience made with the first one, as well as by the knowledge gathered with the 3D-model, while the first itself was overhauled to be equal to the second one.

Figure A-62 Sidecar realized for the Canadian customer

In july 2018 a visit in Canada reported the actual state of the two prototipes: up and running in Toronto!

And eventually, a third prototype was built in spring 2018 to make possible the testing needed for the final set-up of the model – as well as the writing of this script. The frame is ready while the body of the sidecar will be completed shortly.

Figure A-63 Two finished Canadian Sidecars

Attachment B – Sidecar in The World

B.1 Sidecars in England

Sidecaring began in England just after the turn of the century. It is fitting that the history of English sidecar manufacturers begins with Watsonian. Several British sidecar manufacturers in recent prominence include Heddingham, Gemini, and Saluki. The Wessix, well known in the mid fifties, faded, returned, and faded yet again. Only Watsonian-Squire, and Heddingham continue making sidecars today although others have joined recently.

Of all sidecar makers, Watsonian conjures up stability of sidecaring throughout the world and is a household name for many sidecarists and is the only surviving manufacturer who went into business to produce sidecars over 90 years ago and continue to do so today. Watsonian continued activities in racing and competition. They made racing outfits for the best drivers, including world Sidecar Champion, Eric Oliver.

The small wheel development for street hacks in 1954 took advantage of the lower center of gravity of the sidecar, a racing development. A strong chassis and a more robust suspension ended structural problems. Watsonian introduced the Kenilworth and the Maxstoke Saloon, both in two seater configuration. The semi-monocoque body also came from racing. The glass-fibre made pleasant curves and sweeps easy to design and build. More significantly, it lowered production costs when steel and wood construction costs were becoming significantly higher.

By the mid sixties, Watsonian was the only sidecar manufacturer in England - all other competition had lost out to the Austin Mini.

Watsonian, although producing 17 models, sought other markets. They produced thousands of reinforced polyester/glass Bambini sidecars and Bambox commercial side boxes for motor scooters. They expanded into hard tops for MG sports cars, side panels for BSA motorcycles, and dodgem cars for fun fairs. They made children's miniature four wheel one- and two-seater cars with engine sizes up to 120 cmc and more stuff: sidecar production accounted for about one-third of their total production. In simple economics, it was diversify, or fold. This is reason for they to merge with the other largest sidecar manufacturer in the UK, Squire company.

In any case, Watsonian weathered the storm and still produce the Monaco, a single seater with lockable trunk. Other favorites include the Palma, a child-adult version of the Monaco; and the Monza, a super sports single adult. The Monza is an updated Flight. The Grand Prix, another favorite, is a single seater sports version. A recent development is a larger unit based on an improved and strengthened Super Silk chassis. The Oxford can seat three or four adults. The Cambridge, on the same chassis, has a full double bench seat that seats two and includes a spacious trunk.

Figure B-64 Two different Watsonian models

Another important sidecaring company in England was the Squire Sidecars (Bushfield Ltd.) in Warwickshire.

The company, in 1972, restored Rolls Royce Silver Ghost's and other vintage cars. Diversification in 1974 resulted in a high quality single seater sidecar for modern motorcycles. Sidecar interest grew with their first model release in 1975. Sales doubled each year until they became the largest sidecar manufacturer in Europe making over 1000 sidecars each year. Export sales account for nearly 70 percent of production. Squire distributors are in most European countries and account for nearly 70 percent of production.

Their current catalogue illustrates 10 different models including dual width sidecars, trailers, and cargo side boxes. They have special contracts with several countries, including Egypt, Nigeria, Canada, Japan, and Kuwait. Their premature introduction to America failed as liability insurance difficulties became insurmountable. Eventually, they merged with Watsonian in 1988, to form as previously stated the Watsonian-Squire company.

The makers of the humble Swallow sidecar, produced after World War I, can be justly proud of their offspring, the Jaguar racing and saloon cars. William Walmsey, son of a wealthy coal merchant, made the first Swallow sidecar. William had no interest his father's coal business. He preferred to buy and renovate war surplus Triumph motorcycles.

The Swallow had sporty lines and a comfortable passenger seat. Aluminum panels on an ash frame enclosed the octagonal Zeppelin-like body. A polished aluminum disc on the wheel enhanced the sporting image. A touch of luxury was the close fitting coupe top which reduced visibility to nil. Walmsey turned out one unit a week, making almost everything himself. His sister did the upholstery and trim, later done by his wife. The chassis came from Haydons of Birmingham. The price of the sidecar was thirty two guineas or about one hundred and thirty five dollars.

Figure B-65 Swallow sidecar model

Swallow sidecars were raced at the 1924 Isle of Man TT with Harry Reed finishing second on a 344 cc Dot-JAP-Swallow. Tinkler brought a Matador-Blackburn with Swallow chair into third place. Reed remained loyal to Swallow in 1925, though he changed to a Matador motorcycle. A lighter sidecar model intended for competition grew out of this racing activity in 1925.

The Nottingham Police purchased several Brough Superior motorcycles fitted with Swallow sidecars in 1927. A new chapter in the Swallow story opened when they produced the first Austin Seven Swallow two-seater car in 1927. It had a podgy looking body fitted onto an Austin Seven chassis. This started them on the road to auto world glory and away from motorcycles.

The sidecar business carried on for a time. They built a universal chassis for mounting on either side of the bike for left- or right-hand drive. This unit sold very well in Switzerland. A launch style body came in 1928 which avoided the fabric covered body made popular by Weymann.

Cars took over the Swallow factory in the thirties while sidecar construction took only a small section of the factory. Their models included the Standard Swallow of 1930, the elegant SSI and SSII of 1932, and the sporty SS Jaguar i00 in 1936.

They still produced about 100 sidecars a week until the outbreak of World War II. During World War II, Swallow supplied large numbers of box sidecars to all three services and the National Fire Service.

After World War II, development of the SS Jaguar or Jaguar continued. This produced a succession of models from the Le Mans winning C and D Types to the XKE models, to the current XJ's.

Introduction of the Swallow Gadabout scooter, with a 125 cc Villiers engine, came in 1948. An option included a commercial sidecar box. They ceased production prematurely in 1951, just four years before the Scooter boom hit Britain.

Cars were re-introduced with the Swallow Doretti in 1954. It used Triumph TR-2 mechanical components.

Competition from the cheaper and faster TR-2, and the Austin Healey I00, soon brought production to an end in March, 1955.

In October 1956, Watsonian Sidecars purchased Swallow Coachbuilding and transferred operations to their Factory in Greet, Birmingham. Production of this sidecar line ceased in 1967.

The Motor Cycle published an illustrated description of a sidecar with options of electric or acetylene lighting in their November 1922 issue. Montgomery's of Coventry made the chassis. They also made

complete sidecars. In 1924, they switched to a pentagonal body shape and brought the price of the

lightweight touring model down to ninety dollars.

The Coupe-de-Lux with hammock seat, Triplex screen, and a luggage compartment in the pointed

tail sold for one hundred and twenty dollars. They proudly displayed their own sidecars on their own stand at the 1923 Motor Cycle Show. They also had the satisfaction of seeing their sidecars on the Brough Superior, Coventry Eagle, Dot, and Matador stands also. George Brough listed the Coupe-de-Lux model as the standard sidecar on Broughs from 1924 to 1927.

B.2 Sidecars in Germany

Steib's name was legend for quality at home and abroad. So exacting was Steib's production that BMW commissioned Steib to build sidecars for them using the BMW emblem. Steib made sidecars for BMWs and Zundapps during World War I. The heavy outfit was quite successful on the Western Front and in the Sahara Desert. The driven sidecar wheel made the outfit virtually unstoppable. Steib built thousands of units. The Allies destroyed the Nurnberg factory during a bombing raid. Down, but not out, work continued in the bombed out factory in 1945. They made a civilian version of the famous Army model (no gun mount). This was the Grune Elefant TR500 model.

Figure B-66 two Steib different models

By 1949 the factory was turning out 12,000 to 15,000 units per year and exporting them to 36 countries. That was the year the Deutsch Mark replaced the Reich Mark.

Steib produced slight variations on six major sidecar themes. The earliest was the S500/501, the familiar bullet shaped design so loved by sidecar manufacturers of the era. Tension springs supported the body on the early models. The most significant design advance was the leading axle torsion wheel suspension used in later models.

The various Steib models were the LS200, S250, S500, S501, S350, TR500, TR502, RSI, RS2, LT200 and the RSTI. The RS series were for scooters while the last two were tradesmen's boxes. The bodies were of fine quality steel with high quality protective finishes applied. Stelb used highly finished aluminium hardware. The fittings were robust, simple, and straight. Their sidecars fitted most motorcycles.

While the economic recovery made Germany prosper in the fifties, it cast the death knell for the Steib family business. The now affluent populace demanded the people’s car. Agricultural machinery construction replaced sidecar assembly in the Steib shop. The factory ceased building sidecars in 1960 but

Steib is not forgotten. Collectors search eagerly for Steib sidecars. Spares are available while replicas of many models are in Japan, Germany, India and the United States.

B.3 Sidecars in USA

Sidecaring began in America, as in many other countries, just after the turn of the twentieth century, and for the same reasons. The motorcycle could not accommodate a passenger while the 4-wheel car was beyond the reach of the average person.

Sidecars were popular in the early days with many manufacturers in the trade. Most faded from memory. Their popularity declined as inexpensive transportation such as the Model T Ford and the later Model A appeared. There were very few sidecars on the highways in the United States from the early thirties until the late sixties.

Only Harley-Davidson continued to make sidecars from the pioneer days to present. The sidecar revival began in the late sixties with the growth of motorcycle popularity. The International appeared briefly in Minnesota. The Side Strider by Doug Bingham, made its appearance in 1968. Frank Thompson Zuch introduced his Cyclecar in 1971, while the Spirit Eagle came in 1972. Their sidecars had many things in common.

They were lightweight (100 to 140 pounds, that is 45 to 65 kg) with universal mounting systems. They cost between $300 and $425 and were suitable for the lighter bikes of that era, such as the bikes from the UK and from Japan.

Sidecar popularity grew in the early seventies as manufacturers promoted their products. Several articles of and about sidecars appeared in motorcycle journals and periodicals. Over 100 sidecar outfits gathered at the first Griffith Park Sidecar Rally sponsored by Doug Bingham in 1971. This Rally continues today at the same location with up to 500 outfits in attendance. The sidecar returned as practicable vehicle for the small family.

The popularity of the sidecar attracted many entrepreneurs to this field. A partial list of US sidecar manufacturers, past and present, includes:

1973- Simon (now the Motorvation Sypder) .

1974- HitchHiker

Goodwin

*Centaur (later revived as the Zephyr).

*American Easy Rider.

*Freedom.

*Cycle Mate.

1975- *Essix.

*Vetter Terraplane.

1976: *Cycle Camper.

1977 : Kenna (by Automarket) .

Spyder T-I (by Motorvation).

Coupe Royale (by Motorvation) .

1978-*Equalean (by Wallick).

* These models are no longer in production.

Few manufacturers prepared themselves for the serious struggle to produce a long lasting product.

They did not survive the economic recession of the mid seventies. Manufacturers now face the increasing complexity of dealing with governmental regulatory bodies and stringent warranties, as they must ensure the absolute safety of their products and undergo difficult approval process.

Just a few years after the invention of the sidecar, Hugo D. Young obtained a motorcycle sales agency in Mansfield, Ohio. If he allowed the sidecar wheel to tilt as the motorcycle tilted when turning, he could take curves faster and safer.

The sidecar would attach with flexible connections. This invention would also allow the wheel to rise or fall over uneven ground while keeping the sidecar level.

Mr. Young made a flexible unit in 1912 for his own use. A traveling salesman friend suggested he obtain a patent. Seeing commercial possibilities, he suggested manufacturing the device. That patent inspired the "knee-action" design found in later automobile suspension systems.

Carl F. Dudle joined Young in 1913 as a partner in the Flxible Side Car Company. Patent disclosure dictated the unusual spelling. They incorporated the company in 1924.

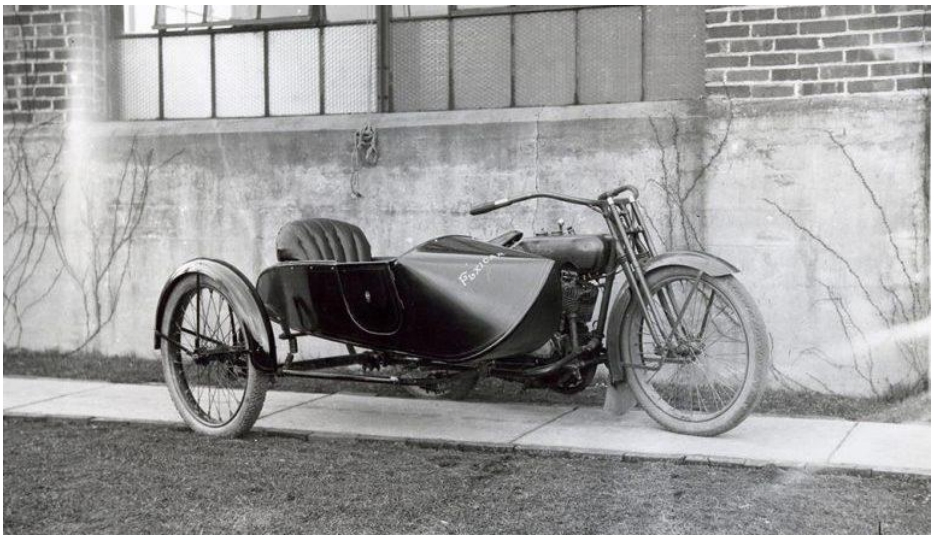

Figure B-67 1913 Flexible model

The Flxible was an improvement over conventional sidecars and soon became a favourite of many sidecarists, notably for sidecar racing.

All major sidecar racing records soon fell to motorcycles equipped with Flxibles. These sidecars fitted Harley-Davidsons. Thors, Hendersons, Indians, Reading-Standards, and Excelsiors. They sold Flxible's

to dealers and individuals. Many went overseas.

The company built its own factory in 1916. It soon became the world's largest exclusive manufac-

turer of sidecars. The single seater with a door was the most popular model. They also had a side-byside

two seater, and a convertible top model. During World War I, they only made olive drab sidecars to fit Excelsior Motorcycles for use by the Allied Armies. The sidecars went to New York for shipment overseas. On arrival, they were uncreated, fitted with a machine gun, and attached to the motorcycle. They were very fast, and an efficient means of destruction in combat areas.

They deleted the word "sidecar" from their name in 1919 to reflect potential diversification. The cost of the Ford T dropped as the result of the depression. Now it competed, dollar for dollar, against the motorcycle and sidecar. The popularity of the sidecar outfit declined while the popularity of the T increased. The Flxible Company moved from the sidecar trade into coach building and the rest is history. Rohr Industries of California purchased Flxible in 1970. The Grumman Corporation bought Flxible four years later, but after another property change the company went into bankrupcy in 1996.

A Flxible Sidecar appears just a page or two ahead of the modern buses in the last company brochure.

There were several other sidecar manufacturer in the US.

The Motorvation Engineering company built Jerry Simons' Spyder T - I, and Ed Millray's Coupe Royale in 1976. Jim Sontag purchased the company in August, 1979. The Roadster Royale, a convertible version of the Coupe Royale, came in 1980.

Figure B-68 Spider T and Coupe Royale models

The Formula II made its debut in 1981 using an exclusive patented adjustable lean-out device by pre-loading the suspension.

Figure B-69 Formula II model

Popularity of the Formula II outstripped production of other models from 1983 to 1987. They returned, by popular demand, with an improved external frame. The heavier models included an adjustable suspension. They offer a wide range of sidecars with quality fittings and mountings, and a Back Pack cargo trailer. The trailer is towed behind a solo motorcycle or a sidecar outfit.

Robert Odell and William Heggarty founded Sidecar Restorations, Inc. in 1970. Heggarty's outfit, a 1966 BMW with Steib TR 500 sidecar, created widespread interest. The two teaching partners spent their summers in Europe on motorcycles.

They looked for old sidecars for restoration and resale. This business soon mushroomed into a full time venture. The Company moved into larger quarters and later Brian Casey joined the organization.

They imported EML sidecars, kits, and complete outfits from Holland a few years ago. The new company name reflects ths success of this venture. EML of St. Louis is the sole United States importer for EML. They have a small dedicated dealer network. They install one half the sidecar units imported while their dealers install the rest.

A related company, BMW Motorrad of St. Louis, is the largest BMW dealership in the world. They operate the largest paint facility for BMW motorcycles outside the BMW factory. Their specialty is applying BMW paints to any BMW part, including complete motorcycles. They carry a huge inventory of BMW parts and support a toll free parts order phone line. They stock mounting sets for all popular BMW models. Universal hardware is generally available for all makes of motorcycles.

Those wishing a classic style sidecar or inexpensive transp, or may choose the Ural imported from Russia. This is a good buy in sidecars. It is solid, a copy of the civilian version of the WW II German military sidecars.

As Sidecar Restoration, they restored over 400 Steib sidecars. Several were re-exported back to Germany. Restoration continues as part of their operation. At least one restoration project is always in progress. Many Steib parts are always on their shelves.

Leaning sidecars have been around since 1903. In the hands of a professional, they outperformed a conventional rigid hack.

P.C. Harrington Johnson built his own rig in 1932 from scrap. He used a picture of a Harley-Davidson banking sidecar as a model. "We had enormous fun with it on the road. It was a real delight to sail up to a Bobby on point duty (traffic cop), stick out your right hand at a quite impossible speed, grin at his horrified gape, and chuck the whole outfit on its right ear (left hand chassis) as you scuttled round the corner...all three wheels banking at an impossible angle as you went around at solo speed. It did not work quite the same to the left and the "independent springing" effect of the sidecar wheel made the light chair hop skittishly over bumps and into potholes.

"The setup did have two serious difficulties...you had to park it offside - on to the kerb, propping the footrest on the pavement as the outfit would not stand straight by itself; the other was that the darned thing skidded just like a solo over wet tramlines (trolley car tracks). The outfit was not really intended for serious sidecar passenger carrying...the passenger had to sit very still, bang in the middle, and let the bike and sidecar wheel lean round him, which was rather unnerving."

(From Motorcycle Sport, November 1978)

Waly Wallick developed another way to pilot an outfit like a solo. His patented linkage allows hands-off driving, with or without a passenger.

An Equalean outfit can lean in curves to the right or the left within allowable lean limits. The independent linkage transfers few stresses to the cycle frame. This is good news to those with late model machines designed for solo operation.

Figure B-70 Equalean leaning sidecar

Such machines may have light frames not suitable for heavy duty sidecar operation. Wear on the sidecar tire is about the same as for the motorcycle front wheel. Gas mileage drops by only two or three mpg. The outfit handles equally well, whether loaded or not. No ballast is necessary for an empty sidecar. Turning requires little effort.

No changes required in the steering department. Heavier front fork oil and possibly air caps are desirable. The sidecar requires only minimum effort to mount or de-mount. Alignment is nearly automatic.

The future of this machine depends on the sidecarist. Does he wish to operate his outfit in a manner similar to his solo bike, or does he prefer a rigid machine?

The Equalean was available from the Jamison Fabrication Company of California. But nowadays it is no longer available.

The earliest sidecars fitted to Harley-Davidsons came from Flxible and other sidecar manufacturers.

Sidecar history is scarce from 1903, the year the factory started, until 1919, when Harley-Davidson made sidecar models for military use.

The H-D factory made sidecars. The Seamen Body Company also made sidecars for H-D.

Some 3257 sidecars were sold in 1924, or 1 for every 2 V-twins sold that year. One Indiana dealer purchased 41 Vtwins, all except 1 sidecar equipped.

A pointed nose graced the 1930 sidecar for 74 model motorcycles. The sidecar featured interchangeable jiffy wheels, and an internal expanding sidecar wheel brake used with the rear brake. It had semi-elliptical springing as standard equipment.

Twin headlights were available for the motorcycle and the improved electrical system included an automatic voltage regulator.

The 1929 Enthusiast, the factory news journal, reminds sidecarists to adjust the connecting bar so the motorcycle leans slightly away from the car (or truck) body. It is wrong for the motorcycle to lean toward the sidecar. With the connecting bar properly adjusted, you will not feel any side pull.

The basics of sidecaring remain the same today. The 1929 Enthusiast also tells how two young Chicago girls drove from Chicago to New York, then from Chicago to the West Coast and back to Chicago on a Harley-Davidson outfit.

Grocery package Harley-Davidson trucks were quite common, according to the photos in the Enthusiast. The 1933 Harley-Davidson Package Truck, Model MXP, and the Servi-Car were given a substantial price reduction.

The basic Harley-Davidson in those years cost less than a 1914 Harley-Davidson. They sold the machine without electrical systems or lights, no footboards, small tires, and a two speeds transmission. It delivered only 8 hp. The 33-LS sidecar for the 45 costs only $90 while the 33-LT sidecar for the 74 costs just $15 more. The former had coil suspension up front. A full combination sold for a modest $415.

An OHV 61 joined the Vee twin line-up in late 1936, while an 80 SV became top of the line. The 45 and the 74 continued in production.

The three larger engines used roller bearings in their flywheel assemblies. The needle pointed sidecar gave way to a pleasing round nosed sidecar, their basic style for the next thirty years. Sidecars and Servi-cars were assembled in the top floor of their extensive ten-acre floor space factory.

William Connelly, A.M.A. Commissioner of District No. 4, with co-pilot Fred Dauria, captured the transcontinental sidecar record. They completed the 3300 mile run from New York City to Los Angeles in only 69 hours, 46 minutes in 1936 on an 80 Harley-Davidson outfit. At no time was the engine stopped for more than 8 minutes at a time during this period. Over one million people who attended the opening of the Boulder Dam saw these pioneers who were guests of honor at the ceremony. Their return home was more leisurely and included many vacation stops and a visit to the Harley-Davidson Factory.

H. Persoon won the International Six-Day Trials in 1936 on a 61 OHV outfit. His passenger was V. Ripel.

Harley-Davidson produced the FLH Classic Sidecar to celebrate their 75th Anniversary. Their famous 80 1340 cc V-twin engine, rated at 80 hp, powers the unit. Fork trail reduction improved maneuverability.

Figure B-71 FLH sidecar model

Increased total gearing retained good acceleration. The three interchangeable die-cast wheels come with MT-90-16 tires. The FLH is two-tone tan and cream with hand applied pin striping.

B.4 Sidecars in Japan

The first motorcycle imported into Japan was an English Thomas in 1904. The first major importer of motorcycles was Fatabaya of Akasuka, Tokyo, who brought Indians from America. Later, Yamaguchi Inc., imported the british Triumph in 1910, and Yamada-Riseikan of Kanda, Tokyo, imported the NSU from Germany in 1912. Importation of Indians increased. In 1916, the Japanese Postal Service imported the Yale, a 950 cc V-Twin from Consolidated Manufacturing, Toledo, Ohio. Toyko had just 37 motorcycles registered in 1916.

The Japanese army used many sidecar combinations in 1918, while the Japanese Police used the Big Red Indian in 1919. Most motorcycles used in Japan in the Twenties were for official purposes although some 3-wheelers did find their way into civilian service.

Narazo Shimazo made the first Japanese sidecar in 1925, the Yero-First. He also made the first domestic motorcycle, the Yero-First motorcycle. It had a 4 stroke side valve engine with a 3-speed transmission and reverse gear. He made a V-Twin in 1935 in premises now owned by Mazda.

Sankyo built a Japanese version of the Harley-Davidson, the Rikuo, under a license from the Milwaukee Factory, in 1931. The 1936 models included a rear transmission to drive the sidecar wheel and the rear wheel.

Military vehicles supplied to the Japanese Army in World War II included the Mazda, Kuroyane and the Rikuo. The military police sidecar drivers are called Kenpei, while sidecar mounted police of the Imperial Families are the Konoe-Hei. Some civilians, usually doctors, drove sidecar outfits.

They used conventional sidecars fitted to Ariel's (imported by Yamada-Rinseikan) or to Moto-Guzzi's (imported by Mikuni-Shoten). Mikuni now (2018) makes carburetors and throttled bodies. The military version of the Rikuo continued in production after World War II, but for civilian purposes. The 252 Rikuos were 90 percent of the total Japanese motorcycle production in 1946. Japan now makes 13 to 16 million motorcycles each year.

Sabaru produced a 169 cmc sv Rabbit scooter with a DS-I sidecar, and Mitsubishi produced a 148 cc sv

Silver-Pigeon scooter, also with a sidecar. Rikuo continued to produce a Japanese 200 cc sv V-Twin

VFD with a 1930's Harley-Davidson style sidecar.

Figure B-72 Rikuo and Kuroyane models.

Surplus aircraft fuel tanks were popular as sidecar bodies because of the shortage of raw materials in the post war era. Journalists and Police Departments favored sidecar units.

The Minato sidecar, produced by Fuji-Kogyo, fitted motorcycles and scooters. The Yasui sidecar, by Yasui-Kogyo fitted the Rabbit Scooter. The Izumi sidecar, by Izumi-Kogyo fitted the L.E. Velocette and other machines.

The Minato sidecars, originally made for Meguro and Honda, were later exclusive to Yamaha. Minato, through their Fuji-Kogyo outlet, made sidecars for other brands. Sidecar production ceased in 1966 because of the introduction of Minicars such as the Daihatsu 3-wheeler 200 cc 2 stroke. The last sidecar of the post war era was the Sanshin boat of fiber glass construction (all prior sidecars were of steel). Sanshin is now part of the Yamaha complex. The detachable Sanshin body also served as a boat with an outboard motor

fitted. The Japanese had lost interest in sidecars by this time.

Sidecar revival came to Japan in 1968. One of the sidecars exhibited in the 1968 Japanese Motor Show was a racing type sidecar fitted to a Kawasaki Mk III. Another was a conventional sidecar fitted to a Kawasaki WISA 650 cc OHV Twin.

These sidecars, built by M. Ohta of Tairiku Motors, were on the Kawasaki stand. The WISA, or WISS in America, was a copy of the British BSA Twin. Meguro designed it for Kawasaki.

Kawasaki obtain their sidecars from Tairiku Motors, the only sidecar manufacturer. Tairiku also made sidecars for private sale to enthusiasts. The President, Mr. Masayoshi Ohta, was the importer for BSA and BMW. He also sold rebuilt Steib TR500's. He developed a streamlined fiber glass body to fit BMW's and Moto Guzzi's. Sidecars cost about the same as a motorcycle because of their hand construction.

The Japanese Land Transportation Office denied Kawasaki permission to sell and register 200 motorcycle combinations because of the unique driving technique for a sidecar combination. They felt it strange to have one technique to turn to the right, and another to turn to the left. They finally allowed that 30 were okay but 200 were dangerous!

This absurd notion remains with the Land Transportation Office. Another oddity is that while Japanese sidecars are “unsafe”, foreign sidecars are “safe”. Watsonian and Harley-Davidson exported sidecars to

Japan in 1970, followed by the Bingham in 1973, and the Bender and Velorex in 1974. The Ural and Dnieper came in 1976, the Squire in 1978, and the American Spirit in 1979. The Chonjian and the Don-hai came from China in 1980 and 1981, respectively. Some imported exclusive models such as the EML and HMO privately. Only dedicated sidecar enthusiasts own and drive sidecars in Japan today.

Attachment C – Sidecar Datasheet

C.1 Vehicle Draw

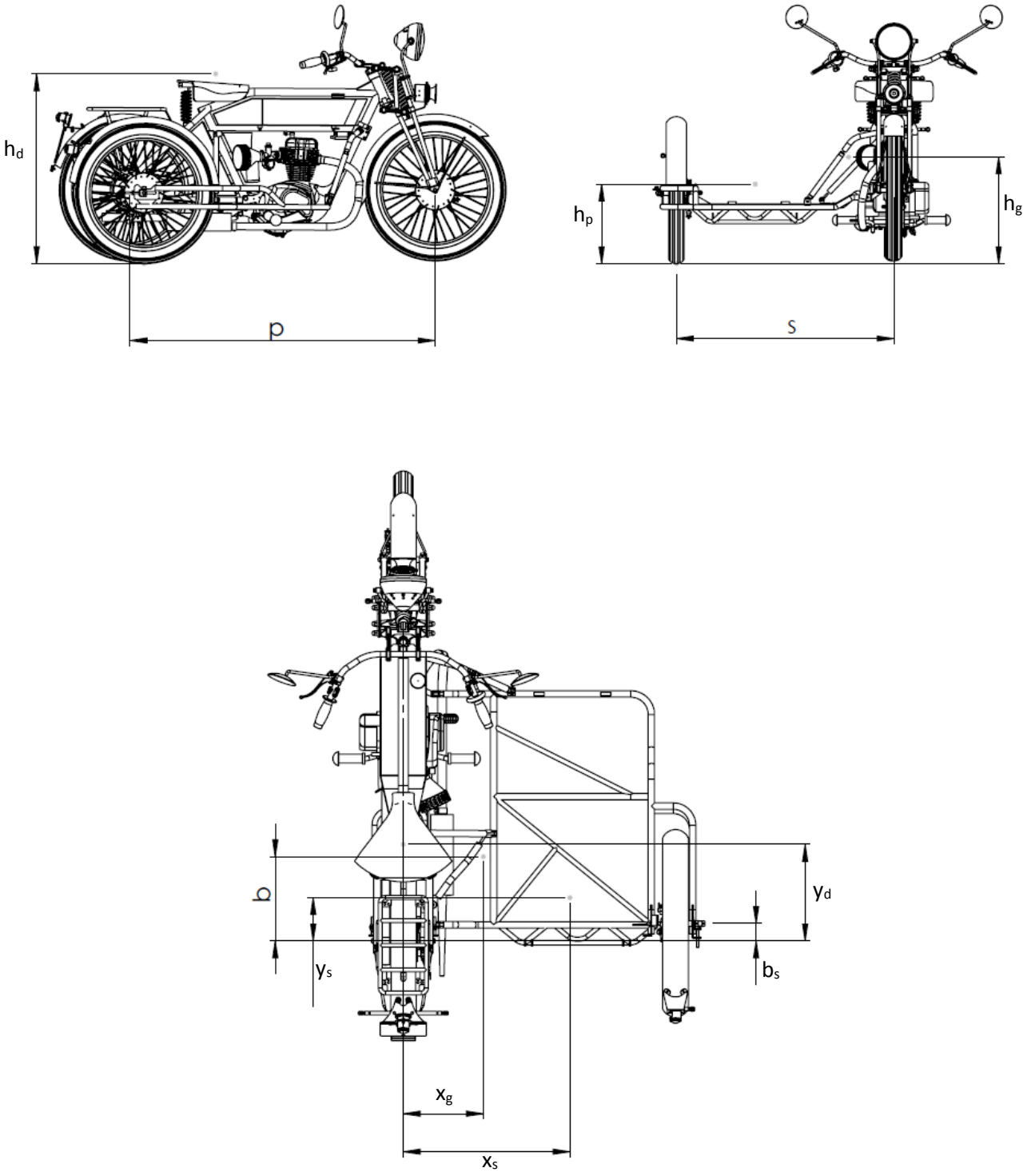

Figure C-73 Characteristc dimensions of the Sidecar vehicle

C.2 Datasheet of the Vehicle

Vehicle Inertia Data					
Motorcycle mass	m_b [Kg]	111.27	Motorcycle inertia	Jz_b [Kgm^2]	31.3280
Sidecar mass	m_s [Kg]	25.47	Sidecar inertia	Jz_s [Kgm^2]	5.2518
Vehicle geometry Data					
Wheel base	p [m]	1.487	Gauge	s [m]	1.054
Front base	a [m]		Rear base	b [m]	
Front shift	a_v [m]		Side wheel shift	b_s [m]	0.06345
Steer slope	ε [deg]	23.5	Roll angle		
Toe angle					
Vehicle Centre of Gravity Position					
longitudinal	x_g [m]	0.725	lateral	y [m]	0.122
height	h_g [m]	0.022			
longitudinal	x [m]	0.237	lateral	y [m]	0.858
height	h [m]	0.014			
Occupants Masses					
Driver mass	m_d [Kg]	75	Passenger mass	m_p [Kg]	75
Driver Position					
longitudinal	x [m]	0.423	Lateral	y [m]	0
height	h [m]	0.8455			
Rear Passenger Position					
Longitudinal	x [m]	0	Lateral	y [m]	0
Height	h [m]	0.8455			
Side Passenger Position					
longitudinal	x [m]	0.2135	Lateral	y [m]	0.5270
height	h [m]	0.345			

Table C.1 - Vehicle Datasheet

Gear Box					
Gear Ratios	0.1031	0.1607	0.2160	0.2609	0.3143
Final Ratio	0.3750				

Table C.2 - Gearbox Datasheet

Attachment D – Preliminary Model Results

In this attachment are reported the results given by the mathematical model without the validation process performing a left and right steering pad with the three different configurations

D.1 Steering pad Left

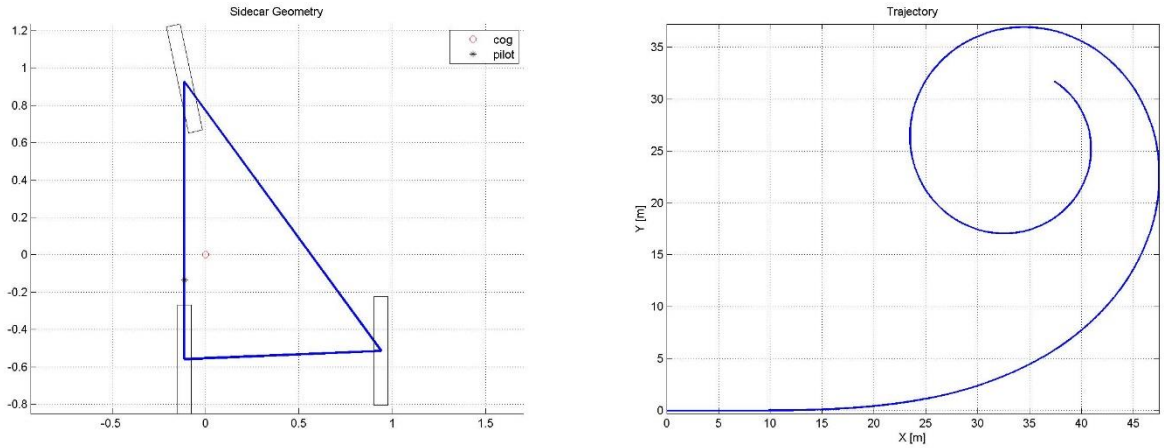

Figure D.1-74 COG and Trajectory for Pilot configuration

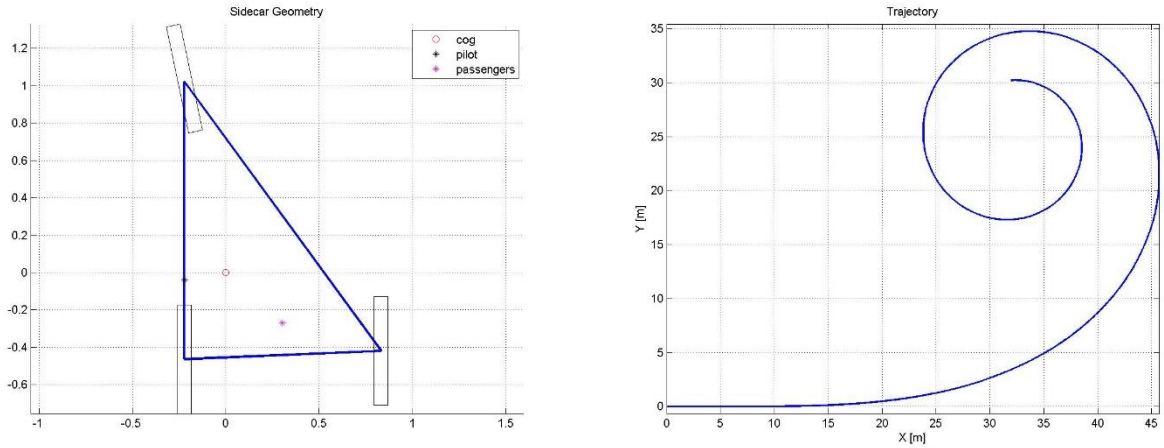

Figure D.1-75 COG and Trajectory for Part Load configuration

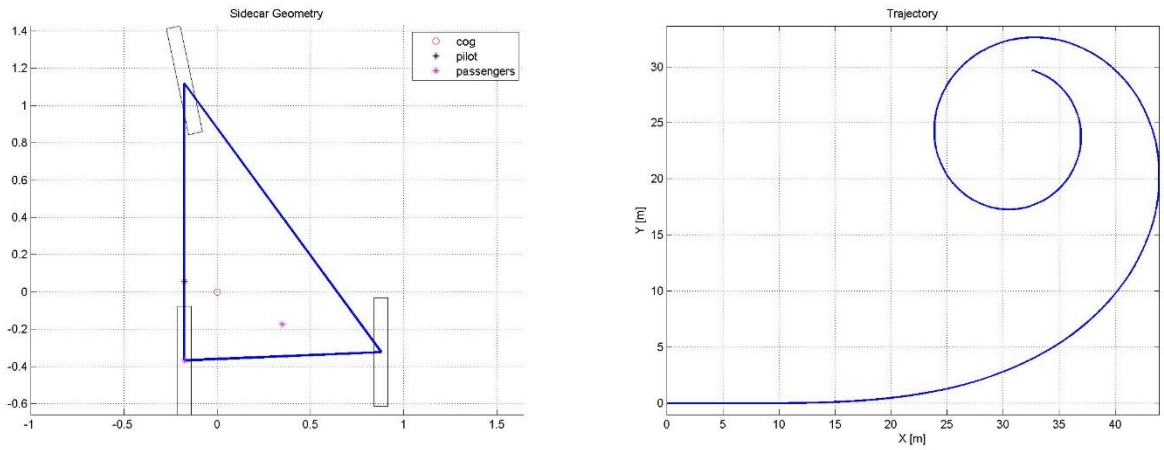

Figure D.1-76 COG and Trajectory for Full Load configuration

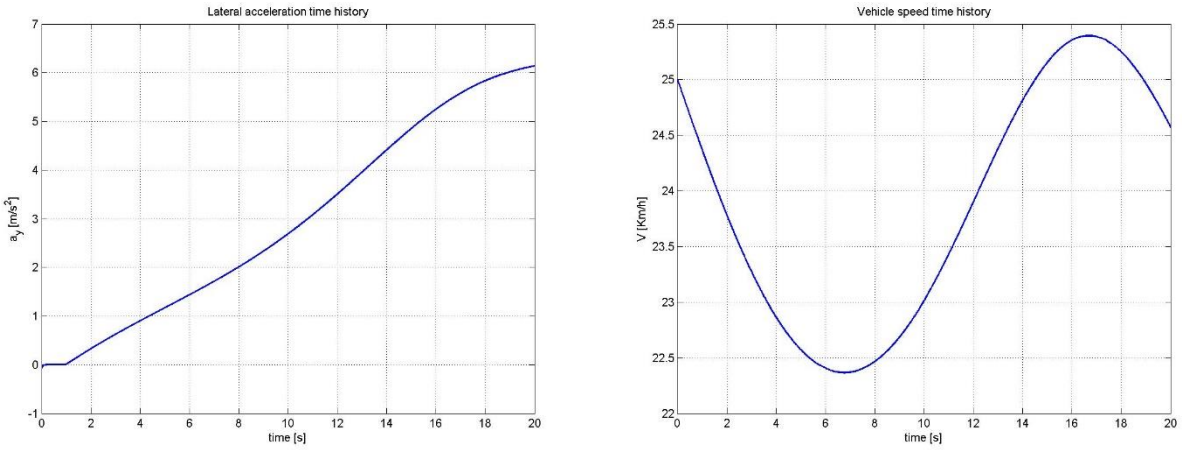

Figure D.1-77 A_y and Speed for Pilot configuration

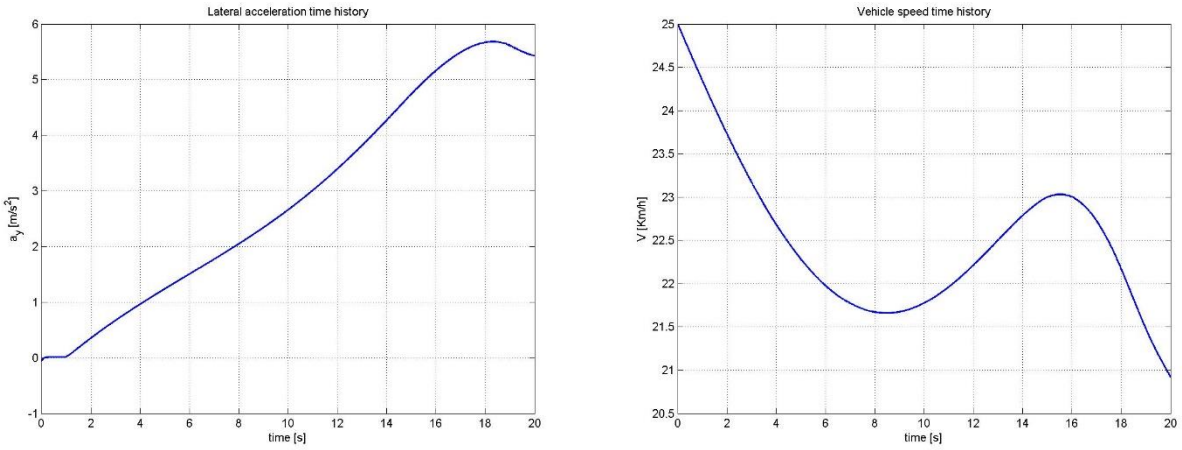

Figure D.1-78 Ay and Speed for Part Load configuration

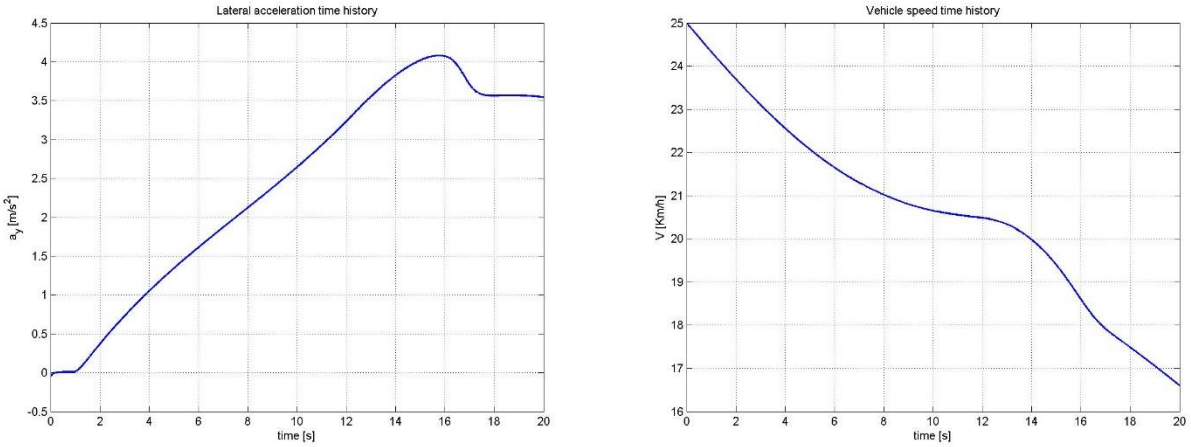

Figure D.1-6 Ay and Speed for Full Load configuration

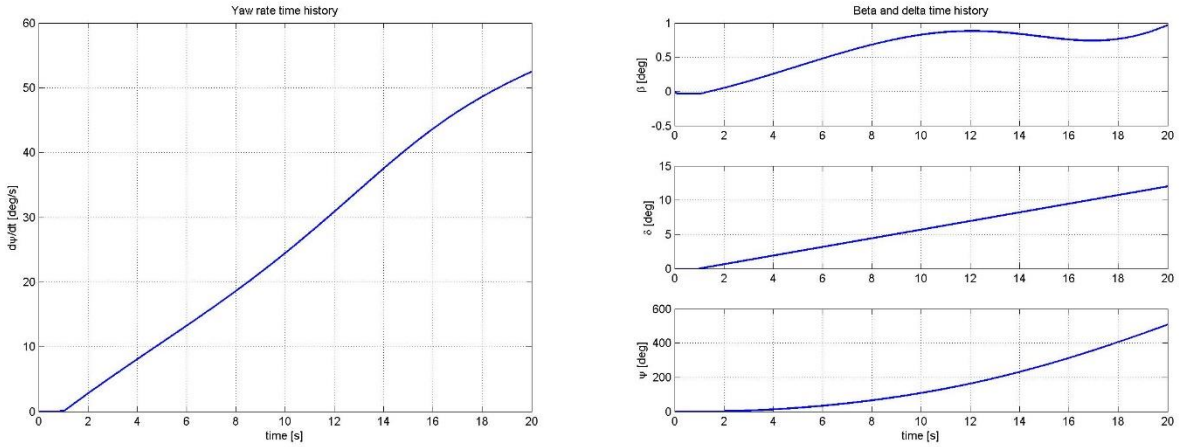

Figure D.1-79 Yaw rate and Angles for Pilot configuration

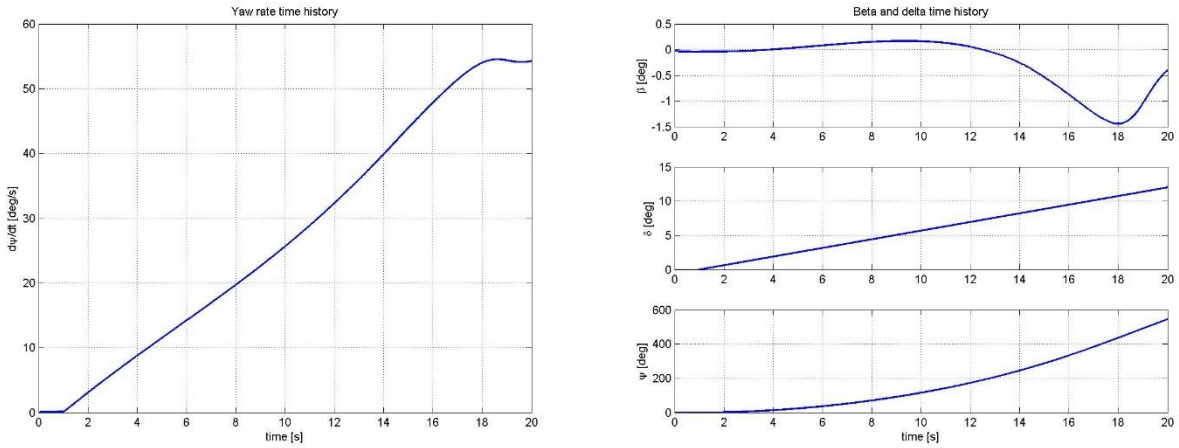

Figure D.1-80 Yaw rate and Angles for Part Load configuration

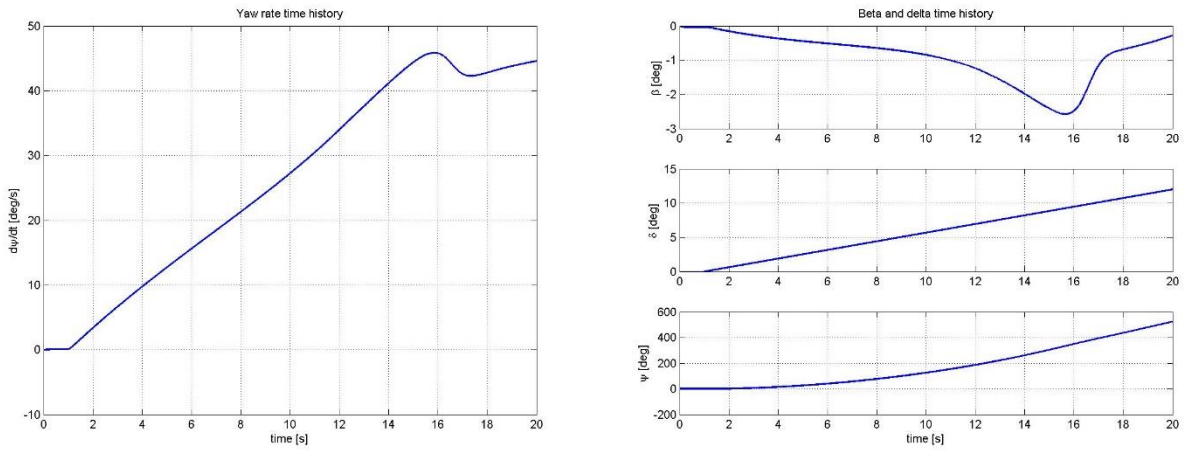

Figure D.1-9 Yaw rate and Angle for Full Load configuration

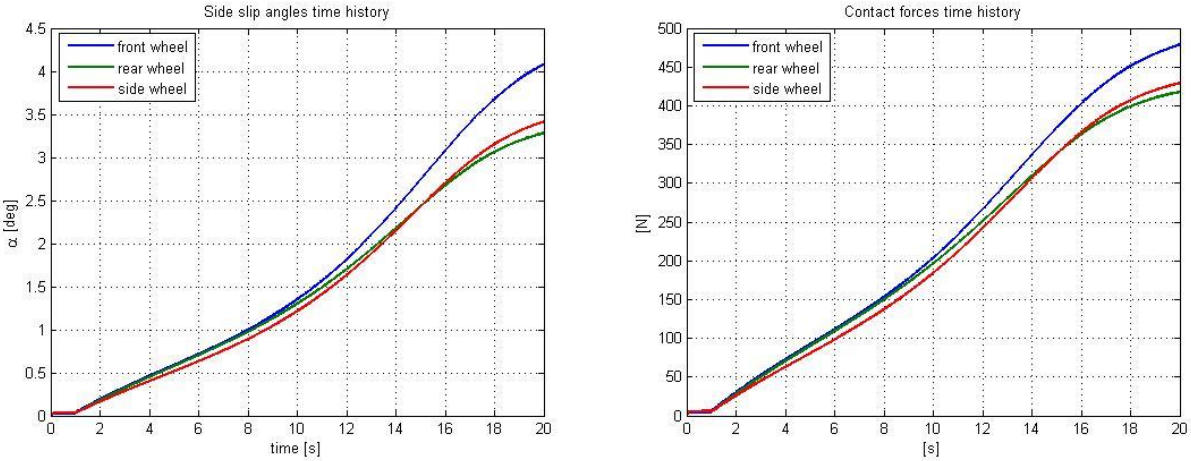

Figure D.1-10 Slip Angles and Contact Forces for Pilot configuration

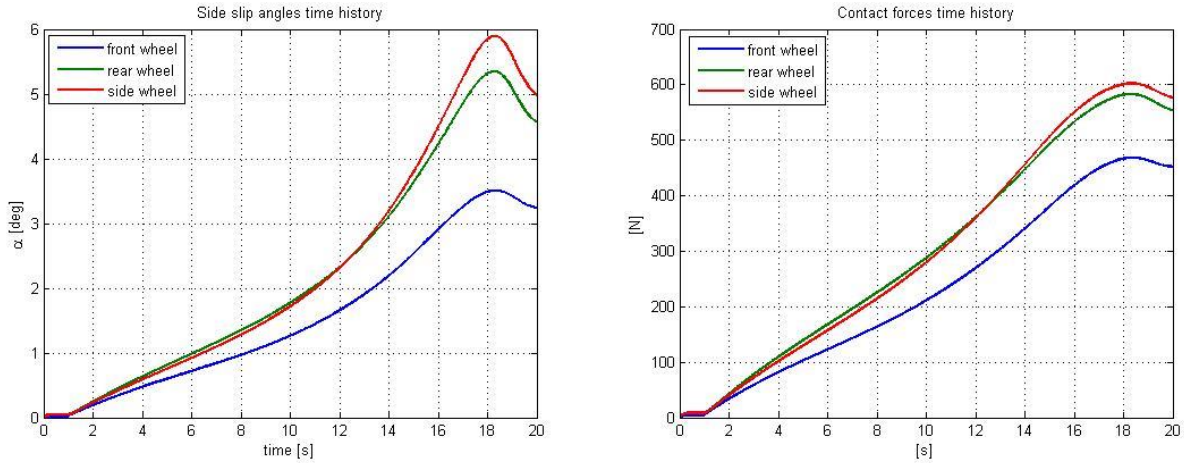

Figure D.1-11 Slip Angles and Contact Forces for Part Load configuration

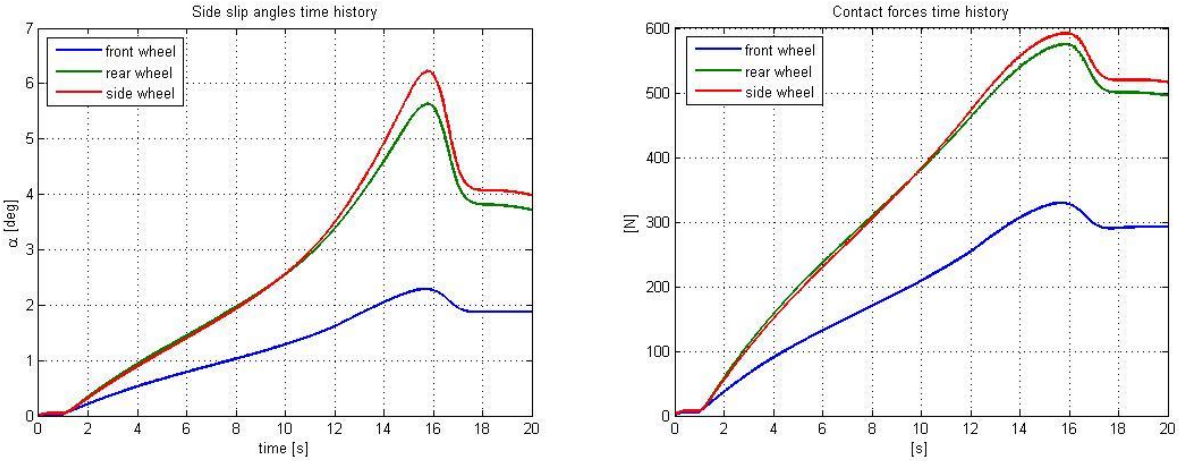

Figure D.1-81 Slip Angles and Contact Forces for Full Load configuration

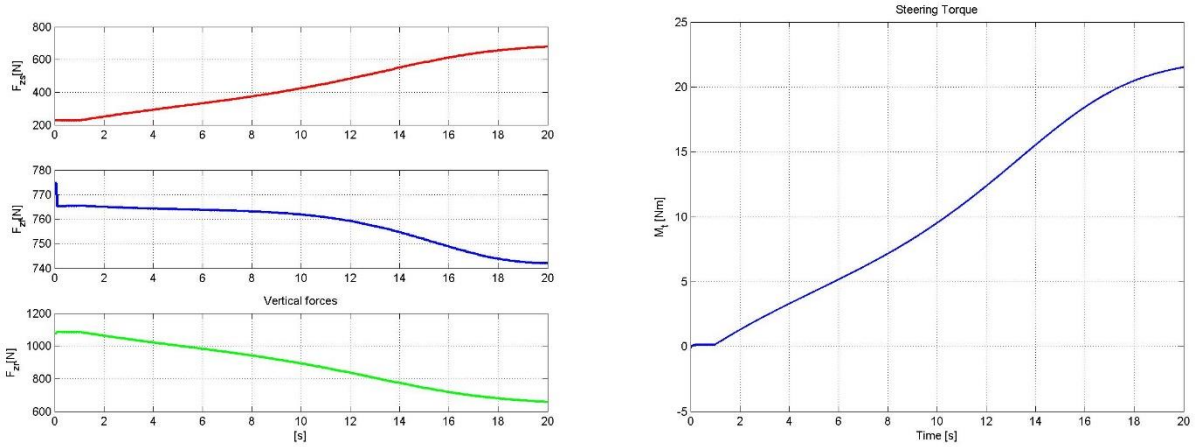

Figure D.1-82 Vertical Forces and Steering Torque for Pilot configuration

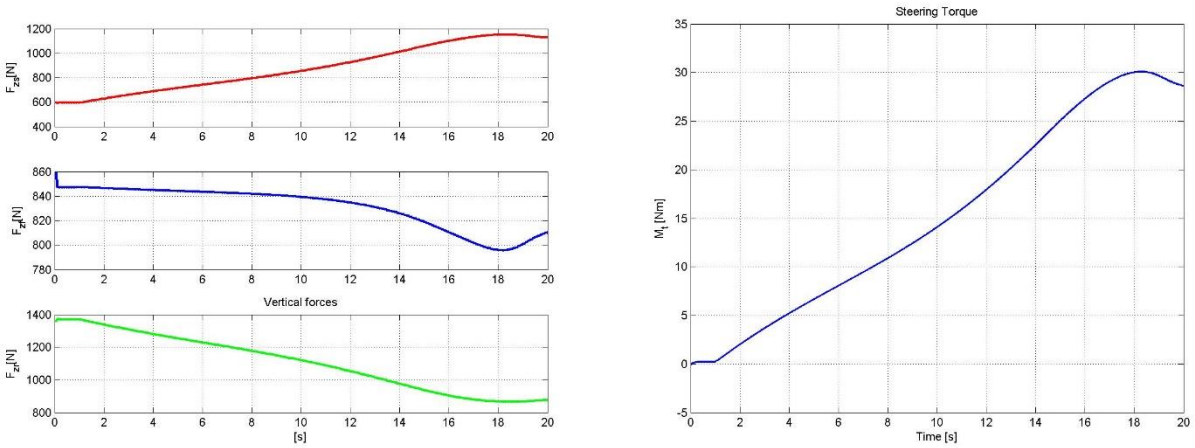

Figure D.1-83 Vertical Forces and Steering Torque for Part Load configuration

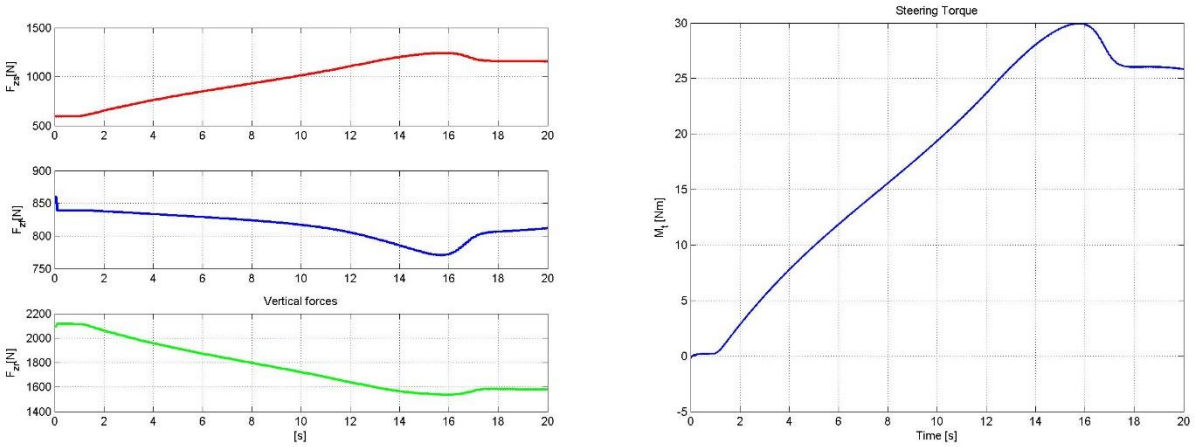

Figure D.1-84 Vertical Forces and Steering Torque for Full Load configuration

D.2 Steering Pad Right

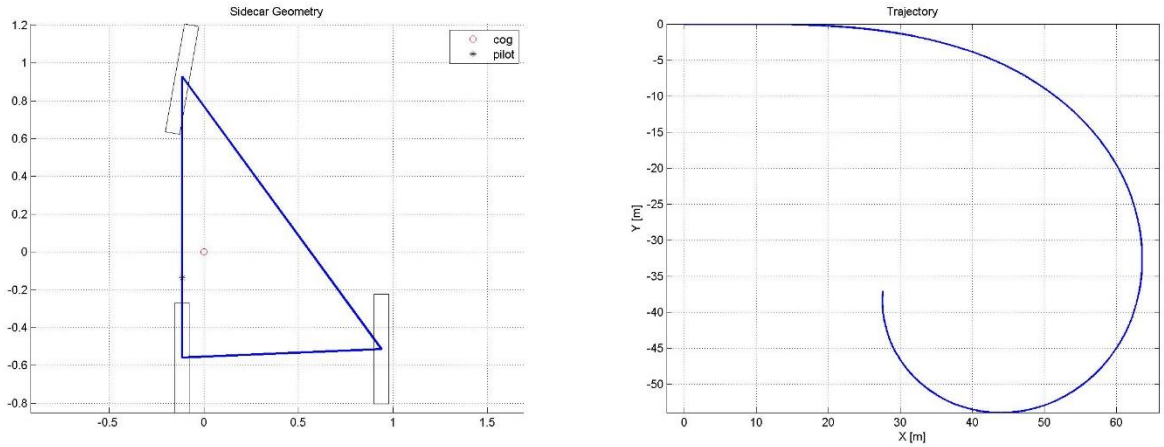

Figure D.2-1 COG and Trajectory for Pilot configuration

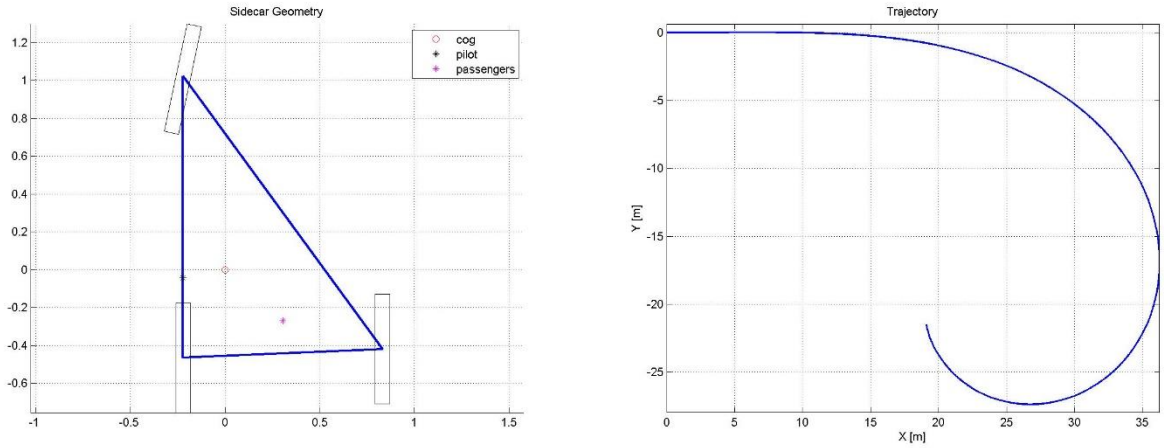

Figure D.2-285 COG and Trajectory for Part Load configuration

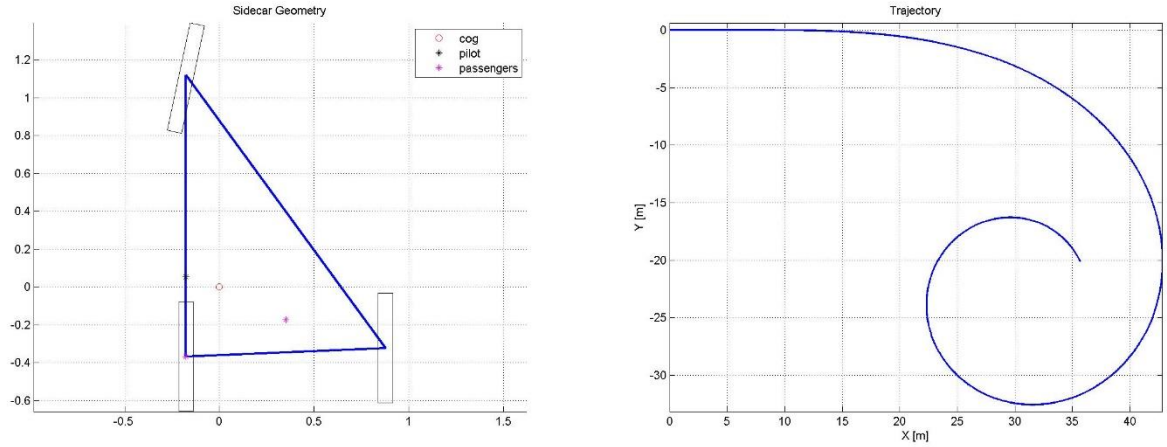

Figure D.2-86 COG and Trajectory for Full Load configuration

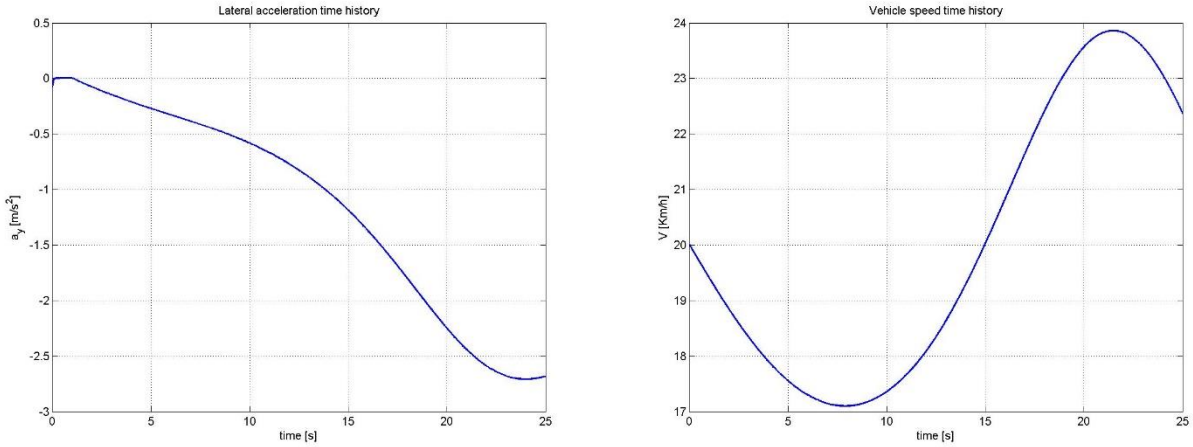

Figure D.2-87 Ay and Speed for Pilot configuration

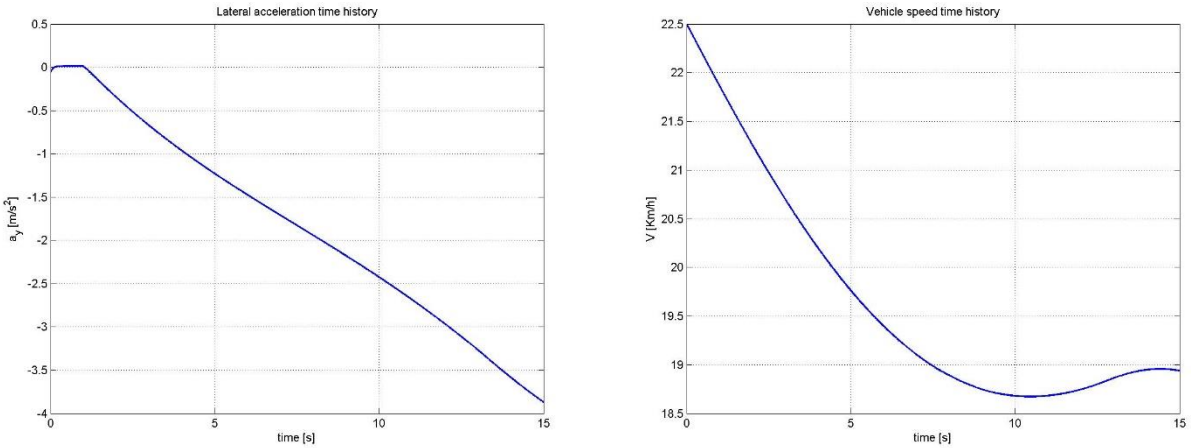

Figure D.2-88 Ay and Speed for Part Load configuration

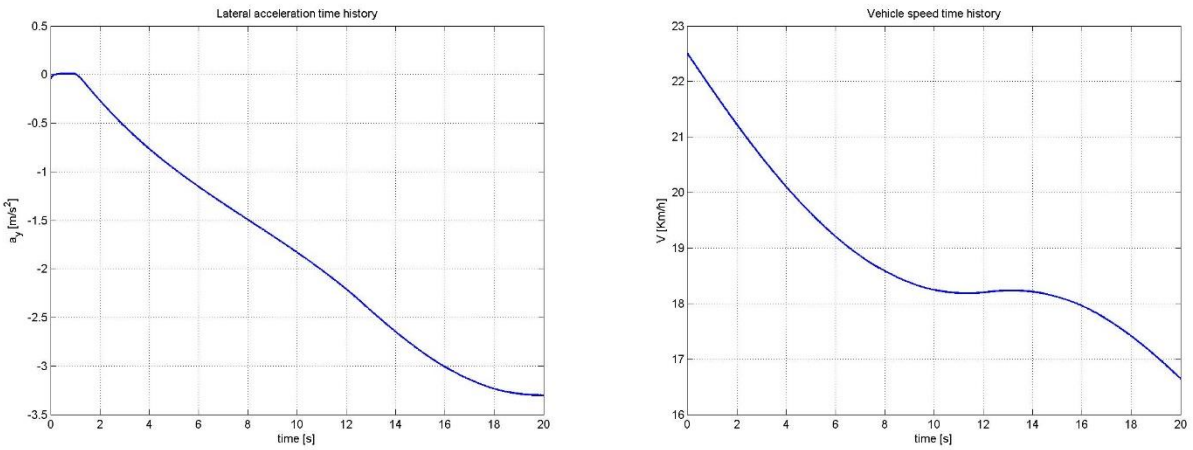

Figure D.2-89 Ay and Speed for Full Load configuration

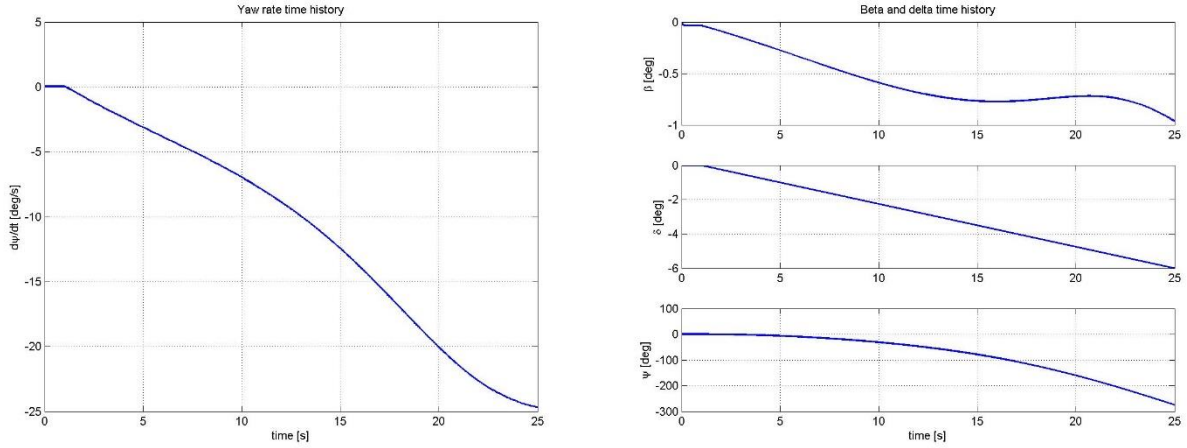

Figure D.2-90 Yaw rate and Angles for Pilot configuration

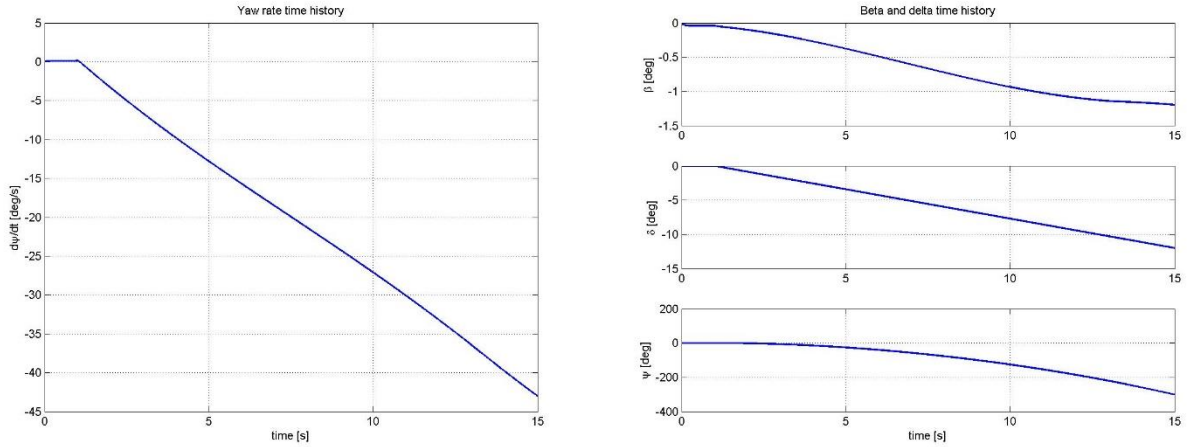

Figure D.2-8 Yaw rate and Angles for Part Load configuration

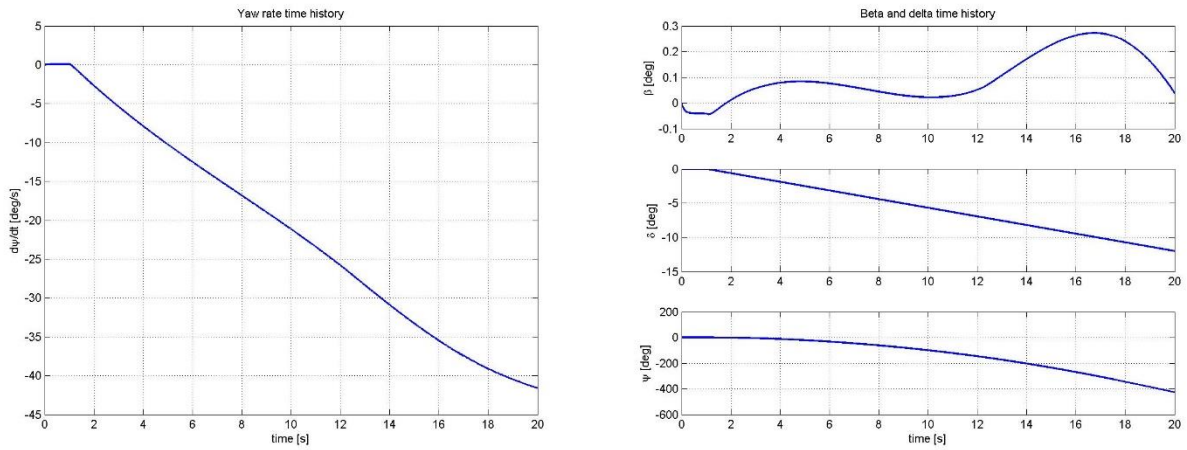

Figure D.2-91 Yaw rate and Angles for Full Load configuration

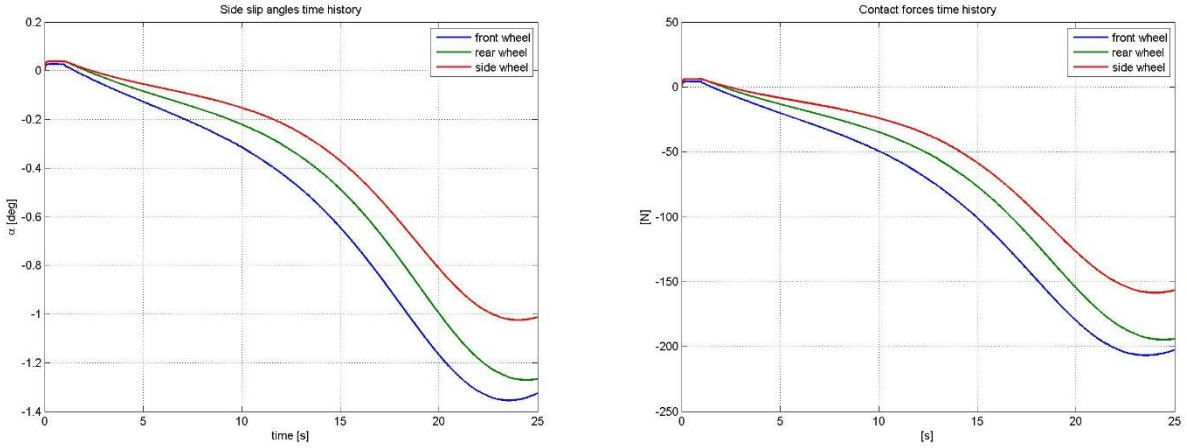

Figure D.2-92 Slip angles and Contact Forces for Pilot configuration

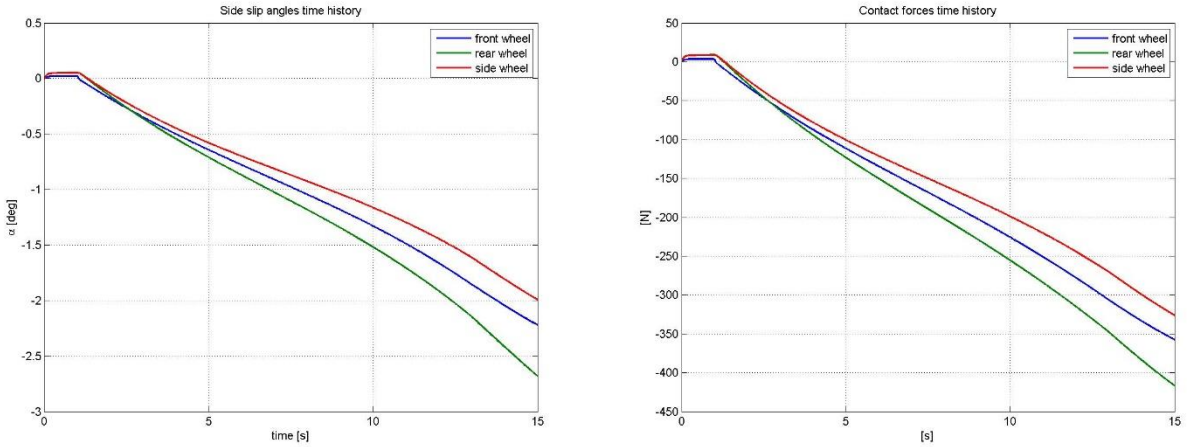

Figure D.2-931 Slip angles and Contact Forces for Part Load configuration

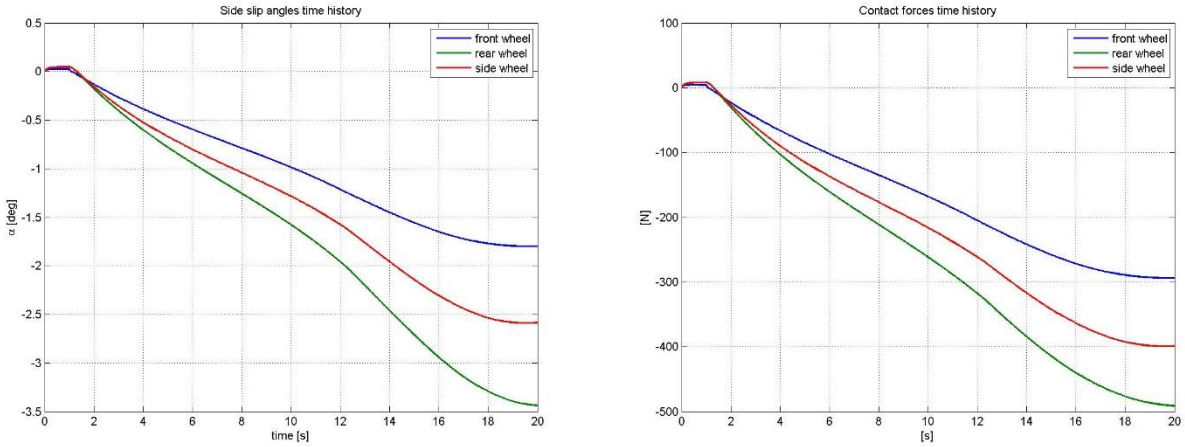

Figure D.2-94 Slip angles and Contact Forces for Full Load configuration

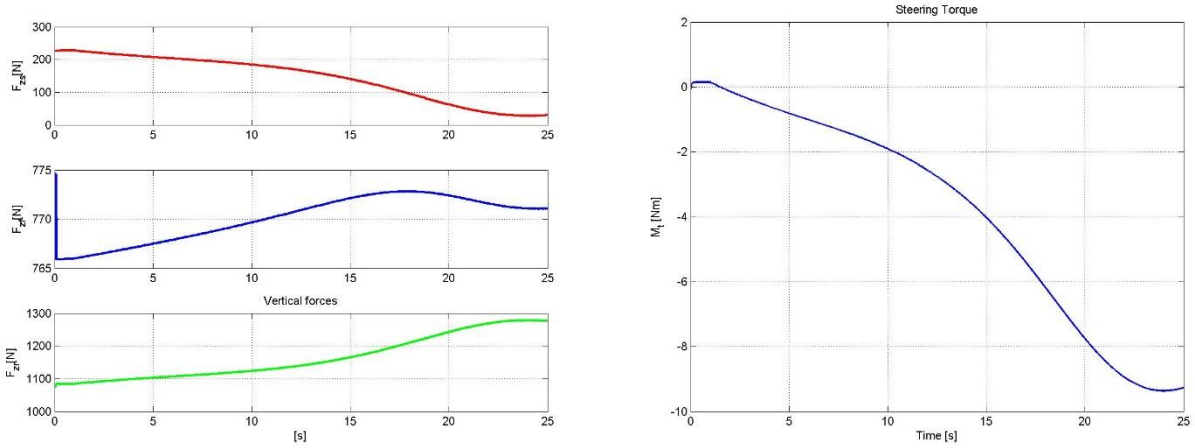

Figure D.2-953 Vertical Forces and Steering Torque for Pilot configuration

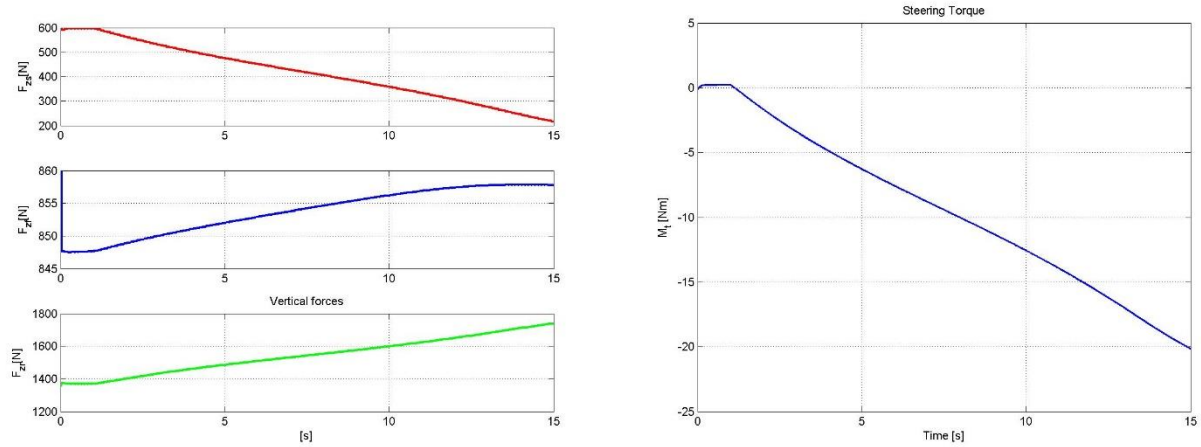

Figure D.2-96 Vertical Forces and Steering Torque for Part Load configuration

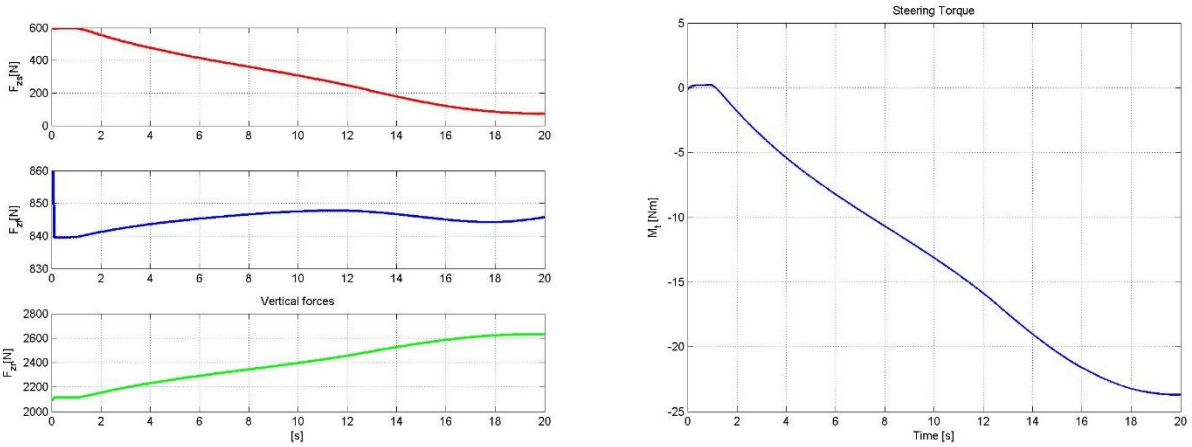

Figure D.2-15 Vertical Forces and Steering Torque for Full Load configuration

Attachment E – Sidecar Validation Results

The following attachment contains the result given from the validation procedure described in Chapter 5

E.1 Straight Line constant speed

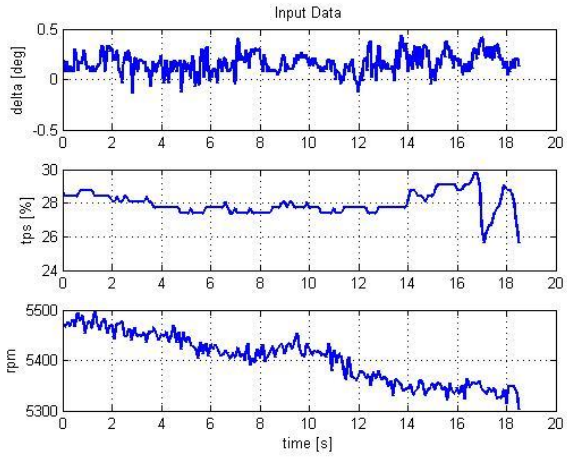

Figure E.1-97 Input data

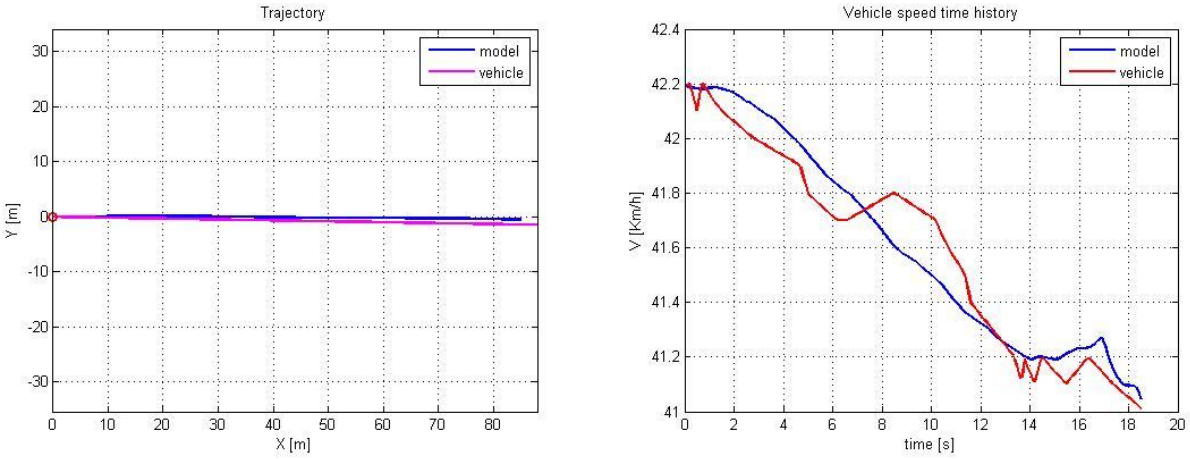

Figure E.1-98 Trajectoy and Speed for constant speed

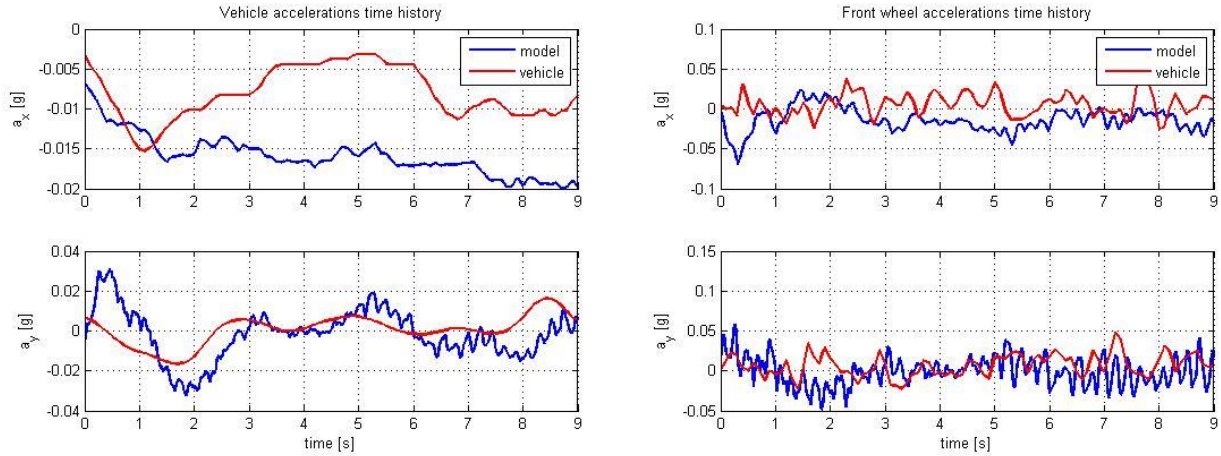

Figure E.1-99 Vehicle and Front wheel accelerations fo rconstant speed

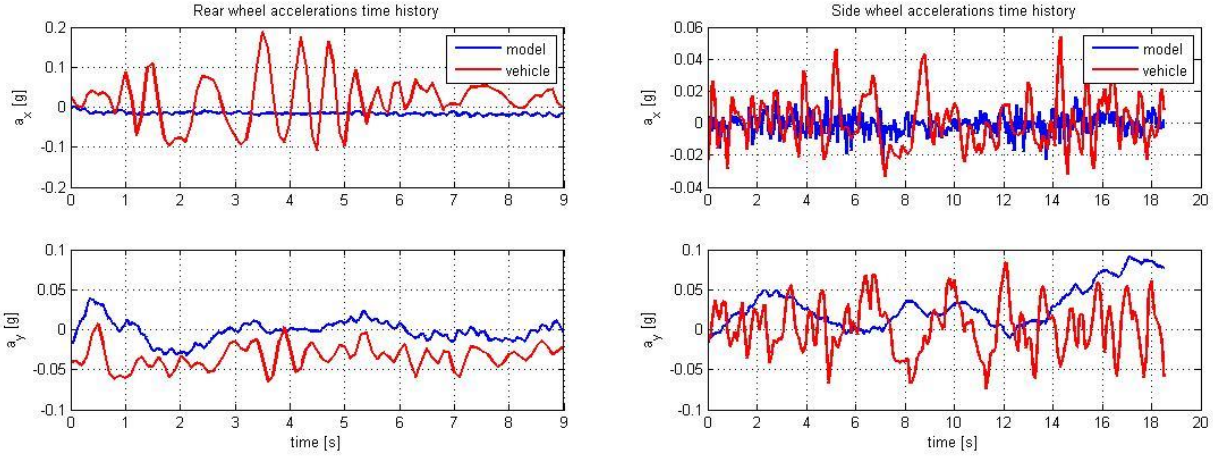

Figure E.1-100 Rear and Side wheel Accelerations for constant speed

E.2 Straight Line Acceleration

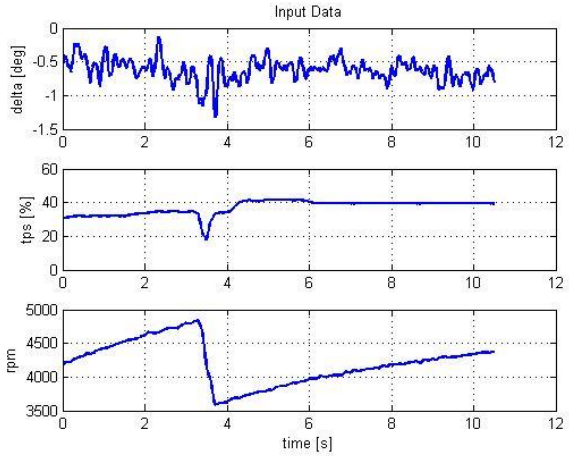

Figure E.2-101 Input data for acceleration

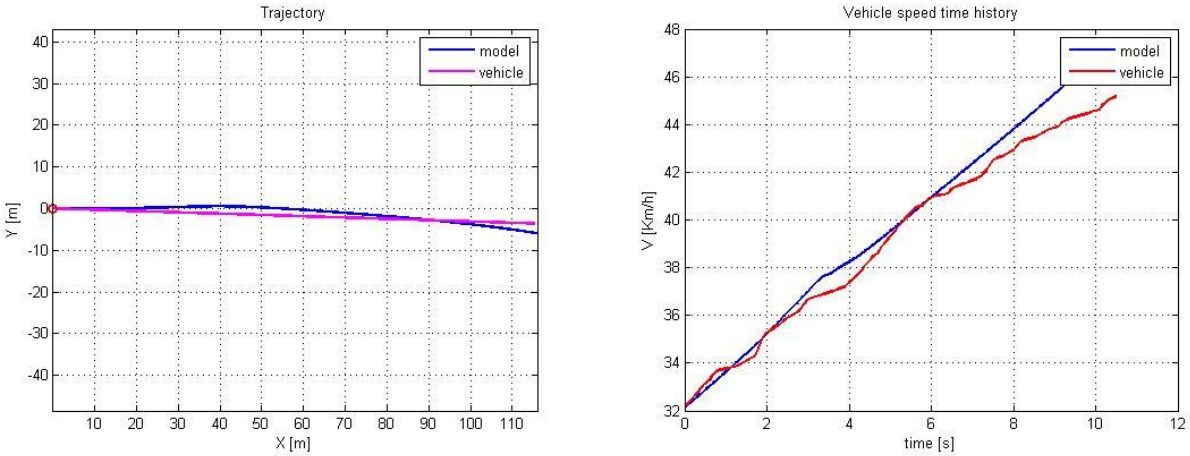

Figure E.2-102 Trajectory and Speed for acceleration

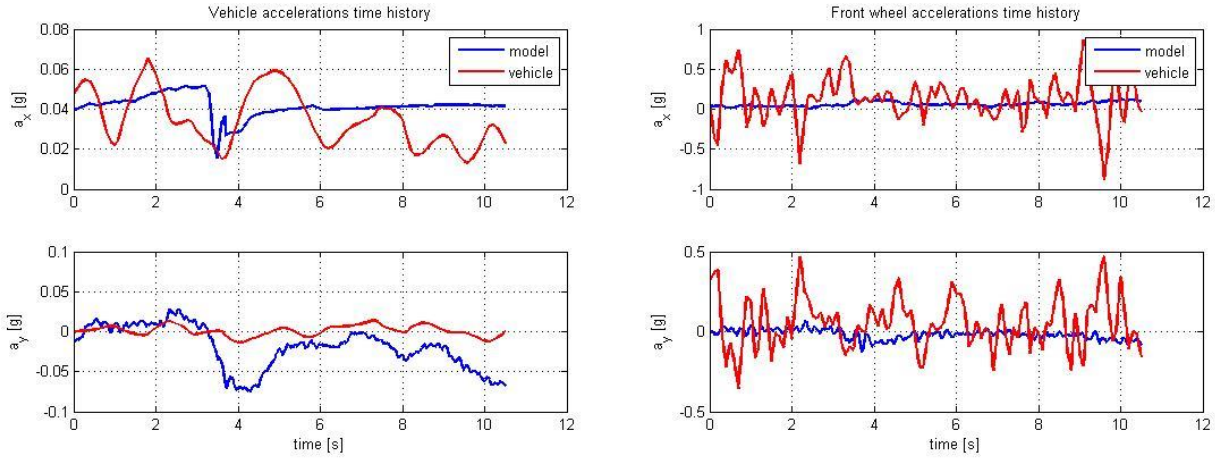

Figure E.2-103 Vehicle and Front wheel accelerations for acceleration

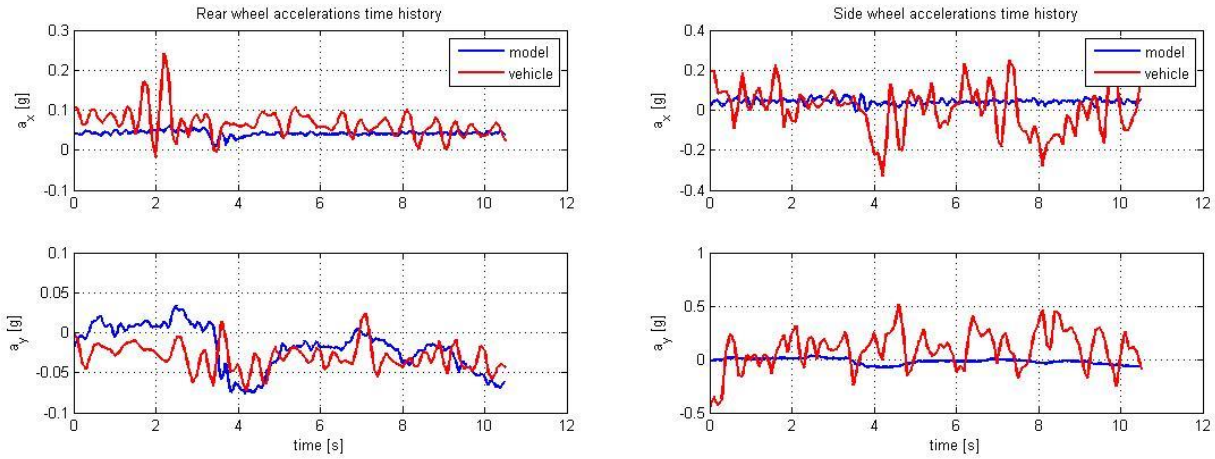

Figure E.2-104 Rear and Side wheel accelerations for acceleration

E.3 Straight Line Braking

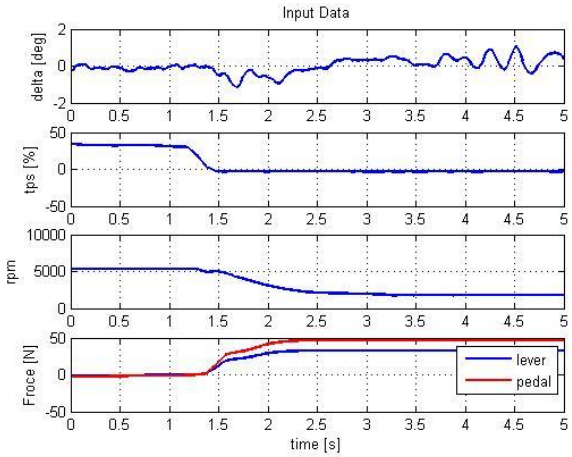

Figure E.3-105 Input data for Braking

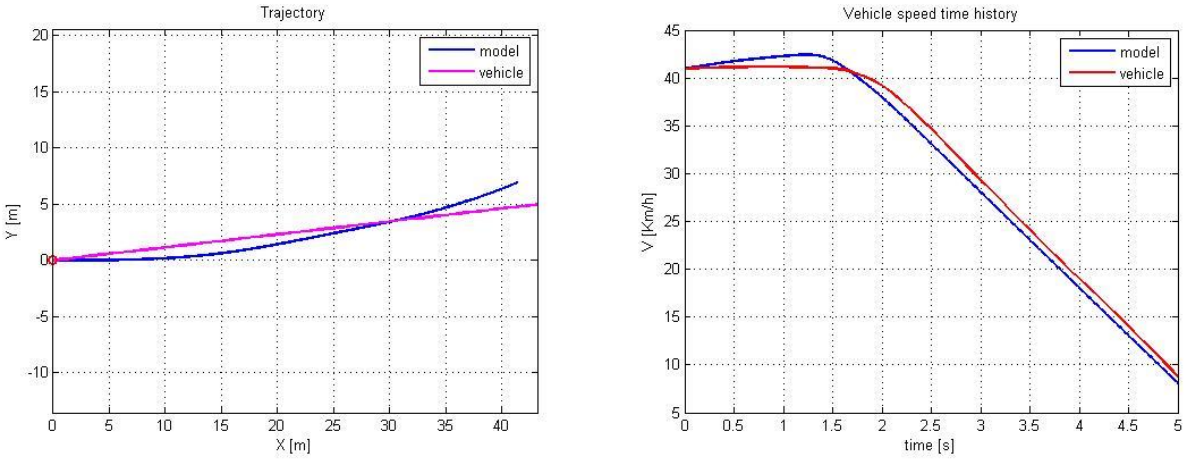

Figure E.3-106 Trajectory and Speed for Braking

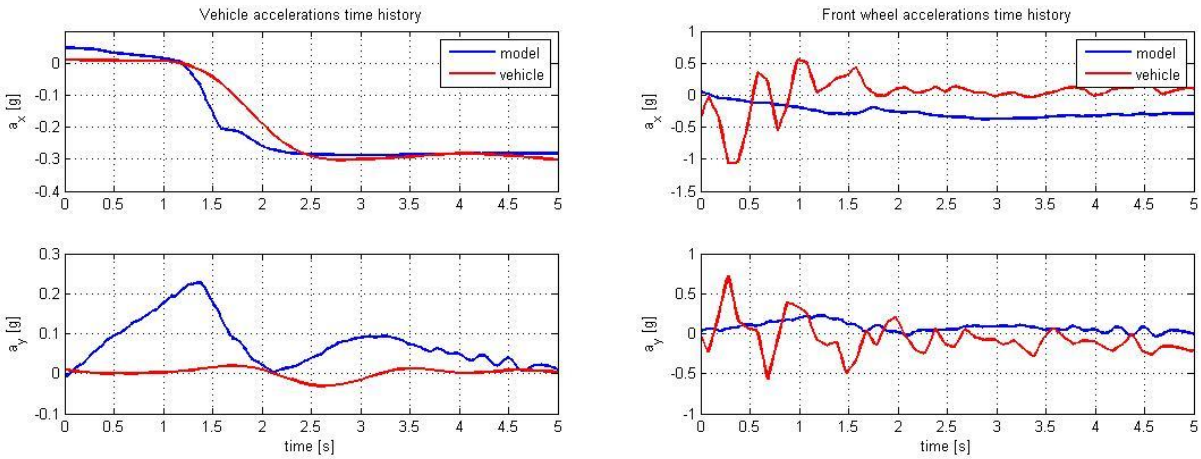

Figure E.3-107 Vehicle and Front wheel accelerations for Braking

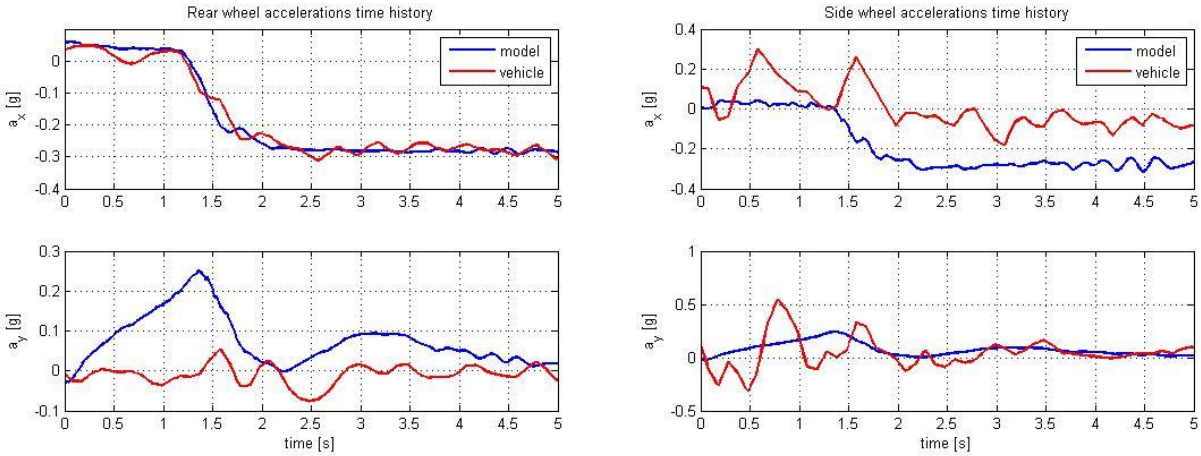

Figure E.3-108 Rear and Side accelerations for Braking

E.4 Steering Pad Left

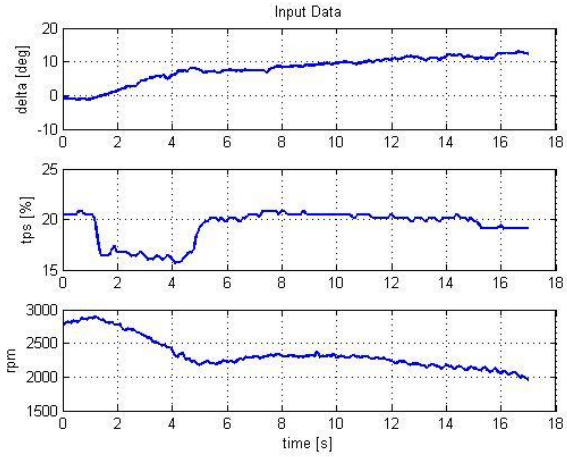

Figure E.4-109 Input data for Steering pad left

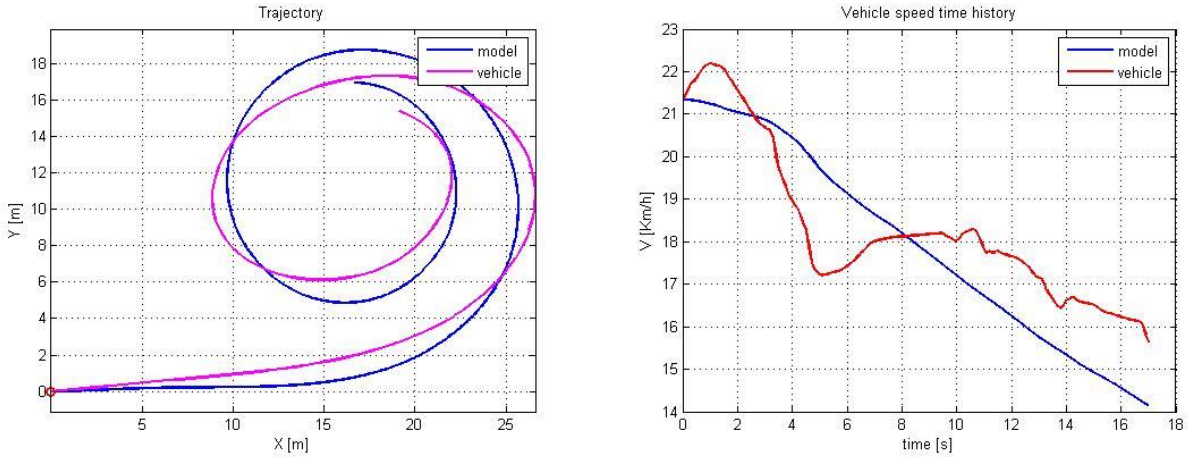

Figure E.4-110 Trajectory and Speed for Steering pad left

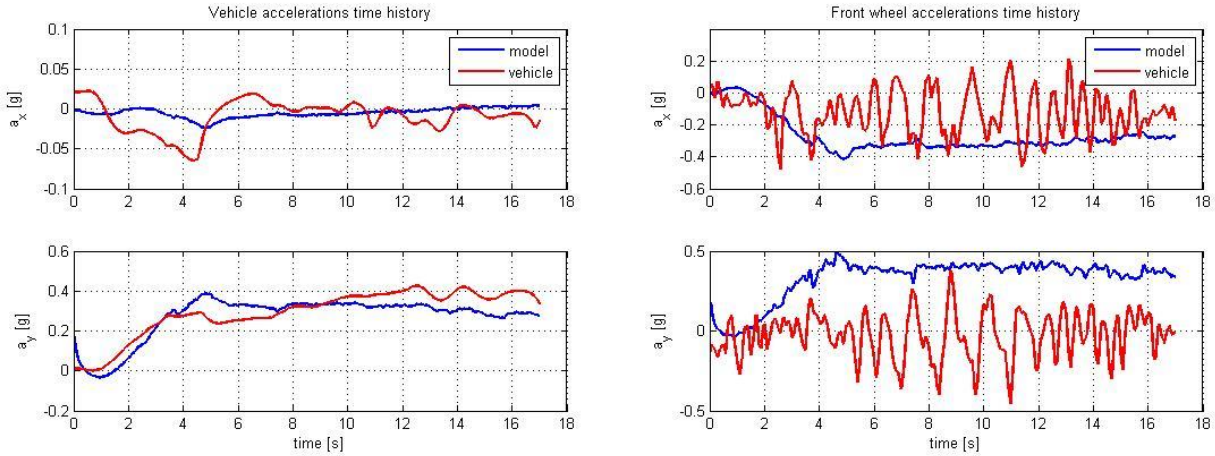

Figure E.4-111 Vehicle and Front wheel accelerations for Steering pad left

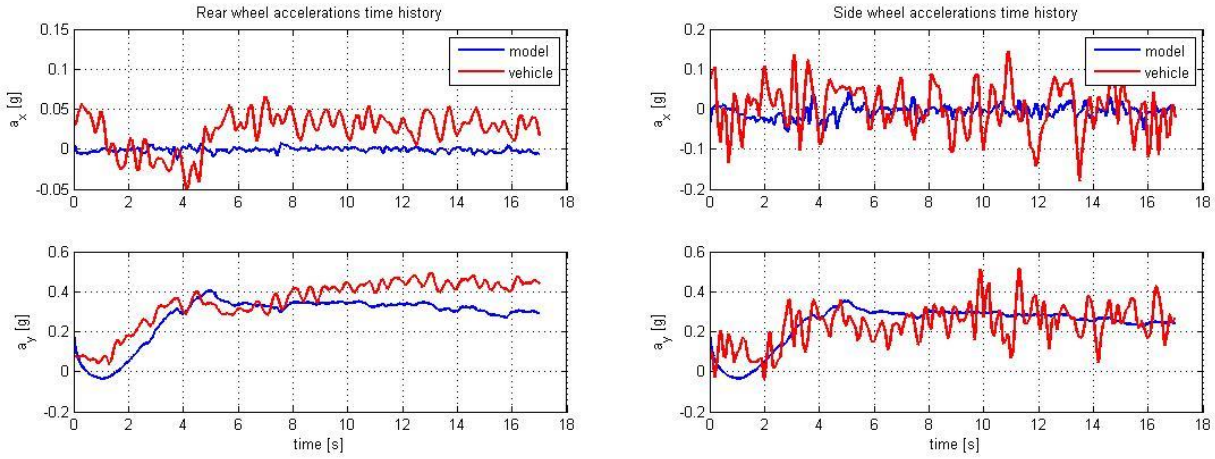

Figure E.4-112 Rear and Side wheel accelerations for Steering pad left

E.5 Steering Pad Right

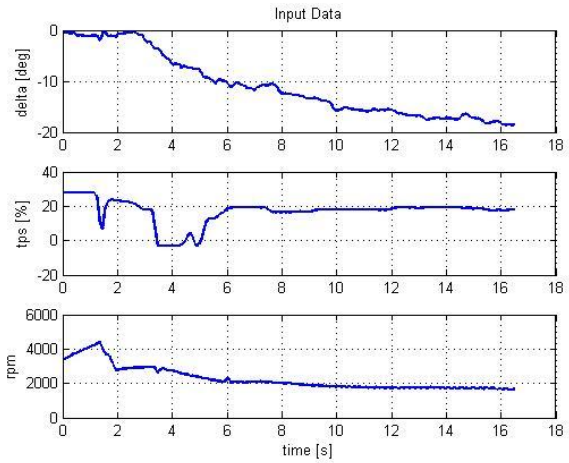

Figure E.5-113 Input data for Steering pad right

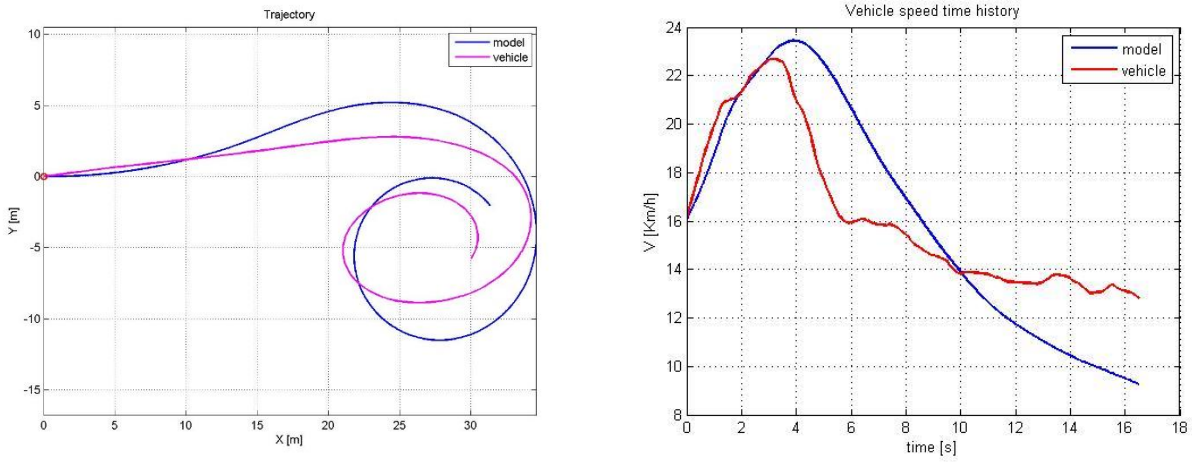

Figure E.5-114 Trajectory and Speed for Steering pad right

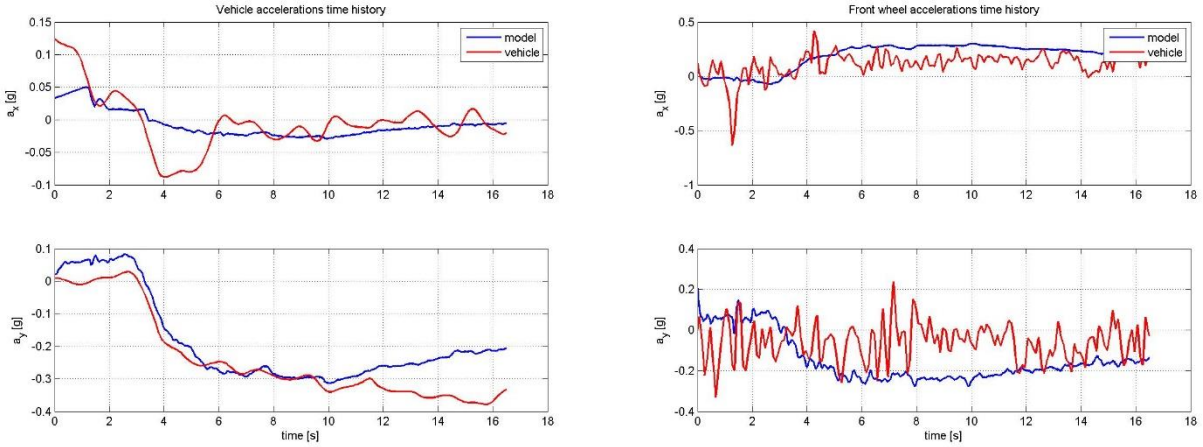

Figure E.5-115 Vehicle and Front wheel accelerations for Steering pad right

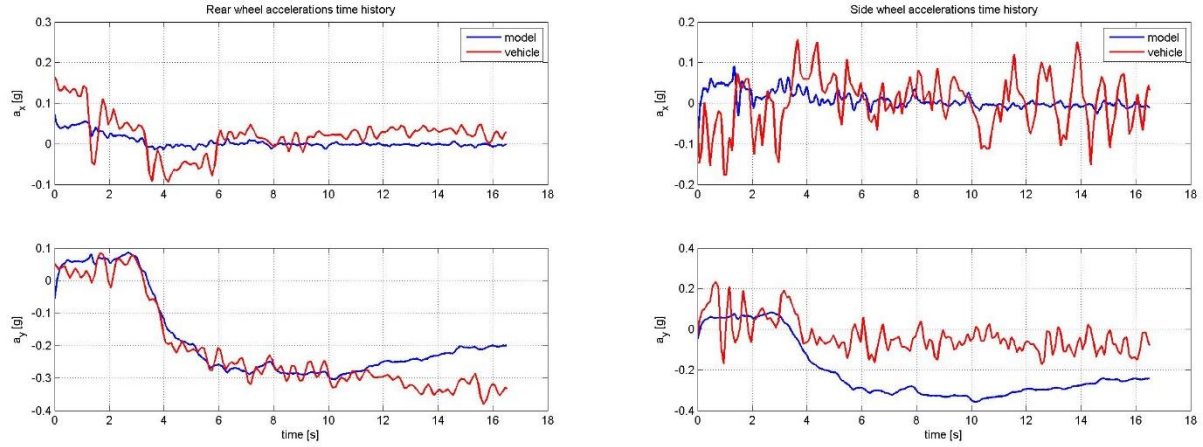

Figure E.5-116 Rear and Side wheel accelerations for Steering pad right

E.6 Wave Pad

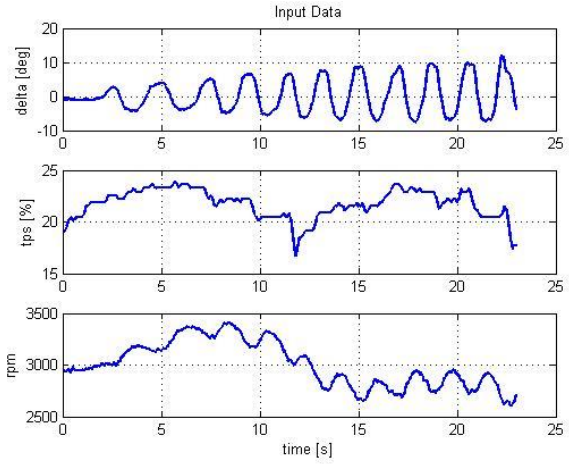

Figure E.6-117 Input data for Wave pad

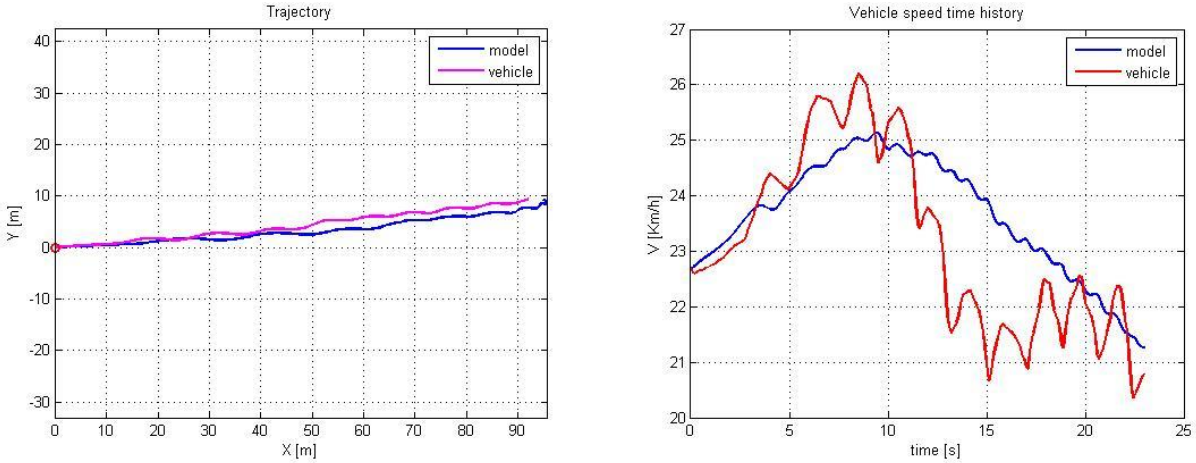

Figure E.6-118 Trajectory and Speed for Wave pad

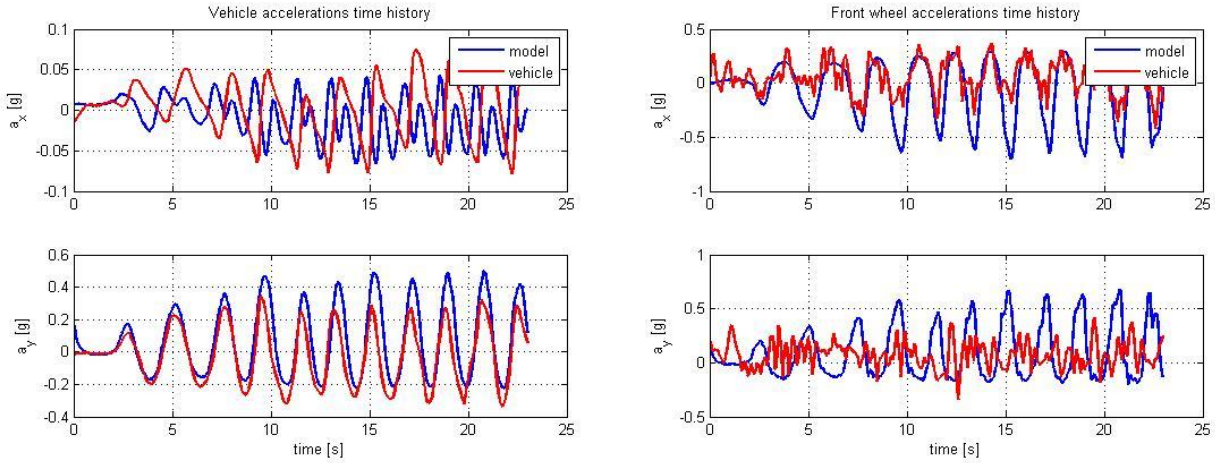

Figure E.6-119 Vehicle and Front wheel accelerations for Wave pad

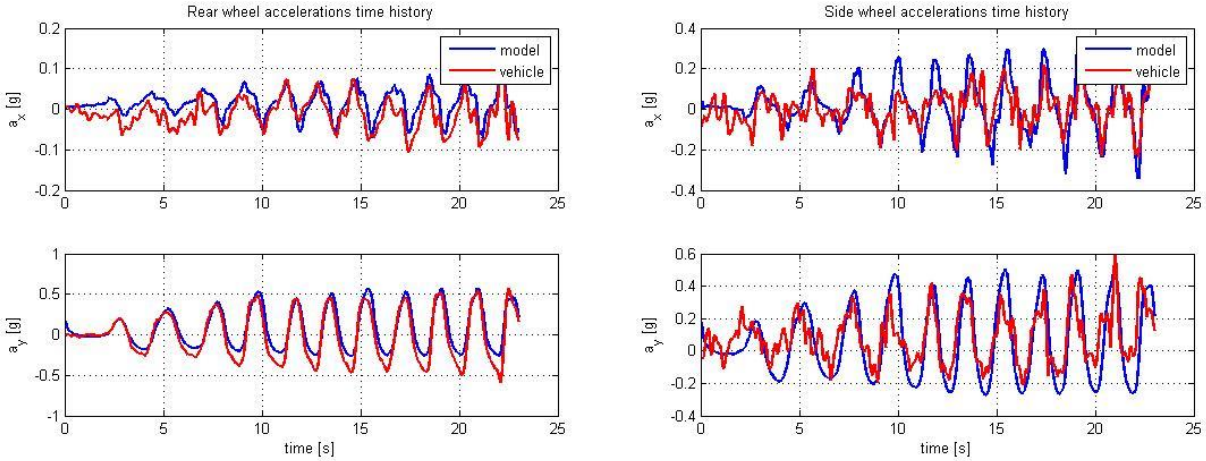

Figure E.6-120 Rear and Side wheel accelerations for Wave pad

E.7 Step Steer

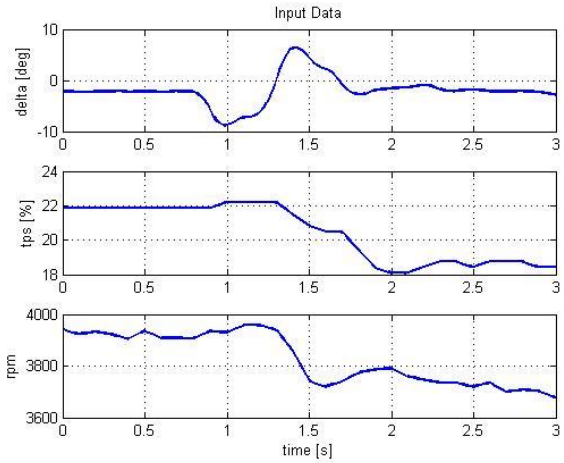

Figure E.7-121 Input data for Step steer

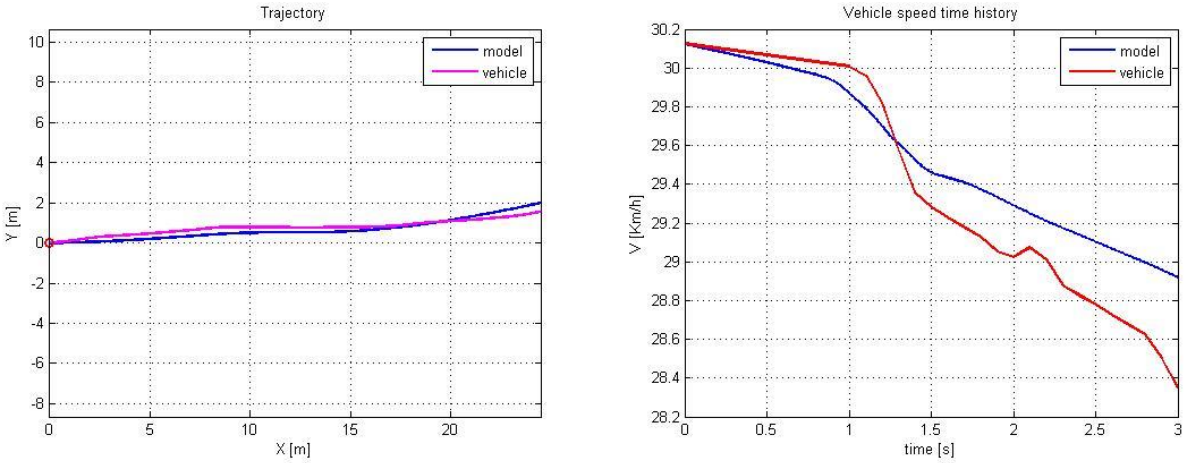

Figure E.7-122 Trajectory and Speed for Step steer

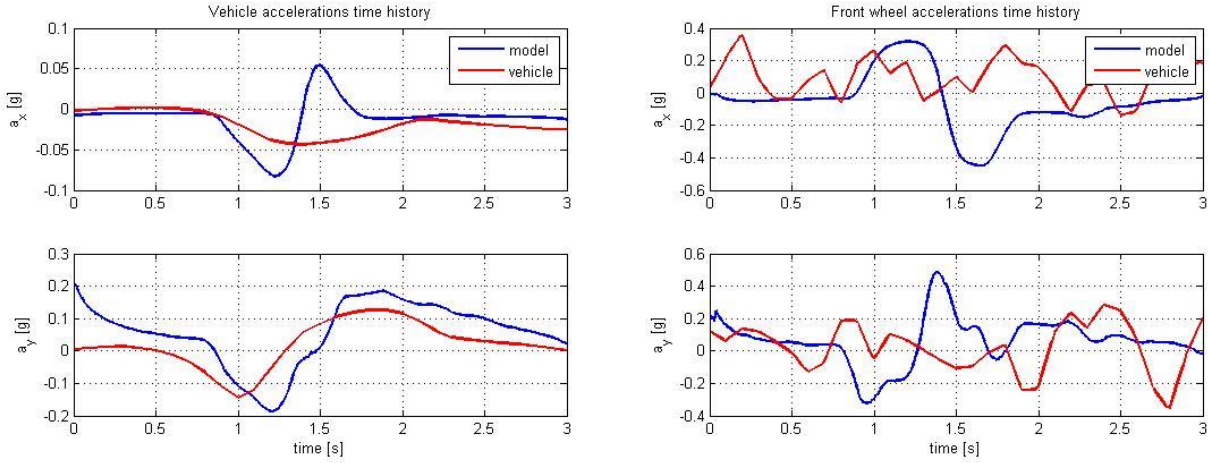

Figure E.7-123 Vehicle and Front wheel accelerations for Step steer

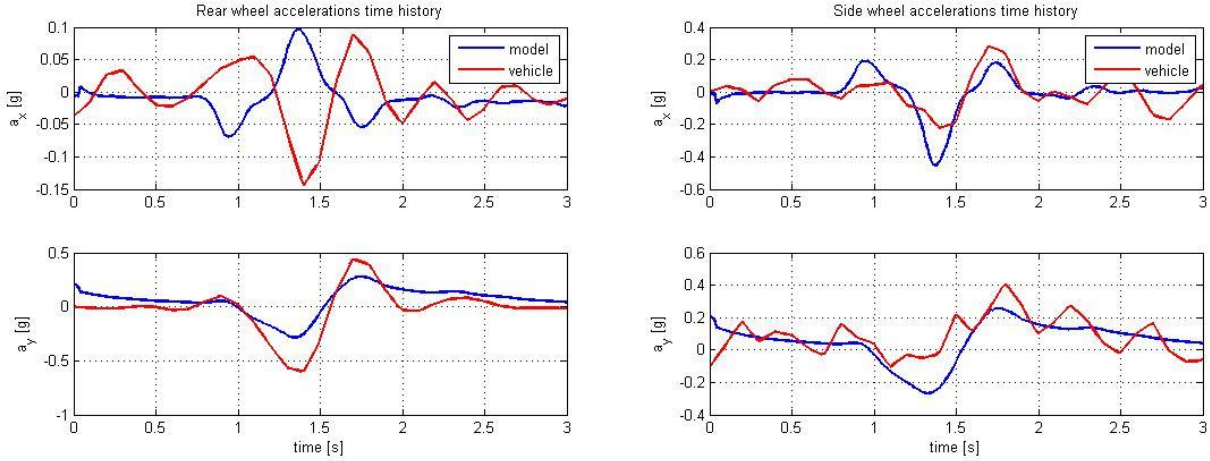

Figure E.7-124 Rear and Side wheel accelerations for Step steer

E.8 Validation Results with Parameters change

In this section we show the results obtained with the validation algorithm with variation of Forward shifting, 65 mm from the rear wheel, and the Camber angle at 2°

E.8.1 Constant Speed with Forward shifting Increase

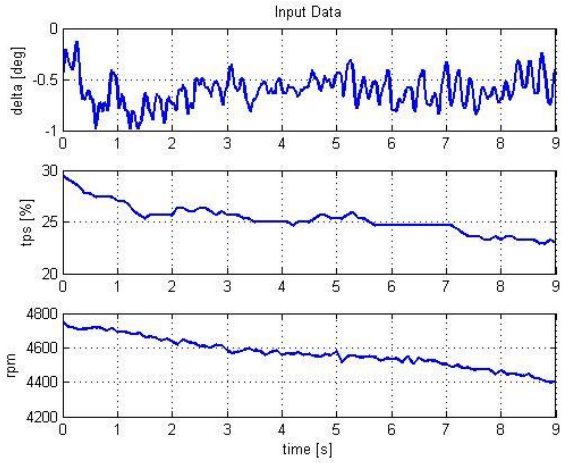

Figure E.8.1-125 Input data with increased Forward shifting

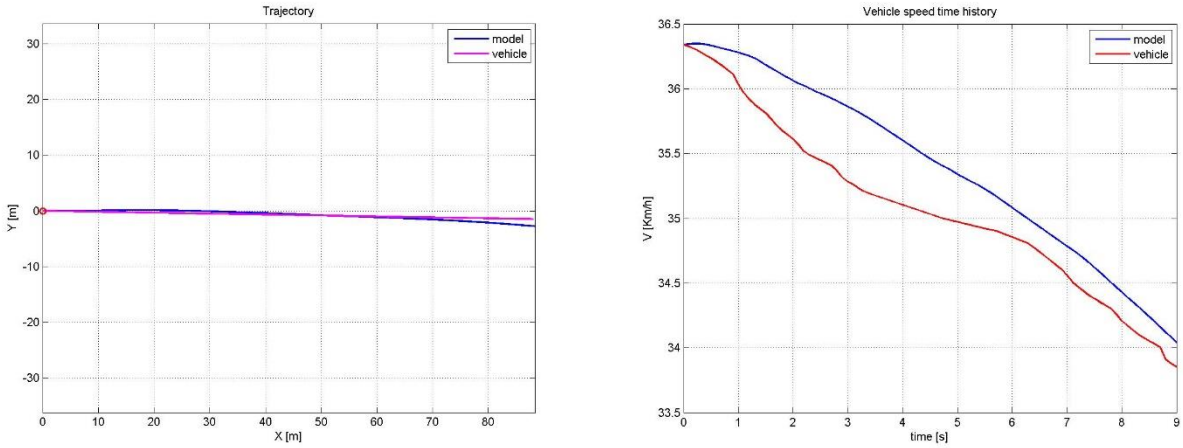

Figure E.8.1-2126 Trajectory and Speed with Forward shifting 65mm

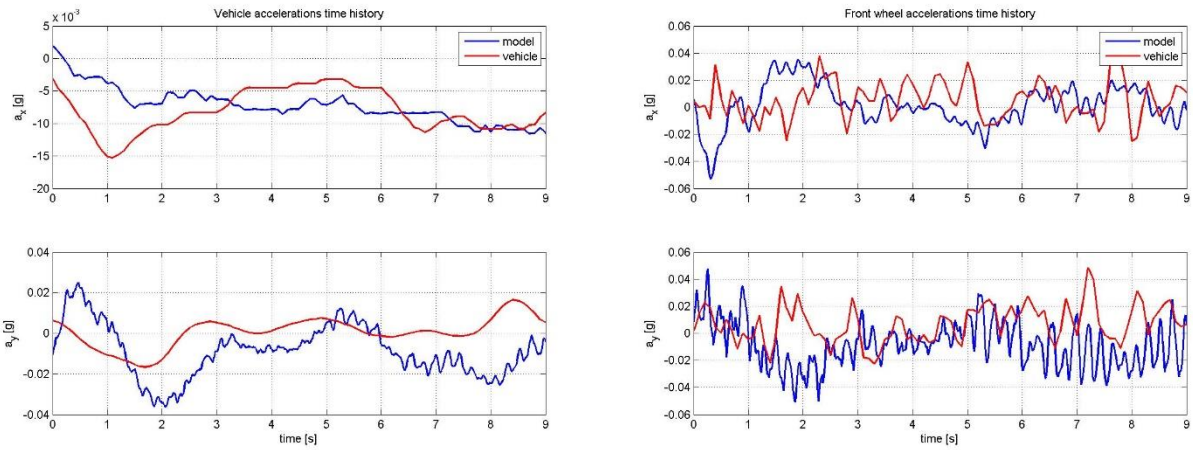

Figure E.8.1-127 Vehicle and Front wheel accelerations with Forward shifting 65mm

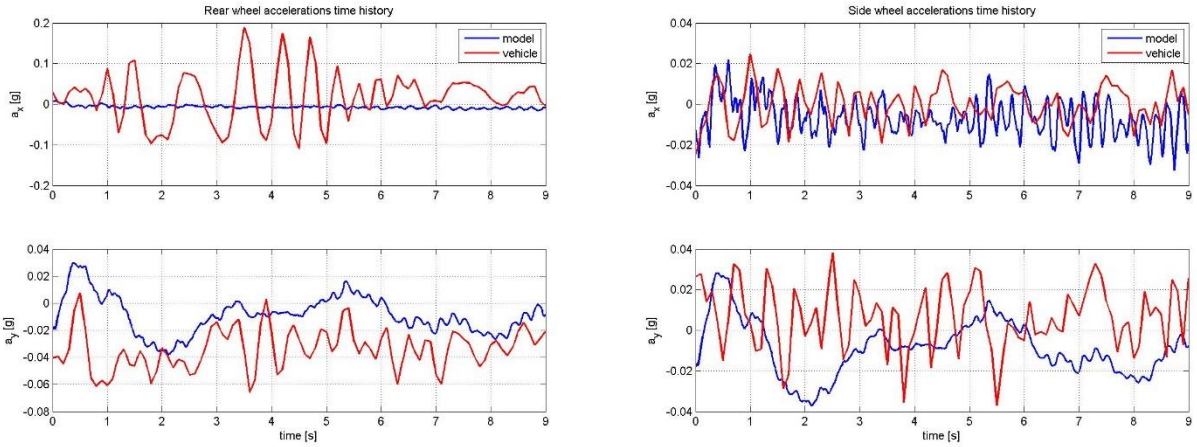

Figure E.8.1-128 Rear and Side wheel accelerations with Forward shifting 65mm

E.8.2 Steering Pad Left with Forward shifting increase

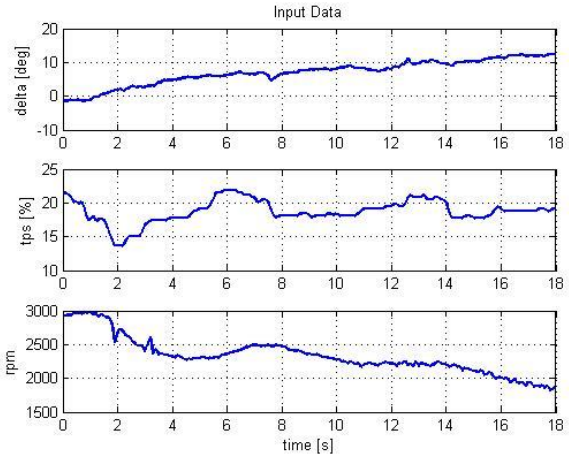

Figure E.8.2-129 Input data with increased Forward shifting

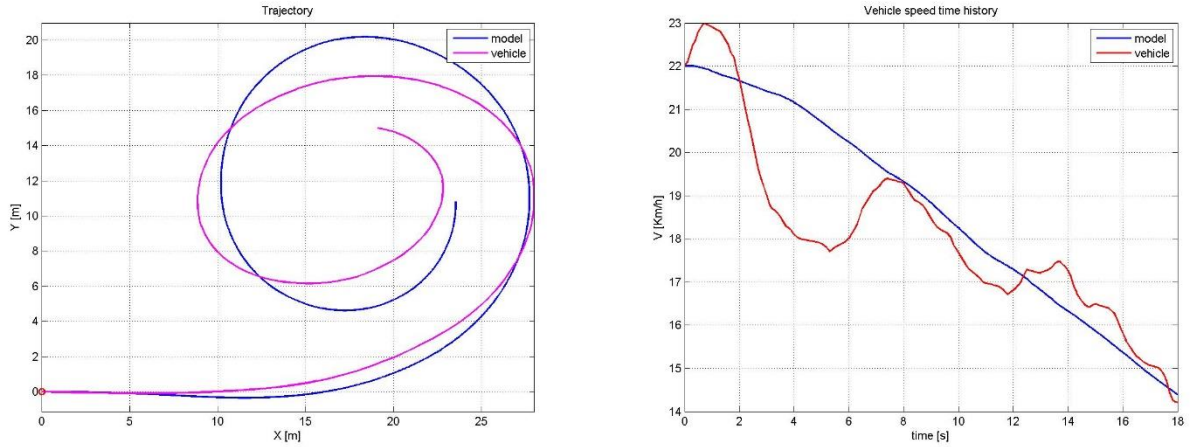

Figure E.8.2-130 Trajectory and Speed with Forward shifting 65mm

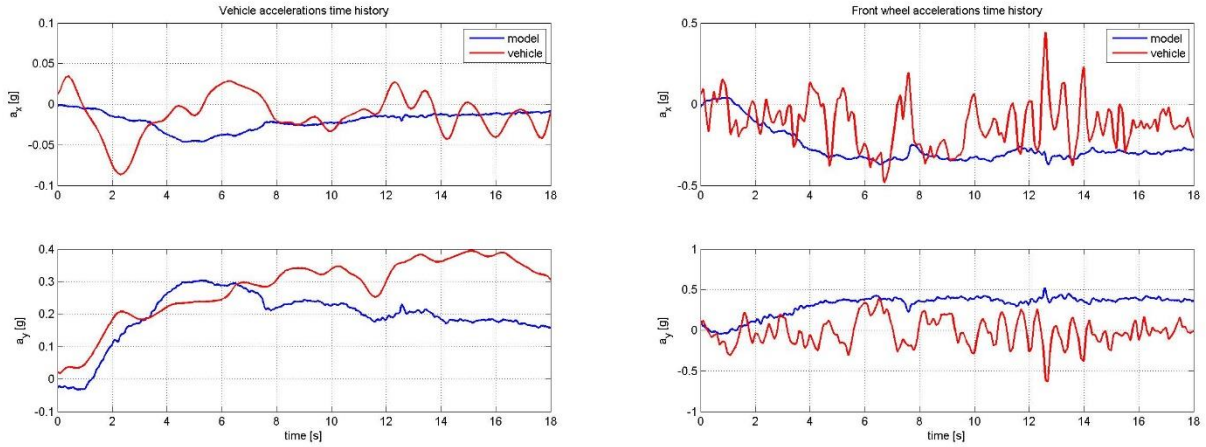

Figure E.8.2-131 Vehicle and Front wheel accelerations with Forward shifting 65mm

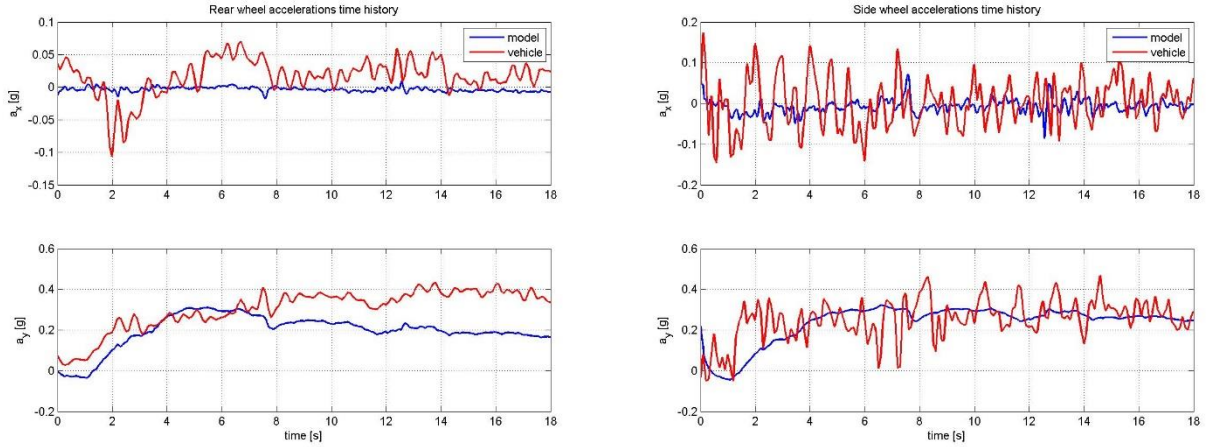

Figure E.8.2-132 Rear and Side wheel accelerations with Forward shifting 65mm

E.8.3 Steering Pad Right with Forward shifting increase

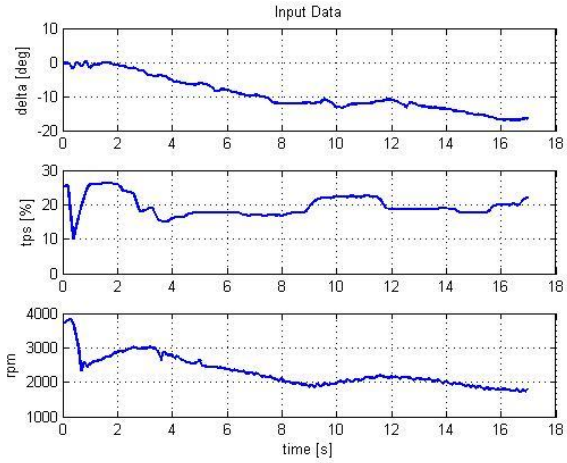

Figure E.8.3-133 Input data with Forward shifting 65mm

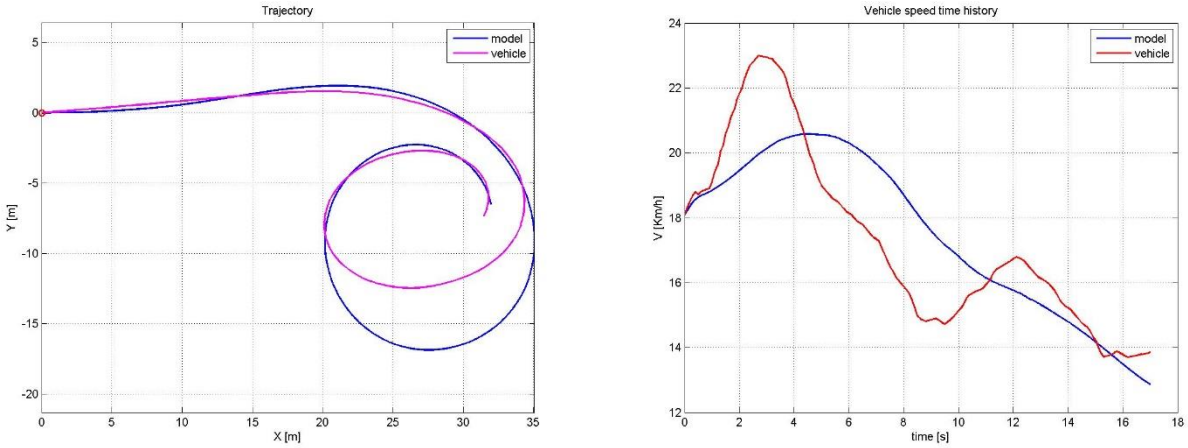

Figure E.8.3-134 Trajectory and Speed with Forward shifting 65mm

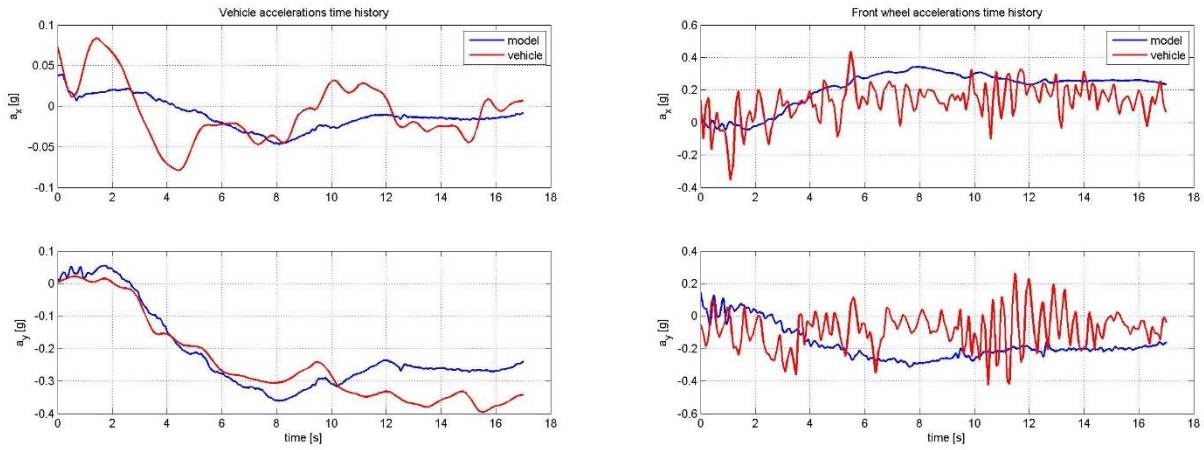

Figure E.8.3-135 Vehicle and Front wheel accelerations with Forward shifting 65mm

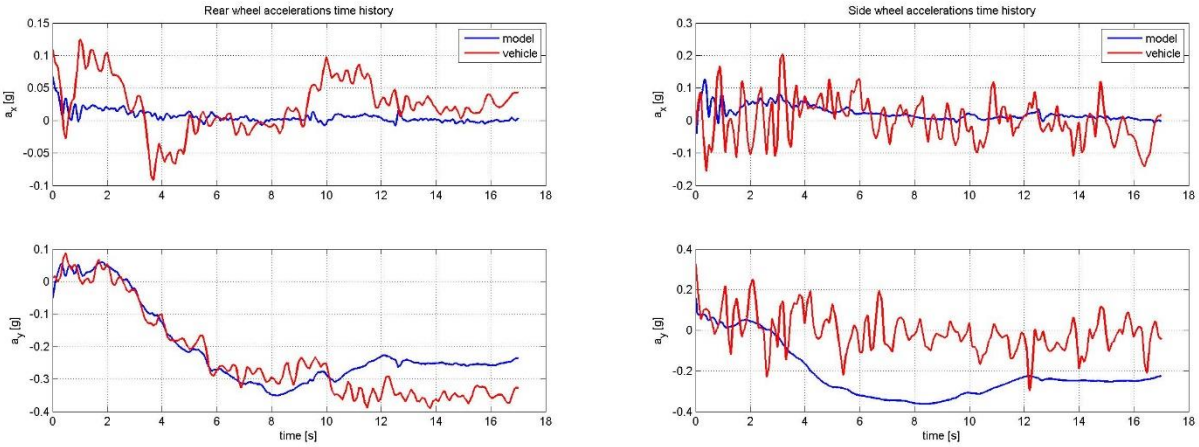

Figure E.8.3-136 Rear and Side wheel accelerations with Forward shifting 65mm

E.8.4 Constant Speed with Camber angle increase

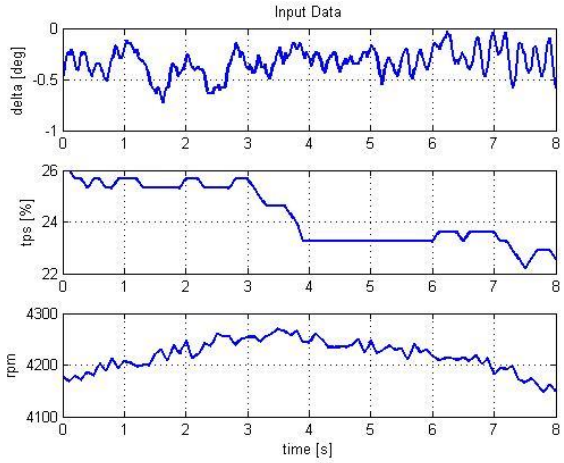

Figure E.8.4-137 Input data with Camber angle 2°

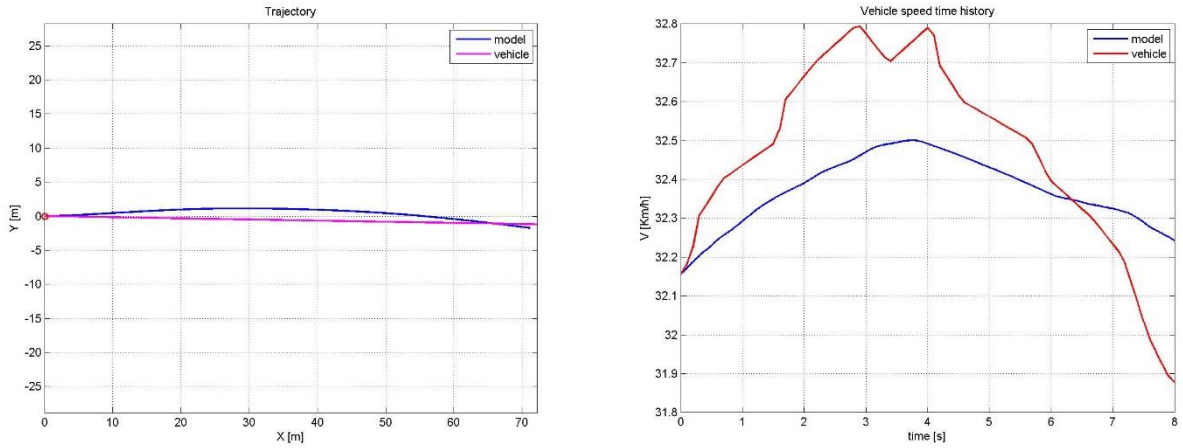

Figure E.8.4-138 Trajectory and Speed with Camber angle 2°

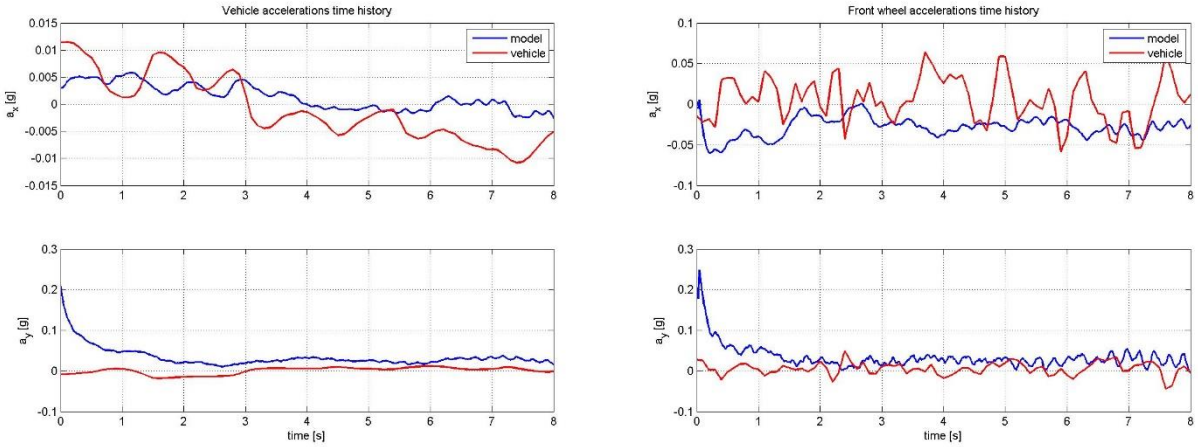

Figure E.8.4-139 Vehicle and Front wheel accelerations with Camber angle 2°

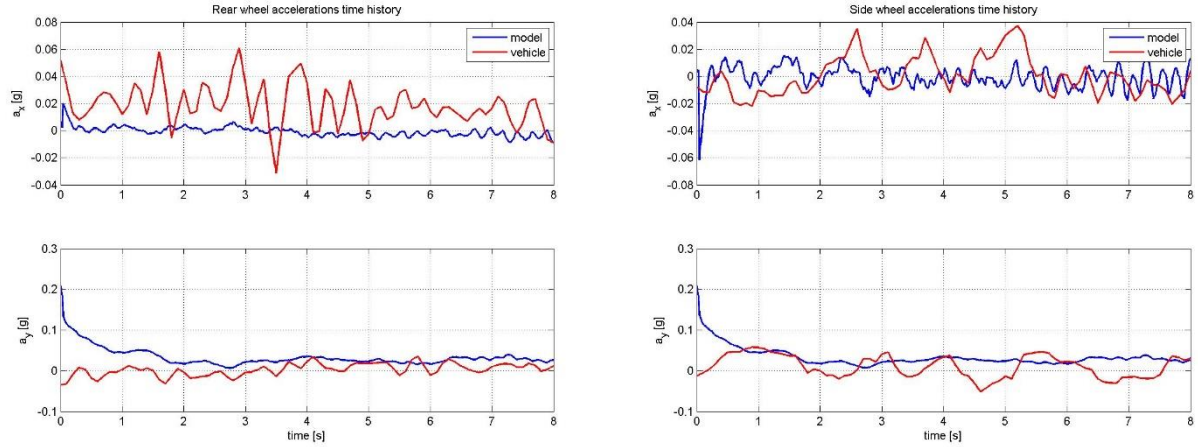

Figure E.8.4-140 Rear and Side wheel accelerations with Camber angle 2°

E.8.5 Steering Pad Left with Camber angle increase

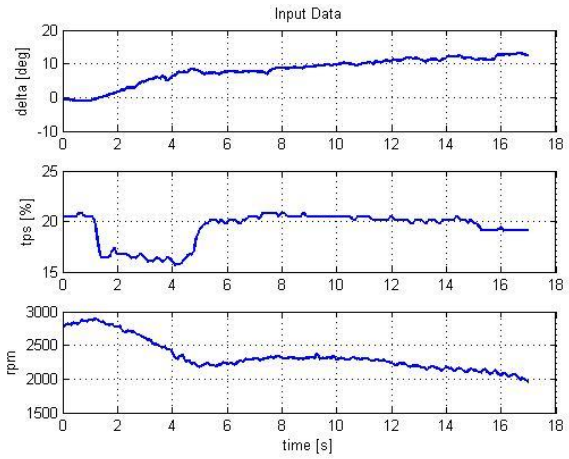

Figure E.8.5-141 Input data with Camber angle 2°

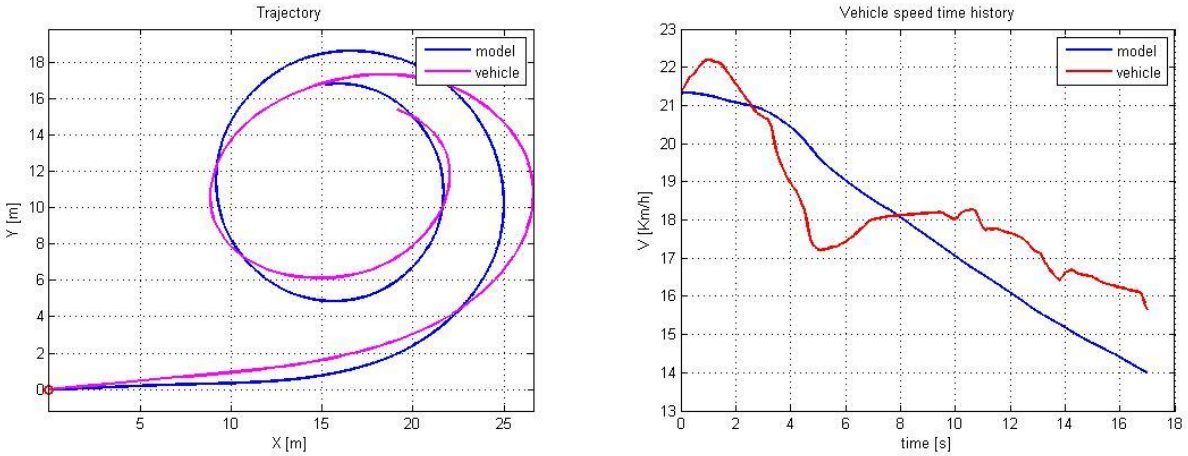

Figure E.8.5-142 Trajectory and Speed with Camber angle 2°

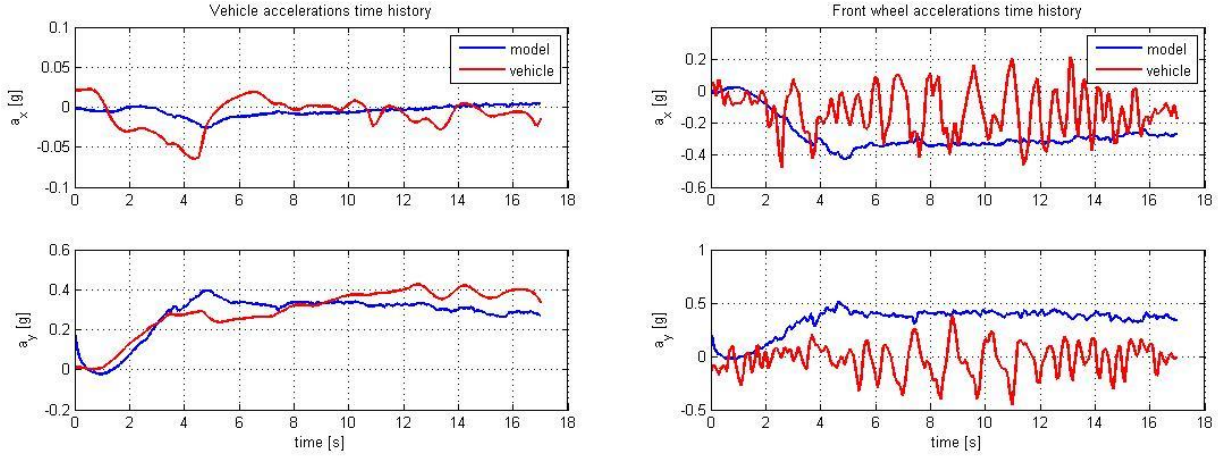

Figure E.8.5-143 Vehicle and Front wheel accelerations with Camber angle 2°

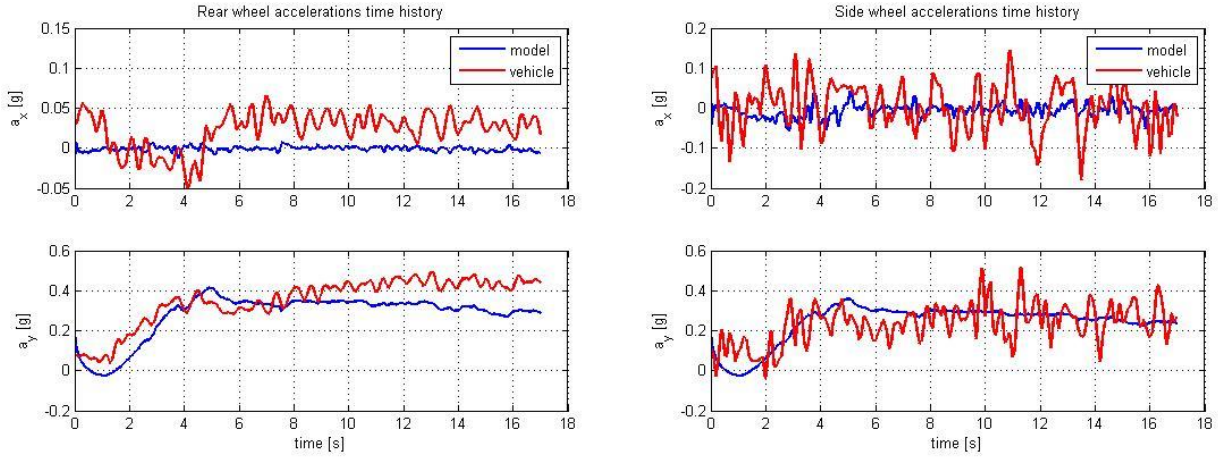

Figure E.8.5-144 Rear and Side wheel accelerations with Camber angle 2°

E.8.6 Steering Pad Right with Camber angle increase

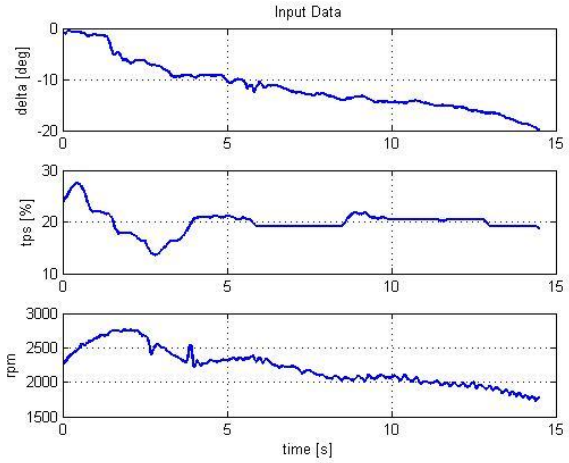

Figure E.8.6-145 Input data with Camber angle 2°

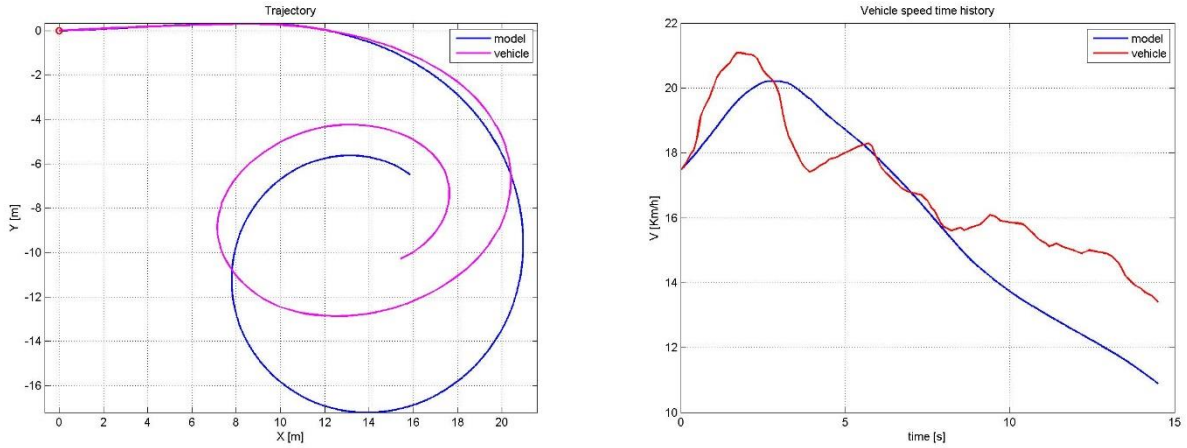

Figure E.8.6-146 Trajectory and Speed with Camber angle 2°

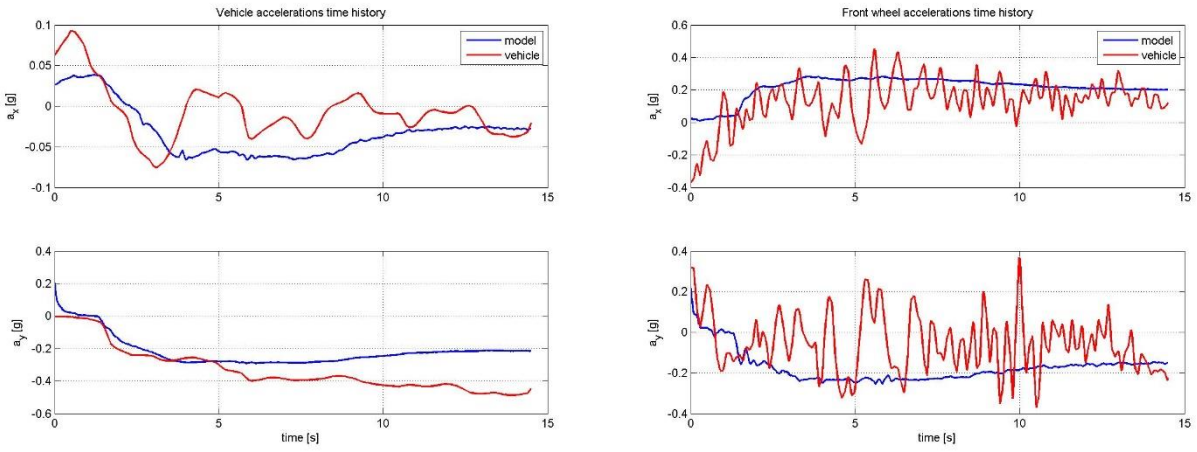

Figure E.8.6-147 Vehicle and Front wheel accelerations with Camber angle 2°

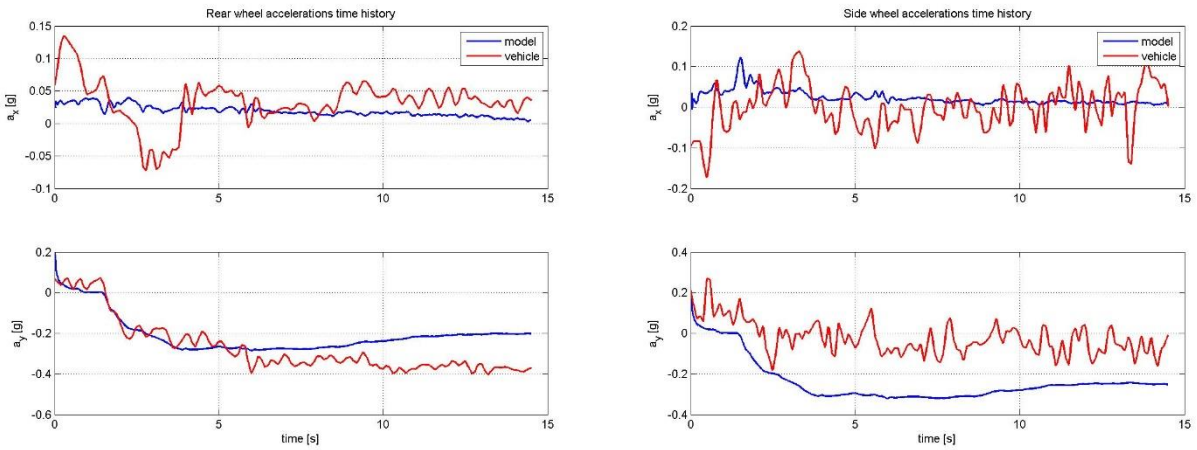

Figure E.8.6-148 Rear and Side wheel accelerations with Camber angle 2°

E.9 Validation Errors

		Constant Speed	Acceleration	Braking	Steering pad Left	Steering pad Right	Wave pad	Step Steer
Trajectory [m]	**μ**	0,493	2,093	2,321	3,252	2,810	9,7	1,024
	σ	0,286	1,171	2,079	1,604	2,051	4,845	0,492
Speed [Km/h]	**μ**	-0,015	3,151	1,019	-0,251	1,080	-0,545	0,042
	σ	0,107	1,696	1,253	1,886	1,549	0,497	0,093
Ax [g]	**μ**	0,000	0,015	0,017	0,003	0,007	0,004	0,000
	σ	0,003	0,014	0,050	0,033	0,019	0,037	0,012
Ay [g]	**μ**	-0,029	-0,037	-0,128	0,431	-0,448	-0,008	-0,052
	σ	0,028	0,027	0,085	0,266	0,194	0,374	0,207
Axf [g]	**μ**	0,036	0,137	0,344	-0,082	0,101	0,071	0,139
	σ	0,048	0,259	0,353	0,111	0,177	0,185	0,239
Ayf [g]	**μ**	-0,027	0,013	-0,195	0,090	-0,308	0,034	-0,019
	σ	0,038	0,153	0,203	0,144	0,204	0,301	0,267
Axr [g]	**μ**	-0,019	-0,088	0,366	-0,027	-0,002	0,018	0,015
	σ	0,013	0,036	0,270	0,059	0,025	0,061	0,030
Ayr [g]	**μ**	-0,051	-0,067	-0,137	-0,029	0,098	-0,042	-0,058
	σ	0,025	0,026	0,089	0,050	0,073	0,070	0,113
Axs [g]	**μ**	0,017	0,007	-0,123	-0,008	0,003	0,092	0,114
	σ	0,016	0,109	0,091	0,069	0,061	0,103	0,103
Ays [g]	**μ**	-0,026	0,058	-0,083	0,182	-0,060	0,114	0,058
	σ	0,042	0,168	0,148	0,114	0,104	0,180	0,116

Table E.1 - Errors from Validation process

Attachment F – Sensitivity Analysis Results

In this attachment are reported the results given by the sensitivity analysis algorithm with the Part Load Configuration along a Left Steering Pad, a Right Steering Pad and Straight Line during braking

F.1 Steering Pad Left

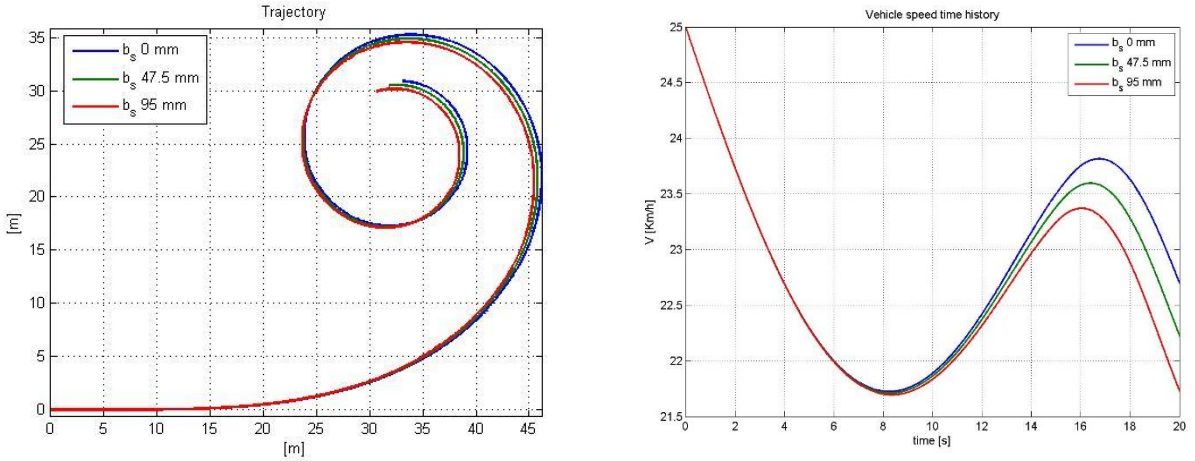

Figure F.1-149 Trajectory and Speed for Forward shifting

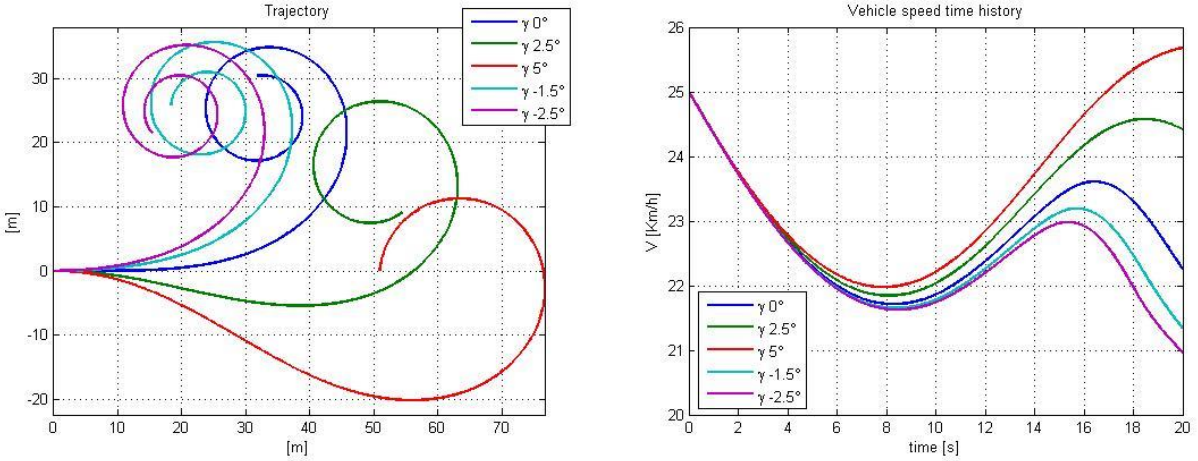

Figure F.1-150 Trajectory and Speed for Camber

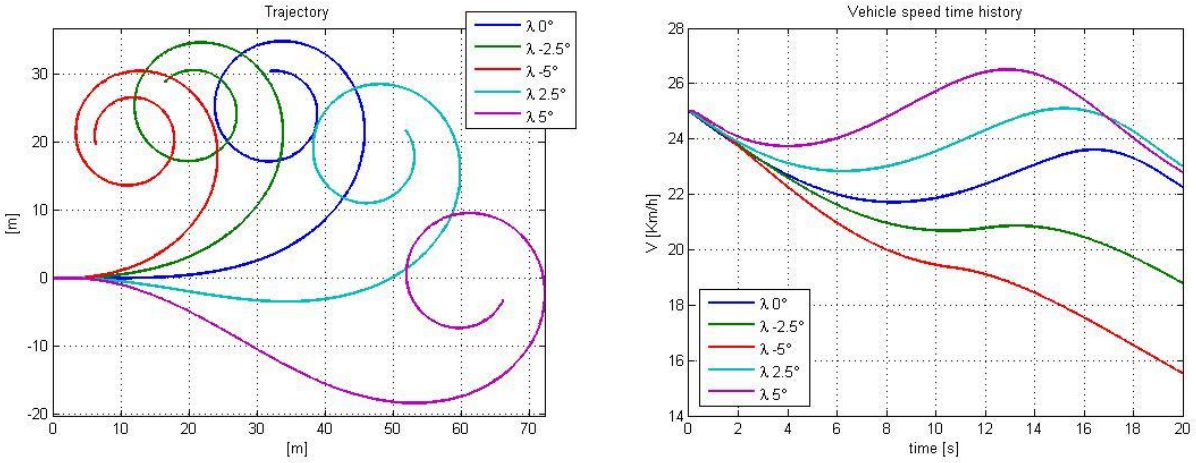

Figure F.1-151 Trajectory and Speed for Toe angle

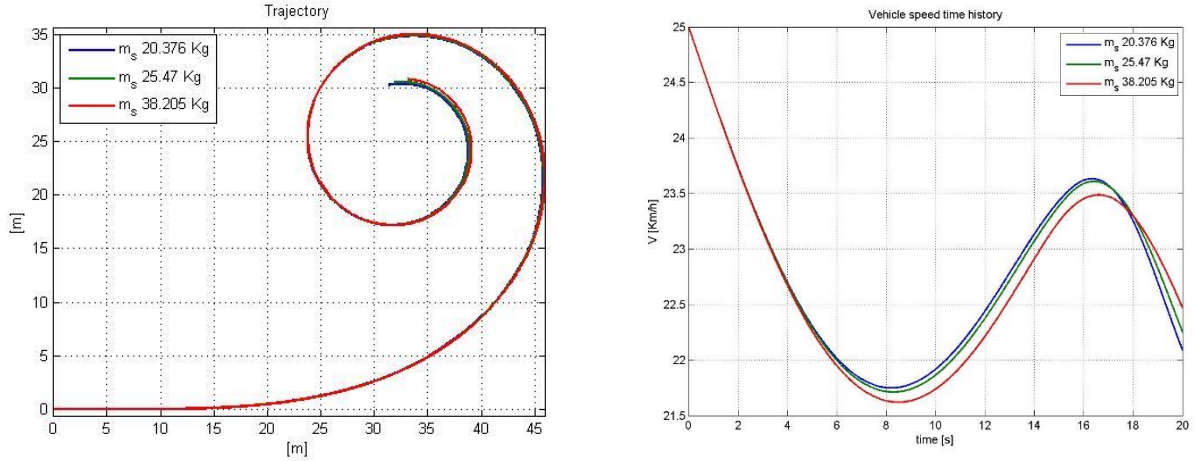

Figure F.1-152 Trajectory and Speed for Sidecar mass

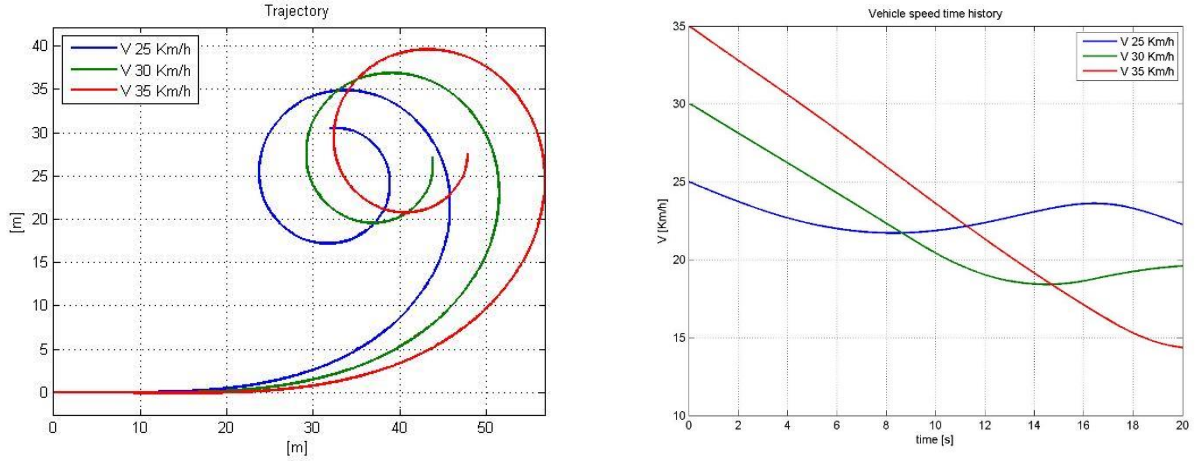

Figure F.1-153 Trajectory and Speed for Initial speed

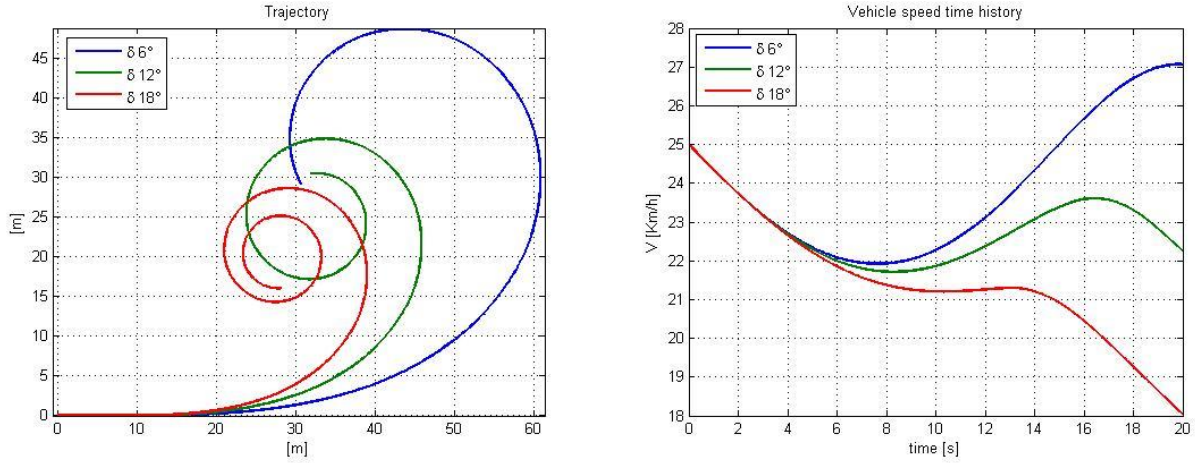

Figure F.1-154 Trajectory and Speed for Maximum steer

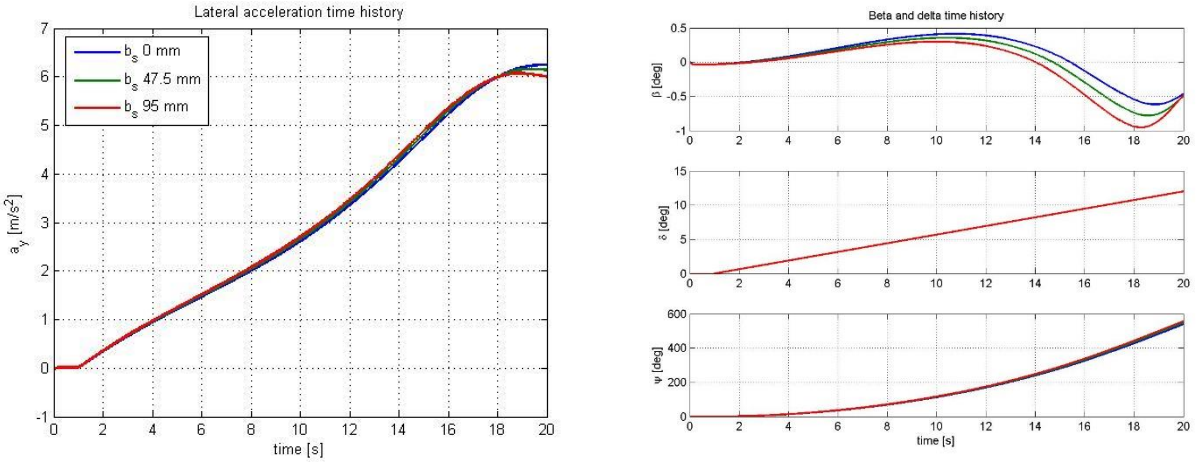

Figure F.1-155 Lateral acceleration and Angles for Forward shifting

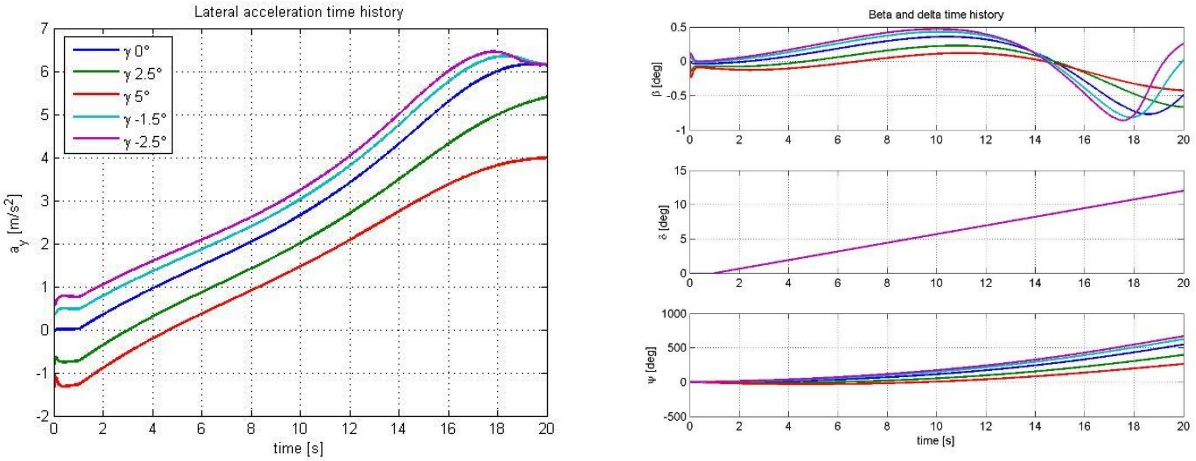

Figure F.1-156 Lateral acceleration and Angles for Camber angle

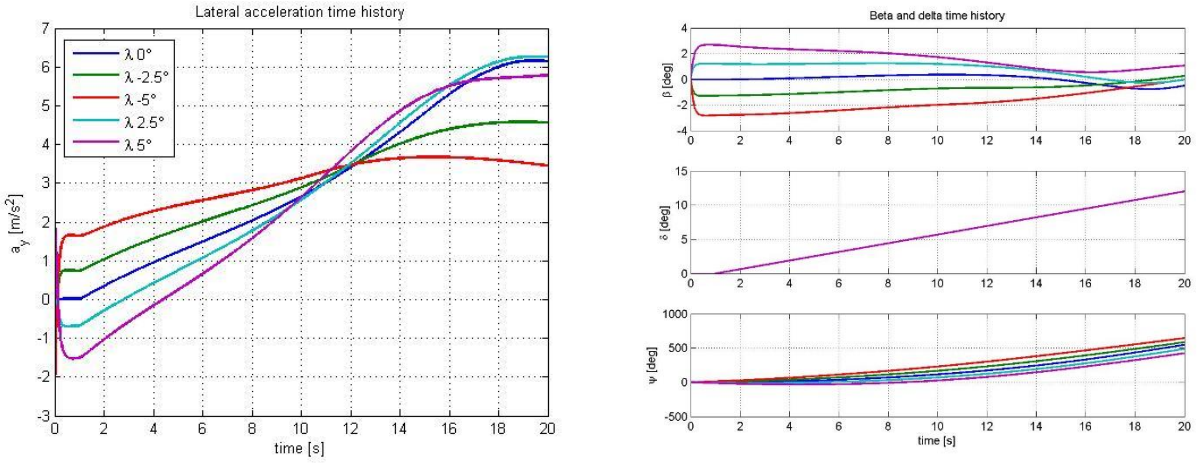

Figure F.1-157 Lateral acceleration and Angles for Toe angle

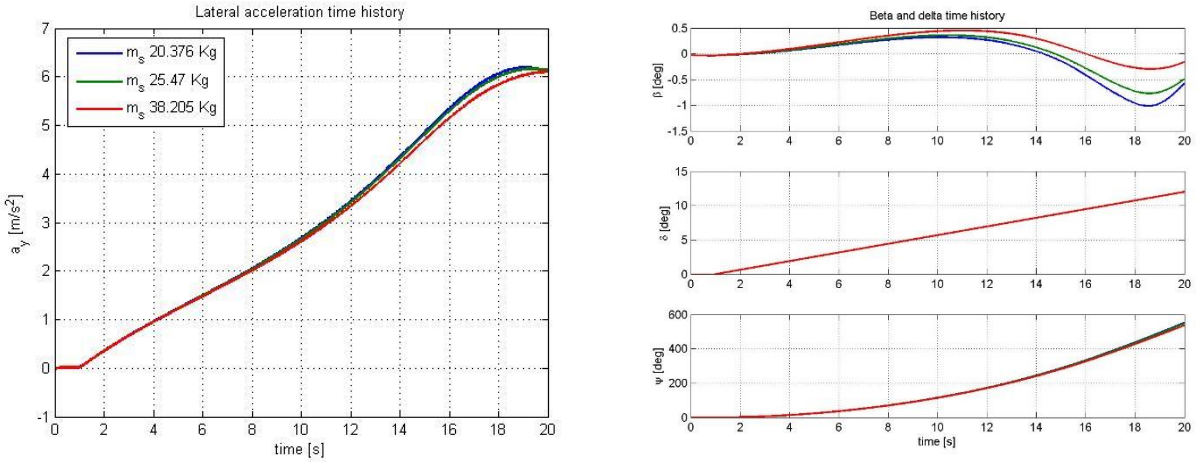

Figure F.1-158 Lateral acceleration and Angles for Sidecar mass

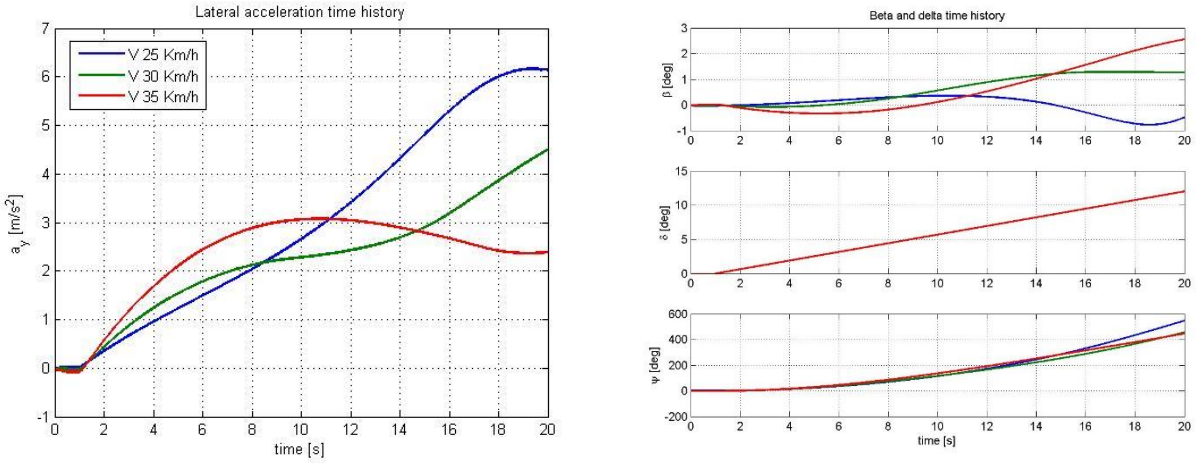

Figure F.1-159 Lateral acceleration and Angles for Initial speed

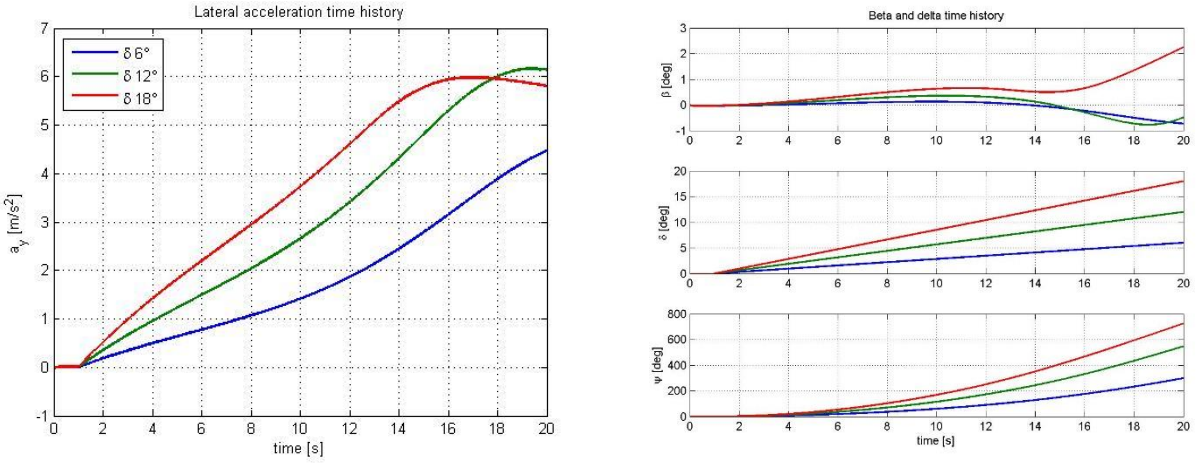

Figure F.1-160 Lateral acceleration and Angles for Maximum steer

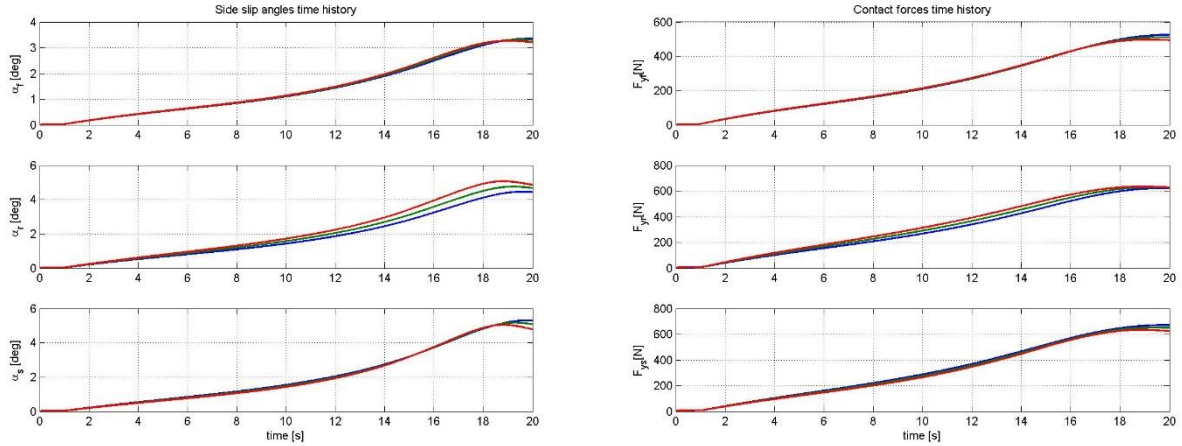

Figure F.1-161 Slip angles and Contact forces for Forward shifting

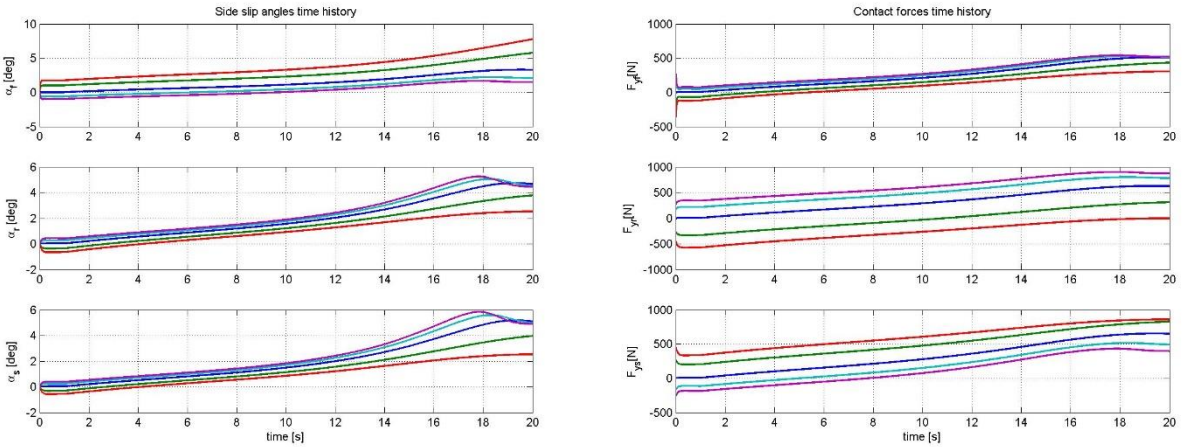

Figure F.1-162 Slip angles and Contact forces for Camber angle

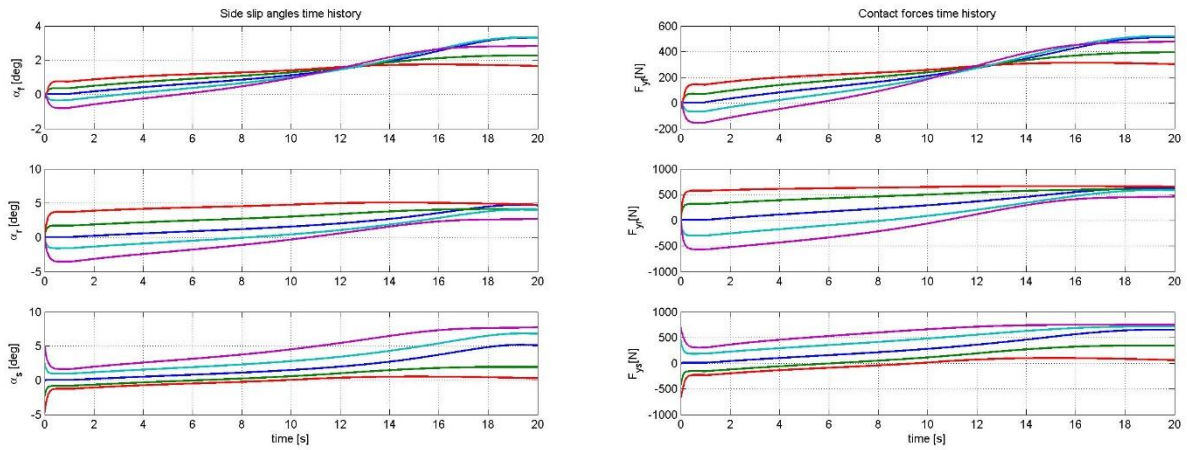

Figure F.1-1635 Slip angles and Contact forces for Toe angle

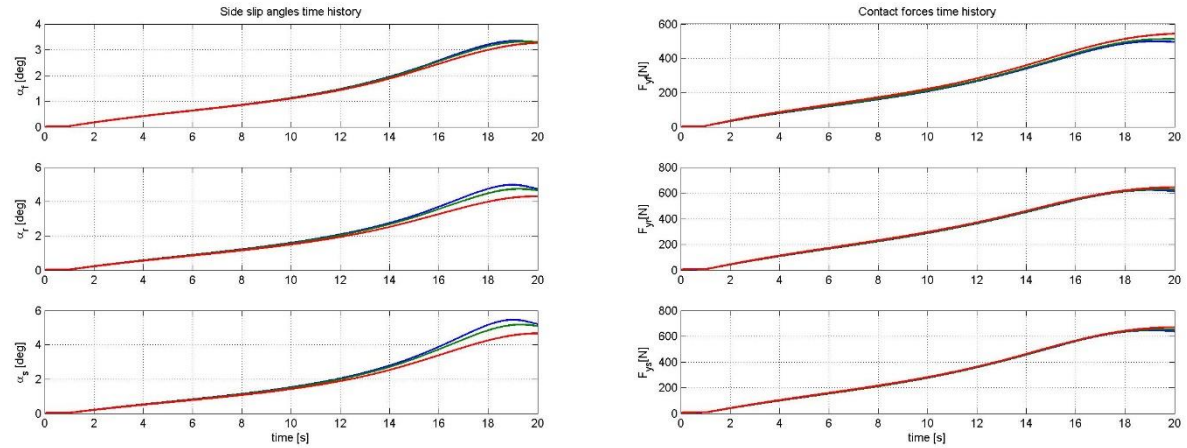

Figure F.1-164 Slip angles and Contact forces for Sidecar mass

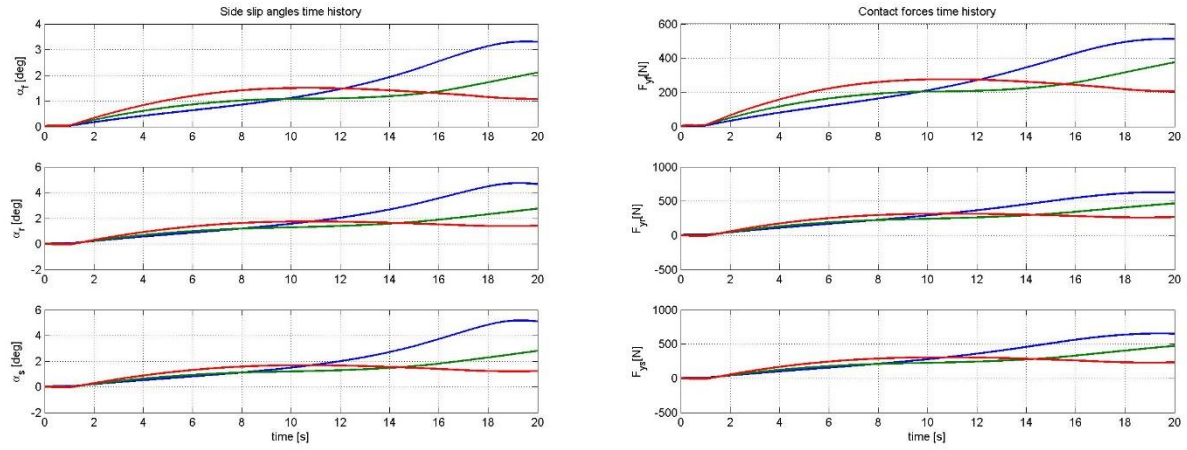

Figure F.1-165 Slip angles and Contact forces for Initial speed

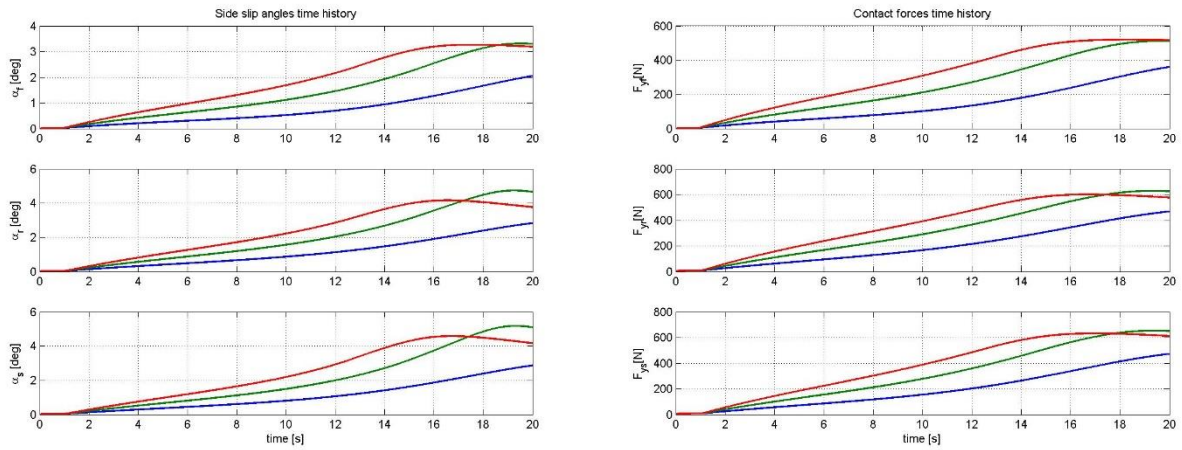

Figure F.1-166 Slip angles and Contact forces for Maximum steer angle

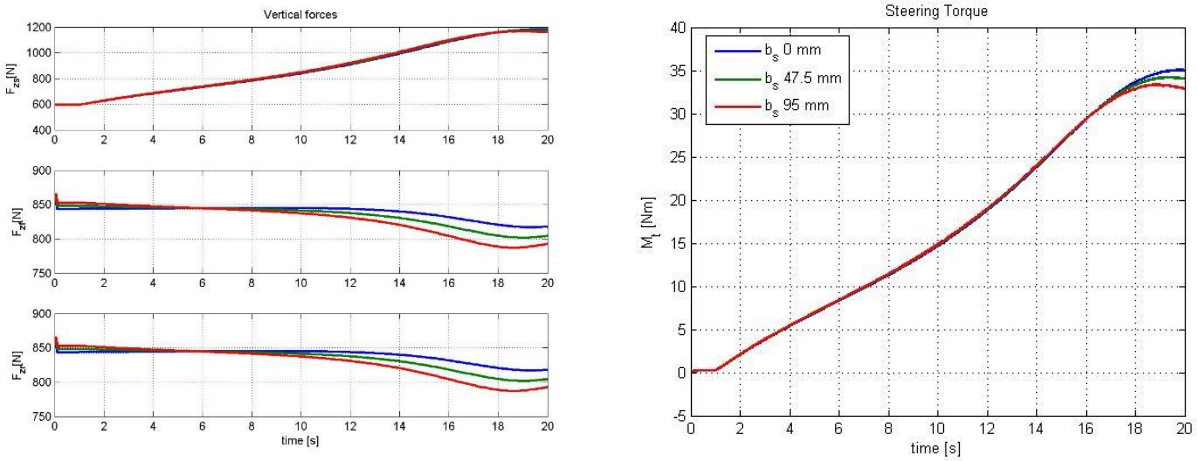

Figure F.1-167 Vertical forces and Steering torque for Forward shifting

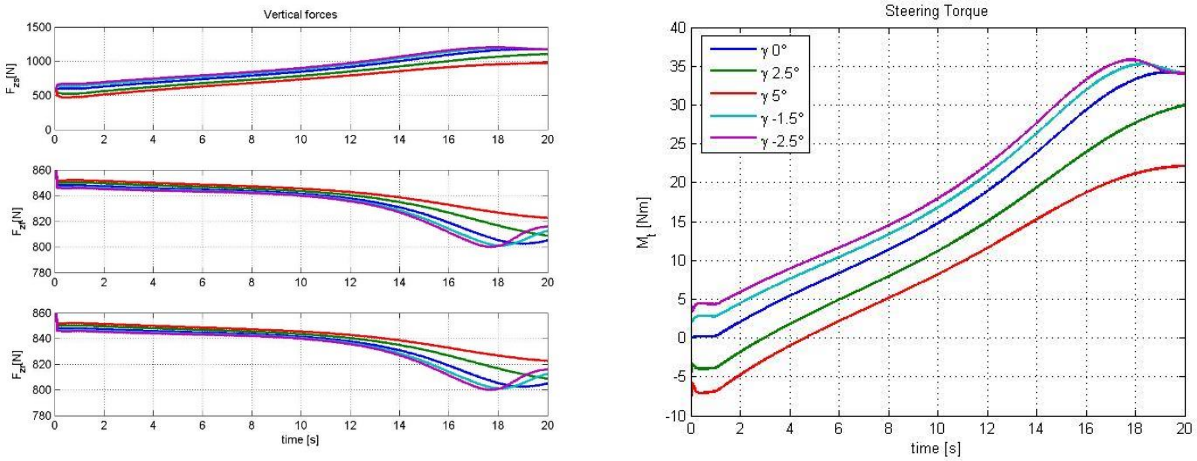

Figure F.1-168 Vertical forces and Steering torque for Camber angle

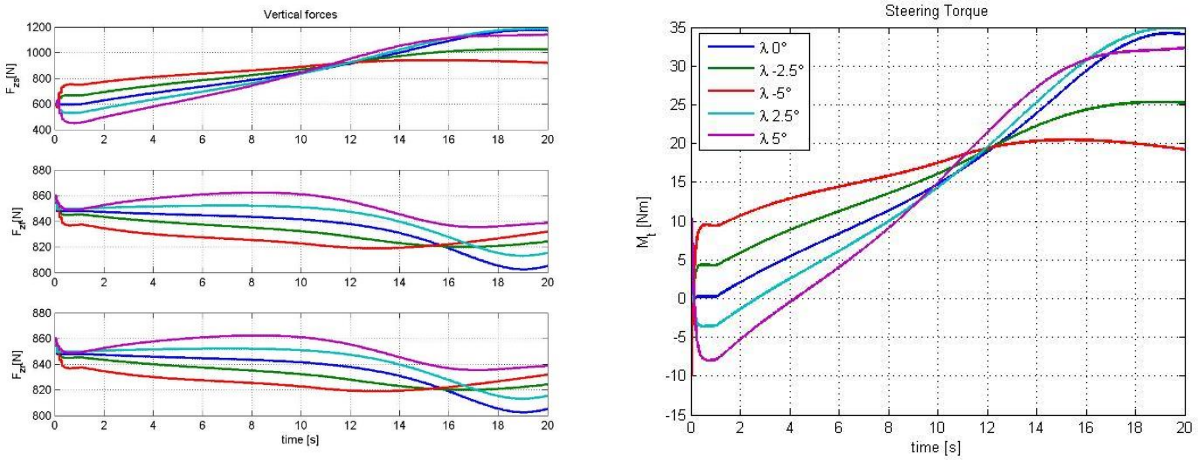

Figure F.1-169 Vertical forces and Steering torque for Toe angle

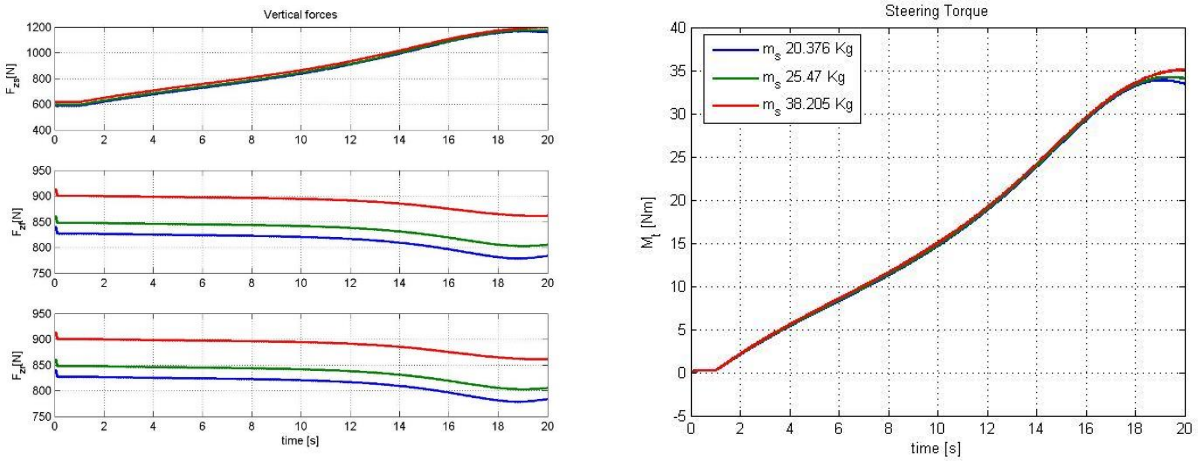

Figure F.1-170 Vertical forces and Steering torque for Sidecar mass

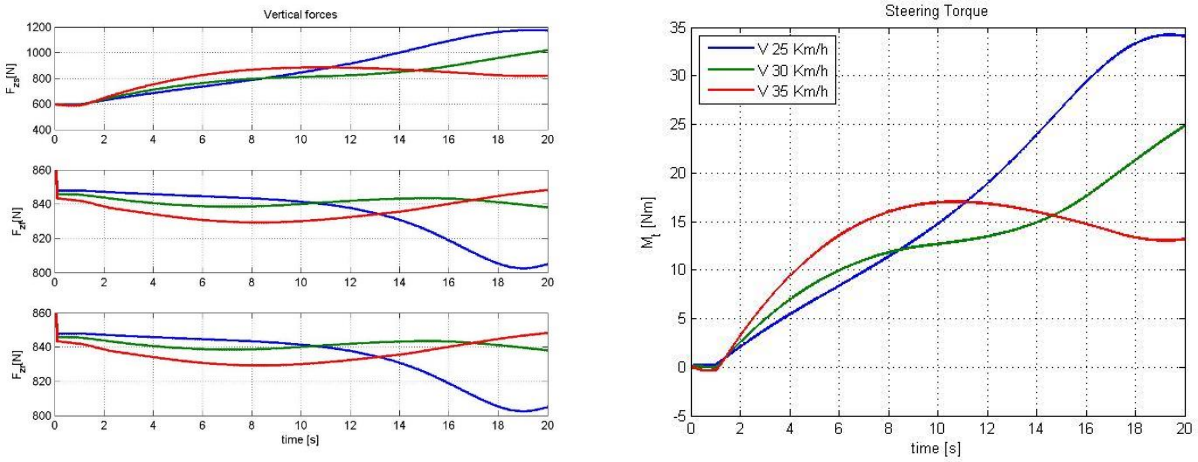

Figure F.1-171 Vertical forces and Steering torque for Initial speed

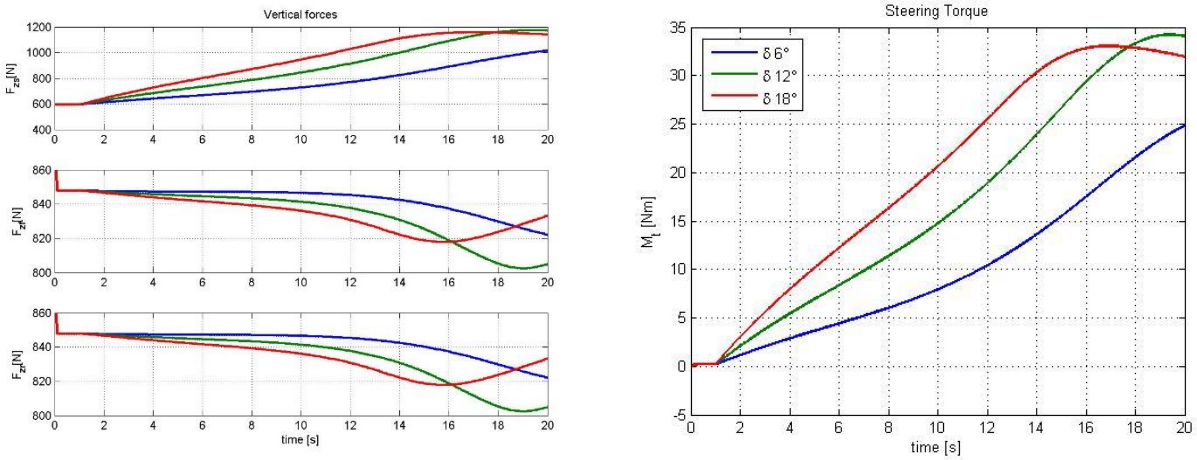

Figure F.1-172 Vertical forces and Steering torque for Maximum steering angle

F.2 Steering Pad Right

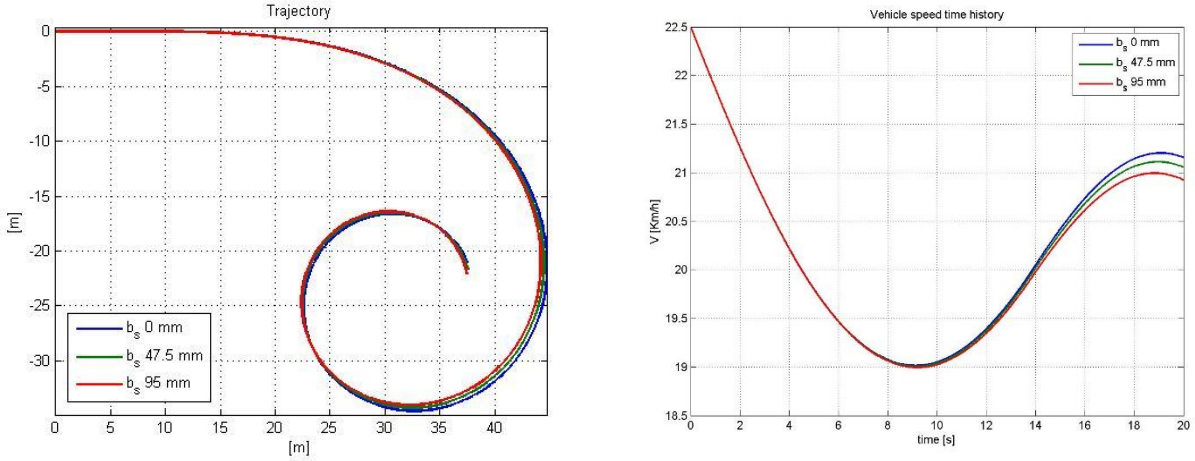

Figure F.2-173 Trajectory and Speed for Forward shifting

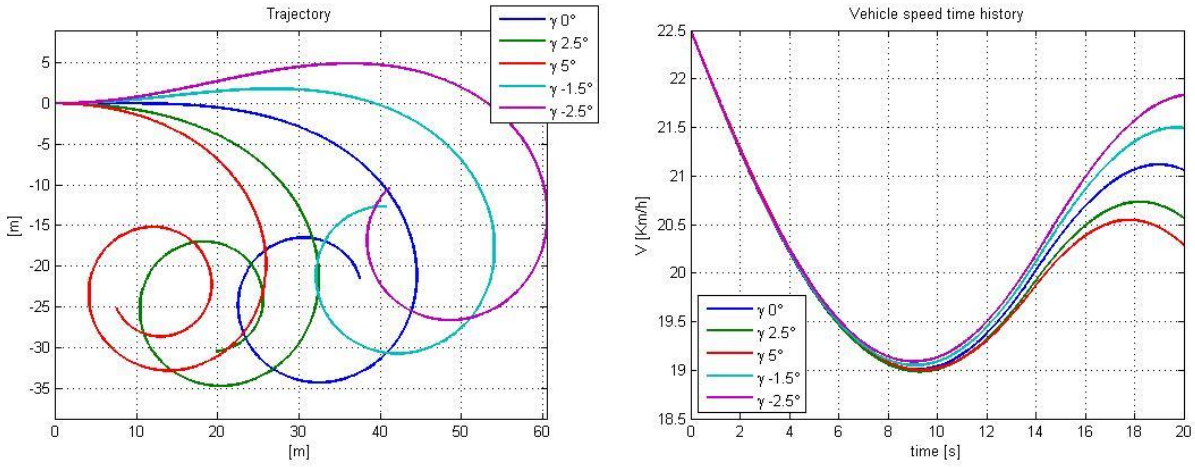

Figure F.2-174 Trajectory and Speed for Camber angle

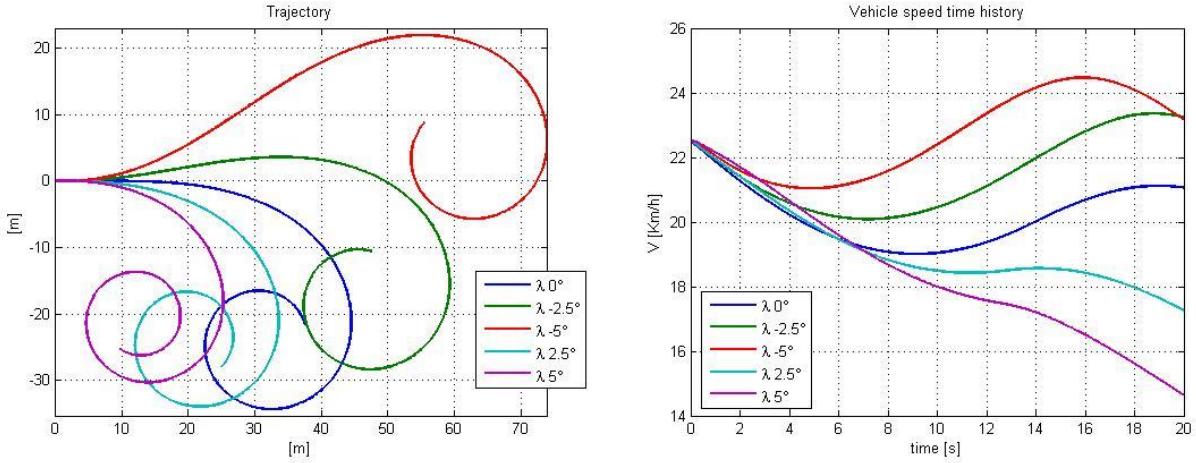

Figure F.2-175 Trajectory and Speed for Toe angle

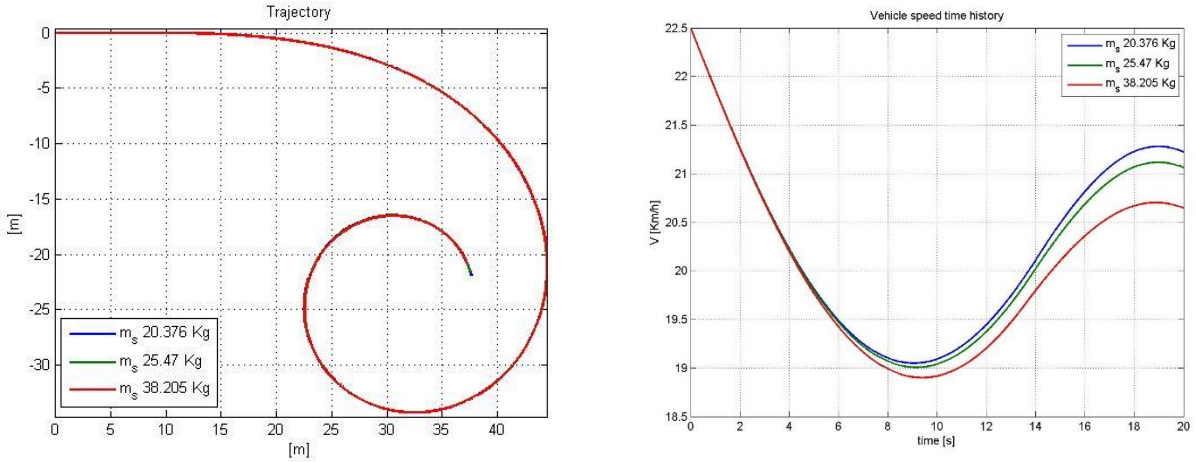

Figure F.2-176 Trajectory and Speed for Sidecar mass

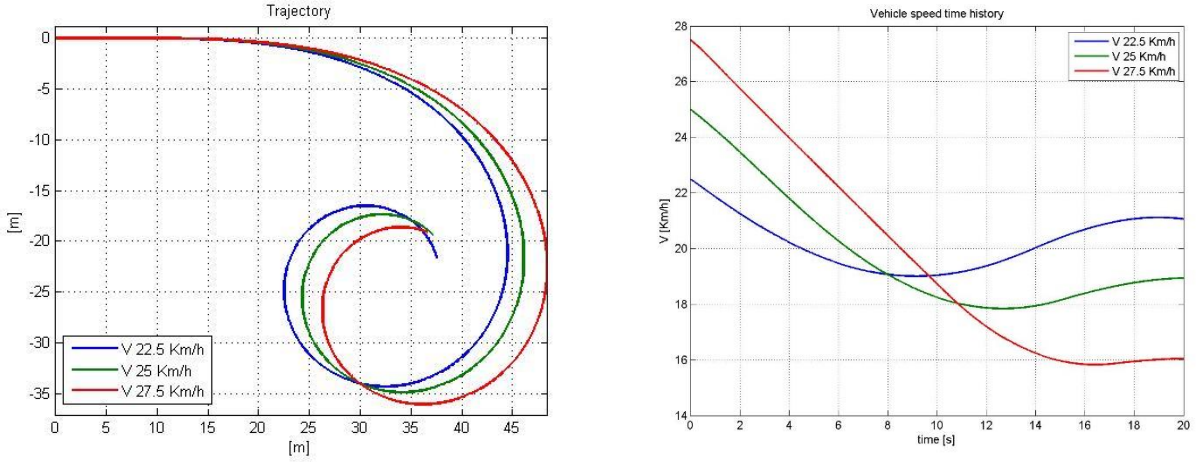

Figure F.2-177 Trajectory and Speed for Initial speed

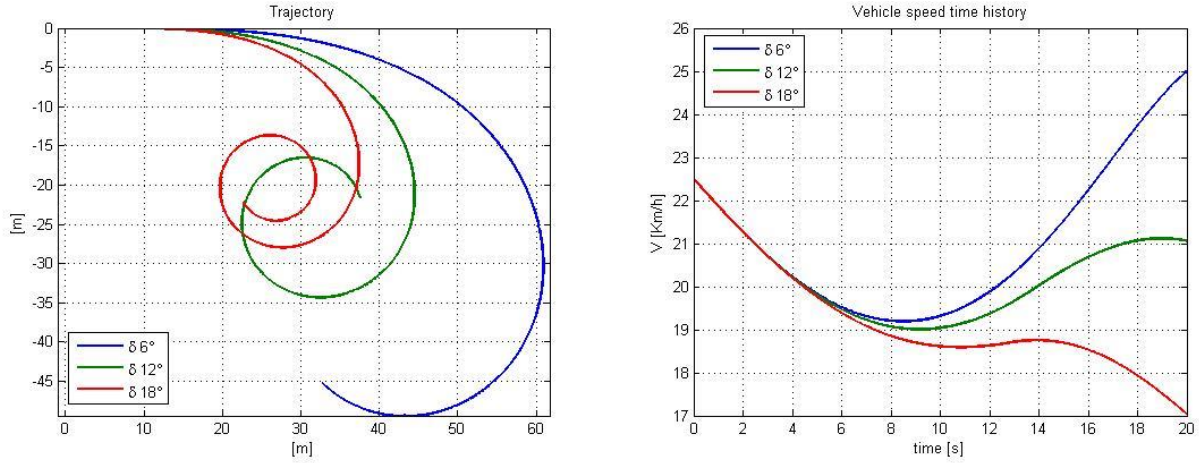

Figure F.2-178 Trajectory and Speed for Maximum steering angle

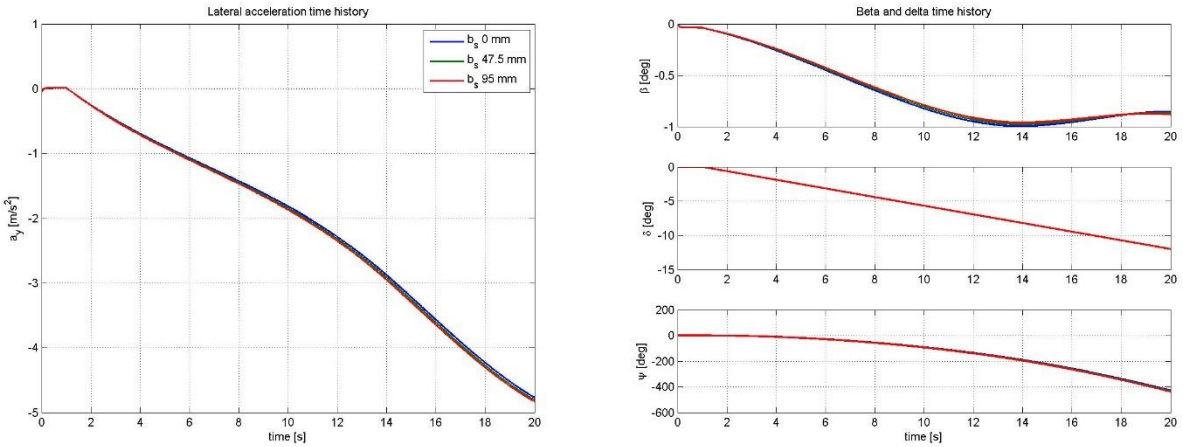

Figure F.2-179 Lateral acceleration and Angles for Forward shifting

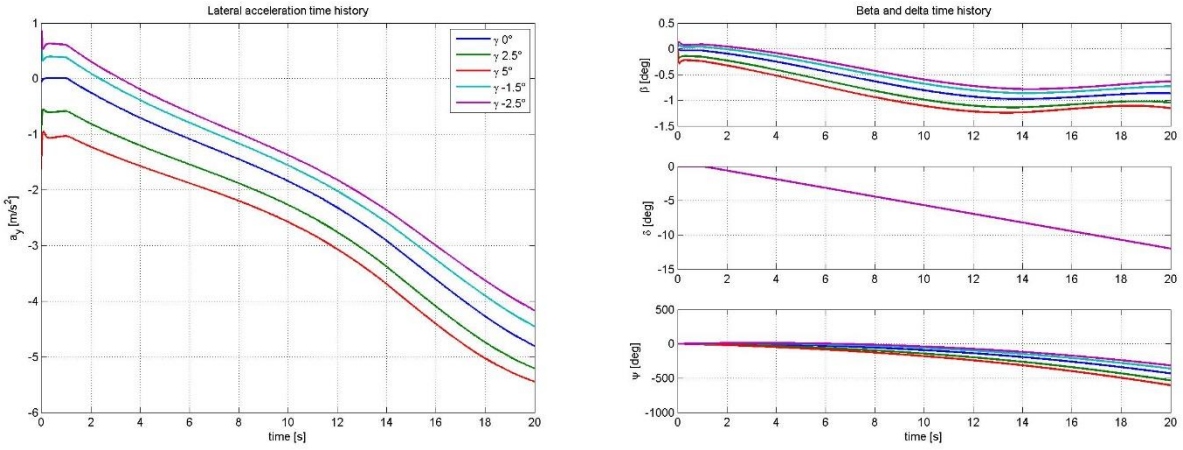

Figure F.2-180 Lateral acceleration and Angles for Camber angle

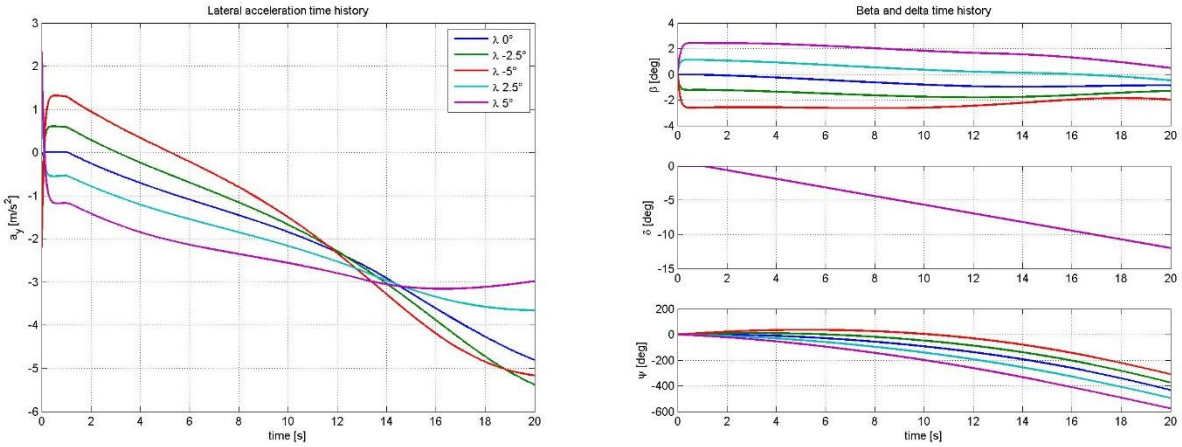

Figure F.2-181 Lateral acceleration and Angles for Toe angle

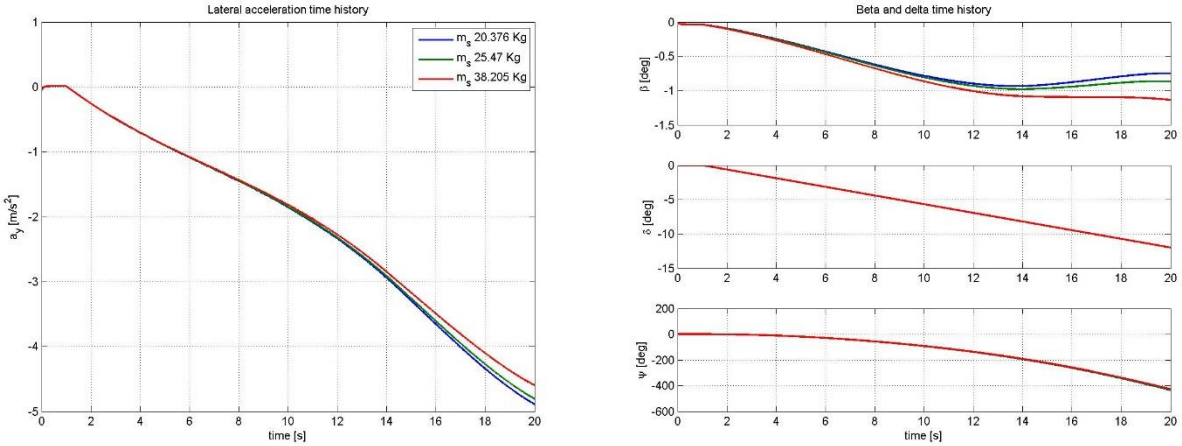

Figure F.2-182 Lateral acceleration and Angles for Sidecar mass

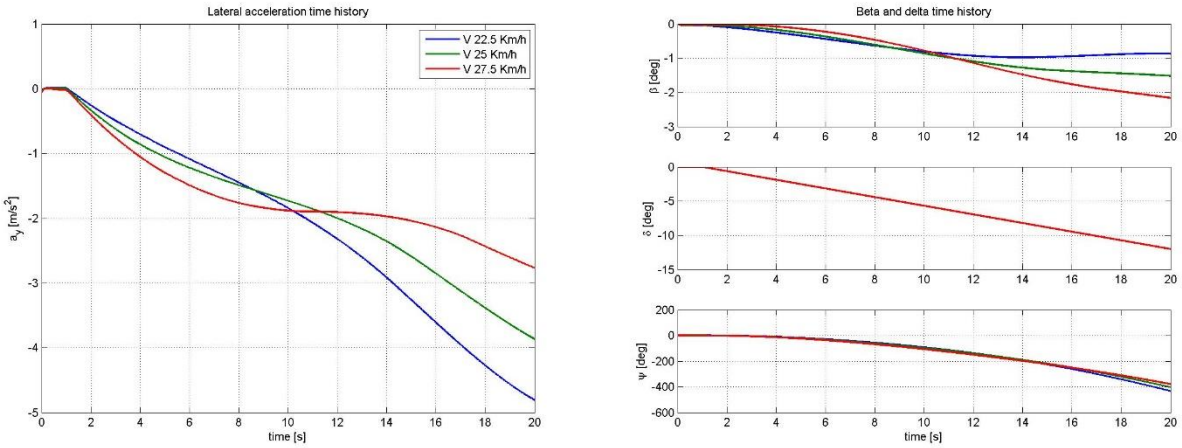

Figure F.2-183 Lateral acceleration and Angles for Initial speed

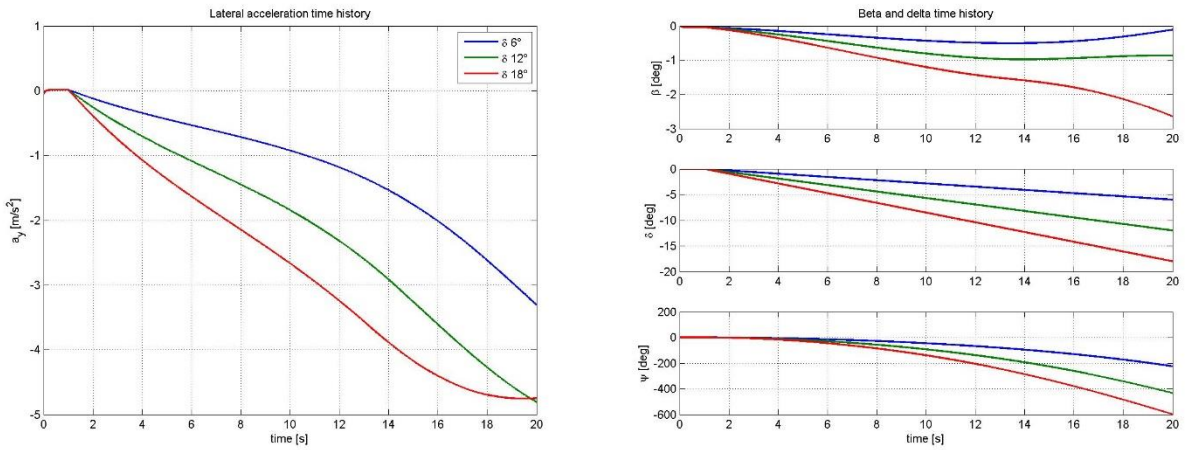

Figure F.2-184 Lateral acceleration and Angles for Maximum steering angle

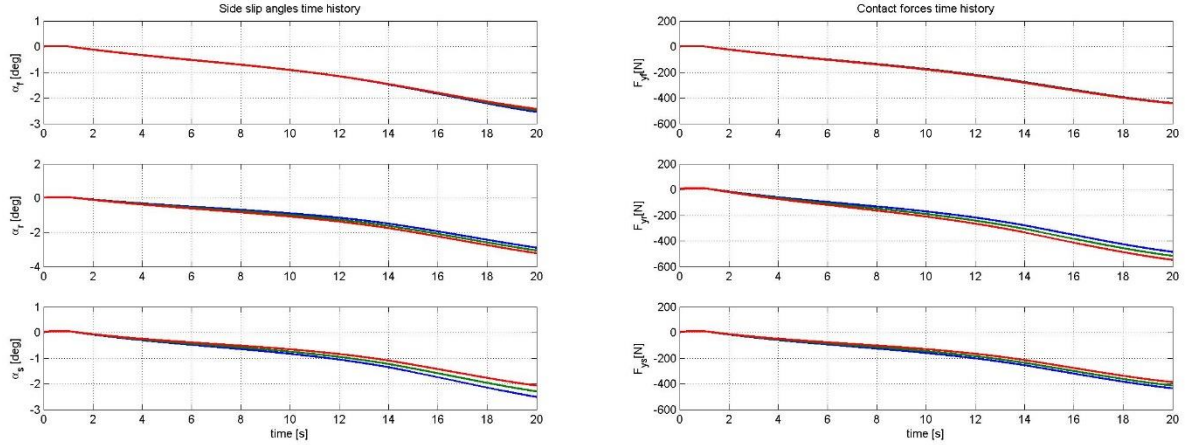

Figure F.2-185 Slip angles and Contact forces for Forward shifting

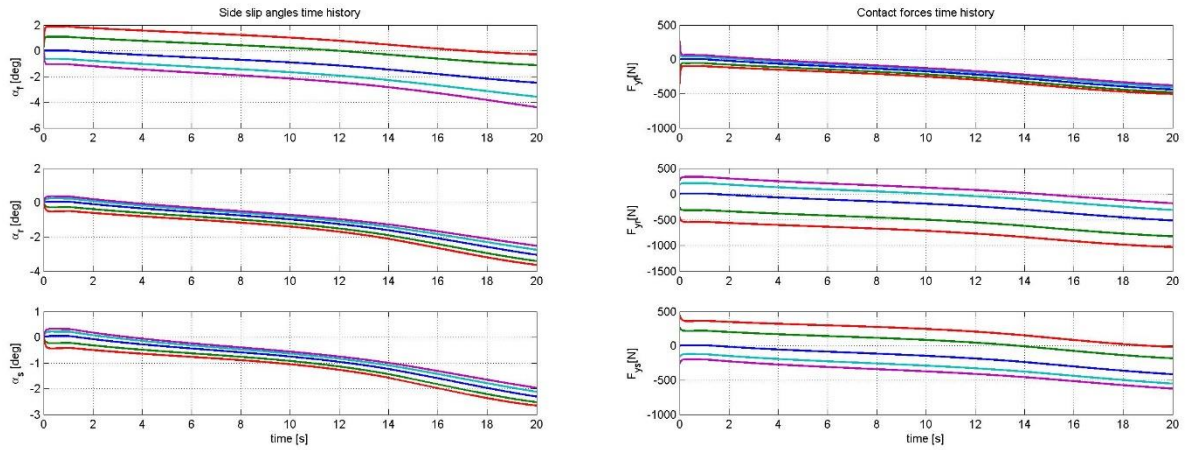

Figure F.2-186 Slip angles and Contact forces for Camber angle

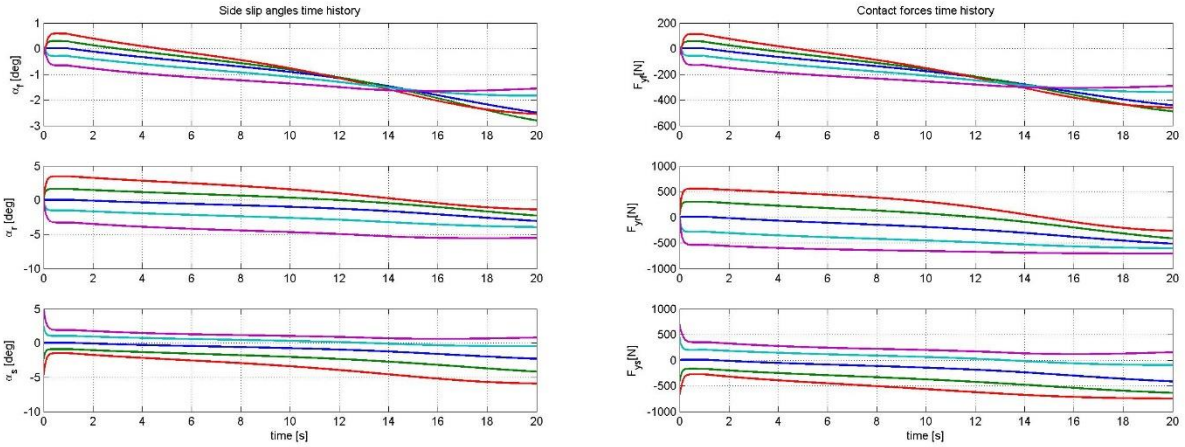

Figure F.2-187 Slip angles and Contact forces for Toe angle

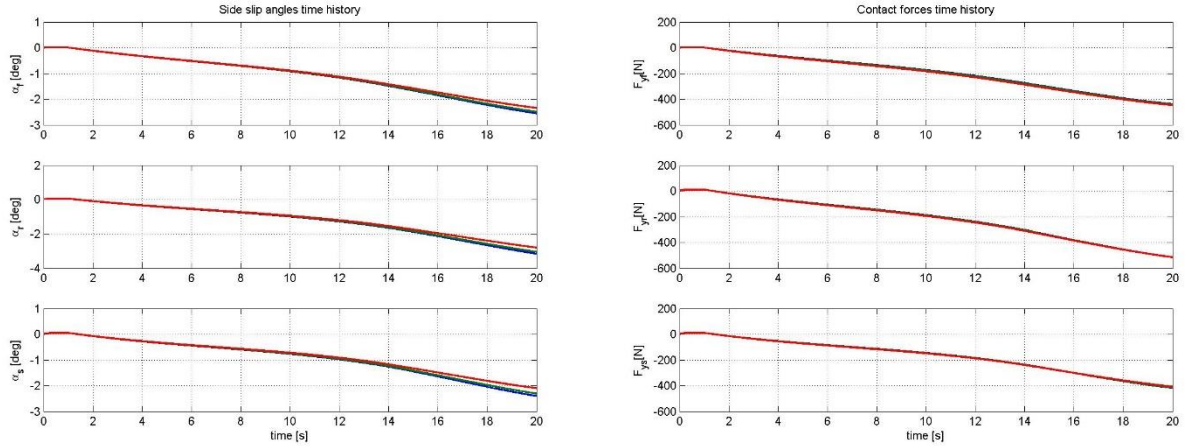

Figure F.2-188 Slip angles and Contact forces for Sidecar mass

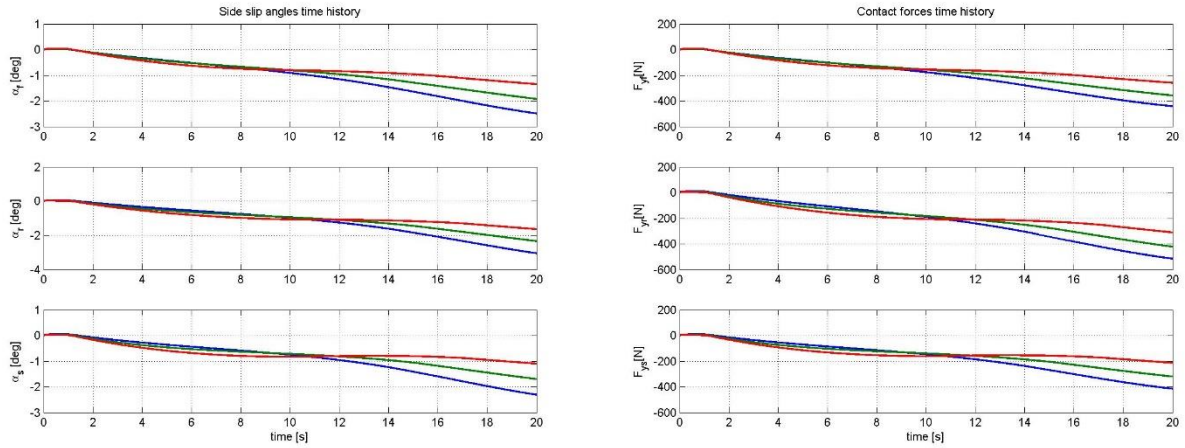

Figure F.2-17 Slip angles and Contact forces for Initial speed

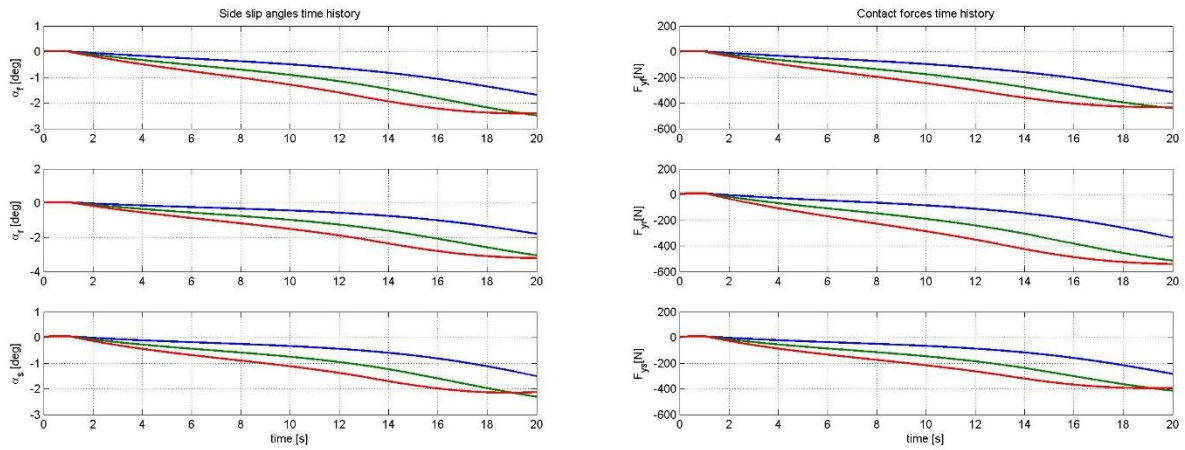

Figure F.2-189 Slip angles and Contact forces for Maximum steering angle

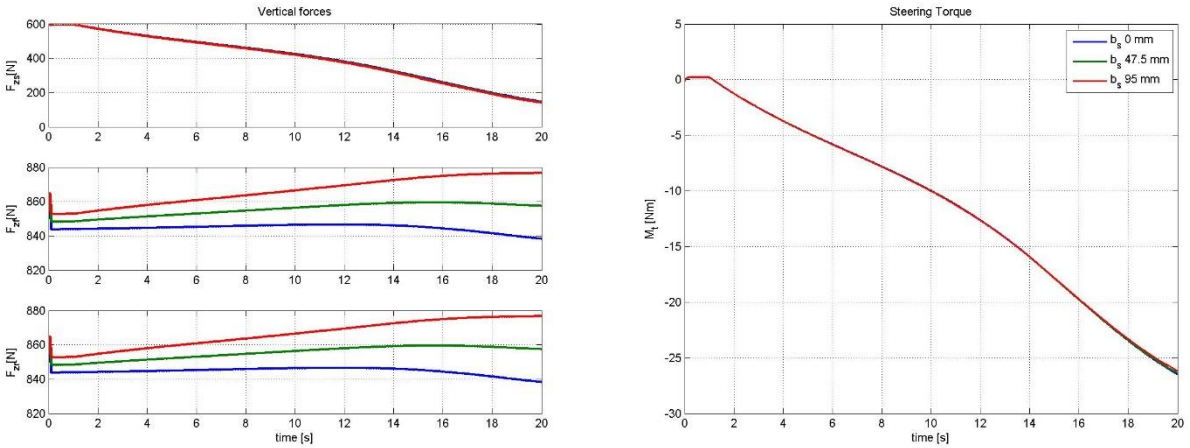

Figure F.2-190 Vertical forces and Steering torque for Forward shifting

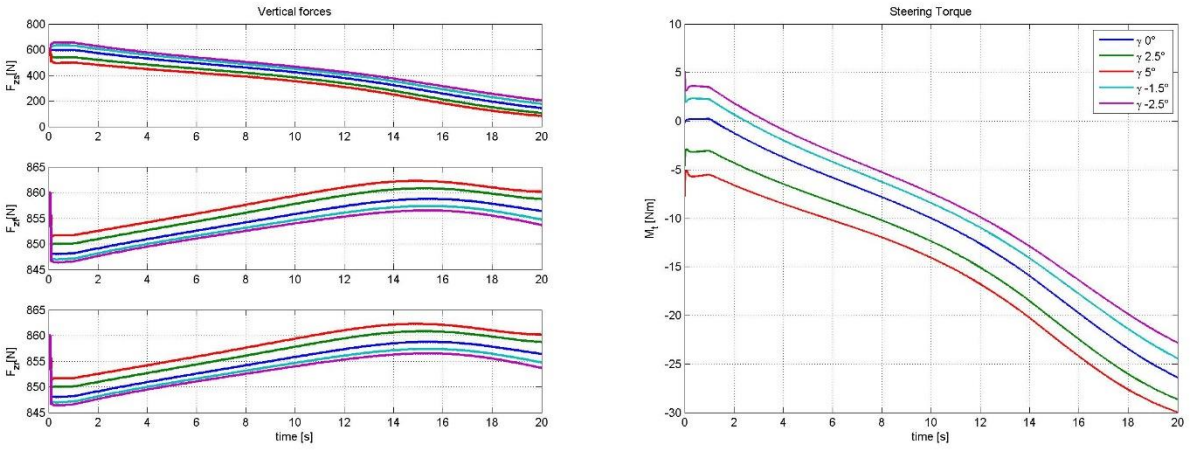

Figure F.2-191 Vertical forces and Steering torque for Camber angle

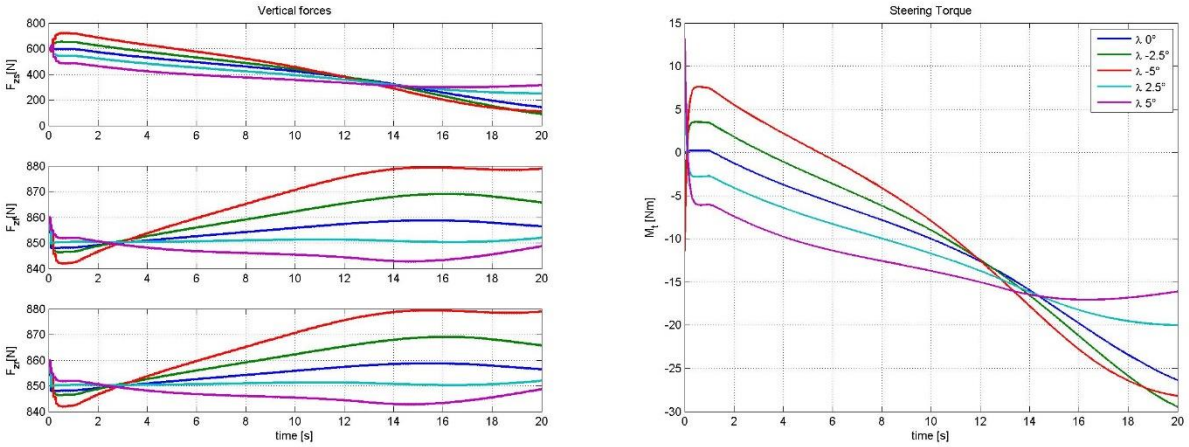

Figure F.2-192 Vertical forces and Steering torque for Toe angle

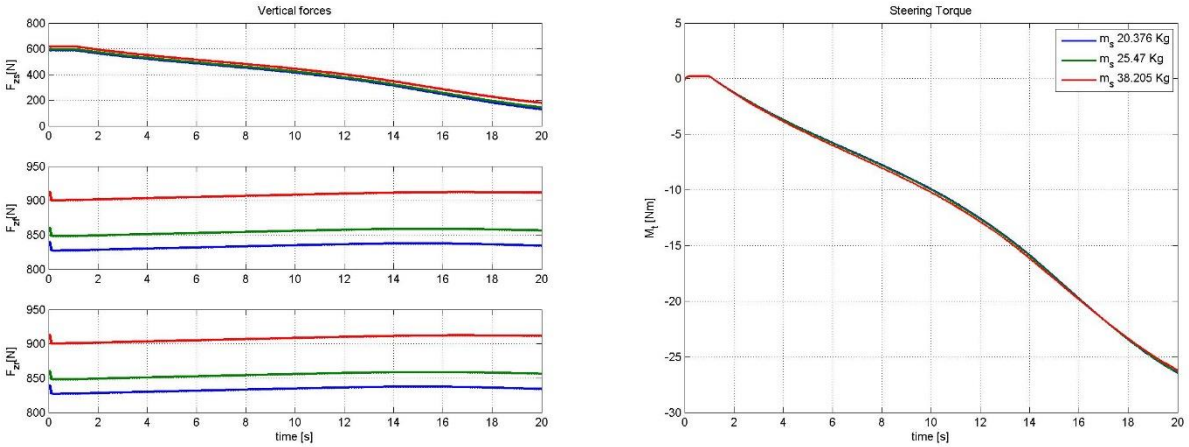

Figure F.2-193 Vertical forces and Steering torque for Sidecar mass

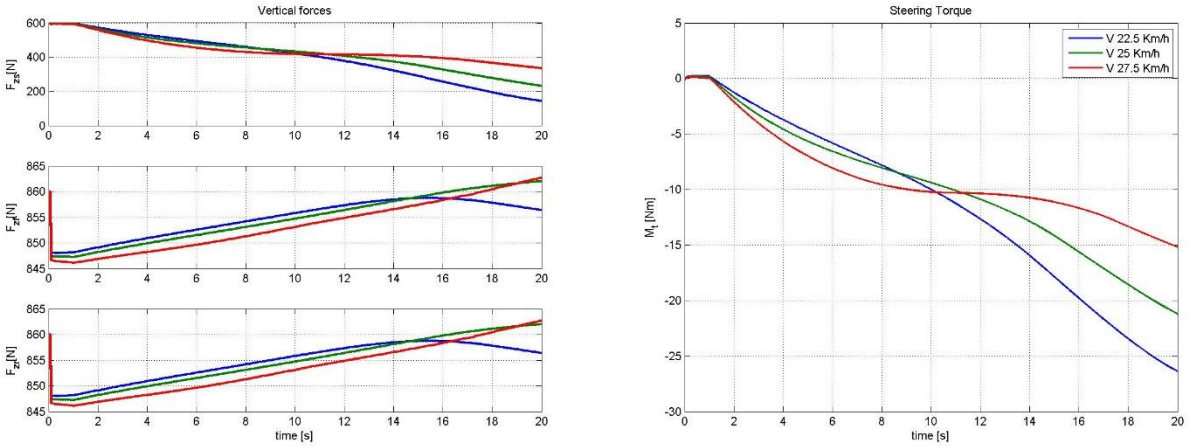

Figure F.2-194 Vertical forces and Steering torque for Initial speed

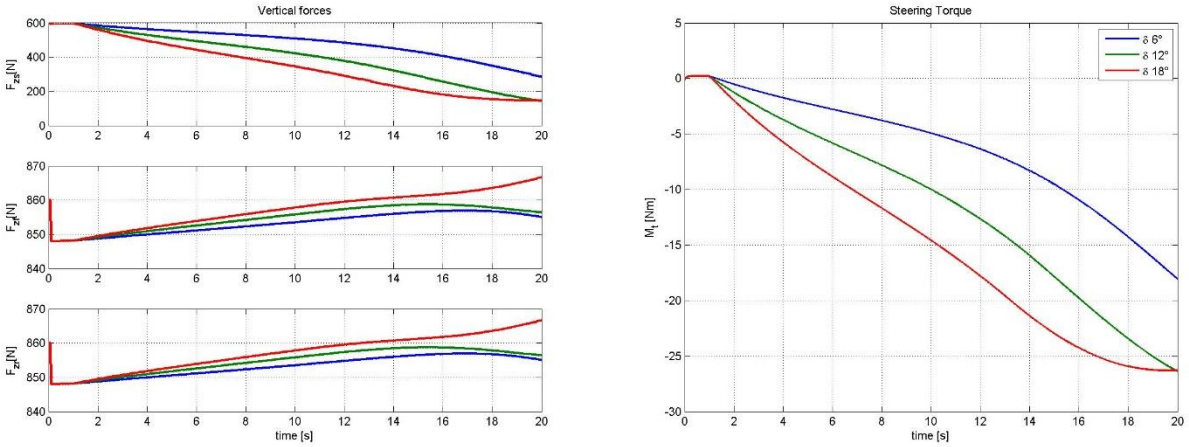

Figure F.2-195 Vertical forces and Steering torque for Maximum steering angle

Attachment G – Optimization Results

In this attachment are reported the results given by the sensitivity optimization algorithm with the Part Load Configuration along a Left Steering Pad, a Right Steering Pad and Straight Line during braking

G.1 Optimization Comparison

G.1.1 Objective Functions

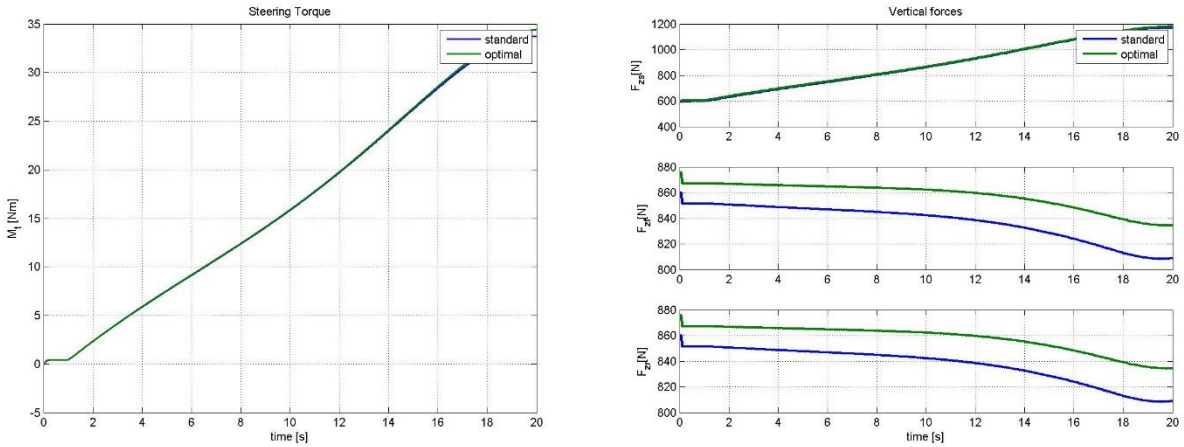

Figure G-196 Steering torque and Vertical forces for Steering pad left

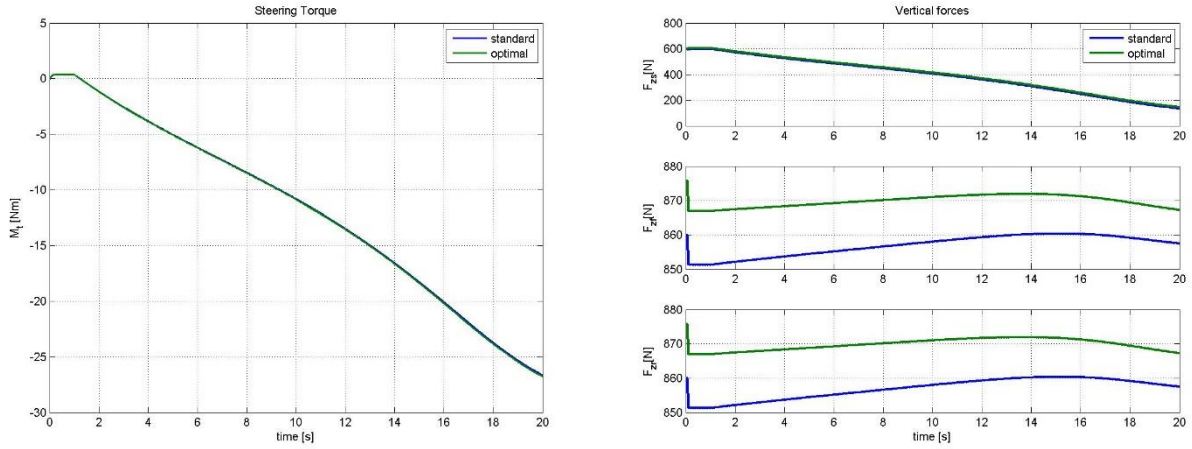

Figure G-197 Steering torque and Vertical forces for Steering pad right

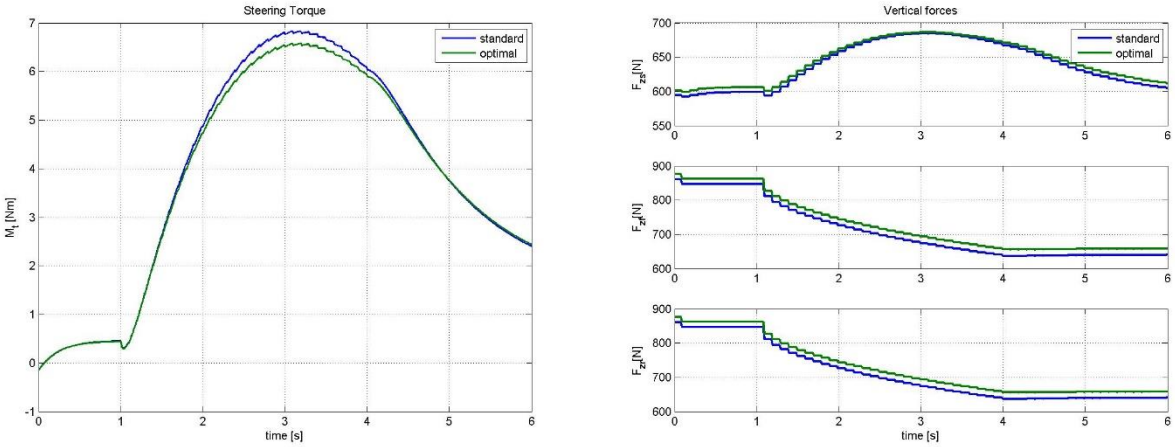

Figure G-198 Steering torque and Vertical forces for Braking

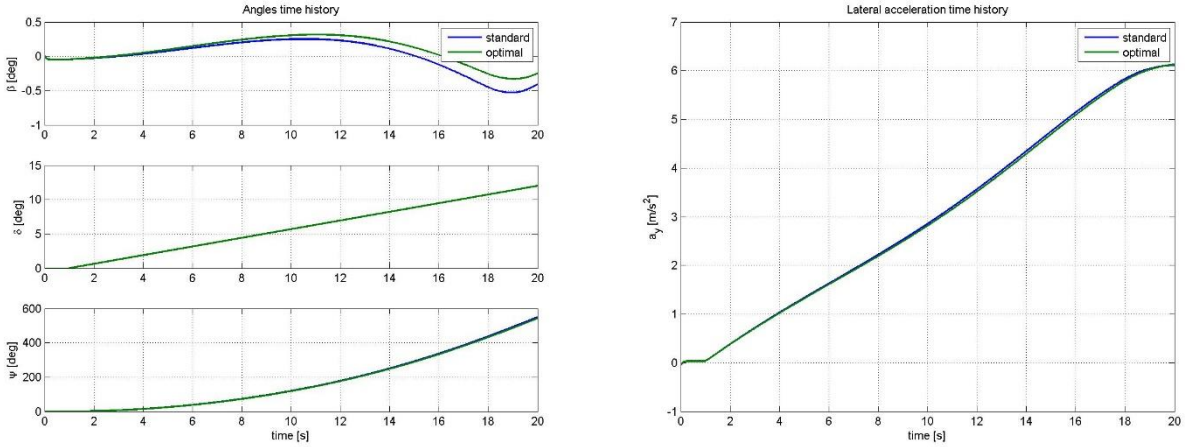

Figure G-199 Angles and Lateral acceleration for Steering pad left

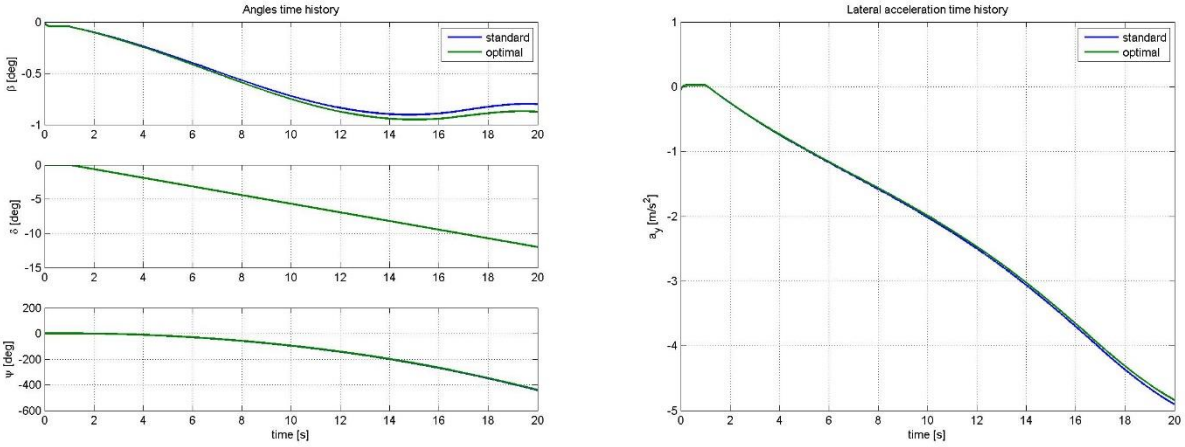

Figure G-200 Angles and Lateral acceleration for Steering pad right

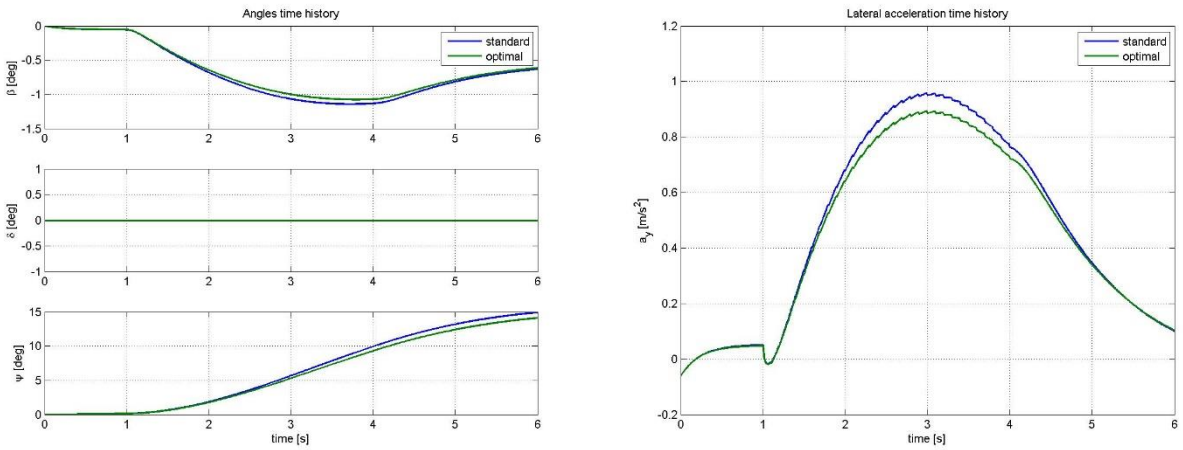

Figure G-201 Angles and Lateral acceleration for Braking

G.1.2 Other Results

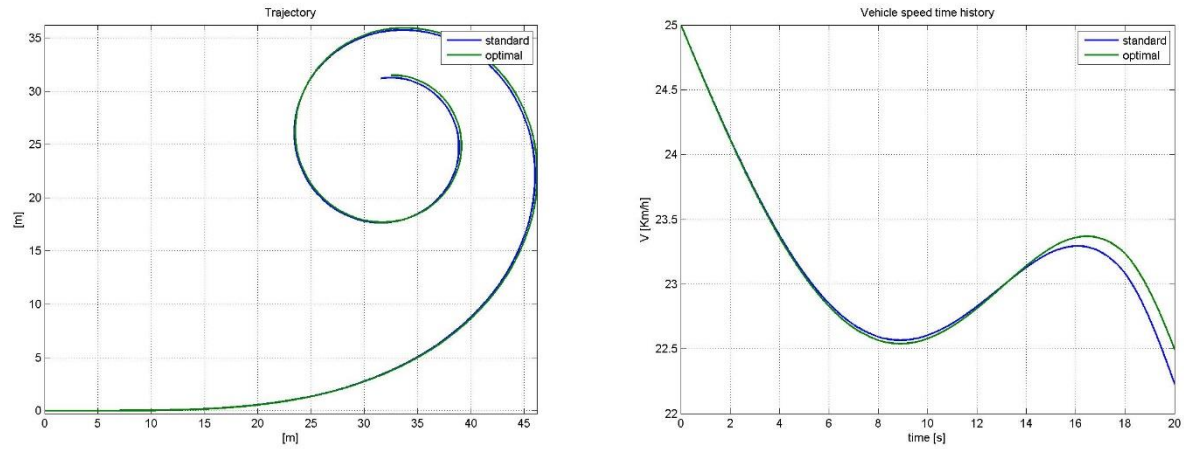

Figure G-202 Trajectory and Speed for Steering pad left

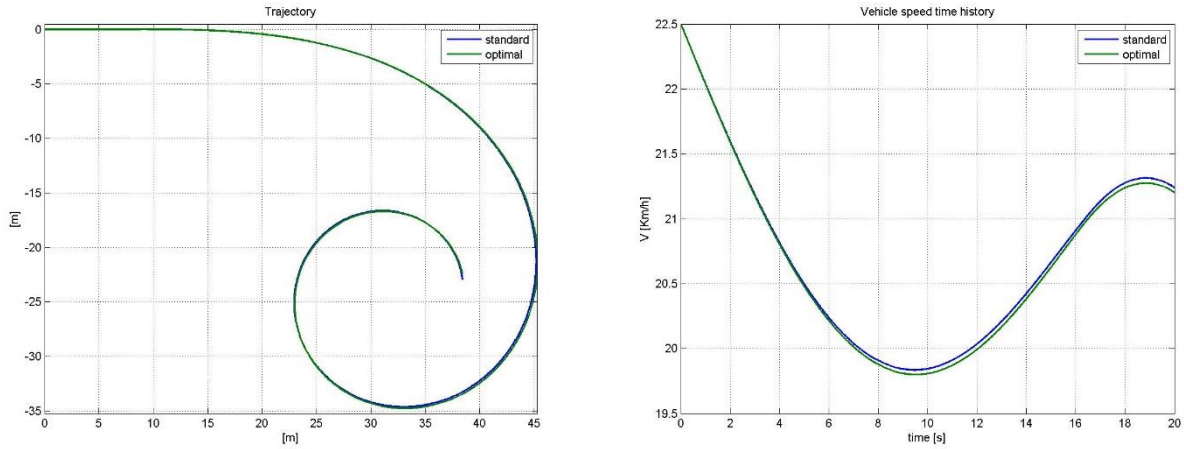

Figure G-203 Trajectory and Speed for Steering pad right

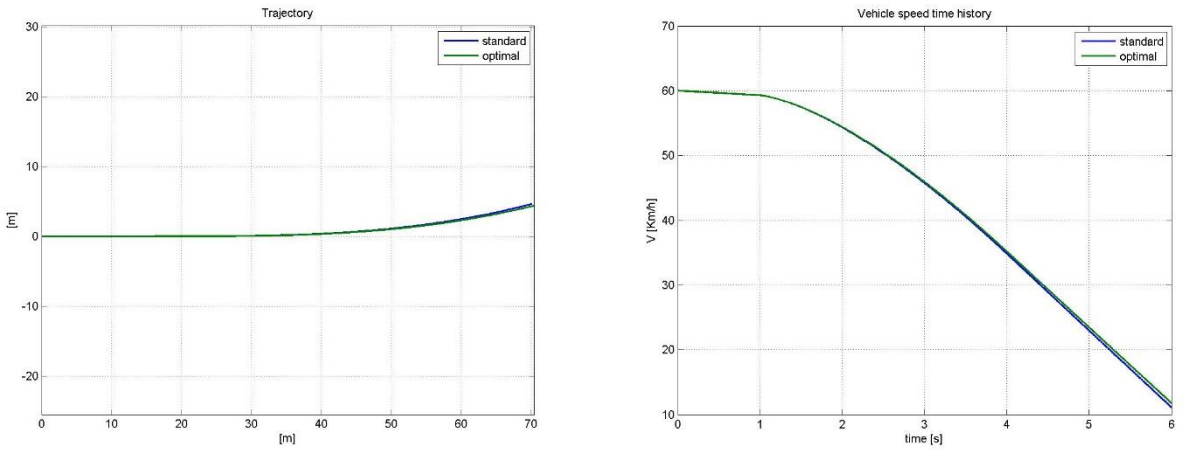

Figure G-204 Trajectory and Speed for Braking

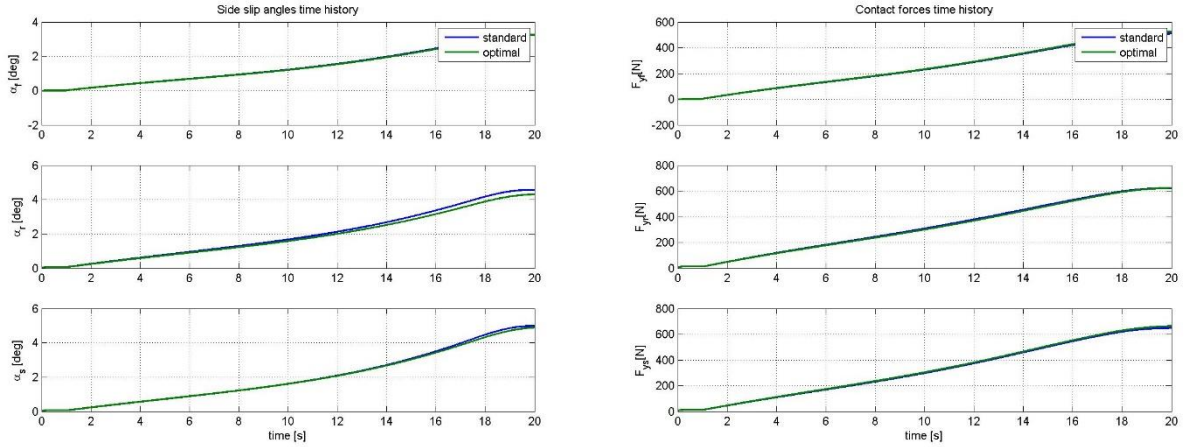

Figure G-205 Slip angles and Contact forces for Steering pad left

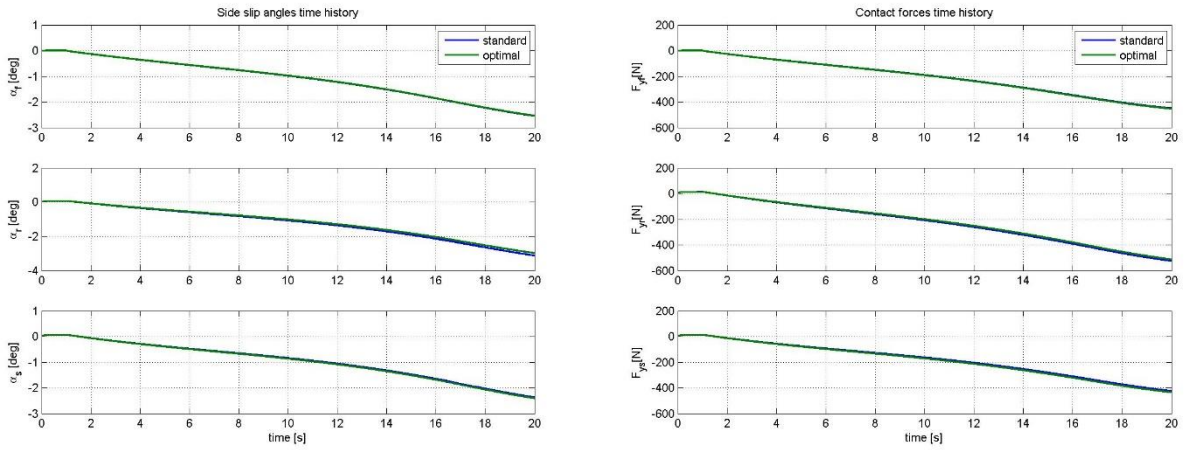

Figure G-206 Slip angles and Contact forces for Steering pad right

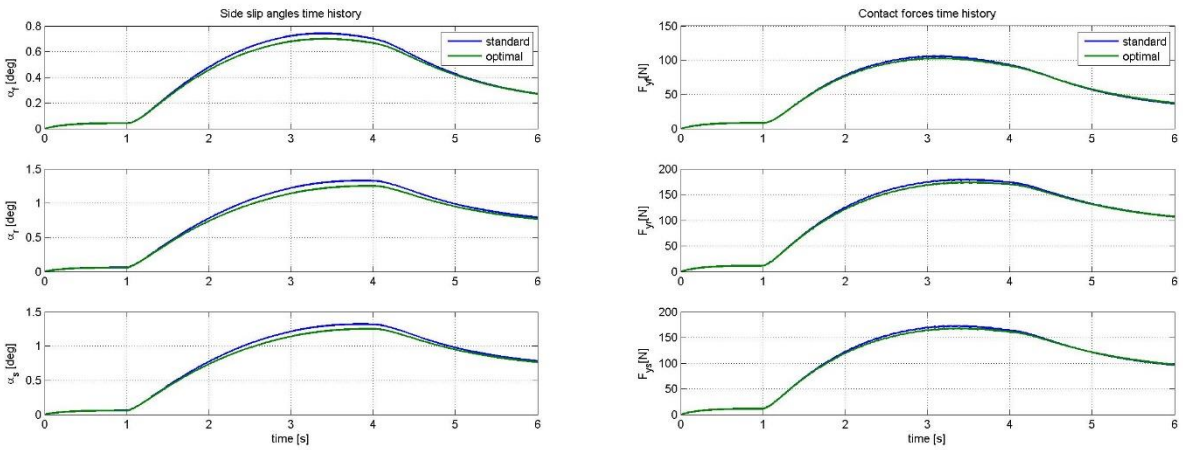

Figure G-207 Slip angles and Contact forces for Braking

G.2 Optimal set

	b_s [mm]	γ [deg]	λ [deg]	m_s [Kg]
1	23,5	0	0	29,744
2	23,5	0	0	25,549
3	25,182	0	0,039	25,689
4	23,780	0	0,078	25,549
5	23,5	0,235	0,019	25,829
	…	…	…	…
50	23,5	0	0,019	30,164
51	23,5	0	0,019	29,744
52	23,5	0	0,019	29,605
53	23,5	0	0	27,367
54	24,341	0	0	27,507
	…	…	…	…
100	23,5	0,627	0	37,016
101	24,341	0,627	0,019	36,596
102	23,5	0,627	0,019	36,876
103	27,986	0,647	0,039	37,016
104	56,866	0,333	0,568	32,192
	…	…	…	…
196	50,978	1,019	0,352	34,149
197	38,360	0,843	0,627	36,876
198	24,341	1,254	0	36,876
199	24,341	1,254	0,058	37,086
200	26,303	1,490	0,019	37,016

Table G.1 - Optimal Set Population

References

Vittore Cossalter : *Motorcycle Dynamics*

Hans B. Pacejka (2006): *Tyre and Vehicle Dynamics*

Prof. Federico Cheli : *Lessons - Multi Body Approach [Vehicle Dynamics and Control]*

Prof. Federico Cheli : *Lessons - Road Vehicle Handling [Vehicle Dynamics and Control]*

Giorgio Diana, Federico Cheli: *Dinamica e Vibrazione dei Sistemi*

Nicolò Bachschmid, Stefano Bruni, Andrea Collina, Bruno Pizzigoni, Ferruccio Resta : *Fondamenti di meccanica teorica e applicata*

Paolo Biscari, Tommaso Ruggeri, Giuseppe Saccomandi, Maurizio Vianello : *Meccanica Razionale per l'Ingegneria*

Ing. Francesco Braghin : *Lesson - Contatto Pneumatico-Strada*

Prof. Massimiliano Gobbi : *Lesson - Introduction to Multi-Objective Programming*

Prof. Massimiliano Gobbi : *Lesson - Progammazione discreta & Algoritmi Evolutivi*

Prof. Massimiliano Gobbi : *Lesson - Global Sensitivity Analysis*

Prof. Massimiliano Gobbi : *Lesson - Global Approximation*

Prof. Massimiliano Gobbi : *Lesson - Multi-Objective Programming*

Hal Kendal (2003) : *The Sidecar Operator Manual*

Dmitri Lurie (2012) : *The Stability of Three-wheeled Vehicles and Two wheel Bicycles*

Ing. Davide Bassi : *Realizzazione del prototipo di un sidecar con l'utilizzo di tecniche di prototipazione virtuale*